The Effect of Compressive Loading and Cement Type on the Fire Spalling Behaviour of Concrete

Jihad Miah

A Thesis Submitted to the University of Pau and Pays de l'Adour
to attain the Degree of Doctor of Philosophy in Civil Engineering

Ecole Doctorale des Sciences Exactes et de leurs Applications

The Effect of Compressive Loading and Cement Type on the Fire Spalling Behaviour of Concrete

Presented by

Md Jihad MIAH

The members of the jury consisted of

Professor Farid Benboudjema	Ecole normale supérieure de Cachan	Reviewer
Professor Izabela Hager	Cracow University of Technology	Reviewer
Dr. Anne-Lise Beaucour	Université de Cergy-Pontoise	Examiner
Professor Roberto Felicetti	Politecnico di Milano	Examiner
Professor Jean Michel Torrenti	University of Paris-Est (Ifsttar)	Examiner
Professor Christian La Borderie	University of Pau and Pays de l'Adour	Supervisor
Dr. Hélène Carré	University of Pau and Pays de l'Adour	Co-supervisor
Dr. Pierre Pimienta	Centre Scientifique et Technique du Bâtiment	Co-supervisor

October 2017

Abstract

Fire spalling of concrete can seriously jeopardise the integrity of the entire structure due to the reduction of the cross-sectional area of the structural elements, which lead to direct exposure of reinforcing bars to the flames (i.e. decay of mechanical properties of steel). In addition, the repair costs of the structures damaged by fire spalling of concrete are generally important. Therefore, from the 1960s, concrete fire spalling has received increased attention (Shorter and Harmathy 1961, Harmathy 1965, and Saito 1965) within the research community. Since the safety of people in case of unexpected fire is one of the today's major issues in the design and construction of concrete structures and infrastructure constructions – such as buildings, tunnels, bridges, nuclear power plants, and shelter structures, it is essential to have exhaustive knowledge about the fire spalling behaviour of concrete to guarantee good fire stability of the structural elements.

Based on the results presented in the literature, two main hypothesis have been proposed to explain the fire spalling behaviour of concrete, where the first mechanism focuses on the build-up of pore pressure (proposed by Harmathy 1965) while the second mechanism focuses on the development of thermal stresses (proposed by Dougill 1972 and Bazant 1997). Actually, to date, the fire spalling mechanism is still not yet completely understood. According to pioneer investigations in the literature, it is shown that the occurrence of fire spalling is influenced by various parameters, the external compressive load being one of them, which role is not well known in detail.

The research presented in this thesis seeks to examine and understand the mechanism of fire spalling role played by the external compressive loading during heating. Within this context, comprehensive experimental studies have been performed within the scope of the work presented in this thesis. Two ordinary concrete (B40-II and B40-III: $fc_{28days} \approx 40$ MPa) specimens (slab, cube and prismatic shape) were exposed to ISO 834-1 fire curve, while a constant uniaxial or biaxial compressive load was applied. The cubic (200 x 200 x 200 mm^3) specimens were heated on one full face (perpendicular to the loading direction) following a temperature curve close to the ISO 834-1 fire curve, while simultaneously being subjected to a vertical uniaxial compressive load (0, 4, 8, 12, 16 and 20 MPa). The mid-size concrete slabs with a nominal dimension of 800 x 800 x 100 mm^3 were heated at the bottom face, according to the ISO 834-1 fire curve, while a constant biaxial compressive load (0, 0.5, 0.75, 1.5, 3, 5 and 10 MPa) was applied before heating parallel to the heated face of the slab. In order to gain a deeper understanding the mechanism of the fire spalling role played by compressive loading and incorporation of slag in cement, comprehensive experimental studies have been performed, such as water absorption porosity and axial gas permeability tests on the unloaded preheating specimens, axial and radial gas permeability tests under different loading conditions (i.e. confining pressure and uniaxial compressive load) of the specimens after preheating under loading and unloading conditions. Additionally, measurements of temperature and pore pressure were carried out on unloaded prismatic specimens under three different heating rate and temperature levels.

Further, in order to better analyse the experimental results and to provide more insight into the mechanism behind the fire spalling behaviour of concrete role played by the external compressive loading, numerical computations were carried out by using the existing thermo-mechanical (TM) model implemented in a finite element code CAST3M, aimed at evaluating the stress profiles and the crack opening through the thickness of the slab and the cube during heating under compressive load (uniaxial and biaxial).

The research studies presented in this thesis clearly showed that the presence of external compressive load (uniaxial and biaxial) and their levels have a significant influence on the fire spalling behaviour of concrete. Loaded specimens are more prone to spalling than unloaded specimens, with increasing amounts of spalling for higher values of applied compressive stress.

In uniaxial tests, spalling was much higher for B40-II (3% of slag) than B40-III (43% of slag) for all the applied values of compressive stress. A similar difference was observed between the results obtained in biaxial tests at lower load (0.5 MPa). On the contrary, the difference appears not so significant from 1.5 to 10 MPa of biaxial fire tests due to the lower influence of the permeability of two different concretes when the biaxial load becomes relatively high.

From this study on two ordinary concretes (initial water content dried at 80°C, B40-II = 3.4-4.5% and B40-III = 3.5-5.4%), it highlights that a certain level of external compressive stress (uniaxial or biaxial) was necessary to induce spalling. A possibility is that the applied compressive stress prevents the creation of cracks naturally due to thermal mismatch between cement paste and aggregates and thermal gradients. For unloaded specimen, the creation of cracks increases the permeability and naturally prevents the pore pressure to exceed a value that favours spalling.

During a real fire, concrete structural members are always loaded or restrained. The presence of compressive loading during heating significantly increases the compressive stress (decreases the tensile stress) and the magnitude of pore pressure, which increase the risk of fire spalling. Then, the applied compressive stress is a very important key factor that the fire resistance design of concrete structures should take into account when considering spalling. Hence, **it is recommended that the fire spalling test should not be carried out only on unloaded specimens, especially for the ordinary concrete.**

Keywords: Concrete, cement, slag, ISO 834-1 fire, high temperature, spalling, compressive loading (uniaxial and biaxial), displacement, confining pressure, permeability, porosity, pore pressure, CAST3M, internal stresses, cracking.

Résumé:

L'écaillage du béton peut sérieusement mettre en péril la structure toute entière en raison de la réduction de la section transversale des éléments structurels, ce qui conduit à une exposition directe des armatures aux flammes (c'est-à-dire la dégradation totale des propriétés mécaniques de l'acier). En outre, les coûts de réparation des structures endommagées par l'écaillage du béton sont généralement importantes. Par conséquent, à partir des années 1960, l'écaillage du béton a été objet d'une attention accrue (Shorter et Harmathy 1961, Harmathy 1965 et Saito 1965) au sein du milieu de la recherche. Étant donné que la sécurité des personnes en cas d'incendie est l'une des principales questions actuelle pour la conception et la construction des structures en béton et celles d'infrastructures (les bâtiments, les tunnels, les ponts et les centrales nucléaires), il est primordial d'avoir des connaissances exhaustives sur le comportement du béton à haute température et le risque d'écaillage afin de garantir une bonne stabilité au feu des éléments structurels.

En se basant sur les résultats présentés dans la bibliographie, deux hypothèses principales ont été proposées pour expliquer le risque d'écaillage du béton à haute température. Le premier mécanisme correspond au développement de la pression des pores au cours du chauffage (proposé par Harmathy 1965) tandis que le second mécanisme correspond au développement des contraintes thermiques (proposé par Dougill 1972 et Bazant 1997). Actuellement, le mécanisme de l'écaillage du béton n'est toujours pas encore bien compris. Selon les recherches disponibles dans la littérature, il est démontré que l'apparition de l'écaillage du béton est influencée par divers paramètres, le chargement mécanique étant l'un d'eux, dont le rôle n'est pas bien connu en détail.

La recherche présentée dans cette thèse vise à examiner et à comprendre le rôle d'un chargement mécanique de compression sur le mécanisme d'écaillage.. Dans ce contexte, différentes études expérimentales ont été réalisées dans le cadre du travail présenté dans cette thèse. Différents spécimens de béton ordinaire (B40-II et B40-III: fc28 ≈ 40 MPa) (Formes : dalle, cube et prisme) ont été exposés à la courbe de feu standard (ISO 834-1), tandis qu'une charge de compression uniaxiale ou biaxiale constante a été appliquée. Les spécimens cubiques (200 x 200 x 200 mm^3) ont été chauffés sur une face (perpendiculaire à la direction du chargement) suivant une courbe de température proche de la courbe de feu ISO 834-1, tout en étant simultanément soumis à une charge de compression uniaxiale verticale (0, 4, 8, 12, 16 et 20 MPa). Quinze dalles de béton de taille moyenne ayant une dimension nominale de 800 x 800 x 100 mm3 ont été chauffées sur la face inférieure, selon la courbe de feu ISO 834-1, tandis qu'une charge de compression biaxiale constante (0, 0.5, 0.75, 1.5, 3 , 5 et 10 MPa) a été appliquée parallèlement à la face chauffée de la dalle. Afin d'acquérir une compréhension plus approfondie sur l'effet sur'écaillage du chargement de compression et de l'incorporation du laitier dans le ciment, différentes études expérimentales ont été réalisées, telles que la mesure de la porosité par absorption d'eau et des essais de perméabilité axiale aux gaz exécutés sur les échantillons préchauffés, des essais de perméabilité axiale et radiale aux gaz sous différentes conditions de chargement (c'est à dire pression de confinement et charge de compressive uniaxiale) des

échantillons après préchauffage sous différentes conditions de chargement). En outre, des mesures de la température et de la pression des pores ont été effectuées sur des échantillons prismatiques non chargés sous trois vitesses de chauffage et différents niveaux de température.

En outre, afin de mieux analyser les résultats expérimentaux et comprendre l'effet du chargement mécanique de compression sur le mécanisme d'écaillage du, des calculs numériques ont été réalisés en utilisant un modèle thermo-mécanique existant (TM) implantée dans un code d'élément fini CAST3M. Ces simulations numériques visent à évaluer les profils de contraintes ainsi que l'ouverture des fissures suivant l'épaisseur de la dalle et du cube pendant le chauffage sous une charge de compression (uniaxiale et biaxiale).

Les recherches présentées dans cette thèse ont clairement montré que la présence d'un chargement de compression externe (uniaxial et biaxial) et leurs niveaux ont une influence significative sur l'écaillage du béton. Les échantillons chargés présentent plus d'écaillage que ceux qui ne sont pas chargés. L'ampleur de l'acillage augmente avec la contrainte de compression appliquée.

Dans les essais au feu sous chargement uniaxial, l'écaillage était beaucoup plus élevé pour le B40-II (3% de laitier) que pour le B40-III (43% de laitier) pour toutes les valeurs de contrainte de compression appliquée. Une différence similaire a été observée pour les résultats obtenus lors d'essai au feu sous chargement biaxial à faible charge (0,5 MPa). Au contraire, la différence n'est pas significative de 1,5 à 10 MPa.

À partir de cette étude sur deux bétons ordinaires, il peut être mis en évidence qu'un certain niveau de contrainte de compression externe (uniaxiale ou biaxiale) est nécessaire pour induire l'écaillage du béton ordinaire. Les pressions des pores se combine avec les contraintes thermiques dûes aux gradients thermiques. Les contraintes de compression appliquées empêchent la création de certaines fissures générées par l'incompatibilité des déformations thermiques de la pâte de ciment et des granulats et des gradients thermiques. Pour l'échantillon non chargé, la création de fissures augmente la perméabilité et empêche naturellement le développement des pressions de pores.

Pendant un feu réel, les membres structurels en béton sont toujours chargés ou retenus. La présence d'un chargement compressif pendant le chauffage augmente considérablement le stress de compression (diminue le stress de traction) et la grandeur de la pression des pores, ce qui augmente le risque d'écaillage. Ensuite, le stress compressif appliqué est un facteur clé très important que la conception de la résistance au feu des structures en béton devrait prendre en compte lors de l'écaillage. Par conséquent, **il est recommandé que les essais d'écaillage ne soientt pas effectués uniquement sur des échantillons non chargés.**

Mots clés : Béton, ciment, laitier, feu standard (ISO 834-1), haute température, écaillage, chargement en compression, déplacement, pression de confinement, perméabilité, porosité, pression de pores, fissuration.

Dedication

I would like to dedicate this thesis to my beloved mother “Most Rahema Begum”, father “Noor Mohammad Bapary” and my wife “Shamima Aktar MIAH” who encouraged me to pursue my dreams and finish my dissertation.

List of Contents

1 Introduction

1.1 Background and motivation of the research

Fire poses one of the most severe environmental conditions that can act on the concrete structures as an external load and can induce severe damages (cracks, fissures and spalling etc.) or even lead to the collapse, which increase the potential risk in terms of human life and financial loss. In the past, there have been a numerous fire accident in tunnels such as the Channel Tunnel (1996 and 2008), Mont Blanc (1999) and Fréjus (2005) in France, Storebealt Tunnel (1994) in Denmark, Tauern (1999) in Austria and the Gotthard Tunnel (2001) in Switzerland, which causes human losses and significant structural damage [1] as well as an economic impact due to repair costs for tunnel reconstruction and indirect cost because of the tunnel not being operational during repair. After inspection, it has been reported that most of the tunnels have been seriously damaged (i.e. spalling) due to severe thermal load caused by fire, for example, as in the case of the first fire accident in the Channel Tunnel, along 50 metre length of the tunnel with 400 mm thick tunnel lining was suffered severe spalling and was reduced on average to 170 mm, exposing the reinforcement, see Figure 1.1 [1-3]. As a result, a great attention has been paid by the researchers around the world on the fire spalling behaviour of concrete to guarantee good fire protection of the structural elements and ensure that the people in the building or tunnel have enough time to save themselves.

Figure 1.1: Damage in the lining of the Channel Tunnel between France and England after the fire accident on November, 18th 1996.

In the case of unexpected fire in the building, the concrete structural elements such as slab, beam, column, and wall are subjected to extreme temperatures which lead to significant degradation of the stiffness (i.e. decrease of modulus of elasticity) as well as strength properties (both in compression and in tension) of the concrete [4], and increase both the elastic deformability and the creep [5] and cracking (due to thermal incompatibility between cement paste and aggregates [5-6], the thermal gradients and the external mechanical loading). Further, explosive spalling of concrete occurs under combined action of pore pressure, compression in the exposed surface region (induced by thermal stress and external loading) and internal cracking [7]. Fire spalling is a sudden and violent breaking away of the hot layers from concrete members which reduces the cross-sectional area and may lead to direct exposure of reinforcing bars to flames (i.e. decay of mechanical properties of steel), with a significant reduction of the load bearing capacity [5-7], which can seriously jeopardise the integrity of the entire structure.

Although numerous experimental and numerical studies have been conducted in order to gain a better understanding of the fundamental physics behind the fire spalling behaviour of concrete, its mechanism is still not yet completely understood. According to pioneer investigations in the literature, it has been shown that various factors, such as material factors (moisture content, permeability, aggregate type, etc.), geometry factors (section size and shape), and external factors (heating rate and level, applied external loading) influence the fire spalling behaviour of concrete in different ways [8-9]. It is worth noting, however, that an enormous number of experimental studies have been reported in the literature on unloaded specimens [6, 10], while comparatively, there are few published data on fire spalling of concrete subjected to external compressive loading condition [11-14]. Despite that, some investigations [11-14] deal with the effect of external compressive loading on the fire spalling behaviour of concrete, its role is still not yet well understood. Furthermore, it is well known that the high strength concrete (HSC) is more susceptible to explosive spalling due to its higher density (caused by reducing the water to binder ratio or adding fine mineral admixture, i.e. low porosity and permeability) than the normal strength concrete (NSC), therefore more attention was paid on the HSC by the scientific community.

The cement industry has recently shown a significant interest in blast furnace slag based cement because of its very good durability performance as low chloride diffusion and lower carbon footprint and reduction of negative environmental effects as well as bring economic benefits [15]. Although slag based cement concrete has been shown to have a significant number of advantages when used in concrete structures, it is essential to have exhaustive knowledge about the spalling behaviour of slag based cement concrete when exposed to high temperatures to answer the question whether concrete members and structures made with slag based cement can give the same fire safety level as those made with 100% Ordinary Portland Cement (OPC) concrete. The existing literature does not provide a detailed investigation of the fire behaviour of concrete made with blast furnace slag based cement (CEM III in Europe), especially spalling process of concrete in fire.

1.2 Aims of the research

As mentioned above, the lack of published test results, limited information and knowledge as well as the presence of some evidence of the effect of external compressive loading on the fire spalling behaviour of concrete provides the motivation of this thesis work. Most of the previous research reports on the fire spalling of concrete were tested on unloaded specimens, as an example, in the previous doctoral thesis of CSTB and SIAME (Jean-Christophe Mindeguia 2009 [10]), comprehensive experimental tests were carried out to analyse the contribution of vapour pore pressure to the thermal instability risk of concrete with different testing configurations, such as different concrete parameters (compactness, aggregate nature and polypropylene fibres), different samples geometries (from little cylindrical sample to mid-size slabs) and different heating procedure (from slow heating to ISO 834-1 fire). No clear link was found between the vapour pore pressure and fire spalling of concrete. It was concluded that vapour pressure is not the only physical origin for concrete spalling, hence both mechanisms (thermo-hydral and thermo-mechanical) should be taken into account.

In order to gain a deeper understanding of the effect of external compressive loading on the fire spalling behaviour of concrete, this current PhD thesis was launched in September 2014 at the Centre Scientifique et Technique du Bâtiment (CSTB) with the research collaboration of laboratory SIAME, Université de Pau et des Pays de l'Adour.

Since there is no existing model which can predict the fire spalling behaviour of concrete due to the complex structure of a composite material, such as variation of porosity, permeability, thermal dilation, opening of cracks, tensile strength, elastic modulus, migration of moisture, pore pressure and internal stress field with temperature, experimental studies appear necessary to investigate this phenomenon. Within this context, comprehensive experimental studies have been performed within the scope of the work presented in this thesis. The main goal of this research project is to study the effect of external uniaxial and biaxial compressive loading and cement type on the fire spalling behaviour of ordinary concrete (B40: $fc_{28days} \approx 40$ MPa) made with CEM II (3% of slag) and CEM III (43% of slag) cements. In order to deeper understand the experimental results and to explain the fire spalling mechanism of concrete, numerical computations were carried out by using an existing thermo-mechanical (TM) model with the finite element code CAST3M. However, data generated from this thesis can be used for future modelling and the development of appropriate design guidelines on the fire spalling behaviour of concrete when exposed to fire and external compressive loading.

1.3 Thesis layout

This thesis consists of seven chapters, as presented in Figure 1.2, as well as an appendix. The first part consists of the introduction in chapter 1.

Chapter 2: Literature review

In this chapter, a review of past research studies on the fire spalling behaviour of concrete is presented. This chapter mainly focused on the mechanism and influencing factors of the fire spalling of concrete, a great attention has been paid to the effect of external compressive loading on the fire spalling behaviour of concrete.

Chapter 3: Behaviour of concrete at high temperature

This chapter presents a detailed overview of the physical properties of concretes at high temperature related to fire spalling. Comprehensive experimental studies have been performed to analyse the effect of thermal load levels on the residual porosity and gas permeability of concrete in unloaded and loaded (only permeability) condition, which could influence the fire spalling behaviour of concrete by directly influencing the build-up of pore pressure during heating. Additionally, measurement of temperature and pore pressure were carried out under 3 different heating rate and temperature levels.

Chapter 4: The Effect of compressive loading and cement type on the fire spalling of concrete

This chapter presents the experimental studies aimed at evaluating the risk of fire spalling of concrete due to pressure build-up in the pores, thermal and load-induced stresses, which is the main goal of this thesis. The experimental test campaign consists of two parts: i) fire spalling tests on cubic specimens under different levels of uniaxial compressive loading and ii) fire spalling tests on the slab specimens under different levels of biaxial compressive loading. A wide range of ISO 834-1 fire spalling tests were carried out and the results are discussed in detail in this chapter.

Chapter 5: The thermo mechanical model

In order to better analyse the experimental results obtained in chapters 3 and 4 and to deeper understand the influence of compressive loading on the spalling mechanism of concrete, an existing thermo-mechanical (TM) model (implemented in a finite element code CAST3M) is described in this chapter, aimed at evaluating the stress profiles and the crack opening through the thickness of the slab and the cube during heating under compressive load (uniaxial and biaxial).

Chapter 6: Fire spalling mechanism of the ordinary concrete

In this chapter, a possible fire spalling mechanism of the ordinary concrete role played by external compressive loading has been discussed. The effect of loading conditions and cement type were also discussed.

Chapter 7: Conclusions and recommendations for future research

This chapter summarises the findings of this thesis and states conclusions on the effect of compressive loading and cement type on the fire spalling behaviour of concrete. Recommendations for future research studies are made.

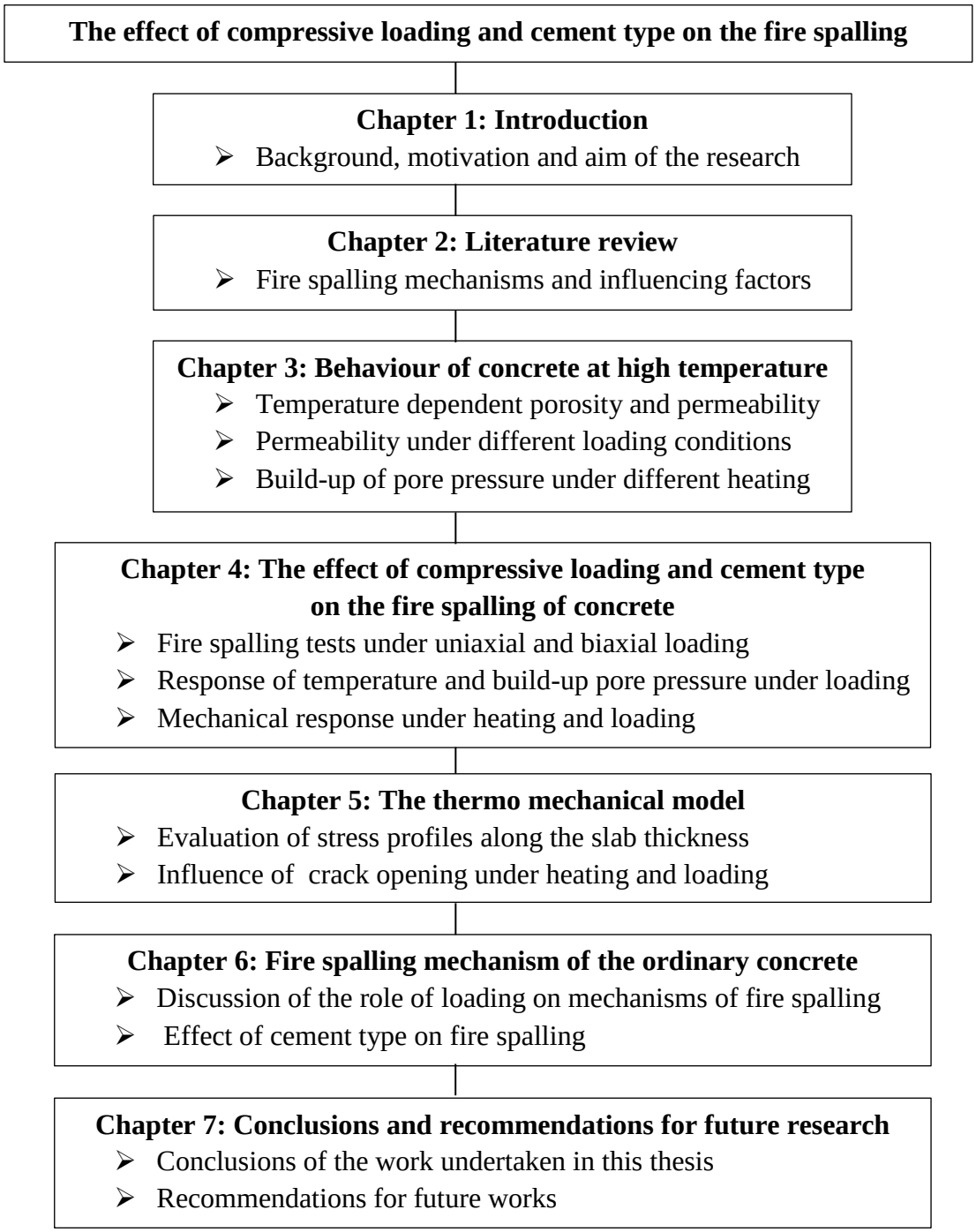

Figure 1.2: Schematic overview of the chapters presented in this thesis.

1.4 References

[1] Haack A. “Catastrophic Tunnel Fires - What have we learnt?”, International symposium on catastrophic tunnel fires (CTF), Ingason H (ed.), SP Swedish National Testing and Research Institute: Borås, Sweden, 2003.

[2] Ulm, F-J., Coussy, O and Bazant, J.P. (1999). “The “Chunnel” fire. I: Chemoplastic softening in rapidly heated concrete”, Journal of Engineering Mechanics, ASCE, Vol. 125, No. 3, March, 1999.

[3] Ulm, F-J., Acker, P and Lévy, M. (1999). “The “Chanel” fire. II: Analysis of concrete damage”, Journal of Engineering Mechanics, Vol. 125, No. 3, March, 1999.

[4] Felicetti, R and Gambarova, P.G. (1998). “Effects of high temperature on the residual compressive strength of high-strength siliceous concretes,” ACI Materials Journal, V. 95, No. 4, July-August 1998.

[5] Bazant, Z.P and Kaplan, M. F. (1996). “Concrete at high temperature: material properties and mathematical models," Book published by Longman Group Limited 1996.

[6] Kalifa, P., Chéné, Grégoire., and Gallé. (2001). “High-temperature behaviour of HPC with polypropylene fibres From spalling to microstructure”, Cement and Concrete Research 31 (2001) 1487–1499.

[7] Khoury G. A and Anderberg Y. (2000), “Concrete spalling review”, Fire safety design, report submitted to the Swedish National Road Administration, Sweden.

[8] Hertz, K.D. (2003). “Limits of spalling of fire-exposed concrete”, Fire Safety Journal 38 (2003) 103–116.

[9] Fu, Y and Li, L. (2011). “Study on mechanism of thermal spalling in concrete exposed to elevated temperatures”, Materials and Structures (2011) 44:361–376.

[10] Mindeguia J-C. (2009). “Contribution Expérimental a la Compréhension des risqué d’Instabilité Thermiques des Béton,” PhDThesis (French), Université de Pau et des Pays de l’Adour, France.

[11] Boström, L. and Jansson, R. (2008). “Self-Compacting Concrete Exposed to Fire”, SP Report 2008:53, Borås, Sweden, 2008.

[12] Carré, H., Pimienta, P., La Borderie, C., Pereira, F. and Mindeguia, J. C. (2013). “Effect of Compressive Loading on the Risk of Spalling”, Proceedings of the 3rd International Workshop on Concrete Spalling due to Fire Exposure, pp. 01007, Paris, France.

[13] Pimienta, P., Anton, O., Mindeguia, J-C., Avenel, R., Cuypers, H. and Cesmat, E. (2010). “Fire Protection of Concrete Structures Exposed to Fast Fires”, 4th International Symposium on Tunnel Safety and Security (ISTSS), March 17-18, 2010, Frankfurt, Germany.

[14] Lo Monte F. and Felicetti R. “Heated slabs under biaxial compressive loading: a test set-up for the assessment of concrete sensitivity to spalling”, Materials and Structures (2017) 50:192.

[15] ACI Committee 233 (2000). “Ground Granulated Blast-Furnace Slag as a Cementitious Constituent in Concrete”, ACI 223R-95, 2000.

2 Literature Review

2.1 Fire spalling behaviour of Concrete

The safety of buildings and large-scale structures exposed to fire is one of the today's major issues in the design of constructions. Fire spalling can occur when concrete is exposed to elevated temperature in buildings, tunnels, underground parks, etc. Fire spalling is a sudden and violent breaking away of the hot layers from concrete members which reduce the cross-sectional area and may lead to direct exposure of reinforcing bars to flames, with a significant reduction of the load bearing capacity [1-2].

According to the literature review, the spalling of concrete can be subdivided into four categories: i) aggregate spalling, ii) explosive spalling, ii) surface spalling, and iv) corner spalling or sloughing off spalling. Among all the types of spalling, explosive spalling is the most dangerous one. The first three types of spalling occur during the first 20-30 min of a severe fire and are influenced by the heating rate, while the fourth occurs after 30-60 min and is influenced by the maximum reached temperature [2].

2.2 Potential mechanisms of fire spalling

Based on the results presented in the literature, two physical mechanisms are often associated with this phenomenon, namely: i) the build-up of pore pressure (the thermo-hydral process [1, 3-5]), ii) development of thermal stresses (thermo-mechanical process [6-10]). While some authors recommended that the spalling is the combined action of both pore pressures and thermal stresses [2, 11-12].

Pore pressure spalling: This mechanism is driven by the pressure build-up inside concrete pores due to water vaporisation, which was identified as the main reason for spalling of concrete as proposed by Shorter and Harmathy 1961 [4] and Harmanthy 1965 [5]. As the temperature of the surface of the specimen exposed to fire reached and exceeded 100 °C and the rate of desorption of moisture in a thin layer adjoining the surface increased, part of the vapour is pushed towards the hot face (where it can be released in the environment), while part is forced towards the inner and cooler core. Since these zones are colder, water vapour starts to condense and a "moisture clog" is gradually created close to the heated surface of concrete (see Figure 2.1 left, Harmanthy 1965 [5]). This clog is assumed to be a region of concrete with high water content, which acts as an impermeable wall for vapour release. With increasing temperature, vapour pressure increases. These pore pressures can locally overtake the tensile strength of concrete and initiate the spalling [1, 13-14].

Thermal stress spalling: This mechanism is attributed to excessive thermal stresses generated by rapid heating, which was identified as the main reason for spalling of concrete as proposed by Bazant 1997 [6], Saito 1965 [7] and Dougill 1972 [8]. The heating of a concrete element involves steep thermal gradients due to the low thermal diffusivity of concrete. These thermal gradients induce compressive stress (due to restrained thermal expansion) distribution parallel to the heated surface and subsequently leading to tensile stress in the direction perpendicular to the heated surface (see Figure 2.1 right, Bazant 1997 [6]). These stresses can locally overtake the tensile strength of concrete and explosive spalling occurs [6, 9-10].

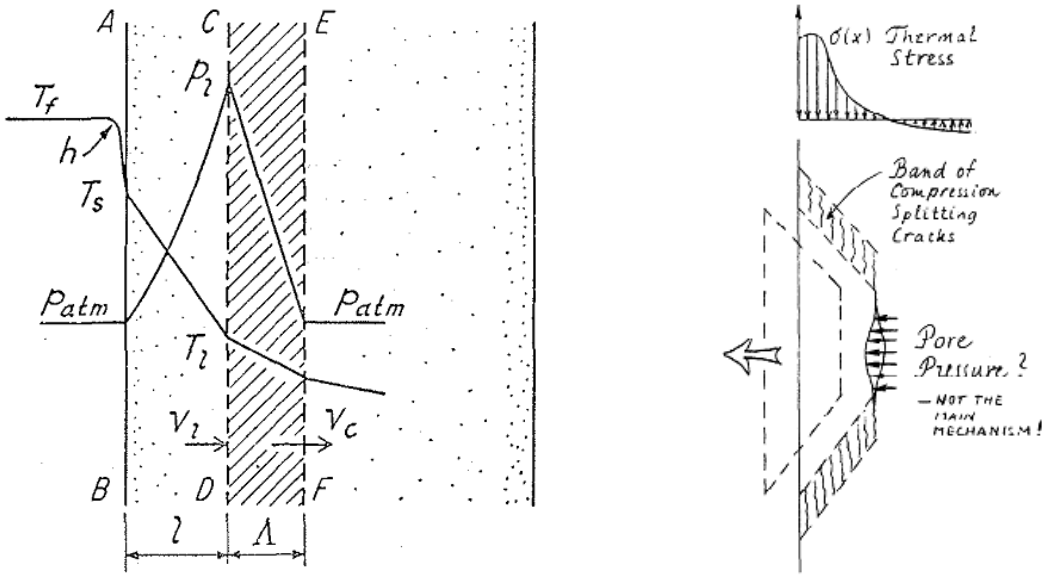

Figure 2.1: Schematic illustration of the moisture clog formation (left) [Note: T = the temperature gradient, p = the build-up of the pore pressure, ***l*** = thickness of dry layer (ABCD), Λ = thickness of moisture clog (CDFE), h = heat transfer coefficient, v = velocity] (Harmanthy, 1965 [5]). Possible mechanisms of explosive thermal spalling (right) (Bazant, 1997 [6]).

Combined pore pressure and thermal stress spalling: It has been found that the spalling occurs due to the combination of tensile stresses induced by thermal expansion and increased pore pressure. According to Khoury and Anderberg 2000 [2] and Khoury 2006 [12], "*explosive spalling of concrete generally occurs under combined action of pore pressure, compression in the exposed surface region (induced by thermal stresses and external loading) and internal cracking"*. Cracks develop parallel to the surface when the sum of the stresses exceeds the tensile strength of the material, which initiates the spalling [12]. However, it is noted that both key mechanisms of pore pressure spalling and thermal stress spalling is influenced by external loading and may change depending upon the section size, type of concrete and moisture content [15]. Zhukov 1976 [11] proposed that the occurrence of the explosive spalling is the development of unstable cracks under the action of the internal compressive stresses, compressive stresses caused by external loading and tensile stresses due to the pore pressure, see Figure 2.2.

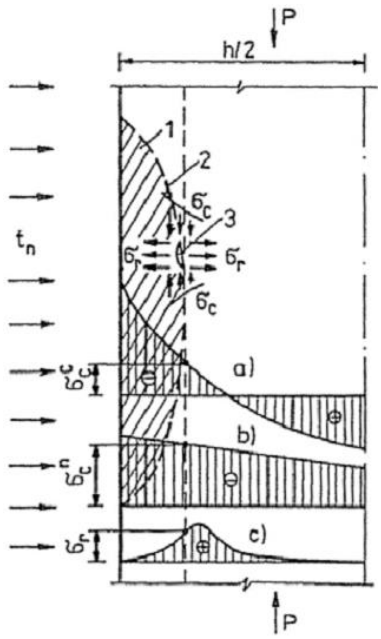

σ_c^c = internal compressive stresses
σ_c^n = compressive stresses caused by external loads
σ_r = tensile stresses due to pore pressure
t_n= fire temperature
P = external load
1 = piece of spalled concrete
2 = trajectory of the crack development
3 = crack

Figure 2.2: Stress distribution around the unstable crack at the moment of explosive spalling of concrete by fire (Zhukov 1976 [11]).

2.3 Factors influencing fire Spalling of concrete

According to pioneer investigations in the literature, it has been shown that various factors, such as material factors (moisture content, porosity, permeability, aggregate type and grading, compressive and tensile strength, presence of cracking, fibres, reinforcement, etc.), geometry factors (section size and shape), and external factors (heating rate and level, applied mechanical loading and level, and constraints) influence the fire spalling behaviour of concrete in different ways [2,15-19].

2.3.1 Observation of fire spalling on unloaded and loaded conditions

2.3.1.1 Fire spalling tests on unloaded specimen

From the 1960s, concrete fire spalling has received increased attention (Shorter and Harmathy 1961 [4]) within the research community around the world. A great number of studies have been conducted on the fire spalling behaviour of concrete on unloaded specimens (Kalifa et al. 2000 [1], Khoury and Anderberg 2000 [2], Phan, L.T. 2008 [3], Mindeguia J-C 2009 [20], Taillefer et al. 2013 [21], and Hager and Tracz 2015 [22]). In the previous doctoral thesis of CSTB and SIAME (Jean-Christophe Mindeguia 2009 [20]), comprehensive experimental tests were carried out on different concretes (B40, B40F2, B40SC, B60 and B60F2) to analyse the influence of the type of aggregates on fire spalling of concrete. The concrete B40 and B60 was made with calcareous aggregates and the B40SC was made with a mix of siliceous and calcareous aggregates. While B40F2 and B60F2 were made with calcareous aggregates and the addition of polypropylene fibres (Ø 18 µm x L 12 mm). The compressive strength of B40 concrete is about

40 MPa, while the B60 and B60F2 concretes are higher than 60 MPa. Mid-size concrete slabs (700 x 600 x 150 mm^3) were exposed to ISO 834-1 standard fire for one hour at the bottom surface of the slab (600 x 420 mm^2) in unloaded condition (free to expand during the fire test).

B40 (ISO 834-1)

B40SC (ISO 834-1)

B60 (ISO 834-1)

B60 (Moderate heating)

Figure 2.3: Exposed faces of the concrete slabs after one hour of ISO 834-1 fire curve.

Additionally, some of the slab specimens were heated under moderate heating (≈ 6.5 °C/min), aimed at to analyse the effect of temperature rate by comparing tests made on slabs at ISO 834-1 and moderate heating rate. For this, the ISO fire furnace was used by voluntarily reducing the power of the burners. Among all the tests, concrete spalling was observed during the ISO 834-1 fire test, for the two B40 and B60 slabs and for one of the B40SC slabs (see Figure 2.3), as well as moderate heating of B60 slab. Concerning the aggregate type, spalling is less severe in the case of the B40SC mixture, i.e. the concrete that contains siliceous aggregates (especially flint

rocks). However, during ISO 834-1 fire tests, some concretes did not show any thermal instability, such as both concretes that contained 2 kg/m^3 of polypropylene fibres (B40F2 and B60F2), and one of the B40SC slab.

An extensive experimental study on the fire spalling behaviour of concrete was presented by Taillefer et al. 2013 [21]. Within the scope of the study, a total of 22 concrete slabs made of normal and high strength concrete (fc ranging from 30 MPa to 75.3 MPa) with different parameters, such as the type of cement, nature of the aggregates, different water to cement ratio and a wide range of size and thickness of the slabs were tested. The slabs were heated on one side through the French Increased Hydro Carbon (HCinc) fire temperature-time curve for the duration of 2 hours. No mechanical load or no restrained were applied during the fire tests. The authors showed that the susceptibility of the concrete spalling increases with the increased moisture content during the fire tests. Some of the specimens suffered severe spalling and were reduced on average to 127 mm (while the thickness of the slab was 550 mm), exposing the reinforcement mesh and the damaged layer crosses the reinforcing mesh, see Figure 2.4. It has been concluded that the spalling depth tends to increase when the compressive strength of concrete increases. The concrete made with silico-calcareous aggregate is less sensitive to fire spalling than the concrete made with calcareous concrete.

Figure 2.4: The exposed face of the slab after 2 hours of heating.

Hager et al. 2015 [22] carried out the fire spalling tests on seven different concretes ($f_{c\ 90days} \approx$ 51 MPa to 96 MPa) aimed at determining the influence of different parameters, such as cement type (CEM I and CEM III), water to cement ratio (0.3, 0.45 and 0.6) and type of aggregates (riverbed = O, granite = G, and basalt = B) on the spalling behaviour of concrete. Fire spalling tests were conducted on concrete slabs with nominal dimensions of 1.2 x 1.0 x 0.3 m^3, which was heated on one side (the area of the specimen exposed to the fire was approximately 0.95 x 0.75 m^2), according to the ISO 834-1 standard fire curve for the duration of 2 hours. Among seven concretes, 6 concrete slabs were spalled during the tests, while the concrete made with

riverbed gravel (O/0.6/CEM I) did not present spalling. An example of the exposed face of the slab after 2 hours of heating can be seen in Figure 2.5. It was concluded that the denser concrete is more sensitive to fire spalling than more permeable concrete. Concerning the aggregate type, the concrete made with riverbed gravel (O/0.3/CEM I) is more prone to spalling than the granite and basalt aggregates. It has been shown that the spalling volume of the concretes made with CEM III (slag based) cement (B/0.30/CEM III and O/0.30/CEM III) was smaller than for the concretes made with CEM I cement (B/0.30/CEM I and O/0.30/CEM I).

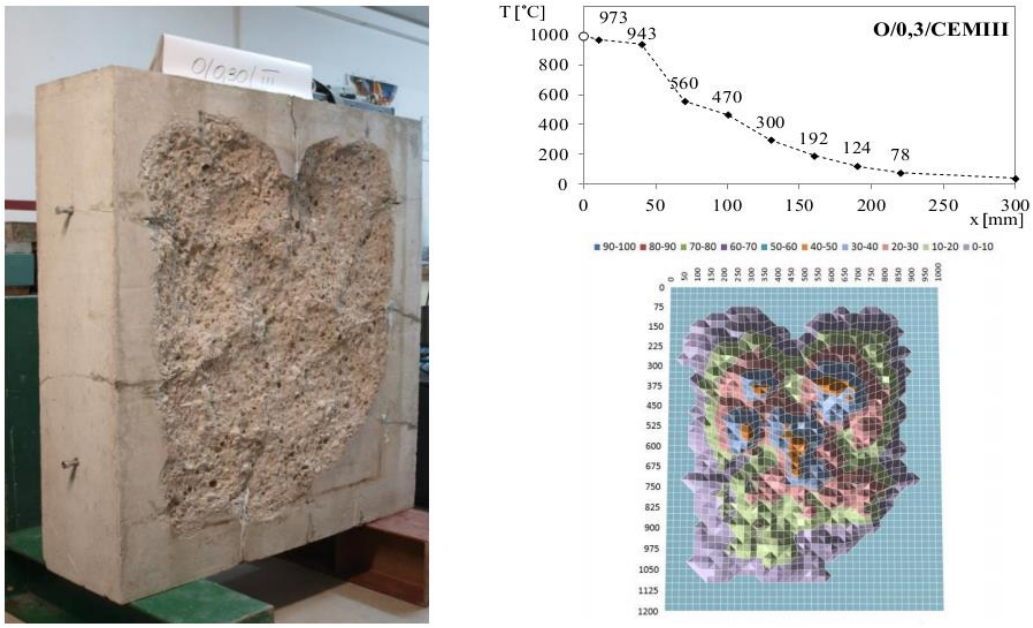

Figure 2.5: The exposed face of the slab (O/0.3/CEM III) (left) and maximum temperature in the slab cross section and spalling map (mesh = 25 x 25 mm, O/0.3/CEM III) (right).

2.3.1.2 Fire spalling tests on loaded specimen

During the period 2004-2017 the Research Institute of Sweden, RISE (old name "SP Technical Research Institute of Sweden) [23-30] performed numerous experimental study on the fire spalling behaviour of concrete in loaded and unloaded conditions (e.g. Jansson and Boström 2004, Boström and Jansson 2008, Boström et al. 2007, Jansson and Boström 2013). Their research studies focused on the effect of specimen size (small slab = 600 x 500 x 200 mm^3 and large scale slab = 1800 x 1200 x 200 mm^3), heating fire curve (ISO 834-1 and hydrocarbon, HC) and mechanical loading (by internal post-tensioning bars and external compressive loading) and restraining conditions (see Figure 2.6). Based on Boström and Jansson 2008 [27] report, in the loaded tests, the maximum tested load levels were 10% of the compressive strength of the actual concrete at room temperature ($f_{c28days} \approx$ 39 MPa to 70 MPa). The load was applied either by post stressing bars going through the centre of the test specimen and or loaded with an externally mounted cradle. It has been found that the mechanically loaded specimens during heating are more susceptible to spalling than unloaded members, see Figure 2.7.

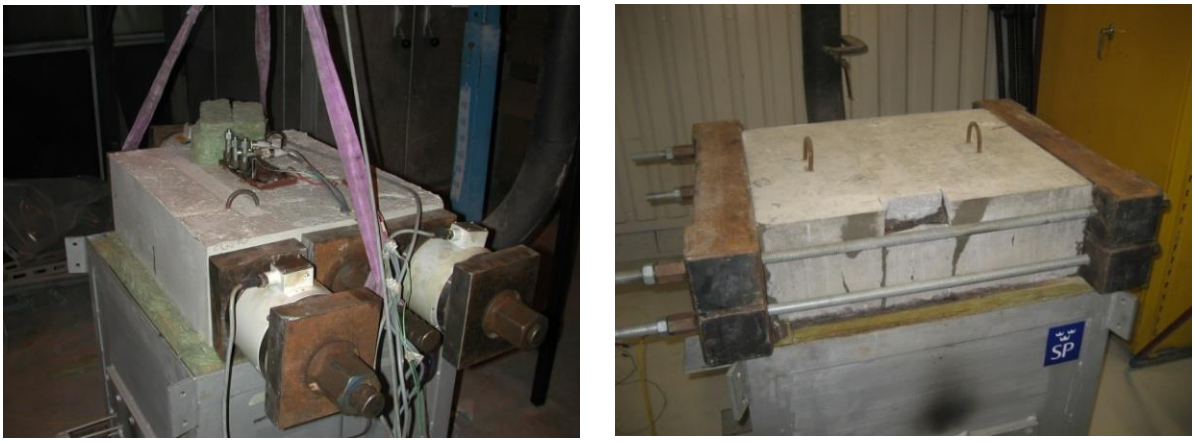

Figure 2.6: Loading with post stressing bars (left) and loading with an external cradle (right) (Boström and Jansson 2008 [27]).

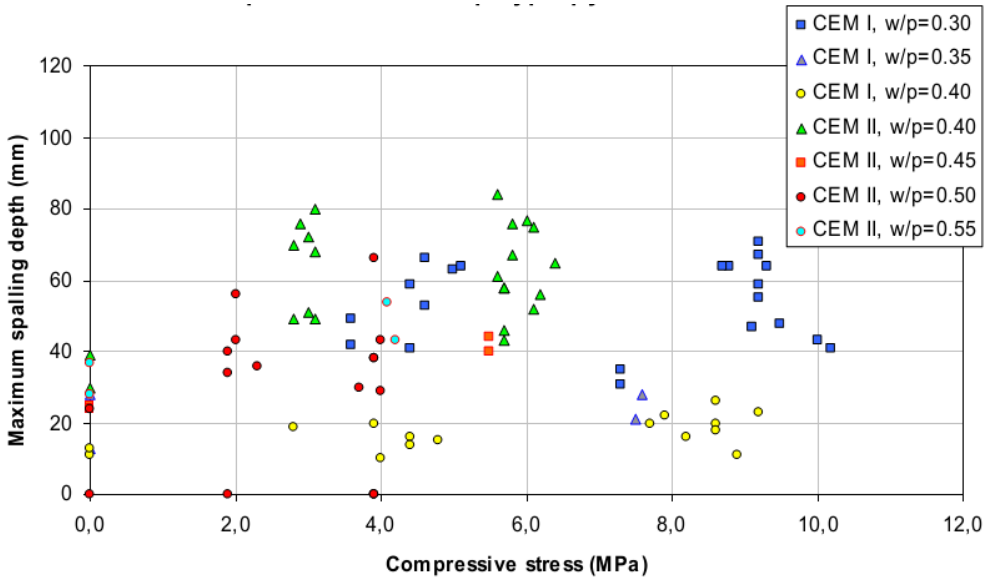

Figure 2.7: Effect of applied compressive stress on the spalling depth (Boström and Jansson 2008 [27]) (Note: w/p = water to powder ratio).

When comparing the method of applying the load to the concrete specimens, see Figure 2.6, a remarkable difference was observed in the amount of spalling. When using an externally mounted cradle the spalling was more severe. An explanation could be that when using the post stressing bars in the centre of the specimen a different crack pattern was formed which may release water vapour and facilitate water transportation within the concrete sample. From their vast amount of research work, they concluded that the loading has an important role on the spalling. It is not only the stress level applied, but also how the load is applied that affects the amount of spalling. The authors recommended that not to perform fire spalling tests on unloaded specimens, except not for a specific reason.

Jansson and Boström 2013 [29] observed that the addition of a load (3.9 MPa by 6 post stressing bars) on concrete ($f_{cat28days}$ = 47 MPa) large slab specimens (1800 x 1200 x 200 mm^3) lead to a longer period and progressive spalling of concrete. Severe spalling causing exposure of the reinforcement to the fire (see Figure 2.8). The authors conclude that the reason for a shorter period of spalling in unloaded specimens is probably that stresses release by cracking of the specimen. Tests were also performed on large slab specimens that were unloaded, but restrained by the loading system. During these tests, the unloaded specimens (but restrained) spalled less than the loaded ones.

Figure 2.8: The test specimen after the fire exposure [29].

Pimienta et al. 2010 [31] investigated the fire test on 6 m x 1 m concrete ($f_{c\ at28days} \approx 40$ MPa) slabs heated on one side through the Increased Hydro Carbon fire temperature-time curve for the duration of 2 hours. An initial compressive stress of 10 MPa was applied to the slab bed that was exposed to fire and then the load kept constant for the whole test. To this aim, a dead load of 1 ton was suspended at the end of the metal beams before heating which creates bending of the slab in the opposite direction of the fire and induces an initial compressive stress of 10 MPa in the slab bed. The slab was longer than the furnace (see Figure 2.9). The ends of the slab have a greater thickness (350 mm) than in the heated zone (200 mm) and were rigidified by dense reinforcements. The stiff metal beams (length = 4000 mm) were fixed on each end of the slab. The concrete slabs were placed on a horizontal gas-burners furnace.

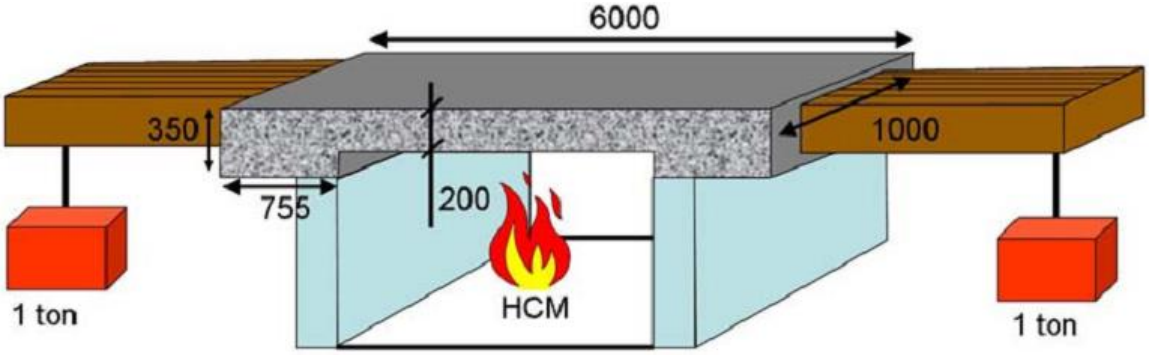

Figure 2.9: Geometry and principle of the “compressive” fire test [31].

The exposed surface of the slab was 4.49 x 1 m². Some tests had been carried out on samples with passive protection (protection thickness = 0, 8, 12.5, 15, 20 and 25 mm). The experimental results have shown that the loaded slabs were more prone to spalling than the unloaded slabs. When concrete slabs were not thermally protected, the maximum spalling depths of silico-calcareous concrete in loaded and unloaded conditions were 85 mm and 30 mm, respectively, while no significant change in maximum spalling depth has been observed for calcareous concrete. On the contrary, when concrete slabs were protected with 8 and 12.5 mm, the maximum spalling depths of calcareous concrete were 63 mm and 137 mm, respectively, in the loaded conditions (see Fig. 2.10) and 50 mm and 0 mm, respectively, in the unloaded condition.

a) Thermal protection = 0 mm
Maximum depth = 49 mm

b) Thermal protection = 8 mm
Maximum depth = 63 mm

c) Thermal protection = 12.5 mm
Maximum depth = 137 mm

Figure 2.10: Fire spalling of loaded slabs (calcareous concrete) with the thermal protection of 0 (unprotected), 8 and 12.5 mm (Pimienta et al. 2010 [31]).

Carré et al. 2013 [32] investigated the effect of compressive loading on the risk of fire spalling of an ordinary concrete ($f_{c28\ days}$ = 37 MPa). To this aim, a specific metallic frame has been developed to apply uniaxial stresses on slabs during the fire tests (see Figure 2.11a). The concrete made with calcareous aggregates and CEM II/A-LL 42.5 R cement has been studied in this experimental campaign. Six concrete slabs with nominal dimensions of 580 x 680 x 150 mm^3 were heated at the bottom face of the slab (500 x 600 mm^2) according to ISO 834-1 fire for the duration of 2 hours under four different levels of uniaxial compressive loading (0, 5, 10 and 15 MPa). The load was applied before heating by means of 2 flat jacks and then the load was kept constant for the whole test. No spalling was observed on the samples loaded at 0, 5 and 10 MPa. Significant spalling was observed on the 2 samples loaded at 15 MPa. Mean and maximum spalling depths were the same in the 2 samples (respectively 20 and 40 mm, see Figure 2.11b).

Lo Monte et al. 2015 [33], Lo Monte and Felicetti 2016 [34], Lo Monte and Felicetti 2017 [35] studied the interaction between pore pressure and stress in triggering spalling. Concrete slabs ($f_{c\ at\ 28days} \approx 60$ MPa) made without fibre and with 2 kg/m^3 of polypropylene fibre (L = 12 mm; $Ø_{eq}$ = 20-48 μm) and steel fibre (40 kg/m^3 of 0.55 x 35mm hooked end fibre). Concrete slabs with nominal dimensions of 800 x 800 x 100 mm^3 were heated (600 x 600 mm^2) according to ISO 834-1 fire curve and subjected to a compressive biaxial membrane load of about 10 MPa.

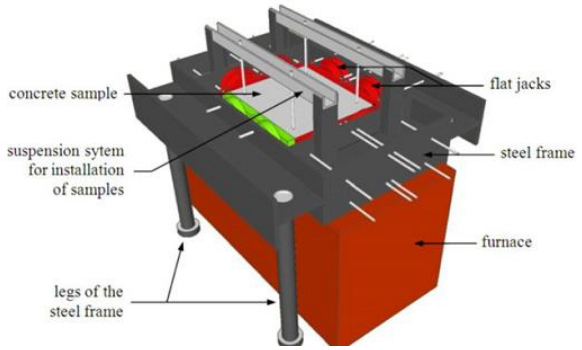

a) Furnace and frame for mechanical loading

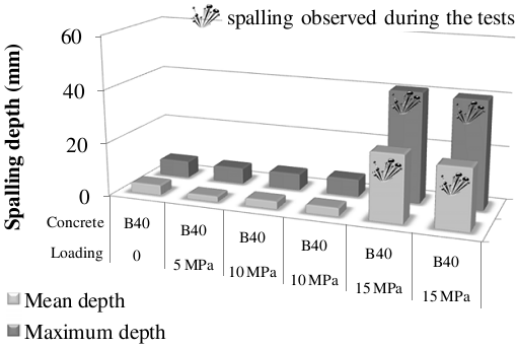

b) Mean and maximum spalling depth

c) Heated face of the slab loaded at 15 MPa

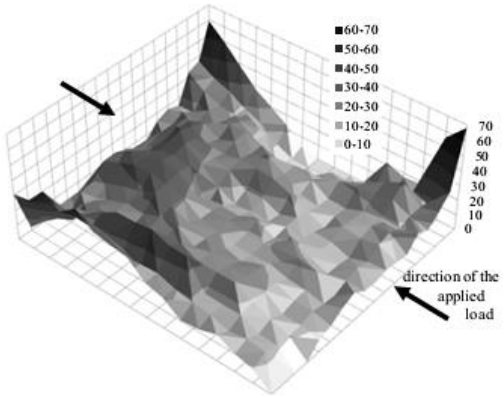

d) Topography of the exposed face

Figure 2.11: Effect of compressive loading on the fire spalling of concrete [32]).

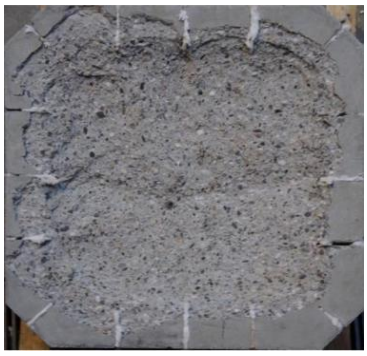

Plain concrete

Steel fibre-reinforced concrete

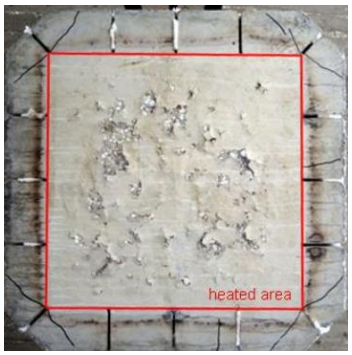

Polypropylene fibre concrete

Figure 2.12: Heated face of slabs after testing for external compressive stress of 10 MPa [34].

Two plain and two steel fibre reinforced concrete slabs were tested under the biaxial compressive stress of 10 MPa. Explosive spalling was observed in both loaded slabs for plain concrete, while only in one slab for steel fibre reinforced concrete. Spalling occurred after 19 and 34 min for plain concrete and after 35 min in steel fibre reinforced concrete. The final spalling depth was very similar for the three specimens (about 45-50 mm, involving all the heated area). While the specimens made with polypropylene (pp) fibre allowed to avoid any form of spalling

during the whole fire duration (120 min), with only a slight superficial scaling observed after cooling, see Figure 2.12.

Maluk et al. 2013 [36] and Maluk et al. 2017 [37] experimentally evaluated fire spalling behaviour of concrete ($f_{cat180days}$ = 103 to 112 MPa) contained different types and dosages of polypropylene fibres. The prismatic concrete slabs (500 mm length x 200 mm wide x 45 or 60 or 75 mm thickness) concrete slabs were heated (400 x 200 mm^2) by radiant panels under uniaxial compressive loading (12.34 MPa) and unloading (0 MPa) conditions. Fire spalling was observed in all the specimens in the loaded condition, while spalling was also observed in the unloaded tests, with the exception of one mix which did not spall in the unloaded condition. The author concluded that the stressed concrete is more likely to spall than unstressed concrete.

Kim et al. 2011 [38] carried out an experimental study on the thermal damage and spalling of concrete under loading conditions in a tunnel fire. The concrete (f_c = 24 MPa) specimen dimension of 600 x 600 x 150 mm^3 was exposed to MHC (Modified Hydrocarbon fire), while the concrete (f_c = 40 MPa) specimen dimension of 600 x 600 x 200 mm^3 were exposed to four different fire scenarios (ISO 834-1 fire, MHC - Modified Hydrocarbon fire, heating rate of 1 °C/sec, and RWS - Rijks Water Staat fire). Five different load ratios (0, 20, 40, 60 and 70% of the compressive strength of concrete at ambient temperature) were applied under the condition of the MHC fire for the duration of 2 hours to investigate the influence of the load ratio on the spalling behaviour of concrete. The load was applied before heating and then maintained constant during the whole tests. The results showed that spalling was observed under unstressed (0% load) conditions, while it was not observed under 20 - 40% loads, which seems to contradict from other researcher's results. The authors explained that in the loaded tests (20 - 40% loads), the development of microcracks occurred inside the concrete, which allows smooth flow of vapour release, which probably mitigates the spalling. Under a load ratio of 70%, the rapid spread of cracks caused failure during 10 minutes of heating.

An extensive experimental study on the effect of loading level on the structural performance of concrete columns in the fire was presented by Ali et al. 2003 & 2004 [39-40]. Within the scope of the study, a total 99 normal ($f_{c28\ days}$ = 43 MPa) and high strength ($f_{c28\ days}$ = 106 MPa) reinforced concrete columns (127 mm x 127 mm and 1800 mm height) were tested under four loading levels (0, 0.2, 0.4 and 0.6 of BS8110 column design strength) and two heating rates (high - represents the BS 476 fire curve and low heating rate, see Figure 2.13 left). The authors observe that the loading levels up to 60% of the design strength have no significant effect on the probability of concrete spalling both under high and low heating rate, which is contradicting from Ali et al. 2010 [41].

Ali et al. 2010 [41] conducted a numerical and experimental investigation of the fire behaviour of high strength ($f_{c28\ days}$ = 104.5 MPa) reinforced concrete (RC) columns of section 127 mm X 127 mm in cross-section and 1800 mm in height. The columns were simply supported at both ends and were tested under five loading levels (0.2, 0.3, 0.4, 0.5 and 0.6 of the BS8110 ultimate design load). The two fire curves were used in columns testing, those were ISO 834-1 fire curve (high heating) and the second curve had an inferior intensity (low heating), see Figure

2.13 left. The numerical and experimental results showed that increasing the loading level has increased the probability of concrete spalling, particularly under low heating regimes (see Figure 2.13 right). The authors also showed that increasing the loading level from 0.2 to 0.6 has reduced the fire resistance of the columns by an average of 65%.

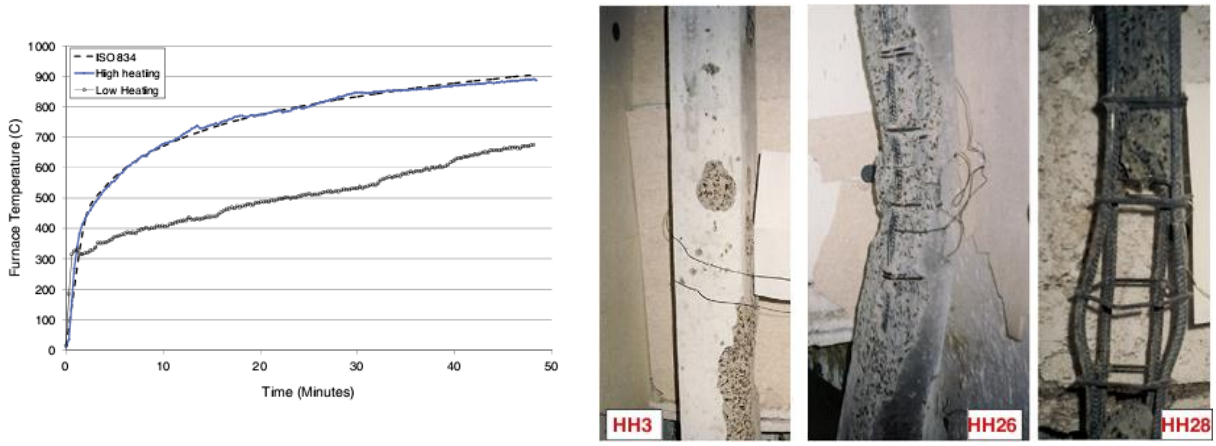

Figure 2.13: Fire curves used in the tests (left) and explosive spalling of columns HH3 (high heating and load level = 0.2), HH26 (high heating and load level = 0.6) and HH28 (low heating and load level = 0.6) (Ali et al. 2010 [41]).

An extensive experimental study on the fire spalling behaviour of concrete in loaded and unloaded conditions was presented by Kodur 2000 [42], Kodur and Phan 2007 [43] and Dwaikat and Kodur 2009 [44]. Dwaikat and Kodur 2009 [44] performed the fire spalling tests on six reinforced concrete (normal strength: $f_{c28\ days} \approx 52$ to 58 MPa and high strength: $f_{c28\ days} \approx 93$ to 106 MPa) beams (3.9 m long x 0.254 m width x 0.408 m high) under two point loads (either 50 kN, which is equal to 55% of the beam capacity, according to ACI 318 or 60 kN or 65% of the beam capacity). The beam specimens were heated (2.44 m of length) under three fire scenarios (ASTM E119 standard fire, short severe design fire, SF and long severe design fire, LF). The severe extent of spalling was observed in higher load ratio (65%) applied to the beam as compared to that the beam with lower load ratio (55%), see Figure 2.14 [44].

Figure 2.14: Fire spalling of normal strength concrete (NSC) Beam B2 (SF and load of 50 kN) and high strength concrete (HSC) Beam B5 (LF and load of 60 kN) [44].

Kodur 2000 [42] concluded that the type of load and its intensity have a significant influence on the fire spalling behaviour of concrete. A loaded structural member is more prone to spalling than an unloaded member.

Morita et al. 2000 [45] performed the ISO 834-1 standard fire spalling tests on both loaded and unloaded specimens. A total of 33 specimens were tested to evaluate the influence of water to cement ratio, the age of concrete, the amount of steel reinforcement, the inclusion of polypropylene fibres, and the time-temperature fire curve. For the loaded tests, concrete ($f_{c\ day\ of\ fire\ test}$ = 63 to 111 MPa) beam specimens (3.6 x 0.5 x 0.4 m^3) were heated from both sides and the bottom according to the ISO 834-1 fire curve for the duration of 3 hours under a vertical compressive load of 44 kN at the middle span of the beam. Fire spalling was not observed for the specimens that contained polypropylene fibres, while the spalling was observed in the loaded beam specimens which were not containing polypropylene fibres, see Figure 2.15. It was found that the lower the water-cement ratio the higher the degree of spalling.

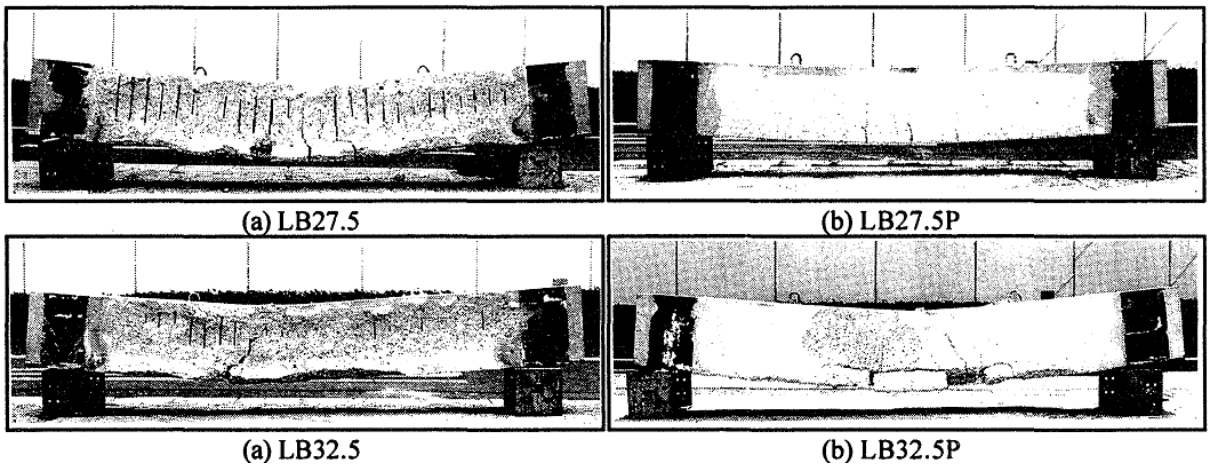

Figure 2.15: Beam after fire test under vertical compressive loading indicating different spalling effects on concrete with and without polypropylene fibre (Note: LB27.5: load (L), beam (B) and 27.5 is the % of water to cement ratio, similar meaning for others) [45].

Castillo et al. 1990 [46], Tao et al. 2010 [47], and Diederichs et al. 1989 [48] have carried out the tests to determine the mechanical properties of concrete subjected to an elevated temperature with a sustained uniaxial compressive stress. Castillo et al. 1990 [46] studied the effect of transient high temperature on compressive strength and load-deformation properties of high-strength concrete under both unloaded and preloaded conditions. The cylindrical specimens (Ø 51 mm x 102 mm) were subjected to temperatures ranging from 100 to 800 °C in increments of 100 °C. In stressed tests, the specimens were preloaded to 40% of their ultimate compressive strength at room temperature. The authors observed that none of the preloaded specimens were able to sustain the load beyond 700 °C. About one-third of the specimens failed in an explosive way in the temperature range of 320 to 360 °C when being heated under a sustained uniaxial compressive stress.

Tao et al. 2010 [47] investigated the compressive strength of self-compacting concrete on cylindrical specimens (Ø 150 mm x 300 mm) heated up to 800 °C, under unstressed and stressed condition (preloaded by 20% of the reference strength of the concrete at 20 °C). Almost all self-compacting concrete specimens tested under the stressed condition failed in explosive spalling between concrete temperatures (measured in the middle of the specimen) of 350 °C and 500 °C. The test results showed that stressed concrete specimens were susceptible to higher spalling than unstressed specimens at the same heating regime.

Diederichs 1989 [48] studied the fire spalling behaviour of concretes (Si, Lt and Tr) on prismatic specimens (100 x 100 x 400 mm^3) heated with 32 K/min (which corresponds to the heating rate at the beginning of the ISO 834-1 fire curve) with an initial constant compressive load corresponding to 15% of the ultimate strength of concrete at 20 °C.

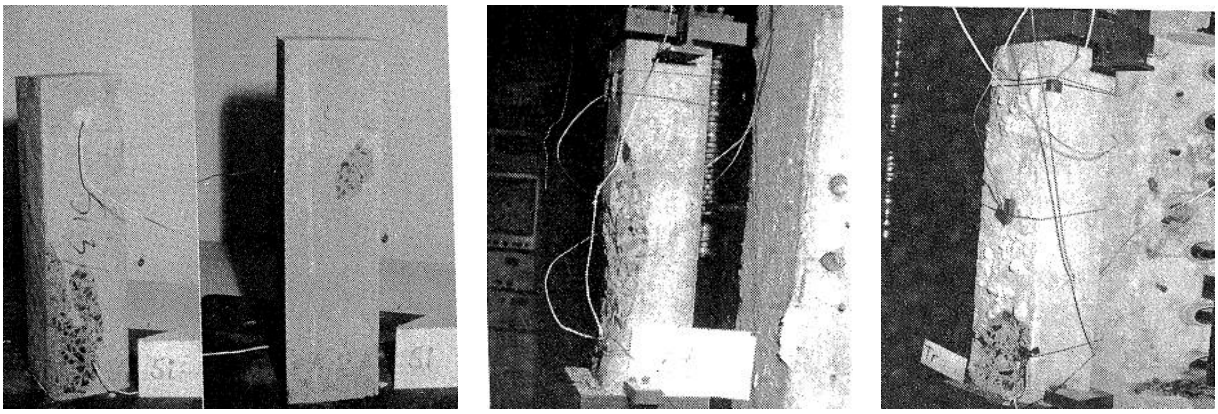

Figure 2.16: Spalling of Si-concrete, Lt-concrete, and Tr-concrete (Diederichs 1989 [48]).

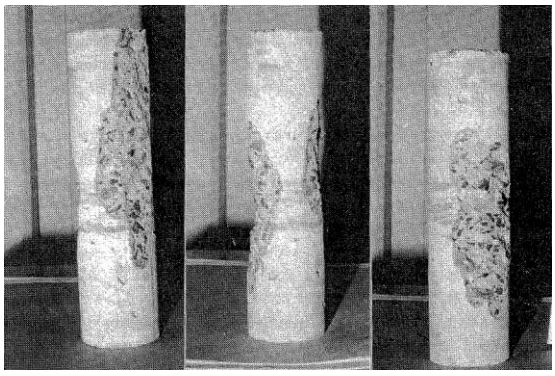

Figure 2.17: Destructive spalling of Lt-concrete specimens loaded during heating [48].

The concretes name as Si, Lt and Tr were made, respectively, with low heat Portland cement contained 9% of silica fume, rapid hardening Portland cement containing 25% of fly ash, and without any pozzolanic binder in addition to blast furnace slag cement with a slag content of slightly over 70%. Compressive strength (100 mm cubes) of three concretes (Si, Lt and Tr) at the

age of 28 days were, respectively, 100, 85.1, 111.1 MPa. The strain was kept constant during the test inducing an increase of the applied load with the increase of the temperature. Spalling was observed in all prismatic concretes (Si, Lt and Tr, see Figure 2.16). Furthermore, Diederichs 1989 [48] also studied the mechanical properties of high strength concrete on cylindrical specimens (Ø 80 mm x 300 mm) heated with 32 K/min with an initial constant compressive load corresponding to 30% of the ultimate strength of concrete at 20 °C. In these tests, destructive spalling was observed in Lt-concrete, see Figure 2.17.

Huismann et al. 2012 [49] measured the transient strain and effects of polypropylene fibres in high strength concrete ($f_{c28\ days}$ = 110 and 113 MPa) exposed to temperatures up to 750 °C. The cylinder specimen diameter of 100 mm and height of 300 mm was loaded to different load levels (0, 10, 20, 30, 40, 50, 60 and 70% of concrete strength at 20 °C), while exposed to a heating ramp of 1 °C/min. The authors reported that the specimens without polypropylene fibres show explosive spalling at 325 °C surface temperature when the load level exceeds 10% of concrete strength at 20 °C. The authors stated that the explosive spalling was attributed to the superposition of the mechanical load and the internal vapour pressure which cannot be released in consequence of the very dense microstructure.

Phan et al. 2002 [50] investigated the mechanical properties of high-strength concrete exposed to elevated temperatures. The cylindrical specimens (Ø 100 mm x 200 mm) were heated at 5 °C/min to temperatures of up to 600 °C for stressed and unstressed conditions. In the stressed test, the specimen was restrained by a preload equal to 40% of the room temperature compressive strength that was applied before heating and maintained during heating. Phan observed that the spalling tendency was reduced in the stressed tests [50].

Arita et al. 2002 [51] performed an experimental study to investigate the thermal spalling of high-performance concrete exposed to ISO 834-1 fire curve. Two different sizes of cylinders (Ø 50 mm x 100 mm and Ø 100 mm x 200 mm) and small prismatic columns (100 x 100 x 400 mm^3) were exposed to ISO 834-1 fire under axial compressive load (axial load ratio = 0, 0.1% and 0.33% of the compressive strength of concrete at 20 °C). Experimental results showed that some of the unloaded specimens spalled more deeply and widely than axially loaded specimens of identical strength. The authors concluded that the effect of axial loading during heating is negative, as the axial load was increased, the degree of spalling seemed to be decreased.

2.3.2 Fire resistance of concrete made with slag based cement

Ground granulated blast furnace slag cement is a by-product of steel production, had been used since the beginning of the 20th century as partial replacement of Ordinary Portland Cement (OPC). The application of such cement receiving more and more attention in the scientific community and concrete industry due to a significant reduction of carbon dioxide gas emissions arising from cement making, cost savings, energy savings, and resource conservation [52-53]. Therefore, it is an environmentally friendly construction material. It has demonstrated very good durability performances as low chloride diffusion. It is mainly used in structures exposed to aggressive chemical environments as building foundations, tunnels, and bridges.

In the past, an enormous number of research works have been focused on the properties of OPC concrete exposed to elevated temperatures, since it is the most widely used binding material for concrete worldwide. The scanty results are available in the literature on the fire resistance behaviour of slag based cement concrete. In the literature, it has been found that the incorporated of slag in the OPC enhances the fire resistance behaviour of concrete [54-61], since the addition of slag reduces the amount of calcium hydroxide ($Ca(OH)_2$) in the binder [54-61]. It was found that an increase in the proportion of slag in the cement paste, in general, led to an improvement in the mechanical properties following exposure to temperatures beyond 400 °C [54-56].

Mendes et al. 2008 [54] demonstrated that, when OPC exposed to a critical temperature of 400 °C, undergo complete breakdown due to the dehydration of $Ca(OH)_2$, followed by the expansive rehydration of lime (CaO) after cooling. The DTG (differential thermogravimetric) results showed that the decomposition peak (related to $Ca(OH)_2$) of OPC at 500 °C was four times higher than the 65% slag peak. Further studies were carried out by Mendes et al. 2009 [55] concluded that the OPC pastes presented no compressive strength after 800 °C either short term (1 week after) or long term (after 1 year) whilst the PC/slag pastes presented compressive strength in the range of 11–14 MPa in the short term and no significant changes in compressive strength were found for the long term after exposed to 800 °C.

Siddique et al. 2012 [57] investigated the mechanical properties of concrete made with partial replacement levels of 0%, 20%, 40%, and 60% of slag by weight of OPC. The specimens were heated in an electric oven with a heating rate of 8 °C/min up to 100, 200, and 350 °C. No significant deterioration of mechanical properties of the concrete was found at a temperature between 27 and 100 °C. While after exposing to 350 °C, the reduction of compressive strength, splitting tensile strength, and modulus of elasticity remained lower than 40% of the initial value.

Xiao et al. 2006 [59] revealed that there were no explosive spalling was found in high-performance concrete with slag at temperatures of 20-800 °C. A similar observation was found by Poon et al. 2001 [60], a distributed network of fine cracks was observed after exposed to 900 °C in all fly ash and slag concretes, but no spalling or splitting occurred, while severe deterioration and spalling was observed in most high-strength concretes containing silica fume and some high strength-OPC concretes.

Hager et al. 2015 [22] carried out the fire spalling tests on seven different concretes aimed at determining the influence of different parameters, such as cement type (CEM I and CEM III), water to cement ratio and type of aggregates on the spalling behaviour of concrete. The authors found that the spalling volume of the concretes made with CEM III (slag based) cement (B/0.30/CEM III and O/0.30/CEM III) was smaller than for the concretes made with CEM I cement (B/0.30/CEM I and O/0.30/CEM I). For example, the spalling volume of concrete made with CEM III and CEM I cements of same mix design was, 6045 cm^3 and 12378 cm^3, respectively.

Rahim et al. 2013 [61] studied the thermal spalling of reinforced concrete ($f_{c28\ days} \approx 73$ to 76 MPa) containing various mineral admixtures (fly ash, silica fume and slag). A total of 108 numbers of cylindrical specimens (Ø 150 mm and 450 mm high) was heated to four different

temperatures (200, 400, 600 and 800 °C, heating rate = 5 °C/min) under preload (25% of the average ultimate load capacity at room temperature) and without preload. The experimental results have shown that the concrete containing silica fume is more vulnerable to spalling than the concrete containing fly ash and slag cement.

2.4 Summary and conclusions

This chapter has presented a large body of literature review, which covered the mechanisms of concrete spalling, the spalling behaviour of concrete on loaded and unloaded test conditions as well as fire resistance of concrete made with slag based cement.

Even though a numerous experimental and numerical studies have been conducted in order to gain a better understanding of the fundamental physics behind the fire spalling behaviour of concrete, its mechanism is still not yet completely understood. Some authors stated that pore pressure is the main driving force of spalling [1, 3-5] while others highlight the significance of thermally induced stresses [6-10], and some other authors recommended that the spalling is the combined action of both pore pressures and thermal stresses [2, 11-12]. Some recent studies have concluded that fire spalling cannot be only explained through the build-up of high pore pressure, even if the concrete experience higher pore pressure (exceeding 3 MPa) [62-64]. The authors stated that many specimens spalled with lower pore pressure (lower than 0.5 MPa) while other specimens did not spall even at pressures higher than 2.5 MPa [63-64]. A similar conclusion has been drawn by Jansson and Boström 2010 [65].

Based on the above review, most of the researchers demonstrated that mechanical loading during fire is a key parameter influencing the spalling behaviour of concrete [23-37, 41-49], while some other researchers found that the presence of higher external load during heating decrease the concrete spalling [38-40, 50-51]. It has been found that the loading levels have an important role on the spalling behaviour of concrete, since the higher load induce microcracks inside the concrete, which allows the release of vapour and then lower risk of spalling. Despite that, some investigations [23-51] deal with the effect of loading on the fire spalling behaviour of concrete, its role is still not yet well understood.

The cement industry has recently shown a significant interest in blast furnace slag based cement because of its superior structural performance and less negative environmental effects as well as economic benefits [52-53]. Although slag based cement concrete has been shown to have a significant number of advantages in virgin condition [52-53] and when exposed to high temperatures [54-61], it is essential to have exhaustive knowledge about the spalling behaviour of slag based cement (CEM III in Europe) concrete when exposed to high temperatures.

Since there is no existing model which can predict the fire spalling behaviour of concrete, comprehensive experimental studies have been conducted within the scope of the work presented in this thesis, which is discussed in the following chapters. The main goal of this research project is to study the effect of external compressive loading (uniaxial and biaxial) and cement type on the fire spalling behaviour of ordinary concrete (B40: $fc_{28days} \approx 40$ MPa).

2.5 References

[1] Kalifa, P., Menneteau, FD and Quenard, D. (2000). "Spalling and pore pressure in HPC at high temperatures", Cement and Concrete Research (2000), Vol. 30, pp. 1915-1927.
[2] Khoury G. A and Anderberg Y. (2000). "Concrete spalling review", Fire safety design, report submitted to the Swedish National Road Administration, Sweden.
[3] Phan, L.T. (2008). "Pore pressure and explosive spalling in concrete", Materials and Structures (2008) 41:1623–1632.
[4] Shorter, G. W., and Harmathy, T. Z. (1961). "Discussion on the Fire-Resistance of Prestressed Concrete Beams", Pro., Institution of Civil Eng. (London), V. 20, 1961, pp. 313-315.
[5] Harmathy, T. Z. (1965). "Effect of moisture on the fire endurance of building elements", ASTM Special Technical Publication, No. 385, pp. 74-95, 1965.
[6] Bazant, Z.P. (1997). "Analysis of pore pressure, thermal stress and fracture in rapidly heated concrete", in: Proceedings, International Workshop on Fire Performance of High-Strength Concrete, NIST, February 13-14, 1997, pp. 155–164.
[7] Saito, H. (1965). "Explosive spalling of prestressed concrete in fire", Occasional Report No.22, Building Research Institute, Japan, 1965.
[8] Dougill, J. W. (1972). "Modes of failure of concrete panels exposed to high temperatures", Magazine of Concrete Research, 24 (79), 71-76, 1972.
[9] Ulm, F-J., Coussy, O and Bazant, J.P. (1999). "The "Chunnel" fire. I: Chemoplastic softening in rapidly heated concrete", Journal of Engineering Mechanics, ASCE, Vol. 125, No. 3, 1999.
[10] Ulm, F-J., Acker, P and Lévy, M. (1999). "The "Chanel" fire. II: Analysis of concrete damage", Journal of Engineering Mechanics, Vol. 125, No. 3, March, 1999.
[11] Zhukov, V. V. (1976). "Reasons of explosive spalling of concrete by fire", Beton i zhlezobeton (Concrete and Reinforcement Concrete), Issue 3.
[12] Khoury, G. A. (2006). "Tunnel concretes under fire: Part 1 - explosive spalling", Tunnels and Tunnelling, CONCRETE November 2006, pp. 62-64.
[13] Anderberg, Y. (1997). "Spalling phenomena of HPC and OC", Proc. of the International workshop on fire performance of high-strength concrete, NIST, Gaithesburg, USA, 1997.
[14] Dal Pont, S., Colina, H., Dupas, A., Ehrlacher, A. (2005). "An experimental relationship between complete liquid saturation and violent damage in concrete submitted to high temperature", Magazine of Concrete Research 57 (no 8) (2005) 455–461.
[15] Khoury, A. G. (2000). "Effect of fire on concrete and concrete structures", Progress in Structural Engineering and Materials, 2000, 2, pp. 429-447.
[16] Hertz, K.D. (2003). "Limits of spalling of fire-exposed concrete", Fire Safety Journal 38 (2003) 103–116.
[17] Fu, Y and Li, L. (2011). "Study on mechanism of thermal spalling in concrete exposed to elevated temperatures", Materials and Structures (2011) 44:361–376.
[18] Majorana, C. E., Salomoni, V. A., Mazzucco, G. and Khoury, G. A. (2010). "An approach for modelling concrete spalling in finite strains", Mathematics and Computers in Simulation 80 (2010) 1694–1712.

[19] Sertmehmetoglu, Y. (1977). "On a mechanism of spalling of concrete under fire conditions", PhD Thesis, King's College, London, 1977.
[20] Mindeguia J-C. (2009). "Contribution Expérimental a la Compréhension des risqué d'Instabilité Thermiques des Béton," PhDThesis, Univ. de Pau et des Pays de l'Adour, France.
[21] Taillefer, N., Pimienta, P., and Dhima, D. (2013). "Spalling of Concrete: A Synthesis of Experimental Tests on Slabs", 3rd IWCS due to Fire Exposure, pp. 01008, Paris, France.
[22] Hager, I. and Tracz, T. (2015). "Parameters influencing concrete spalling severity – intermediate scale tests results", 4th IWCS due to Fire Exposure, Oct. 2015, Leipzig, Germany.
[23] Jansson, R. and Boström, L. (2004). "Experimental Investigation on Concrete Spalling in Fire", Proceedings of the Workshop on Fire Design of Concrete Structures: What now? What next?, 2-3 December, 2004, pp. 109-113, Milan, Italy.
[24] Boström, L. and Jansson, R. (2006). "Spalling of self compacting concrete", Proceedings of the 4th International Workshop on SIF, 10-12 May, 2006, pp. 757-766, Aveiro, Portugal.
[25] Boström, L. and Larsen, C. K. (2006). "Concrete for Tunnel Linings Exposed to Severe Fire Exposure", Fire Technology, 42, 351–362, 2006.
[26] Boström L., Wickström, U. and Adl-Zarrabi B. (2007). "Effect of Specimen Size and Loading Conditions on Spalling of Concrete", Fire and Materials, 2007, 31, pp. 173-186.
[27] Boström, L. and Jansson, R. (2008). "Self-Compacting Concrete Exposed to Fire", SP Report 2008:53, Borås, Sweden, 2008.
[28] Jansson, R., and Boström L. (2012). "Determination of fire spalling of concrete – Relevance of different test methods", Proceedings of the 7th International Conference on Structures in Fire, 6-8 June, 2012, pp. 581-587, Zurich, Switzerland.
[29] Jansson, R. and Boström, L. (2013). "Factors Influencing Fire Spalling of Self Compacting Concrete," Materials and Structures, 2013, 46, pp. 1683-1694.
[30] Sjöström, J., Lange, D., Jansson. R. and Boström, L. (2017). "Anisotropic Curvature and Damage of Unbonded Post-tensioned Concrete Slabs During Fire Testing", Fire Technology, 53, 1333–1351, 2017.
[31] Pimienta, P., Anton, O., Mindeguia, J-C., Avenel, R., Cuypers, H. and Cesmat, E. (2010). "Fire Protection of Concrete Structures Exposed to Fast Fires", 4th International Symposium on Tunnel Safety and Security (ISTSS), March 17-18, 2010, Frankfurt, Germany.
[32] Carré, H., Pimienta, P., La Borderie, C., Pereira, F. and Mindeguia, J. C. (2013). "Effect of Compressive Loading on the Risk of Spalling", Proceedings of the 3rd International Workshop on Concrete Spalling due to Fire Exposure, pp. 01007, Paris, France.
[33] Lo Monte, F., Rossino, C., and Felicetti, R. (2015). "Spalling Test on Concrete Slabs Under Biaxial Membrane Loading", 4th IWCS due to Fire Exposure, Oct. 8-9, 2015, Leipzig, Germany.
[34] Lo Monte F. and Felicetti R. "Spalling sensitivity test on concrete", Proceedings of the Italian Concrete Days (giornate aicap 2016, congresso cte), October 27-28, 2016, Rome, Italy.
[35] Lo Monte F. and Felicetti R. (2017). "Heated slabs under biaxial compressive loading: a test set-up for the assessment of concrete sensitivity to spalling", Materials and Structures (2017) 50:192.

[36] Maluk, C., Bisby, L. and Terrasi, G. (2013). "Effects of polypropylene fibre type on occurrence of heat-induced concrete spalling", 3rd IWCS, pp. 01005, Paris, France.
[37] Maluk, C., Bisby, L. and Terrasi, G. P. (2017). "Effects of polypropylene fibre type and dose on the propensity for heat-induced concrete spalling", Eng. Structures 141 (2017) 584–595.
[38] Kim, H-J., Kim, H-Y., Lee, J-S. and Kwan, K-H. (2011). "An Experimental Study on Thermal Damage and Spalling of Concrete under Loading Conditions in a Tunnel Fire", Journal of Asian Architecture and Building Engineering, November 2011, Vol.10, No.2, pp. 375-382.
[39] Ali, F. A., Nadjai, A., Glackin, P., Silcock, G. and Abu-Tair, A. (2003). "Structural Performance of High Strength Concrete Columns in Fire", Fire Safety Science - Proceedings of the Seventh International Symposium, pp. 1001-1012. doi:10.3801/IAFSS.FSS.7-1001.
[40] Ali, F., Nadjai, A., Silcock, G., and Abu-Tair, A. (2004). "Outcomes of a Major Research on Fire Resistance of Concrete Columns," Fire Safety Journal 39 (2004), pp. 433-445.
[41] Ali, F., Nadjai, A. and Choi, S. (2010). "Numerical and Experimental Investigation of the Behavior of High Strength Concrete Columns in Fire", Eng. Structures 32, pp. 1236-1243.
[42] Kodur, V. K. R. (2000). "Spalling in high strength concrete exposed to fire – Concerns, causes, critical parameters and cures", Proc. of ASCE Structures Congress, Philadelphia, 1–8.
[43] Kodur, V. K. R. and Phan, L. (2007). "Critical factors governing the fire performance of high strength concrete systems", Fire Safety Journal 42 (2007), pp. 482-488.
[44] Dwaikat, M. B., and Kodur, V. K. R. (2009). "Response of Restrained Concrete Beams under Design Fire Exposure," Journal of Structural Engineering, V. 135, No. 11, pp. 1408-1417.
[45] Morita, T., Nishida, A., Yamazaki, N., Schneider, U and Diederichs, U. (2000). "An experimental study on spalling of high strength concrete elements under fire attack", 6th International Symposium on the Fire Safety Science (IAFSS), pp. 855-866, Poitiers, France.
[46] Castillo, C. and Durrani, A. J. (1990). "Effect of Transient High Temperature on High-Strength Concrete", ACI Materials Journal, V. 87, No. 1, pp. 47-53.
[47] Tao, J., Yuan, Y., and Taerwe, L. (2010). "Compressive Strength of Self-Compacting Concrete during High-Temperature Exposure", Journal of Materials in Civil Engineering, ASCE, Vol. 22, No. 10, pp. 1005-1011.
[48] Diederichs, U., Jumppanen, U-M and Penttala, V. (1989). "Behaviour of High Strength Concrete at High Temperatures", Espoo 1989, Helsinki University of Technology, Department of Structural Engineering, Julkaisu/Report 92, 76 pages.
[49] Huismann, S., Weise, F., and Meng, B., and Schneider, U. (2012). "Transient Strain of High Strength Concrete at Elevated Temperatures and the Impact of Polypropylene Fibers," Materials and Structures, 45, pp. 793-801.
[50] Phan, L. T. and Carino, N. J. (2002). "Effects of Test Conditions and Mixture Proportions on Behavior of High-Strength Concrete Exposed to High Temperatures", ACI Materials Journal, V. 99, No. 1, pp. 54-66.
[51] Arita, F., Harada, K. and Miyamoto, K. "Thermal Spalling of High-Performance Concrete During Fire", 2nd International Workshop on SIF, Mch 18-19, 2002, Christchurch, New Zealand.

[52] ACI Committee 233 (2000). "Ground Granulated Blast-Furnace Slag as a Cementitious Constituent in Concrete", ACI 223R-95, 2000.
[53] Hooton, R. D. (2000). "Canadian use of ground granulated blast-furnace slag as a supplementary cementing material for enhanced performance of concrete", Canadian Journal of Civil Engineering (2000), Vol. 27, pp. 754–760.
[54] Mendes, A., Sanjayan, J and Collins, F. (2008). "Phase transformations and mechanical strength of OPC/slag pastes submitted to high temperatures", Mat. and Structures 41:345–350.
[55] Mendes, A., Sanjayan, J.G and Collins, F. "Long-term progressive deterioration following fire exposure of OPC versus slag blended cement pastes", Mat. and Str. (2009) 42:95–101.
[56] Mendes, A., Sanjayan, J.G and Collins, F. (2011). "Effects of slag and cooling method on the progressive deterioration of concrete after exposure to elevated temperatures as in a fire event", Materials and Structures (2011) 44:709–718.
[57] Siddique, R and Kaur, D. (2012). "Properties of concrete containing ground granulated blast furnace slag (GGBFS) at elevated temperatures", Jour. of Adv. Research (2012) 3, 45–51.
[58] Aydın, S. (2008). "Development of a high-temperature-resistant mortar by using slag and pumice", Fire Safety Journal 43 (2008) 610–617.
[59] Xiao, J., Xie, M and Zhang, Ch. (2006). "Residual compressive behaviour of pre-heated high-performance concrete with blast–furnace–slag", Fire Safety Journal 41 (2006) 91–98.
[60] Poon, C-S., Azhar, S., Anson, M and Wong, Y-L. (2001). "Comparison of the Strength and Durability Performance of Normal- and High-strength Pozzolanic Concretes at Elevated Temperatures", Cement and Concrete Research 31 (2001) 1291–1300.
[61] Rahim, A., Sharma, U. K., Murugesan, K. and Arora, P. (2013). "Effect of load on thermal spalling of reinforced concrete containing various mineral admixtures", Proceedings of the 3rd IWCS due to fire exposure, 25-27 September 2013, pp. 01006, Paris, France.
[62] Felicetti, R., Lo Monte, F and Pimienta, P. (2017). "A new test method to study the influence of pore pressure on fracture behaviour of concrete during heating", Cement and Concrete Research 94 (2017) 13–23.
[63] Mindeguia, J-C., Pimienta, P., Noumowé, A and Kanema, M. (2010). "Temperature, pore pressure and mass variation of concrete subjected to high temperature—Experimental and numerical discussion on spalling risk", Cement and Concrete Research 40 (2010) 477–487.
[64] Mindeguia, J-C., Carré, H., Pimienta, P and La Borderie, C. (2015). "Experimental discussion on the mechanisms behind the fire spalling of concrete", Fire Mater.2015;39:619-635.
[65] Jansson, R and Boström, L. (2010). "The Influence of Pressure in the Pore System on Fire Spalling of Concrete", Fire Technology, 46, 217–230, 2010.

3 Behaviour of Concrete at High Temperature

The literature review presented in chapter 2 demonstrated that the fire spalling of concrete is influenced by various parameters [1-3]. It is worth noting, however, that an enormous number of experimental studies have been reported in the literature on unloaded specimens, while comparatively, there are few published data on fire spalling of concrete subjected to the compressive loading condition. The literature review also showed that the incorporation of slag in the Ordinary Portland Cement (OPC) enhances the fire resistance behaviour of concrete [4-7].

Various experimental and numerical studies have shown that the permeability of concrete was identified as one of the key parameters controlling internal fluid transfer, which influences the magnitude of the pore pressure within the concrete structure [8-9] and then influence the risk of fire spalling [10]. It was found that when the concrete is subjected to fire under external compressive loading, the transport of moisture might be strongly affected due to lower damage [11-12] (i.e. lower permeability), which could enhance the risk of fire spalling. Hence, in order to gain a deeper understanding the fire spalling mechanism of concrete, porosity, permeability and build-up of pore pressure measurements were carried out on both concretes (B40-II and B40-III). The main goal of this chapter is to study the effect of thermal loading on the porosity and gas permeability of concretes in unloaded and loaded (only permeability) conditions of two ordinary concretes made with CEM II (3% of slag) and CEM III (43% of sag) cements. Additionally, the build-up of pore pressure and temperature (PT) were measured in order to a deeper understanding the thermo-hydral process of spalling.

3.1 Materials, mix design and curing conditions

Two ordinary concretes (B40-II and B40-III) made respectively, with CEM II (CEM II/A-LL 42.5 R CE CP2 NF) and CEM III (CEM III/A 42.5 N CE CP1 NF) cements have been investigated. The same mix design was used for both concretes; the only difference is the cement type. The CEM II cement contains 85% of clinker, 3% of slag and 12% of limestone, while the CEM III cement contains 54% of clinker, 43% of slag and 3% of limestone. Chemical compositions and mechanical properties of cement are presented in Tables 3.1 and 3.2.

The compressive strength (f_c), modulus of elasticity (E), and tensile strength (splitting, f_t) of both concretes were measured on the cylindrical (Ø 160 mm x h 320 mm) samples at the age of 28 and 90 days. Constituents and concrete properties at the fresh and hardened state as well as slump flow values are reported in Table 3.3. In Table 3.3, it can be seen that the mechanical properties of both concretes are almost the same at both ages, while higher workability of B40-III than B40-II according to its higher slump value. Similar results were found in the literature

[13]. Table 3.4 presents a summary of the concrete batches that were used to prepare all the test specimens. An example image of the cast concrete specimens can be seen from the PT test and biaxial fire spalling test (see Figure 3.1).

Table 3.1: Chemical compositions of CEM II and CEM III cement

Cement	Chemical composition (%)										
	SiO_2	Al_2O_3	Fe_2O_3	TiO_2	MnO	CaO	MgO	SO_3	K_2O	Na_2O	P_2O_5
CEM II	18.3	4.1	2.1	0.3	0.0	61.7	2.0	3.1	0.69	0.09	0.2
CEM III	26.3	7.3	1.6	0.5	0.1	53.4	4.2	3.3	0.6	0.14	0.2

Table 3.2: Mechanical properties of CEM II and CEM III cement

	CEM II	CEM III
Compressive strength at 28 days [MPa]	55	55
Initial/final setting time [min]	165/220	215/240
Heat of hydration 12/41 h [J/g]	200/326	128/295
Density [g/cm^3]	3.04	3.01
Surface area [cm^2/g]	4300	4400

Table 3.3: Concrete mixture proportions and properties of fresh and hardened concrete

B40 Concrete	Unity	B40-II	B40-III
Cement (C)	kg/m^3	350	
Calcareous 8/12.5 gravel	kg/m^3	330	
Calcareous 12.5/20 gravel	kg/m^3	720	
0/2 siliceous sand	kg/m^3	845	
Water (W)	l/m^3	189	
Superplasticizer	% of C	1	
Water / cement ratio (w/c)		0.54	
Slump	cm	**9.9** (8.8 – 12.0)	**21.7** (19.0 – 24.0)
28 days compressive strength	MPa	**41.1** (36.4 – 46.8)	**41.0** (36.1 – 46.5)
90 days compressive strength	MPa	**50.9** (49.0 – 52.3)	**50.4** (47.8 – 55.3)
28 days tensile strength	MPa	**3.9** (3.9 – 4.0)	**3.8** (3.7 – 3.9)
90 days tensile strength	MPa	**4.8** (4.1 – 5.5)	**4.3** (4.0 – 4.7)
28 days modulus of elasticity	GPa	**36** (34.0 – 38.9)	**37.9** (35.7 – 41.0)

Table 3.4: Global view of the concrete batches and the age of the test specimens.

Batch No.	Date of casting	Test	B40-II	B40-III
1	09/04/2014	Porosity	-	> 270 days
		Permeability	-	> 270 days
		PT	-	> 180 days
2	12/09/2014	Unloaded slab ISO fire	-	> 180 days
3	13/04/2015	Porosity	> 300 days	-
		Permeability	> 300 days	-
		Uniaxial cube ISO fire	≈ 90 days	≈ 90 days
4	14/05/2015	Biaxial slab ISO fire	> 90 days	> 90 days
5	26/05/2016	Biaxial slab ISO fire	> 90 days	> 90 days

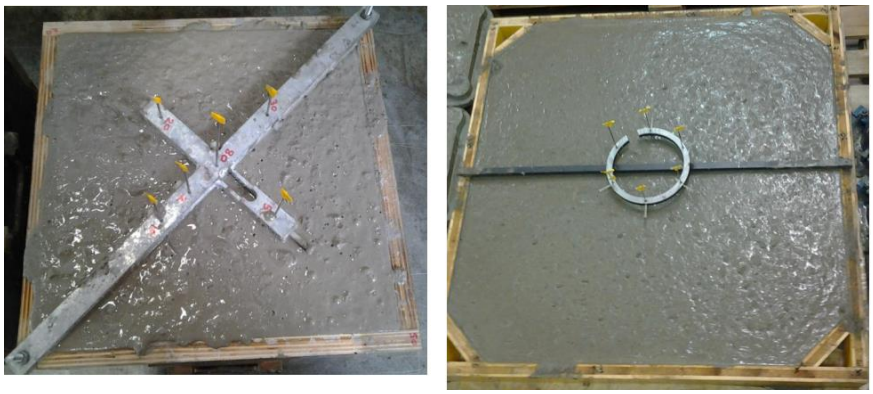

Figure 3.1: The images right after cast concrete from PT test (left) and biaxial fire test (right).

After demoulding the concrete (B40-III) specimens from batch 1 and 2, all the specimens were covered by the plastic film for 7 days inside the laboratory room. Specimens were then stored in the laboratory without the plastic film up to the day of the tests (ISO fire, porosity, permeability, and PT tests). 24 hours after casting of concrete batch 3, all the concrete specimens (B40-II and B40-III) were well covered by the plastic film, then kept at ambient conditions inside the laboratory up to the day of the test (Uniaxial cube ISO fire, porosity and permeability tests). Concerning concrete batches 4 and 5, after demoulding, all the concrete specimens (B40-II and B40-III) were cured for 7 days in wet condition, after that the specimens were stored in the laboratory up to the day of the fire test.

The initial water content was assessed on both concretes (B40-II and B40-III) by drying unsealed and sealed concrete cube samples (100 x 100 x 100 mm^3) at the age of 90 days at 80 °C until a constant value of the mass was reached (around 2 months). Stabilisation was considered achieved when the difference in terms of mass in an interval of more than 24 h was lower than 0.1%. Six specimens (3 for unsealed and 3 for sealed) from each batch of concrete were used. The cubes were previously stored in the same storage condition than the fire test specimens.

After casting, the unsealed cubes were exposed on 6 sides to the ambient temperature during the storage period, while some other cubes were sealed on 4 sides by the aluminium film and 2 other sides of the specimens were exposed to ambient temperature. After 90 days of the storage period, the aluminium film was removed from the sealed specimens and then all the specimens (sealed and unsealed) were dried at 80 °C. This water content refers to the initial free water of the fire test specimens. The initial water content of five different batches is presented in Table 3.5.

Table 3.5: The initial water content of five different batches of B40-II and B40-III concretes

Water loss in %		Batch 1	Batch 2	Batch 3	Batch 4/5
B40-II	Unsealed	**3.8** (PT test)	-	**3.4** (3.4 – 3.5)	**4.0** (3.9 – 4.1) / **4.5** (4.5 – 4.6)
	Sealed	-	-	**3.9**	-
B40-III	Unsealed	**3.0** (2.9 – 3.1)	**3.1** (3.0 – 3.2)	**3.5**	**5.3** (5.2 – 5.4) / **5.4** (5.3 – 5.4)
	Sealed	**3.4** (3.3 – 3.5)	**3.6** (3.4 – 3.9)	**4.1**	-

3.2 Apparatus and test procedures

3.2.1 Water absorption porosity tests after unloaded preheating

The residual porosity of concrete was investigated by means of a technique based on water absorption porosity according to the French standard NF P18-459 [14]. This technique was performed on a quarter-cylinder of 104 mm in diameter and 50 mm thickness concrete specimens, see Figure 3.2 right. Three specimens were used for each thermal load and then the final porosity was calculated by the arithmetic mean of three specimens.

1: Specimen, 2: Water, 3: Desiccator, 4: Pump isolation valve, 5: Water flow controller, and 6: Water input

Water absorption porosity test specimens

Figure 3.2: Porosity test setup (left) and the specimens (right).

The residual porosity of concrete was investigated at room temperature after applying thermal loads of 120, 250, 400 and 600 °C at a slow heating rate of 1 °C/min. The slow heating rate of 1 °C/min was chosen to limit undesirable thermal stress. After reaching the target temperatures, the temperatures were stabilised for 28, 10, 6 and 6 hours, respectively, for the temperatures of 120, 250, 400 and 600 °C [15] to reach a uniform temperature in the concrete. The stabilisation time at the lower temperatures was much longer to ensure that most of the physico-chemical transformations and that the departure of water from the specimen was achieved. The specimens were then cooled down to room temperature at a rate of about 0.3 °C/min inside the closed furnace. The low cooling rate avoided thermal shocks. The reference specimens were dried in an oven at the temperature of 80 °C until a constant value of mass was reached (around 2 months). Stabilisation of the specimen was followed by the measurement of initial water content stabilisation method (see section 3.1).

The residual porosity P_a (in %) of concrete is calculated by measuring the mass of concrete specimens in various states of saturation:

● **Mass of dry test specimen (m_{dry})**: the mass of the specimen was measured in the air after oven drying at 80 °C or heating up to at 120, 250, 400 and 600 °C.

● **Apparent mass of immersed test specimen (m_{sat}^{imm})**: the mass of the specimen was measured in a saturated state when it was immersed in water. In order to measure this value, the samples were placed in an airtight vessel, see Figure 3.2 left. After sealing the vessel, evacuate it until a pressure of not more than 25 mbar is attained and then maintained this vacuum for at least 4 h. After stabilization of pressure, the liquid (drinking water) was introduced progressively, so that the test pieces were covered by about 20 mm of liquid. The pressure was maintained for 24 h, while the specimens were immersed in water. Then the pump was disconnected and the cover of the desiccator was then removed. During this period, the porous network is assumed to be fully saturated with liquid water. The mass of the immersed specimen was then measured by hydrostatic weighing.

● **Mass of soaked test specimen (m_{sat})**: the saturated specimens were removed from the water and immediately wiped it quickly and carefully with a damp cloth in order to remove surface water, without removing the water from the pores. Then the mass of the wet specimen was measured in the air immediately.

Knowing the mass in these three states (dry, immersed in water, and saturated in air), water porosity of concrete is calculated according to Equation 3.1:

$$P_a = \frac{m_{sat} - m_{dry}}{m_{sat} - m_{sat}^{imm}} * 100 \quad (3.1)$$

3.2.2 Residual axial gas permeability tests after unloaded preheating

The residual gas permeability of concrete was measured on 150 mm diameter and 50 mm thickness concrete disc (see Figure 3.3) at room temperature after heating at 80, 120, 250, 400 and 600 °C. The drying (80 °C) and heating (120, 250, 400 and 600 °C) procedures are described

in section 3.2.1. The concrete discs were cut from a cylindrical specimen of 150 mm diameter and 300 mm height using a diamond blade saw, being careful not to keep the upper and lower discs to avoid the edge effect which could influence the measurements of permeability. The curved side of the specimen was wrapped with aluminium foil tape (see Figure 3.3b) to ensure a sealing to prevent leakage of gas through the curved side of the specimen so that the flow occurs uniaxially through the thickness of the specimen. Two specimens were used for each thermal load.

a) Specimen after heating

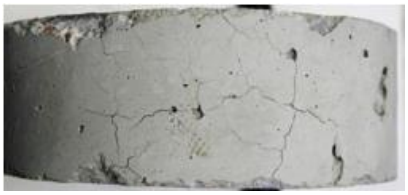

Crack patterns

b) Wrapped with aluminium tape

c) Specimen ready to be tested

Figure 3.3: Preparation of the specimen for the permeability test heated after at 600 °C.

The residual gas permeability of concrete was measured using a Cembureau constant pressure permeameter with nitrogen as the neutral percolating gas [16], see Figure 3.4. To do that, the specimen was placed into the polyurethane rubber ring, and then the permeability cell has been closed. Air pressure was then applied to the inflated tire, which expanded laterally and produced a uniform confining pressure (P_c) around the specimen, see Figure 3.4 left. To ensure the tightness of the setup and to prevent leakage of gas through the curved side of the specimen, air pressure of 8 bars was applied to the rubber ring.

Three levels of pressure difference ΔP (the difference between the injection pressure P_{inj} and the atmospheric pressure P_{atm}) were chosen depending on preheating temperatures in order to determine the intrinsic permeability of concretes according to the Klinkenberg's approach [17]. The downstream gas flow rate through the test piece was measured using a soap bubble flow meter. At each pressure stage, the flow rate was stabilised for concrete samples, which was normally achieved between 20 and 60 seconds (depending on the heat treatment). This condition was verified by taking at least two measurements separated by a 15 minutes time interval. If two values differ by less than 2%, the steady state flow condition is assumed to be achieved. To ensure reproducibility, each measurement was obtained as the arithmetic mean of no less than three such records.

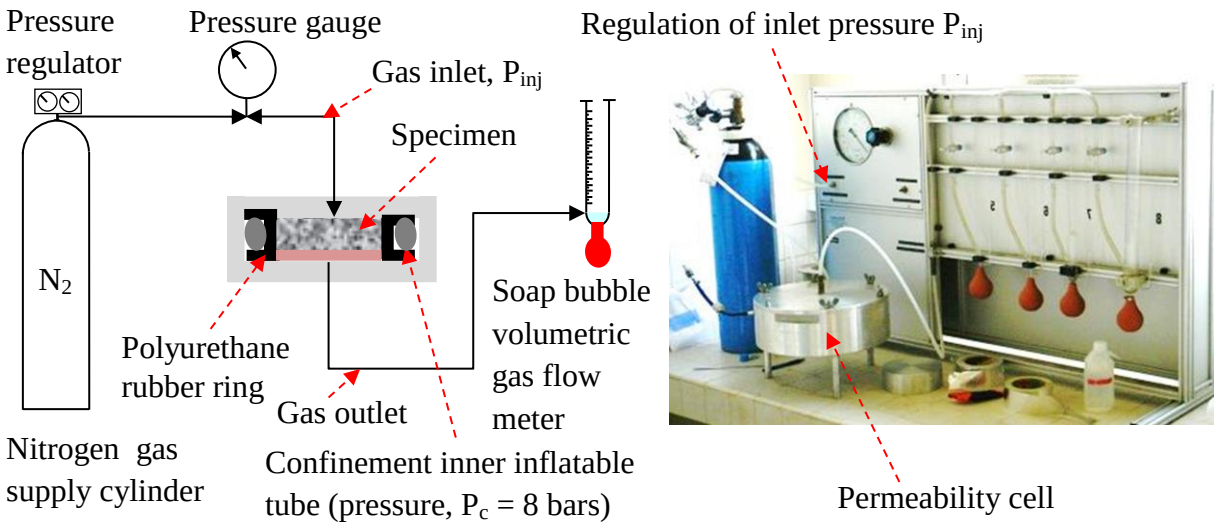

Figure 3.4: Test setup according to the RILEM-CEMBUREAU method [16].

For each applied pressure, the apparent coefficient of permeability k_{app} (m^2) is calculated from the Hagen-Poiseuille relationship for laminar flow of a compressible fluid through a porous body with small capillaries under steady-state conditions [16]. The relationship as follows:

$$K_{app} = \frac{2.\mu.Q.L.P_{atm}}{A(P_{inj}^2 - P_{atm}^2)} \quad (3.2)$$

where: Q [m^3/s] = measured gas flow; A [m^2] = cross-sectional area; L [m] = thickness of the sample; μ [Pa.s] = coefficient of viscosity (1.76 x 10^{-5} Pa.s for nitrogen gas at 20 °C); P_{inj} [Pa] = inlet pressure, i.e., applied absolute pressure; P_{atm} [Pa] = atmospheric pressure.

Permeability obtained from equation (3.2) is dependent on pressure and it is valid for the specific pressure at which the permeability is measured. However, when gases are transported through porous media, the flow consists of viscous flow as well as slip flow [17-18]. In order to compare the gas permeability to liquid permeability, it is necessary to correct for the slippage of the gas, which is commonly referred to as the Klinkenberg correction [17]. By measuring the gas permeability under a variety of pressure gradients, the intrinsic permeability is derived by fitting the data to an equation of the form:

$$K_{app} = K_{int}\left(1 + \frac{b}{\overline{P}}\right) \quad (3.3)$$

where: $\overline{P} = (P_{inj} + P_{atm})/2$, k_{app} [m^2] = apparent permeability; K_{int} [m^2] = intrinsic permeability; b [Pa] = Klinkenberg coefficient; $\overline{P}$ [Pa] = mean pressure of the inlet and outlet streams.

Intrinsic permeability (K_{int}) is the limiting value of gas permeability when the mean pressure $\overline{P}$ tends toward infinity. The determination of intrinsic permeability (K_{int}) consists of measuring

apparent permeability (K_{app}) at different pressures (P_{inj}) and in plotting it against the inverse of the mean pressure ($1/\overline{P}$) (see Figure 3.5).

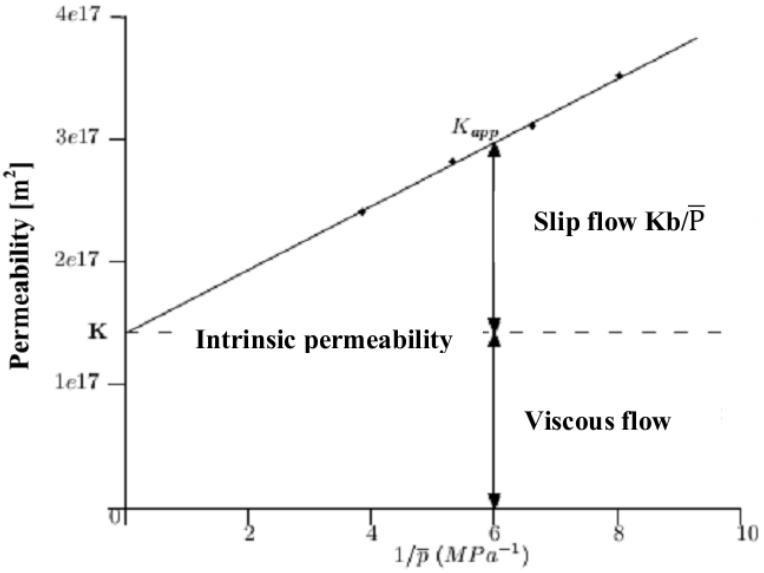

Figure 3.5: Determination of the intrinsic permeability of the material according to Klinkenberg approach. Differentiate the types of gas movement (Dal Pont 2004 [18]).

3.2.3 Residual gas permeability tests in loaded condition

In order to gain a deeper understanding of the role of different loading conditions in compression on the permeability of concrete, 3 different gas permeability tests were carried out in SIAME and CSTB. They are as follows:

- Residual axial permeability tests under radial confining pressure after unloaded preheating,
- Residual axial permeability tests under radial confining pressure after preheating under uniaxial loading,
- Residual radial permeability tests under uniaxial loading after unloaded preheating.

The summary of the experimental program is described in Table 3.6. Testing temperatures, applied compressive stresses and number of tested samples are given. Except test iii) at 600 °C, two specimens for each temperature and each compressive load were used for both concretes, see Table 3.6.

3.2.3.1 Residual axial permeability tests under radial confining pressure after unloaded preheating

The residual axial gas permeability tests under radial confining pressure was similar to the test method described in section 3.2.2, see Figure 3.4. The main difference between this current test and the former test (in section 3.2.2) was the applied radial confining pressure to the specimen. In the former test, a confining pressure of 0.8 MPa was used for all the tests. It is a low pressure

usually used to ensure the lateral tightness during the tests. In this current section, different levels of confining pressures (Pc) were applied to study the effect of confining pressure (perpendicular to the gas flow) on the gas permeability of concretes (B40-II and B40-III), see Figure 3.6 right. The heating rate and the temperature levels were same as described in section 3.2.1, see Table 3.6. In this test campaign, additional tests at 800 °C of both concretes were performed. The specimens were heated at 1 °C/min and then stabilised for 6 hours. To ensure that the lowest applied load (0.3 MPa) is sufficient to prevent leakage of gas through the curved side, blank tests on an aluminium disc of the same dimensions (150 mm diameter and 50 mm thickness, see Figure 3.7) were performed at 0.3 and 0.6 MPa. No outflow occurred at these lower confining pressures. Therefore, these blank tests demonstrated that the permeability test results of the concrete specimens were not affected by leakage through the curved side when applying the lower load value.

Table 3.6: Global view of the experimental program for all the permeability tests (Note: – No test, B40-II/B40-III).

T [°C]	80	120	250	400	600	800
i) Residual axial permeability tests under radial confining pressure (Pc = 0.3, 0.6, 0.9 and 1.2 MPa) after unloaded preheating	2/2	2/2	2/2	2/2	2/2	2/2
ii) Residual axial permeability tests after heating-cooling under uniaxial loading (σ = 0, 0.5, 1.5, 3 and 5 MPa; Pc = 0.6 MPa)	–	–	–	2/2	–	–
iii) Residual radial permeability tests under uniaxial loading (σ = 0.6, 0.9, 1.2, 2, 3, 5 and 10 MPa) after unloaded preheating	–	2/2	2/1	2/2	1/–	–

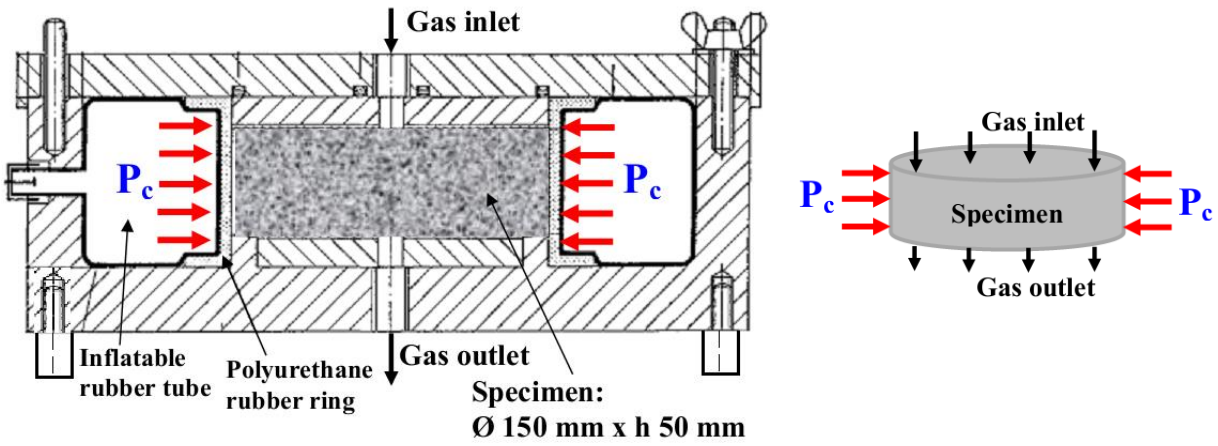

Figure 3.6: Test setup according to the RILEM-CEMBUREAU method (left) [16] and detail application of confining pressure (Pc) and axial gas flow to the specimen (right).

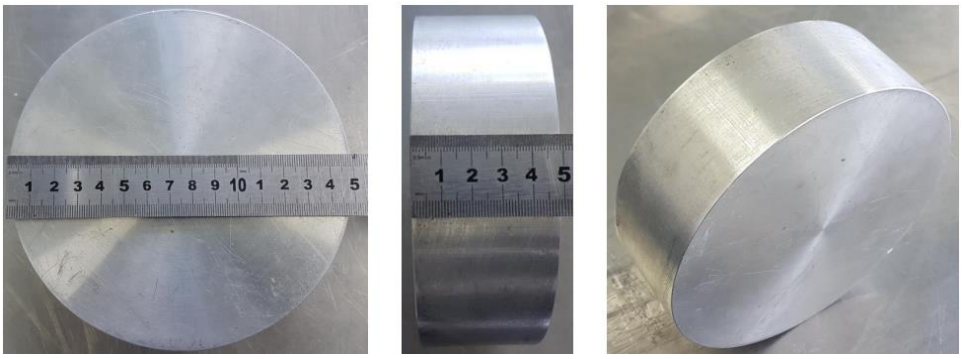

Figure 3.7: The aluminium disc specimen for blank permeability test.

Axial gas permeability was performed at four different levels of radial confining pressure, Pc: 0.3, 0.6, 0.9 and 1.2 MPa (see Table 3.6) to investigate the role of confining pressure on the gas permeability of heated concretes (B40-II and 40-III). This was achieved by increasing the inflatable rubber tube pressure applied to the polyurethane rubber ring, see Figure 3.6 left. In order to study the reversibility of the loading, the unloading (0.9, 0.6 and 0.3 MPa) permeability tests were also carried out right after the test at a maximum confining pressure of 1.2 MPa.

3.2.3.2 Residual axial permeability tests under radial confining pressure after preheating under uniaxial loading

This test method was similar to the test method described in section 3.2.2. The difference was that the specimens were preheated under a constant uniaxial compressive loading, see Figures 3.8 and 3.9. The size of the specimens was same as described in section 3.2.2. Only one heating temperature (400 °C) was studied and the permeability tests were performed with one confining pressure (Pc = 0.6 MPa).

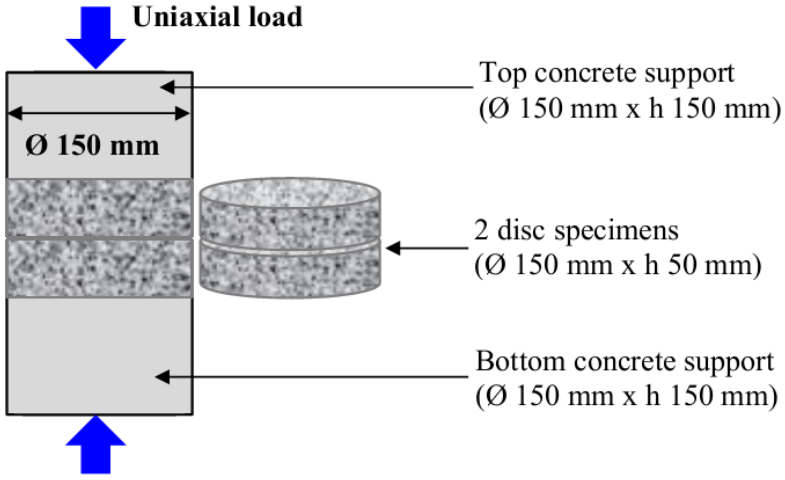

Figure 3.8: Schematic diagram of the preheating under uniaxial loading of the test specimens.

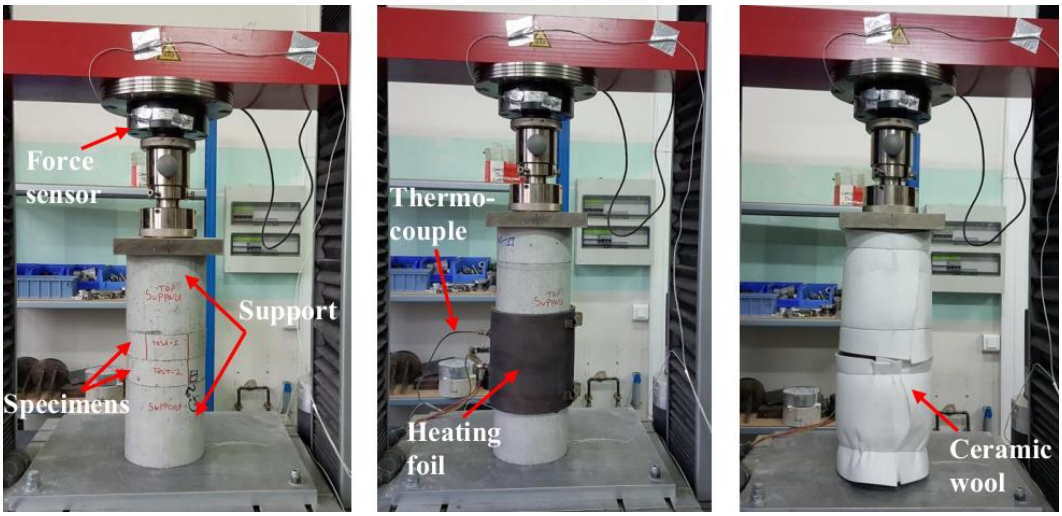

Figure 3.9: Preheating under uniaxial loading of the test specimens.

Prior heating, all the specimens, as well as concrete supports, were grinded in order to obtain two faces (upper and lower faces) parallel and plane to ensure a uniform stress distribution in the specimens. The specimens were surrounded with a heating foil (see the second image in Figure 3.9) and a thermal insulator made with ceramic wool and were positioned in the hydraulic press. The specimens were heated with a slow heating rate of 1 °C/min up to 400 °C, stabilised for 8 hours, and then cooled down to ambient temperature inside the heating device. Before heating, a constant uniaxial compressive load was applied and then maintained constant during heating and cooling. Five different levels of uniaxial compressive stresses (0, 0.5, 1.5, 3 and 5 MPa) have been investigated on both concretes (B40-II and B40-III), see Table 3.6.

3.2.3.3 Residual radial permeability tests under uniaxial loading after unloaded preheating

The principle of this test was to measure the radial permeability by injecting the nitrogen gas inside a hollow concrete cylindrical disc and then measure the radial gas flow of the specimen. The size of the hollow discs was 123 mm in outer diameter and 52 mm internal diameter with 50 mm in height, see Figure 3.10. The concrete hollow discs were cut from a cylindrical specimen of 150 mm diameter and 300 mm height using a diamond blade saw and then grinded in order to obtain two faces (upper and lower faces) parallel and plane to ensure a uniform stress distribution in the specimens, while the radial sides of the specimens were grinded in order to obtain 123 mm in outer diameter as well as to have better gas transfer (to avoid edge effect) through the radial sides during the permeability test. The top and bottom faces of the specimens were sealed with aluminium foil tape to prevent leakage of gas along the interface. The heating rate and the temperature levels were same as described in section 3.2.1.

A schematic diagram of the experimental device is shown in Figure 3.11. This experimental setup allows the measurements of radial gas permeability of the concrete disc specimens. First, the specimen was placed in the cell of permeameter composed of a system with two metal platens. Then, the inert gas (nitrogen) was injected into the cylindrical borehole through the perforated

bottom platen. A pressure difference ΔP (the difference between the injection pressure P_i and the atmospheric pressure P_{atm}) was applied and maintained until gas flow stabilisation. The relative pressure and mass flow rate were measured at the upstream of the specimen by the flowmeters, after that the volumetric gas flow was calculated.

Figure 3.10: Radial permeability test specimens.

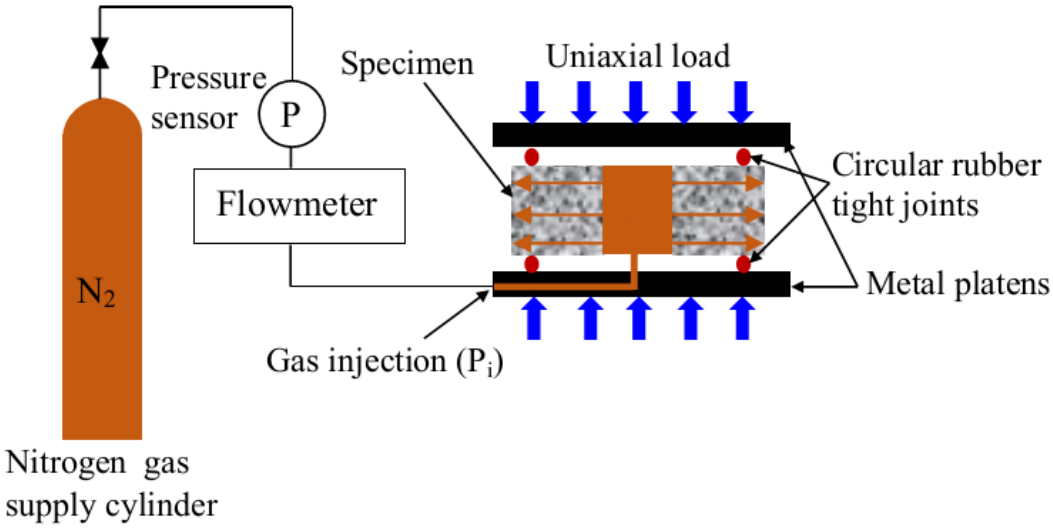

Figure 3.11: Schematic diagram of the radial permeability test under uniaxial loading device.

Darcy's law and mass balance equation [19] lead to the determination of an apparent permeability K_a [m^2]. When the injection flow rate Q_i [m^3/s] is known, the permeability K_a [m^2] can be calculated as follows:

$$K_a = \frac{Q_i P_i \mu \ln\left(\frac{r_2}{r_1}\right)}{\pi h \left(P_i^2 - P_{atm}^2\right)} \quad (3.4)$$

where μ [Pa.s] is the dynamic viscosity of the inlet gas used (nitrogen), P_{atm} [Pa] is the atmospheric pressure; r_1 [m], r_2 [m], h [m] are the inner radius, outer radius, and height of the cylindrical specimen respectively.

A small constant uniaxial compressive stress of 0.6 MPa was applied. This small load ensures the tightness of the permeability cell, hence, radial gas flow only. This permeability assumed as reference permeability for this test program, since it is believed that this small load will modify slightly the crack pattern of the specimen. To study the effect of uniaxial compressive loading on the radial gas permeability of concrete, seven different levels of compressive loading (0.6, 0.9, 1.2, 2, 3, 5 and 10 MPa, see Table 3.6) have been investigated on both concretes (B40-II and B40-III). Four different levels pressure difference ΔP were applied to the samples depending on preheating temperatures in order to determine the intrinsic permeability of concretes according to the Klinkenberg's approach [17].

3.2.4 Measurement of pore pressure and temperature (PT)

The build-up of pore pressure and temperature tests were carried out according to the test methods described by Kalifa et al. 2000 [20]. The experimental campaign consisted of 12 tests with 3 different thermal loadings, 6 specimens for each type of cement concrete (B40-II and B40-III). Two specimens for each thermal loading were used to assess repeatability. Among 12 tests, 6 tests of B40-III concrete have been carried out and the results were compared with the ones with B40-II concrete which have already been published [21]. Prismatic concrete samples of 300 x 300 x 120 mm^3 were used for all PT tests. Specimens were instrumented with five gauges placed at 10, 20, 30, 50 and 80 mm depths from the exposed surface of concrete specimens for simultaneous pressure and temperature measurements (see Figure 3.12 right). The measurement of the gas pore pressure and the temperature was performed by using capillary steel pipes (inner diameter 1.6 mm), fitted with sintered metal round plate (Ø 12 x 1 mm), see Figure 3.13. For more details about the experimental set-up, the reader should refer to Kalifa et al. 2000 [20].

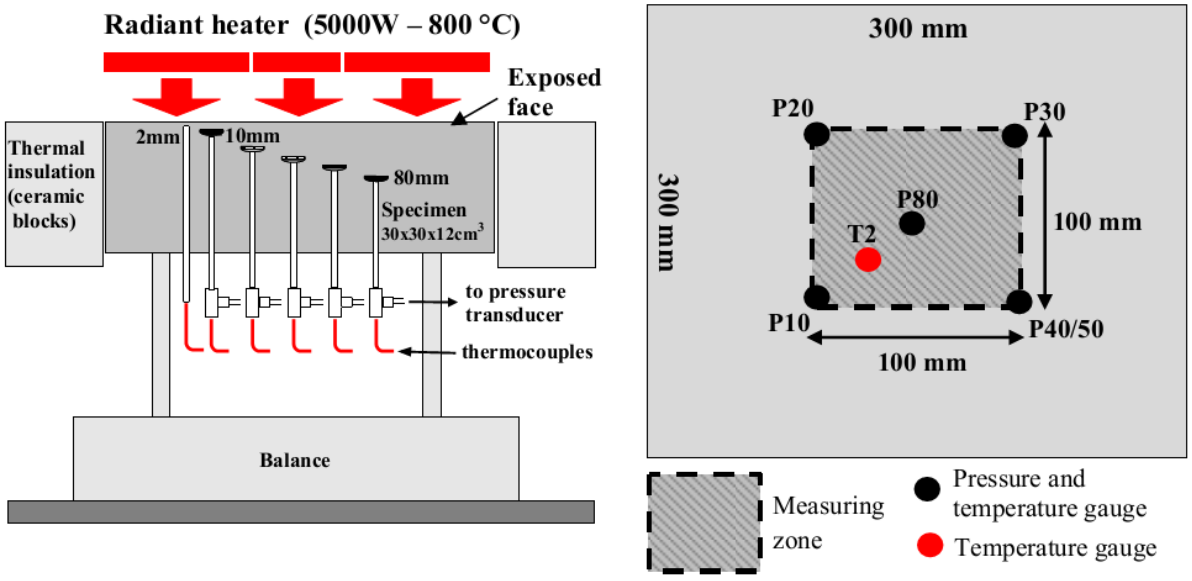

Figure 3.12: Test set-up (left) and position of the pressure-temperature gauges (right).

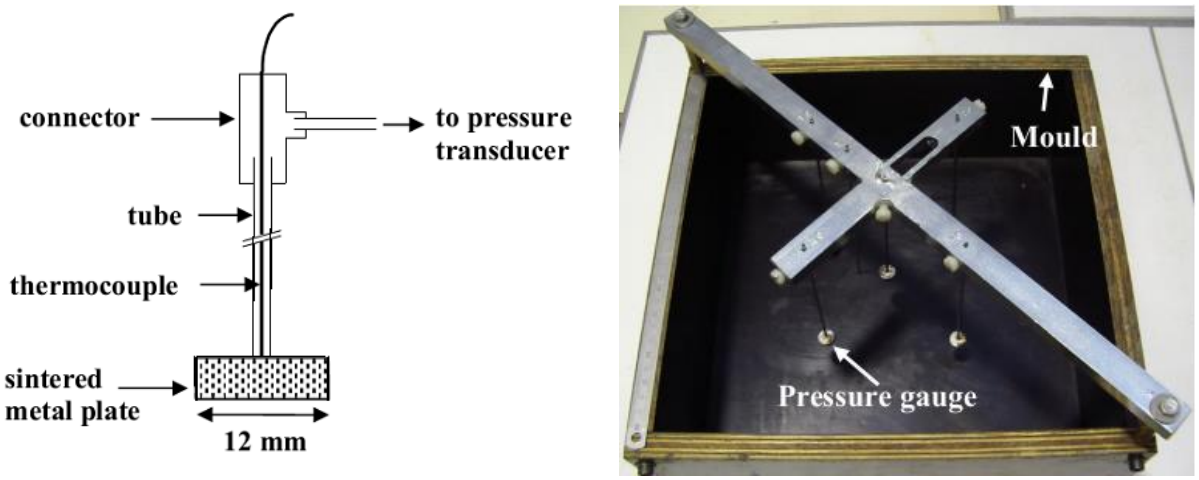

Figure 3.13: Pressure–temperature gauge

In order to better understand the role played by cement type in the behaviour of concrete at high temperature, particularly the influence of heating rate on both thermo-hygral behaviour and instability risk of concrete, 3 different thermal loadings have been applied (see Figure 3.14). The heating system consists of one radiant panel positioned 3 cm above the exposed surface of the prismatic sample. The sample lateral faces were insulated with porous ceramic blocks to favour quasi-unidirectional heat transfer.

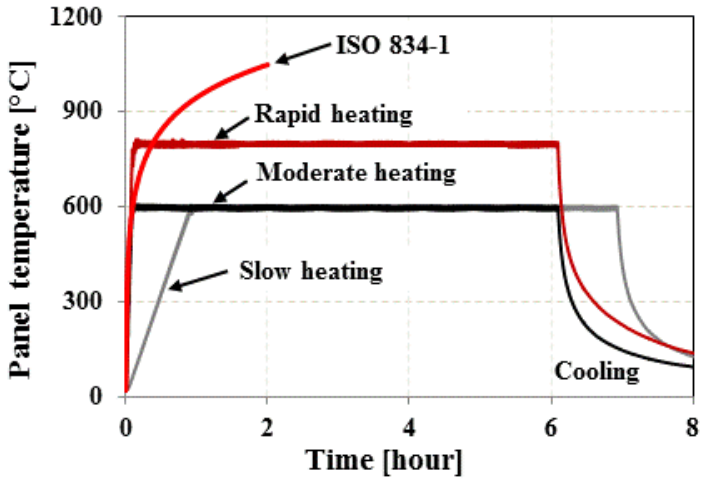

Figure 3.14: The thermal loads for PT tests and comparison with ISO 834-1 fire curve.

The three different thermal loads are as follows:

Slow heating: The radiant panel was controlled with a heating rate of 10 °C/min up to 600 °C (after about 1h of heating) and then this temperature was maintained constant for 6 hours. After 6 hours of stabilisation, samples were naturally cooled down to the room temperature (20 °C).

Moderate heating: The radiant panel was controlled in such a way that the temperature reached as quickly as possible 600 °C (after about 5 minutes of heating). The heating panel temperature

was maintained constant for 6 hours. After that, samples were naturally cooled down to the room temperature (20 °C).

Rapid heating: The heating system was the same as the moderate heating; the only difference was that the radiant panel temperature reached as quickly as possible 800 °C (after about 5 minutes of heating).

3.3 Experimental results and discussion

3.3.1 Residual porosity and axial permeability tests after unloaded preheating

Porosity measurement is related to total pore volume, whereas permeability is related to the interconnectivity of the pores in the concrete, which measures how fast the gases or liquids will flow through it, due to a pressure gradient. Knowledge of porosity and permeability will allow us to better understand the fluid transport behaviour in concrete, which could influence the fire spalling behaviour of concrete by directly influencing the build-up of pore pressure during heating. The porosity and intrinsic permeability of the B40-II and B40-III tested concrete specimens subjected to different preheating temperatures are presented in Figure 3.15a-b.

Mass evolution was also carried out on the specimens which have been tested in porosity and permeability. The specimens were weighed before and after each heat treatment (to calculate the average mass loss of each temperature, three specimens for porosity and two specimens for permeability tests were used), see Figure 3.15c. In Figure 3.15b, the y-axis presents the permeability in $\log_{10}$ scale and the x-axis present temperature in arithmetic scale. Good repeatability of the porosity and permeability tests have been observed for both concretes. It can be seen that as the temperature increased, the porosity and permeability increased, with especially higher increment at the higher thermal load, see Figure 3.15a-b.

At temperatures 80 °C and 120 °C, a sharp increase on both characteristics were observed for both concretes. This behaviour was observed by Khalifa et al. 2001 [22] in the temperature between 80 °C and 105 °C. This behaviour could be due to accessible pore volume caused by the withdrawal of free water and a loss of physically bound water (which leaves empty pores behind) that could not be withdrawn at 80 °C. This behaviour consistent with the measurement of average mass loss at this temperature (see Figure 3.15c), a higher mass loss was observed at 120 °C than at 80 °C, which indicates a higher porosity and permeability. It should not correspond to a significant change of the matrix itself [22] and not due to cracking. This sudden upward jump of permeability was also observed by Bazant 1997 [23], which was more than 2 orders of magnitude (about 200 times) when passing from 95 °C to 105 °C.

It can be seen that a low increase in porosity has been observed in the temperature between 120 °C and 250 °C in comparison to their evolutions at the temperature between 80 °C and 120 °C. A quite similar behaviour was observed in the permeability measurement, especially in the B40-III. These results are in good agreement with the measurements of mass loss, a lower increment of mass loss was observed at that temperature range compared to the 80 °C and 120 °C, see Figure 3.15c. At temperatures ranging from 250 °C to 400 °C, the porosity and

permeability increases, respectively, approximately 1.3 times and one order of magnitude as compared to the value at 80 °C. Since no visible surface cracking was observed after the heat treatment, which can be seen in Figure 3.16a, d, it could be due to the increase in macroporosity and the increase in capillary porosity due to the beginning of the Portlandite decomposition [24].

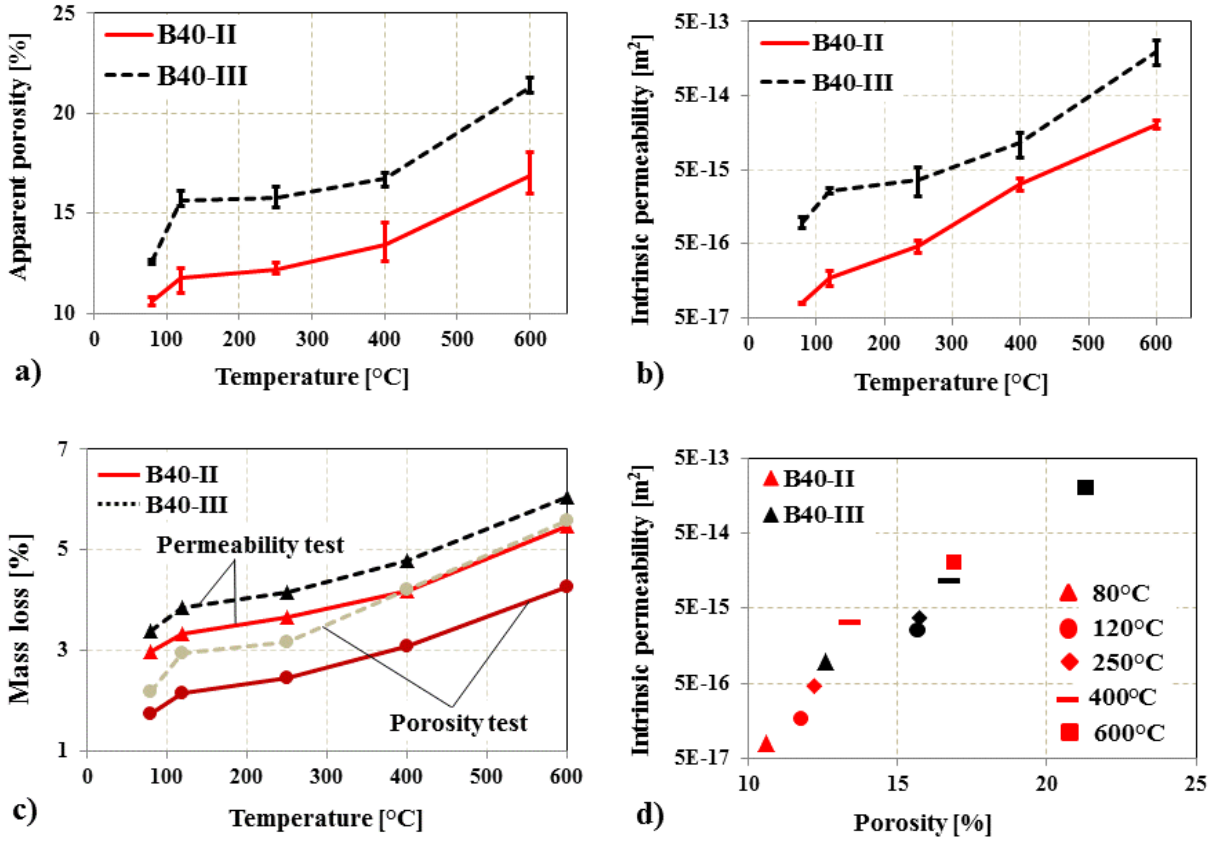

Figure 3.15: Residual porosity (a) and gas permeability (b) as a function of temperature. Mass loss of porosity and permeability test specimens after heated to the target temperatures (c). The relation between permeability and porosity of concretes at a different levels of temperatures (d).

Beyond 400 °C, a much more significant change in porosity and permeability were observed, which could be due to the development of cracks mainly caused by the thermal incompatibility between the cement paste and the aggregates, since at high temperature the cement paste shrinks due to dehydration, while the aggregates dilate due to their positive thermal expansion [22]. This mismatch brings in tensile stresses in the matrix and compressive stress in the aggregates leading cracking. The evidence of cracking after heat treatment at 600 °C can be clearly seen in Figure 3.16b-c, e-f. The cracks mainly located at the aggregate-cement paste interface as well as through the aggregates were stained with red colour.

An important observation from Figure 3.15a-b is that the residual porosity and permeability of B40-III are higher than B40-II for all the temperatures. These two results observed on both porosity and permeability are in good agreement and consistent with the results of mass loss. After being exposed to the same temperature, the mass loss of B40-III is always higher than the

B40-II (see Figure 3.15c). The average mass loss of porosity and permeability test specimen at 80 °C are, respectively, 1.7% and 3.0% for B40-II and 2.2% and 3.4% for B40-III, while at 600 °C, 4.3% and 5.5% for B40-II and 5.6% and 6.0% for B40-III, respectively. Moreover, in B40-III, a network of minor cracks, as well as major cracks at the aggregate-cement paste interface and through the aggregates were observed, while comparatively low cracking was observed in B40-II. This higher mass loss and higher cracking justify the higher porosity and permeability of B40-III than B40-II at elevated temperatures (see Figure 3.15c and 3.16).

a) 400 °C (B40 II) b) 600 °C (B40 II) c) 600 °C (B40 II)

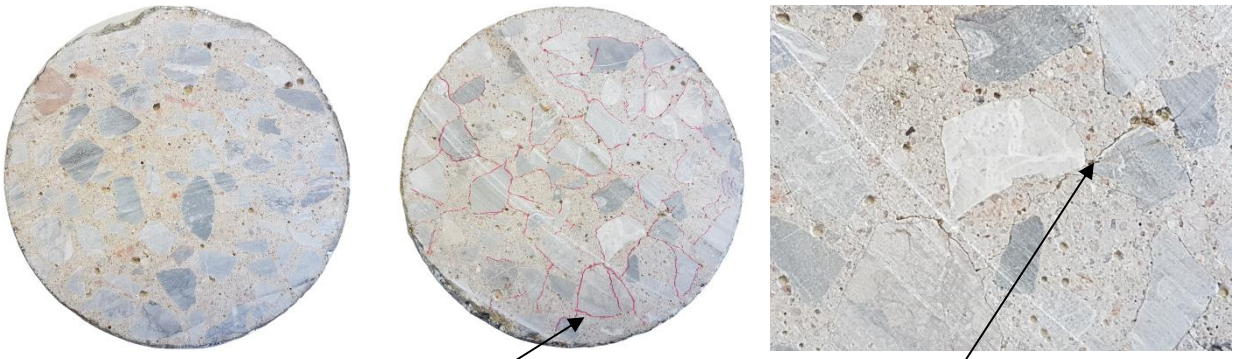

Almost no cracks were observed by the naked eye at the aggregate-cement paste interface of B40-II and B40-III specimens (a, d)

Cracks located at the aggregate-cement paste interface and through the aggregates of both concretes were stained with red colour (b, e)

Cracks can be seen clearly by the naked eye heated after at 600 °C

d) 400 °C (B40 III) e) 600 °C (B40 III) f) 600 °C (B40 III)

Figure 3.16: a-b, d-e) The images of B40-II and B40-III concrete specimens subjected to elevated temperature before permeability test; c, f) zoom images of the preheated specimens.

The relation between residual gas permeability and porosity of two concretes heated at a different level of temperatures was also analysed. Interestingly, a good correlation between residual porosity and gas permeability of both concretes can be noticed in Figure 3.15d, the

permeability increased with the increase in porosity. It can be seen that a gradual increment of permeability and porosity was observed up to 250 °C, as the temperature increased above 250 °C, the difference became wider, especially in the B40-III. This behaviour could be due to the formation of larger cracks at 600 °C (see Figure 3.16b-c, e-f), especially in B40-III, which is the main factor controlling the evolution of gas permeability of concrete. From Figure 3.15d, it also represents two different behaviours of two different concretes at the elevated temperatures, even though the same mix design was used for both concretes (only difference is the cement type).

3.3.2 The effect of loading on the residual gas permeability of concrete

A detail description of the results on the effect of loading on the gas permeability of concrete is given in the sections below.

3.3.2.1 Residual axial permeability tests under radial confining pressure after unloaded preheating

Figure 3.17a presents the residual axial intrinsic permeability (K_{int}) of concretes (B40-II and B40-III) specimens subjected to different preheating temperatures at different levels of radial confining pressure (Pc). In the Figure 3.17, the lines represent the average value and the vertical line (i.e. error bar) represents the range of data. The results were reproducible. For a deeper analysis of the influence of radial confining pressure on the axial permeability, it is worthwhile to study the variation in permeability, normalised with respect to the reference value of confining pressure, i.e. K_{int} (Pc)/K_{int} (Pc = 0.3 MPa). The permeability results at 0.3 MPa was considered as a reference permeability for this test (as discussed in section 3.2.3.1). The representation of the normalised axial permeability is shown in Figure 3.17b.

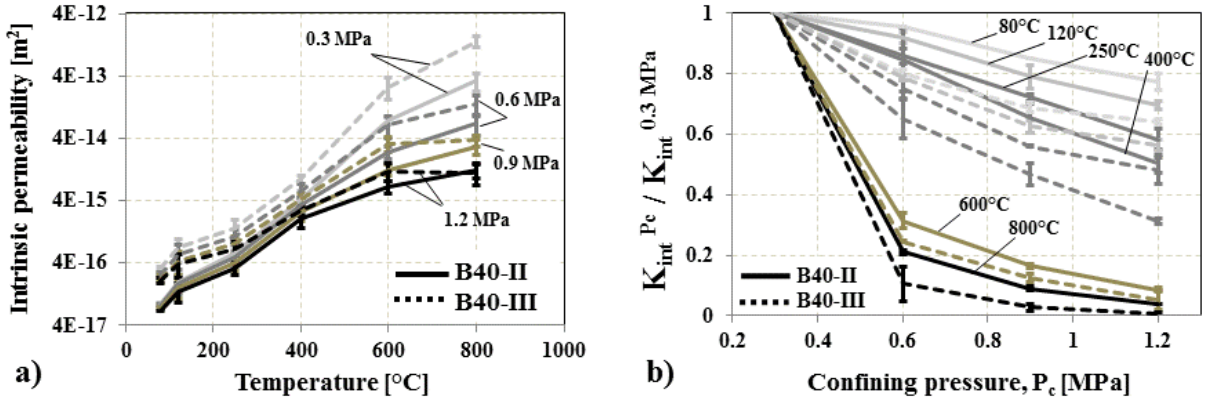

Figure 3.17: Residual axial intrinsic permeability (K_{int}) of concretes under different levels of confining pressure (Pc = 0.3, 0.6, 0.9 and 1.2 MPa) as a function of temperature (a) and normalised permeability versus radial confining pressure (b).

The experimental results showed that the axial permeability of the 2 concretes (B40-II and B40-III) decreased with increasing radial confining pressure (Pc perpendicular to the gas flow, see Figure 3.6 right). It can be seen that the residual permeability after preheating at 80 °C and

120 °C are quite insensitive to confining pressure. This could be due to the reduced amount of microcracks and cracks induced by the lower thermal loads. By opposite, these effects are more pronounced as the temperature treatment has been increased (e.g. at 600 °C and 800 °C). It is important to notice that, as written before, the decreased trend of permeability is not due to leakage of gas, since no outflow occurred at confining pressure starting from 0.3 MPa during the blank test. This behaviour could be attributed to the partial closure of heat induced microcracks and cracks (parallel to the gas flow) probably located at the aggregate-cement paste interface as well as through the aggregates when the specimens were compressed by the radial confining pressure. Indeed, the width of cracks perpendicular to the applied compressive stress (here stress due to confining pressure) closed [25] while those parallel to the stress tended to open [26-28], see an example in Figure 3.18a-b.

Interestingly, a sharp decrease of permeability can be seen when the confining pressure was doubled (Pc = 0.6 MPa) than the reference pressure (Pc = 0.3 MPa). When the confining pressure continues to increase beyond 0.6 MPa, the rate of decreasing trend seems to be much smaller, and the permeability tends to stabilise for the high thermal loads, while it continues to decrease for the intermediate thermal loads (e.g. at 250 °C and 400 °C).

The Figure 3.17b suggests that the crack closure and the decrease in permeability could continue if the confinement would have been increased beyond 1.2 MPa (which was the limitation of the test device), in particular for the specimens which were exposed to intermediate temperatures. The presented results are in good agreement with the results reported in the literature even though most of the studies have been carried out at confining pressures that are much higher than in our tests [25, 29-30]. For example, Pei et al. 2017 [25] carried out permeability and porosity tests under different levels of confining pressure (5, 10, 20, 30 and 40 MPa). In their study, mortar specimens were heated to 105, 400, 500 and 600 °C with a heating rate of 20 °C/h. Their results showed that permeability has an increased sensitivity to confining pressure at higher temperatures due to the closure of the cracks. Chen et al. 2013 [29] tested the gas permeability of heat-treated mortars at four different levels of confining stresses (Pc = 5, 12, 15 and 25 MPa). The authors observed that the permeability of mortars heat-treated above 400 °C was sensitive to confining pressure and the intrinsic permeability decreased by up to 23% when the confining stress increased from 5 to 25 MPa. Likewise, Lion et al. 2005 [30] reported that the apparent permeability was decreased when confining pressure was increased from 4 to 28 MPa and this was more significant for the higher thermal load.

Since the gas permeability has an increased sensitivity to confining pressure at higher temperatures (600 °C and 800 °C), it is necessary to monitor the intrinsic permeability during unloading right after the maximum confining pressure (Pc = 1.2 MPa) test to evaluate the reversibility of the loading. To this aim, Figure 3.19 has been drawn for both concrete specimens subjected to heating at 600 and 800 °C. It was found that there was no changing in permeability during unloading tests at 80 °C and 120 °C, since the permeability at these temperatures are less sensitive to confining pressure, as seen above. In higher temperature levels (600 °C and 800 °C), it can be seen that the axial permeability is a bit reduced during unloading than the loading tests.

Before permeability tests

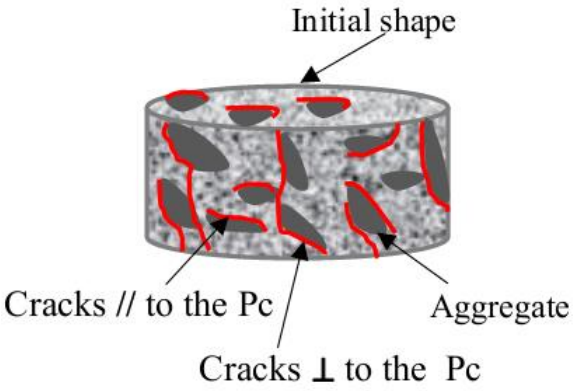

a) Multiple cracks due to thermal load

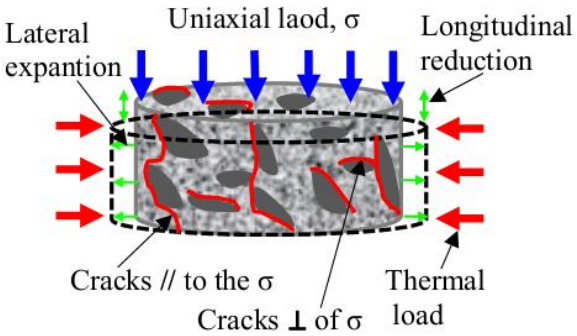

c) Width of cracks // to the uniaxial load (σ) increases and decreases ⊥ to the σ during heating-cooling

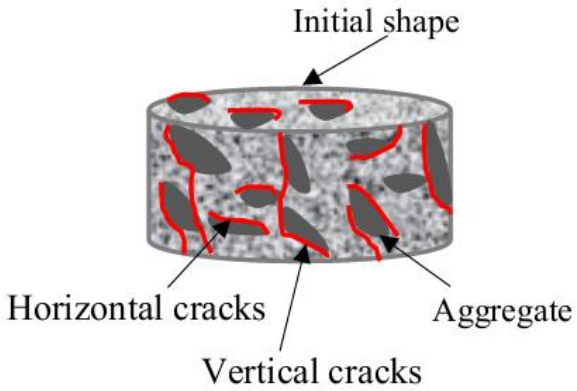

e) Multiple cracks due to thermal load

During permeability tests

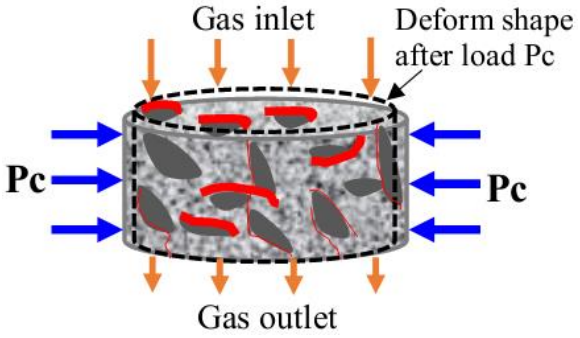

b) Width of cracks ⊥ to the Pc decreases and // to the Pc increases

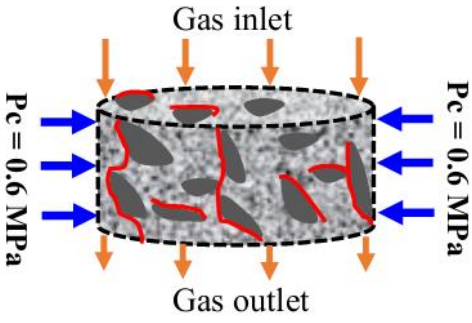

d) Axial gas flow (// to the vertical cracks) under confining pressure of 0.6 MPa

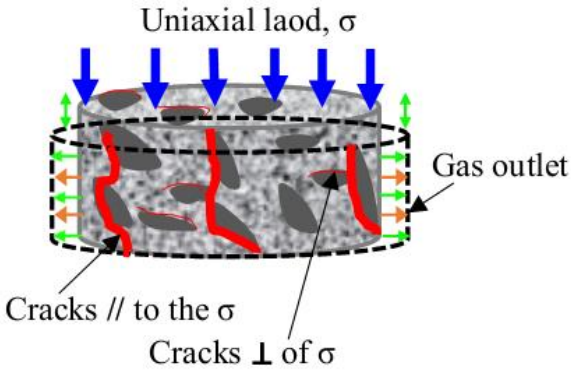

f) Width of cracks ⊥ to the load decreases

Figure 3.18: Schematic diagram of the crack patterns and their effect on heating and different loading conditions (Note: ⊥ = perpendicular, // = parallel).

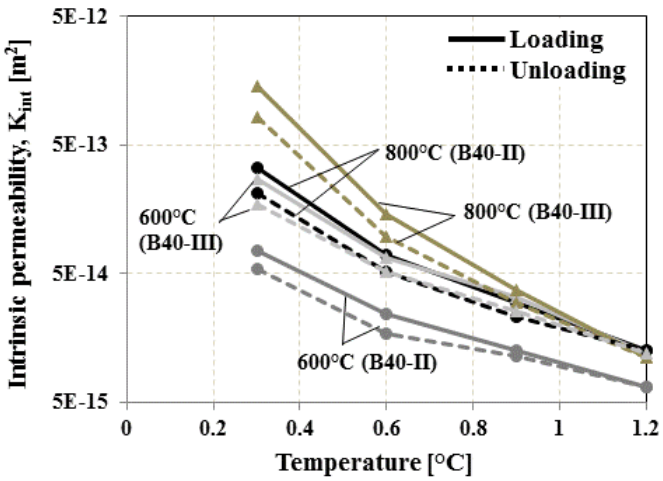

Figure 3.19: Residual axial intrinsic permeability of concretes (B40-II and B40-III) during loading and unloading confining pressure heated after at 600 °C and 800 °C.

The damage of the specimen should not expect due to applied maximum confining pressure (1.2 MPa), since it is very small compared to the strength of concrete. Probably, when unloading, some of the cracks remain closed and some of the pores were completely compressed during loading tests, which could explain the low permeability of the unloading tests.

Figure 3.17 allows us to compare the axial gas permeability of B40-II (3% of slag) and B40-III (43% of slag). It can be observed that the permeability of B40-III is higher for all the temperatures under 0.3 MPa confining pressure. These results are in good agreement with the measured axial permeability as described in section 3.3.1. The permeability difference decreases when confining pressure increases.

3.3.2.2 Residual axial permeability tests under radial confining pressure after preheating under uniaxial loading

The residual axial intrinsic permeability of the B40-II and B40-III concrete specimens subjected to preheating (400 °C) under different levels of uniaxial compressive loading is presented in Figure 3.20. In the graph, the lines represent the average value and the vertical line (i.e. error bar) represents the range of data. In this experimental test campaign, an increasing trend of intrinsic axial gas permeability was observed with the increased uniaxial compressive loading (parallel to the gas flow) during heating-cooling. Interestingly, a higher increase of intrinsic axial gas permeability was observed in the specimens which were loaded at low compressive loading (0.5 MPa) during heating-cooling. These results tend to show that very small compressive loading can influence the axial gas permeability of concrete, even though 0.5 MPa stress is very small compared to the compressive strength of concrete (51 MPa at the day of the test).

When concrete is heated under a constant uniaxial compressive loading, its longitudinal strain is reduced. This reduction is mostly induced by transient thermal strain [26]. By opposite, radial strains tend to be higher. This is mainly explained by the formation and opening of cracks

parallel to the loading [26-28], see an example in Figure 3.18c. The evidence of cracks parallel to the loading direction after heat treatment at 400 °C under uniaxial loading (5 MPa) can be clearly seen in Figure 3.21c-d. No similar cracking was observed in the unloaded specimens, see Figure 3.21a-b. These axial cracks explain the higher axial gas permeability measured in these tests, since the injected gas flow was axial to the loading direction of the specimens (see Figure 3.18d).

B40-II (3% of slag) exhibited lower permeability than the B40-III (43% of slag), which is in good agreement with the former tests we have presented in sections 3.3.1 and 3.3.2.1.

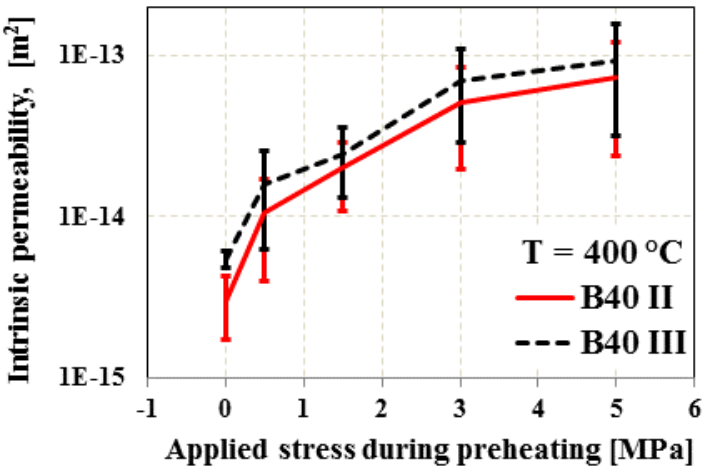

Figure 3.20: Residual axial intrinsic permeability of concretes measured after preheating under different levels of uniaxial compressive loading.

a) B40 II (0 MPa)

b) B40 III (0 MPa)

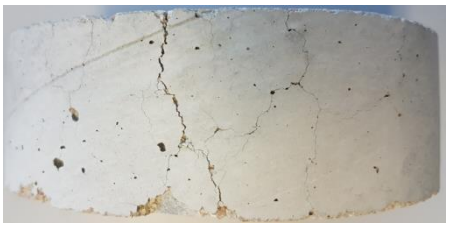

c) B40 II (5 MPa)

d) B40 III (5 MPa)

Figure 3.21: Images of B40-II and B40-III concrete specimens preheated (400 °C) under no load (0 MPa) and a compressive stress (5 MPa).

3.3.2.3 Residual radial permeability tests under uniaxial loading after unloaded preheating

Figure 3.22a presents the residual radial intrinsic permeability (K_{int}) of concretes (B40-II and B40-III) as a function of uniaxial compressive stress, while the relationships between the normalised permeability and the uniaxial compressive stress are shown in Figure 3.22b. It can be seen that in Figure 3.22, at lower temperatures (120 and 250 °C), permeability decreases when applied compressive stress increases, while at the higher temperatures (400 °C and 600 °C), the permeability decreases up to a certain level of load, after that stabilises and then increases when the compressive stress increases.

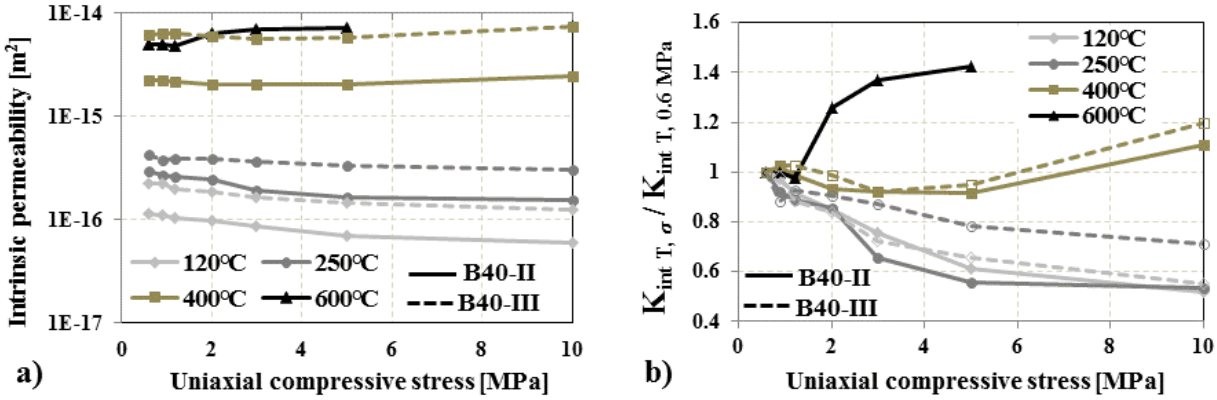

Figure 3.22: Effect of uniaxial compressive loading on the radial gas permeability of concretes.

In general, the trend presented in Figure 3.22b clearly indicates distinct phases in the variation in radial permeability with the load. First, permeability decreased with the increasing applied compressive loading (for all temperature levels). This phenomenon is attributed to the partial closure of heat-induced microcracks and cracks (perpendicular to the load) caused by the increase in the applied compressive loading [31]. It appears between 0.6 and 5 MPa for the heating at 120 °C and 250 °C, between 0.6 and 2 MPa for 400 °C and between 0.6 and 0.9 MPa for 600 °C.

Secondly, a very small change or even almost constant permeability was observed. In this phase, it is believed that there is a combination of crack initiation, crack growth, and crack closure [31]. This phase is observable up to 5 MPa for 120 and 250 °C, between 2 and 5 MPa for 400 °C, between 0.9 and 1.2 MPa for 600 °C.

Finally, an increase in permeability was observed with the further increase of the compressive stress. At 120 °C and 250 °C, the applied stress is not sufficient (10 MPa) to observe increase of permeability due to additional mechanical damage. For B40-II specimens heated at 400 °C and 600 °C, the phenomenon is observed above 5 and 1.2 MPa, respectively (see Figure 3.22b). Almost similar behaviour was found for the B40-III preheated at 400 °C, while the specimens preheated at 600 °C were more damaged during heating, hence it was not possible to measure the permeability of these specimens due to very fast gas flow. The increasing permeability with increasing loads of this behaviour could be due to the extension of the existing cracks (i.e. remaining unclosed cracks) and creation and opening of new cracks [31]

due to Poisson's effect (i.e. increase transversal deformation due to crack opening in the direction of the gas flow) and begin to join together in somehow, which make the permeability to reach the maximum in this phase. These observations are in good agreement with the ones of Banthia et al. 2005 [32]. Banthia et al. 2005 [32] found that a significant increase in radial permeability of plain concrete when the applied uniaxial stress was beyond $0.3f_u$ (where f_u is the strength in compression at room temperature).

As we have seen in sections 3.3.1, 3.3.2.1 and 3.3.2.2, B40-II (3% of slag) always exhibited lower permeability than B40-III (43% of slag) in all the heating levels (see Figure 3.22a), which is really a good agreement among all the tests.

3.3.3 Temperature and pore pressure development

Figure 3.23 presents the temperature measured into the B40-II and B40-III concrete exposed to 3 different thermal loads at different depths from the exposed surface as a function of time. In each heating test (slow, moderate and rapid), no significant change in the development and magnitude of temperatures was observed in both concretes. Higher temperatures were observed close to the heated surface of all heating tests and then a decreasing trend towards the inner depths of both concretes, except for the temperature at 2 mm of B40-III exposed to slow heating test is a bit lower compared to at 10 mm of the same test (see Figure 3.23b), which is inconsistent with the other measurements. This scatters may be partly explained by the uncertainty of the thermocouple position due to technical offsets during installation.

When comparing the development of temperatures into the concrete specimens exposed to 3 different thermal loads, the evolution of temperature is a bit slower in the slow heating tests than moderate heating tests, especially at the beginning of the tests, while a quite higher development and higher magnitude of temperature was observed in the rapid heating of both concretes. This behaviour is in good agreement with the applied thermal loads to the specimens in three different tests, see Figure 3.14.

For all heating levels and almost each measuring depths, a slight temperature plateau has been observed. The temperature plateau is caused by the water phase change (vaporisation). This transformation is endothermic and consumes part of the energy that is brought by heating. As a consequence, the temperature rise of the concrete sample is slowed down. It can be emphasised that water vaporisation can induce additional temperature gradients [33]. Additionally, the vaporization of water creates pressure gradient, the vapour moves towards the hot face and the cold face. The part moving to the hot face cools the concrete as the part moving to the cold face heats it, and can turn back into liquid releasing additional heating.

A steep and the higher temperature gradients were observed in rapid heating of concrete compared to the slow and moderate heating tests (see Figure 3.24). The higher temperature for rapid heating could accelerate the vaporisation as well as induce higher thermal stresses due to the higher thermal gradient, as a result, higher thermal damage and cracks. Thermal damage and release of moisture in the B40-III concrete specimen was noticed when exposed to rapid heating (see Figure 3.25 right), while the thermal damage and release of moisture in the B40-II specimen

was reported by Mindeguia J-C 2009 [21], see Figure 3.25 left. The release of hot moisture was observed around the cracks, while no similar cracking was observed in concrete specimens subjected to slow and moderate heating.

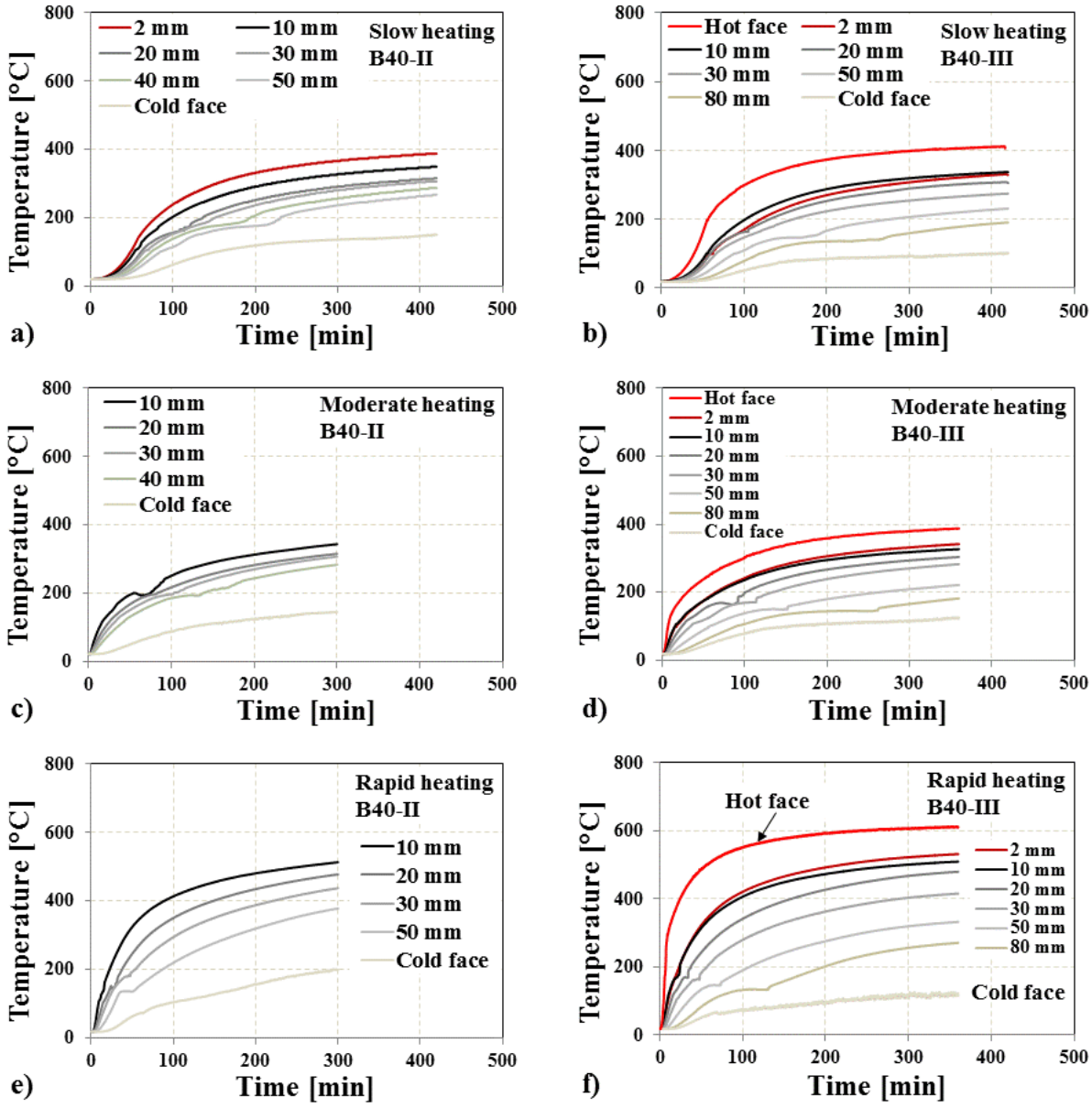

Figure 3.23: (a-c) Evolution of temperatures inside the B40-II [21] and B40-III concrete exposed to 3 different thermal loads.

Figure 3.26 presents the development of pore pressure as a function of time, while Figure 3.27 represents the pressure-temperature plots which are compared with the saturation vapour pressure curve, P_{sv} (T). The saturation curve represents a limit condition of pressure-temperature relation. Theoretically, pressure-temperature curves cannot pass beyond the saturation curve. It can be observed that measured pressures of B40-II and B40-III followed the P_{sv} curve during the

ascending branch. Except for rapid heating, at 50 mm depth in B40-II and at 80 mm depth in B40-III, measured pore pressure is slightly higher than the saturation vapour pressure curve (see Figure 3.27e-f). This overpressure could be attributed to the partial pressure of the dry air enclosed within the porous network [20, 33]. The partial pressure of air in the pore is strongly dependent on its liquid water saturation: the higher the water saturation, the lower the free volume available for the air to expand during heating. Also, the size and number of the pores can increase or decrease the free volume available for the air.

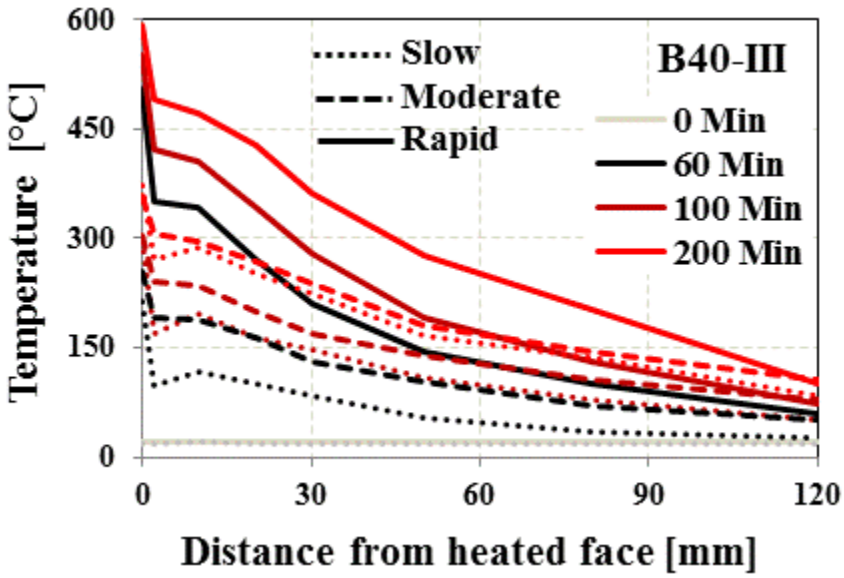

Figure 3.24: Temperature profile through the thickness of B40-III concrete exposed to 3 different thermal loads.

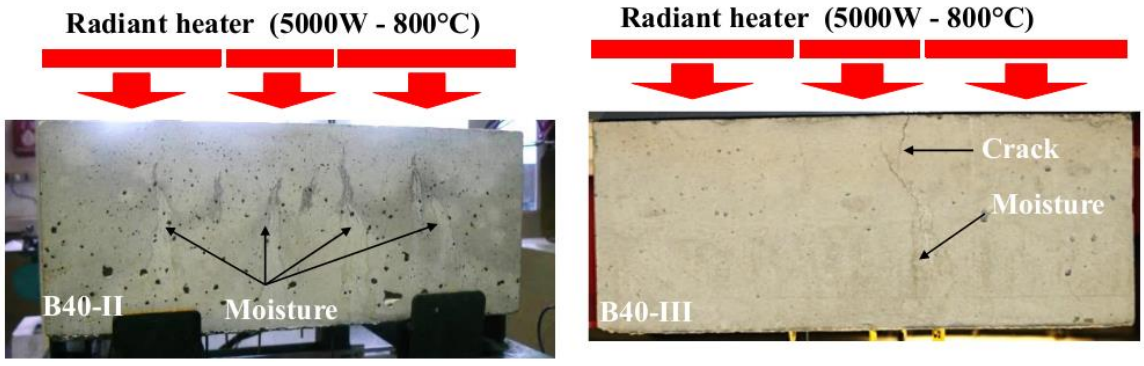

Figure 3.25: Cracking and released of hot moisture in the B40-II (left, [21]) and B40-III (right) concrete when exposed to rapid heating.

Maximum pore pressure determined at different depths of both concretes exposed to 3 different thermal loads is represented in Figure 3.28. Maximum pore pressures determined

during PT tests of B40-II and B40-III are, respectively, 1.51 MPa and 0.73 MPa. This behaviour could be attributed to the lower value of porosity and permeability of the B40-II at high temperature (see Figure 3.15). Indeed, lower permeability reduces transport of water vapour inside the concrete and then induces faster build-up and higher value of pore pressure. When comparing the magnitude of pore pressure obtained with the 3 different thermal loads, no significant change in pore pressures were observed in B40-III concrete specimens, while very different pore pressure has been measured in B40-II concrete specimens (see Figure 3.28).

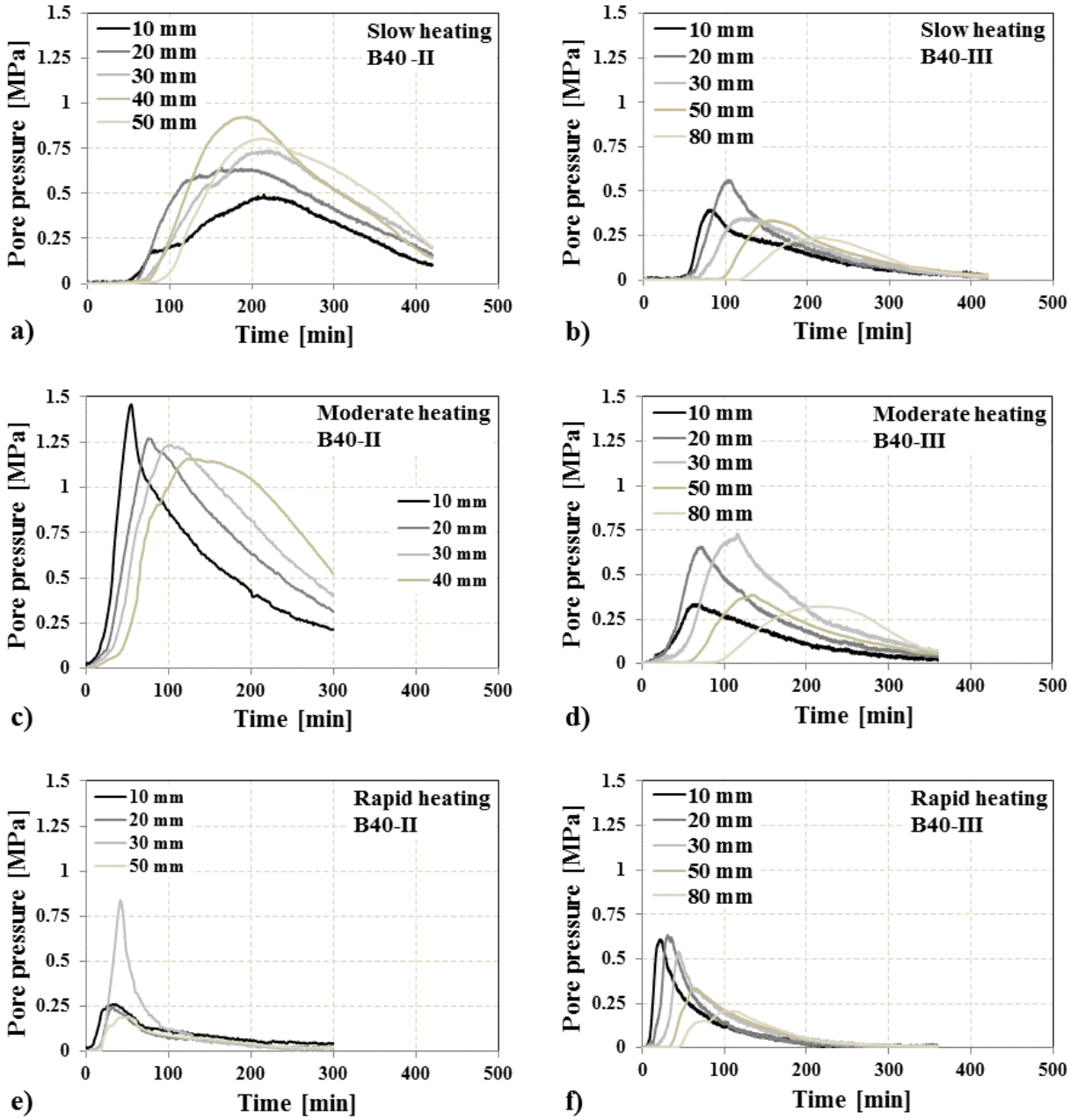

Figure 3.26: Development of pore pressure inside the B40-II [21] and B40-III concrete exposed to 3 different thermal loads.

A quite slow rise of pore pressure with time has been measured in slow heating of both concretes, while a very sharp increase of pore pressures has been observed in moderate heating of B40-II than B40-III (see Figure 3.26, c). This slow rise of pore pressure behaviour could be due to the drying of the specimens during the first hour of slow heating (slow heat diffusion into the concrete due to slow heating rate), which significantly affect the rising of pore pressure, as a consequence, lower pore pressure was measured in slow heating than moderate heating. Almost no pore pressure was measured during the first hour of slow heating test, while maximum pore pressure (1.51 MPa for B40-II) was reached at 10 mm depth of B40-II concrete before 1 hour of moderate heating, see Figure 3.26a, c.

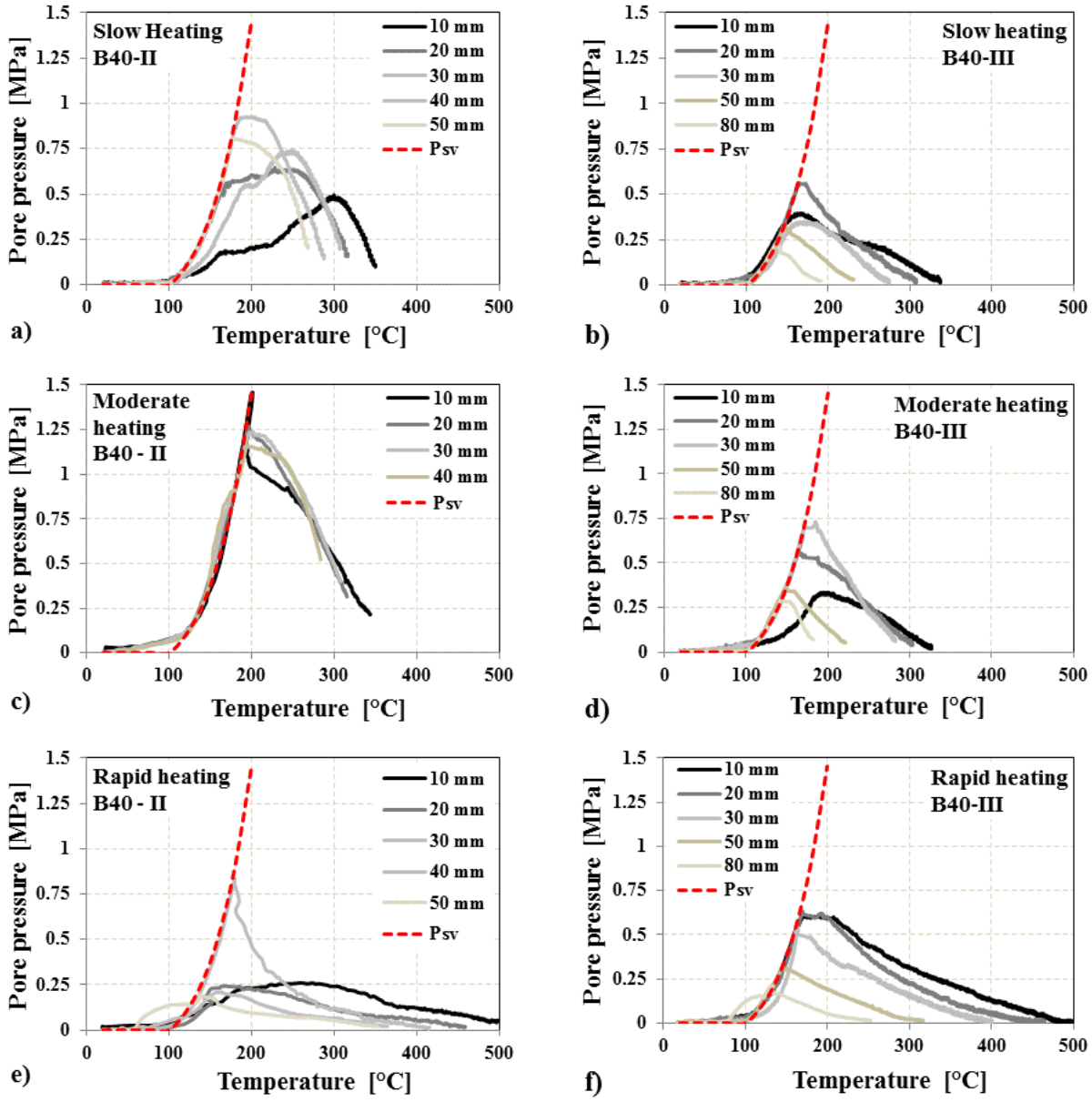

Figure 3.27: Pore pressure versus temperature curves and comparison with the saturation vapour pressure curve P_{sv}.

Low pore pressures were measured in rapid heating of B40-II than B40-III, except one measurement at the depth of 30 mm (see Figure 3.26e). As mentioned above, an increased rate of microcracking and cracks can be expected at a higher heating rate and the higher temperature (i.e. rapid heating) due to high thermal gradients (see Figure 3.24), resulting in higher thermal stresses and then induce higher thermal damage and microcracking, which could increase the permeability and then increase the release of moisture. A more distributed network of fine cracks on the exposed side and few long vertical cracks on the lateral sides were observed due to the higher thermal gradient of rapid heating (see Figure 3.25), while no similar cracking was observed in concrete specimens subjected to slow and moderate heating. As cracks were formed, significant amounts of vapour and liquid water migrated out of the specimens on the lateral side, which could reduce the build-up of pore pressure by favouring the moisture transport. This suggests that the internal cracking is an important factor for pore pressure build-up when concrete is exposed to fast heating rate.

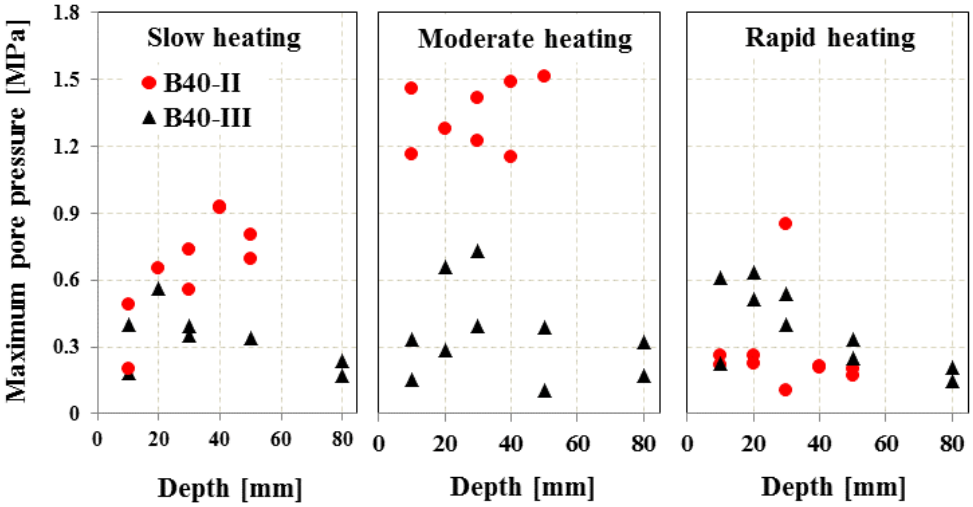

Figure 3.28: Maximum pore pressure measured in B40-II and B40-III concretes during PT tests.

3.4 Summary and conclusions

This chapter has presented the testing methodology and apparatus to investigate some physical properties of concrete made with CEM II (3% of slag) and CEM III (43% of slag) cements at high temperature related to fire spalling. Special interest was driven by four issues: (i) effect of heating on the porosity and permeability of concretes, (ii) effect of heating and mechanical loading on the permeability of concretes, (iii) effect of heating rate and levels on the build-up of pore pressure of concretes and (iv) incorporation of slag in the cement on the behaviour of concrete at high temperatures.

The main findings regarding the influence of heating rate, temperature levels, the presence of loading and cement type on the behaviour of ordinary concrete can be summarised as follows:

It was found that the permeability of concrete made with CEM III cement (B40-III: 43% of slag) is higher than the one of concrete made with CEM II cement (B40-II: 3% slag) in all heating and loading conditions.

As the thermal load increases the permeability and porosity of concrete increases, with especially higher increment at the higher thermal load due to the development of cracks mainly caused by the thermal incompatibility between the cement paste and the aggregates. Both results observed on porosity and permeability are in good agreement.

It has been clearly shown that the presence of loading and their levels have a significant influence on the gas permeability of concrete. It was found that the axial permeability decreases when confining pressure increases by reducing the width of the axial cracks. While the axial permeability increases with uniaxial compressive stress applied during preheating. In the residual radial gas permeability measurements, at lower temperatures (120 °C and 250 °C), the permeability decreases when applied compressive stress increases. At the higher temperature (400 °C and 600 °C), the permeability decreases up to a certain level of load, after that stabilises and then increases when the compressive stress increases. From the analyse of this behaviour, it can be proposed that this finding arises from the combined effect, and competition of both, closing of the cracks perpendicular to the load (permeability decrease) and the opening of the cracks parallel to the load (permeability increase).

As a result, permeability increases or decreases depends on the orientation and opening of cracking and these two parameters are influenced by compressive loading. Hence, the stress state, by governing the orientation and opening of the opened cracks is a very important key factor which control the internal fluid transfer (i.e. permeability) and then directly triggers the build-up and magnitude of the pore pressure within the concrete structure. Stress state has then 2 major roles on concrete fire spalling: (1) a direct influence in the thermo mechanical mechanism and (2) an indirect influence in themo-hydral mechanism by influencing the cracks opening and orientation and then, the permeability.

In the PT tests, none of the specimens spalled during slow, moderate, and rapid heating tests. This behaviour could be due to higher thermal damage of the specimens, since the specimens were unloaded and no restraint during heating, which could avoid the risk of spalling.

B40-II presented higher pore pressure for moderate and slow thermal loadings than B40-III. This result is in good agreement with the lower B40-II permeability and porosity at high temperature. It is to note that during rapid heating, a larger number of surface cracks and few long cracks were observed due to the higher thermal gradient of rapid heating that explain the very low values of pore pressure in B40-II. This suggests that the internal cracking is an important factor for pore pressure development when concrete are exposed to fast heating rate.

Even if pore pressure is not the only driving force of fire spalling, these results (i.e. lower pore pressure due to higher permeability and porosity at high temperatures) tends to show that the B40-III (43% of slag) is less sensitive to fire spalling than the B40-II (3% of slag). This is in good agreement with the fire spalling tests on both concretes, which are discussed in chapter 4.

3.5 References

[1] Khoury G. A and Anderberg Y. (2000). "Concrete spalling review", Fire safety design, report submitted to the Swedish National Road Administration, Sweden.
[2] Hertz, K.D. (2003). "Limits of spalling of fire-exposed concrete", Fire Safety Journal 38 (2003) 103–116.
[3] Fu, Y and Li, L. (2011). "Study on mechanism of thermal spalling in concrete exposed to elevated temperatures", Materials and Structures (2011) 44:361–376.
[4] Mendes, A., Sanjayan, J and Collins, F. "Phase transformations and mechanical strength of OPC/slag pastes submitted to high temperatures", Mat. and Struc. (2008) 41:345–350.
[5] Mendes, A., Sanjayan, J.G and Collins, F. "Long-term progressive deterioration following fire exposure of OPC versus slag blended cement pastes," Mat. and Struc. (2009) 42:95–101.
[6] Xiao, J., Xie, M and Zhang, Ch. (2006). "Residual compressive behaviour of pre-heated high-performance concrete with blast–furnace–slag," Fire Safety Journal 41 (2006) 91–98.
[7] Poon, C-S., Azhar, S., Anson, M and Wong, Y-L. (2001). "Comparison of the Strength and Durability Performance of Normal- and High-strength Pozzolanic Concretes at Elevated Temperatures," Cement and Concrete Research 31 (2001) 1291–1300.
[8] Gallé, C and Sercombe, J. (2001). "Permeability and pore structure evolution of silico-calcareous and hematite high-strength concretes submitted to high temperatures", Materials and Structures, Vol. 34, December 2001, pp. 619-628.
[9] Noumowe, A.N., Siddique, R and Debicki, G. "Permeability of high-performance concrete subjected to elevated temperature (600°C)", Const. and Build. Mat. 23 (2009) 1855–1861.
[10] Phan, L.T. (2008). "Pore pressure and explosive spalling in concrete", Materials and Structures (2008) 41:1623–1632.
[11] Felicetti, R and Lo Monte, F. (2016). "Pulse-Echo Monitoring of Concrete Damage and Spalling during Fire", 9th International Conference on SIF, June 8-10, 2016, Princeton, USA.
[12] Choinska, M., Khelidj, A., Chatzigeorgiou, G and Pijaudier-Cabot, G. (2007). "Effects and interactions of temperature and stress-level related damage on permeability of concrete", Cement and Concrete Research 37 (2007) 79–88.
[13] ACI Committee 233 (2000). "Ground Granulated Blast-Furnace Slag as a Cementitious Constituent in Concrete", ACI 223R-95, 2000.
[14] NF P18-459 (2010). "Essai Pour Béton Durci-Essai de Porosité et de Masse volumique", French Standard, NF P18-459, MARS 2010.
[15] Hager, I.G. (2004). "Comportement à haute température des bétons à haute performance-évolution des principales propriétés mécaniques", PhD Thesis (French), 5 November 2004, l'Ecole Nationale des Ponts et Chaussées etl'Ecole Polytechnique de Cracovie.
[16] Kollek, J. J. (1989). "The Determination of the Permeability of Concrete to Oxygen by the Cembureau Method - A Recommendation", Materials and Structures (1989), 22, pp. 225-230.
[17] Klinkenberg, L. J. (1941). "The Permeability of Porous Media to Liquid and Gases", American Petroleum Institute, Drilling and Production Practice (1941), pp. 200-213.

[18] Dal Pont, S. (2004). “Lien entre la perméabilité et l'endommagement dans les bétons à haute température, ”. PhD Thesis (French), l'Ecole Nationale des Ponts et Chaussées (France).
[19] Darcy, H. (1856). “Les fontaines publiques de la ville de Dijon. Exposition et application des principes à suivre et des formules à employer dans les questions de distribution d'eau”, Victor Dalmont, 1856.
[20] Kalifa, P., Menneteau, FD and Quenard, D. (2000). “Spalling and pore pressure in HPC at high temperatures”, Cement and Concrete Research (2000), Vol. 30, pp. 1915-1927.
[21] Mindeguia JC. (2009). “Contribution Expérimental a la Compréhension des risqué d’Instabilité Thermiques des Béton”, PhDThesis (French), UPPA, France.
[22] Kalifa, P., Chéné, Grégoire., and Gallé. “High-temperature behaviour of HPC with polypropylene fibres From spalling to microstructure”, CCR 31 (2001) 1487–1499.
[23] Bazant, Z.P. (1997). “Analysis of pore pressure, thermal stress and fracture in rapidly heated concrete”, in: Proceedings, International Workshop on Fire Performance of High-Strength Concrete, NIST, February 13-14, 1997, pp. 155–164.
[24] Gallé, C., and Sercombe, J. (2001). “Permeability and pore structure evolution of silicocalcareous and hematite high-strength concretes submitted to high temperatures”, Materials and Structures (2001), Vol. 34, pp. 619-628.
[25] Pei, Y., Agostini, F and Skoczylas, F. (2017). “The effects of high temperature heating on the gas permeability and porosity of a cementitious material”, CCR 95 (2017) 141–151.
[26] Mindeguia, J-C., Hager, I., Pimienta, P., Carré, H and La Borderie, C. “Parametrical study of transient thermal strain of ordinary and high performance concrete”, CCR 48 (2013) 40–52.
[27] Ring, T., Zeiml, M., Lackner, R and Eberhardsteiner, J. (2013). “Experimental Investigation of Strain Behaviour of Heated Cement Paste and Concrete”, Strain (2013)49, 249–256.
[28] Huismann, S., Weise, F. and Schneider, U. (2009). “Influence of the preload on the mechanical properties of high strength concrete at high temperatures”, 1st IWCS due to Fire Exposure, MFPA Institute, Leipzig, September 3–5 2009, pp. 189–200.
[29] Chen, X-t., Caratini, G., Davy, C.A., Troadec, D and Skoczylas, F.. “Coupled transport and poro-mechanical properties of a heat-treated mortar under confinement”, CCR 49 (2013) 10–20.
[30] Lion, M., Skoczylas, F., Lafhaj, Z and Sersar, M. (2005). “Experimental study on a mortar. Temperature effects on porosity and permeability. Residual properties or direct measurements under temperature”, Cement and Concrete Research 35 (2005) 1937 – 1942.
[31] Bian, H., Hannawi, K., Takarli, M., Molez, L and Prince, W., “Effects of thermal damage on physical properties and cracking behavior of ultrahigh-performance fiber-reinforced concrete”, Journal of Materials Science, Springer Verlag, 2016, 51 (22), pp. 10066–10076.
[32] Banthia, N., Biparva, A and Mindess, S. (2005). “Permeability of concrete under stress”, Cement and Concrete Research 35 (2005) 1651–1655
[33] Mindeguia, JC., Pimienta, P., Noumowé, A., and Kanema, M. “Temperature, Pore Pressure and Mass Variation of Concrete Subjected to High Temperature-Experimental and Numerical Discussion on Spalling Risk”, Cement and Concrete Research (2010), Vol. 40, pp. 477-487.

4 The Effect of Compressive Loading and Cement Type on the Fire Spalling of Concrete

In chapter 2, it is shown that the occurrence of fire spalling is influenced by various parameters, external compressive loading being one of them, which role is not well known in detail. Despite that, some investigations considered the effect of loading on fire spalling, there still seems to be a dearth of published data, and to date, there has been no detailed experimental investigation highlighting the effect of biaxial compressive loading on fire spalling. Since a great attention has been paid by some laboratories due to the evidence of the effect of compressive loading on the fire spalling of concrete (discussed in chapter 2), this becomes the centre of attention in the research work described herein.

Since there is no existing model which can predict the fire spalling behaviour of concrete due to the complex structure of a composite material, experimental studies appear necessary to investigate this phenomenon. Within this context, comprehensive experimental studies have been conducted to investigate the interaction between pore pressure and thermo-mechanical stresses in triggering spalling. The concrete specimens (cubic, prismatic, and mid-size concrete slabs) were heated according to the ISO 834-1 fire curve, while a constant uniaxial or biaxial compressive loading was applied. To do that, a test setup has been used at the Université de Pau et des Pays de l'Adour, SIAME to perform fire spalling tests on the cubic and prismatic specimens under different levels of uniaxial compressive loading. While in order to deeper investigate the role of membrane biaxial compressive loading and their levels on the fire spalling of concrete, an extensive experimental campaign has been conducted by means of the test setup developed at the Politecnico di Milano (Italy) [1]. The experimental campaign has been carried out within a research collaboration with the Centre Scientifique et Technique du Bâtiment (CSTB), France and the Université de Pau et des Pays de l'Adour, SIAME, France.

4.1 Apparatus and test procedures

4.1.1 Fire spalling test under uniaxial compressive loading

A small mobile gas furnace was designed (see Figure 4.1) to perform fire spalling tests under the uniaxial compression loading. The furnace has an opening of 200 mm x 200 mm, which can adapt the cubic and prismatic specimens to perform the fire spalling test. The furnace was equipped with three sheathed K type thermocouples placed at 40 mm (TC furnace bottom), 100 mm (TC furnace middle) and 160 mm (TC furnace top) from the bottom surface of the furnace opening and 20 mm from the heated surface of the concrete specimen. The furnace was made of expanded metal with 100 mm of ceramic wool on the outskirts. The shape of the pavilion of the

furnace greatly influences the temperature distribution in the furnace as well as in the concrete. Previously to this study, after manufacturing the furnace, several tuning tests were carried out. To be sure that the measure temperatures are homogenous in the concrete, a concrete cube specimen (200 x 200 x 200 mm^3) was heated which was instrumented with five thermocouples placed at the same depth (10 mm from the heated surface of concrete) in different places from one to another.

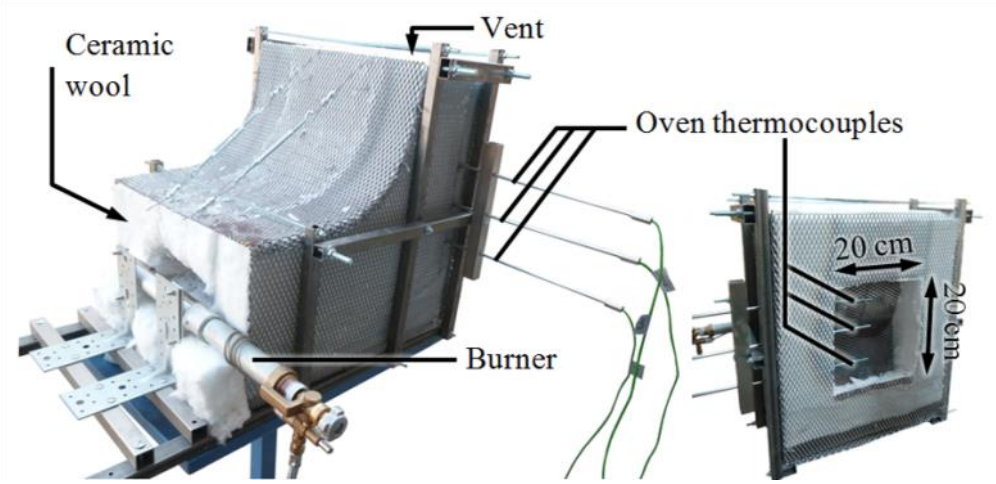

Figure 4.1: A mobile gas furnace for the fire test under uniaxial compressive loading.

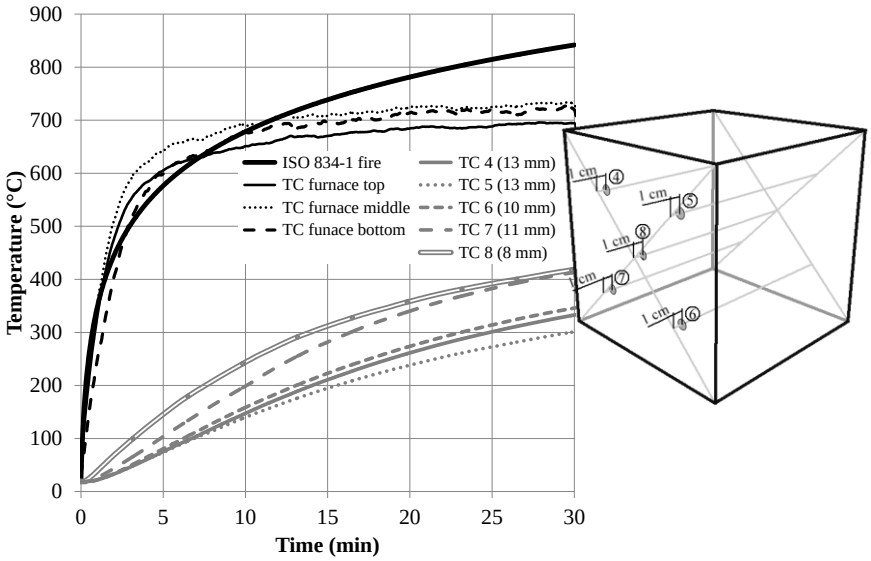

Figure 4.2: Evolution of temperature inside the furnace as well as in the concrete specimen.

Figure 4.2 presents the evolution of the temperature inside the furnace and in the concrete specimen. The heating curve was very similar to the ISO 834-1 fire curve during the first 2 minutes and then a little more severe. The temperature stabilises after about 10 minutes of fire. Quite satisfactory and uniformity of the temperatures were measured at three different places of

the furnace, see Figure 4.2. Even though all the thermocouples were in the same depth of 10 mm from the exposed surface of concrete, a little scatters have been observed from one thermocouple to another. These scatters were explained by the uncertainty of the thermocouple position due to technical offsets during installation. This was confirmed by making holes in the specimen after cooling. The actual measured depth of the thermocouples was, respectively, 13 mm for TC4 and TC5, 10 mm for TC6, 11 mm for TC7 and 8 mm for TC8, see Figure 4.2. The actual depth of the thermocouples was consistent with the measured temperatures. Indeed, TC8 was the closest to the exposed surface, which gives the highest temperatures. While TC4 and TC5 were the furthest away from the exposed surface of concrete, which gives lower temperatures than TC8. These measurements showed a satisfactory temperature homogeneity in the concrete specimen.

To perform the fire spalling test under a constant uniaxial compressive loading, the furnace was placed in front of the hydraulic press (see Figure 4.3 right) to heat the specimen according to ISO 834-1 fire curve, while simultaneously being subjected to a constant uniaxial vertical compressive loading. The specimens (cube: 200 x 200 x 200 mm^3 and prismatic: 200 x 200 x 100 mm^3) were set in front of the furnace between two high strength polypropylene fibres concrete cubes (same size than the fire test cubic specimen), see Figure 4.3 left, to avoid the press temperature rise and to ensure homogeneous mechanical loading during heating.

Figure 4.3: Tested sample in the hydraulic press (left) and complete test setup (right).

Before fire test, all the concrete specimens were well grinded to obtain two faces (upper and lower faces) parallel and plane for uniform load distribution on the concrete specimens during loading. The specimens were heated by means of a natural gas burner for 30 min (since the spalling phenomena occurring in the first thirty minutes of heating) on one full face (perpendicular to the uniaxial compressive loading direction) following a temperature curve close to the ISO 834-1 fire curve, while the lateral sides of the specimens were insulated by 10 mm thick rock wool in order to avoid the cooling of lateral faces of the specimen.

Six different levels of uniaxial compressive stress (0, 4, 8, 12, 16 and 20 MPa) have been investigated on cubic specimens (200 x 200 x 200 mm^3). While three different loading-unloading cycles have been carried out on the prismatic specimens (200 x 200 x 100 mm^3, see Figure 4.4).

Since the first spalling event occurred within 5 min of fire in the cube test, the loads were changed starting from 5 min of fire. In the Case 1 (see Figure 4.4), the specimens were loaded at 20 MPa up to 5 min of fire, then the load was completely released (0 MPa) within a minute without bothering fire and then continue up to the end of the fire test. While in the Case 2, the specimens were heated without loading up to 5 min of fire, then a compressive loading of 20 MPa was applied (taken at around a minute to reach the target load) and then the load was maintained constant for the rest of 25 min of the fire test. Concerning the Case 3, the specimens were loaded at 8 MPa for 5 min of fire, then the load was increased to 20 MPa within a minute and then the load was maintained constant for the rest of the fire test. The summary of the experimental program for cubic and prismatic specimen tests are presented in Table 4.1 and 4.2.

Table 4.1: Global view of the experimental program for cubic specimens.

Applied load [MPa]	0	4	8	12	16	20
B40-II	3	1	2	2	1	2
B40-III	3	1	1	2	1	2

Table 4.2: Summary of the loading-unloading cycle test program for prismatic specimens

Loading condition	Case 1	Case 2	Case 3
B40-II	2	2	2
B40-III	2	2	2

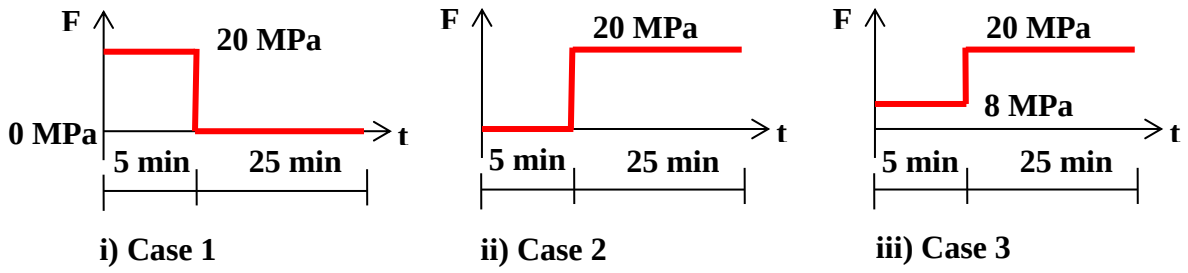

Figure 4.4: Loading-unloading cycles of prismatic specimens

During the fire test, the position of the jack was constant, hence induced an increase of the loading during heating (about 5% at the end of the fire test) due to the thermal dilation of the concrete specimen. After the fire test, the height profile of the spalled area was measured at room temperature using a sliding calliper. The spalling depths were measured in a 2-dimensional grid with a spacing of 20 mm.

In order to gain a deeper understanding of the role played by compressive loading on the build-up and magnitude of pore pressure during the ISO 834-1 fire test, 9 concrete cubes (4 for

B40-II and 5 for B40-III, see Table 4.3) were instrumented with four pressure gauges placed at 10, 20, 30 and 50 mm depths from the exposed surface of concrete specimens for simultaneous pressure (P) and temperature (T) measurements (see Figure 4.5). The measurement of the pore pressure and the temperature was performed according to the system described by Kalifa et al. 2000 [2].

Table 4.3: Global view of the experimental program for pore pressure and temperature measurements under uniaxial loading and unloading conditions (/ = no test).

Applied load [MPa]	0	8	16	Total
B40-II	2	/	2	4
B40-III	2	1	2	5

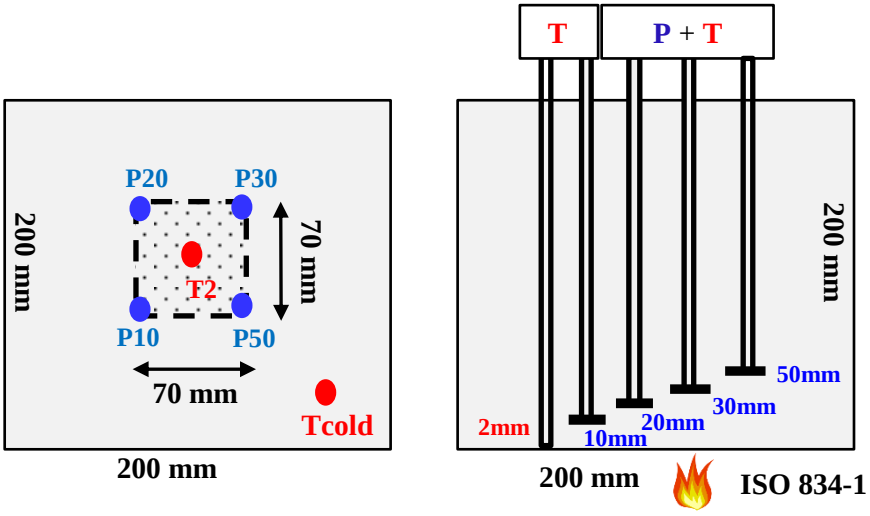

Figure 4.5: Cube specimen (left) and measuring the position of pressure and temperature (right).

4.1.2 Fire spalling test in the unloaded condition

Fire spalling tests were conducted on 4 mid-size concrete slabs (1 of B40-II and 3 of B40-III) with nominal dimensions of 700 x 600 x 150 mm^3. Among the 4 slabs, 3 slabs (1 of B40-II and 2 of B40-III) were heated for 60 minutes at the bottom surface of the slabs according to the ISO 834-1 fire curve (see Figure 4.6a). The third slab of B40-III concrete was heated slowly and then exposed to a thermal shock to investigate the effect of a sudden rise of temperature on the spalling of concrete. In the first part of the test, the ISO fire furnace was used by voluntarily reducing the power of the burners. The mean temperature rate was close to 6 °C/min with a maximum value of 15 °C/min. Then, a thermal shock was applied before reaching the pore pressure peak (after at around 60 min of slow heating) by increasing the power with a heating rate of 80 °C/min. The temperature increased from 400 °C to 800 °C in less than 5 min (see Figure 4.6b).

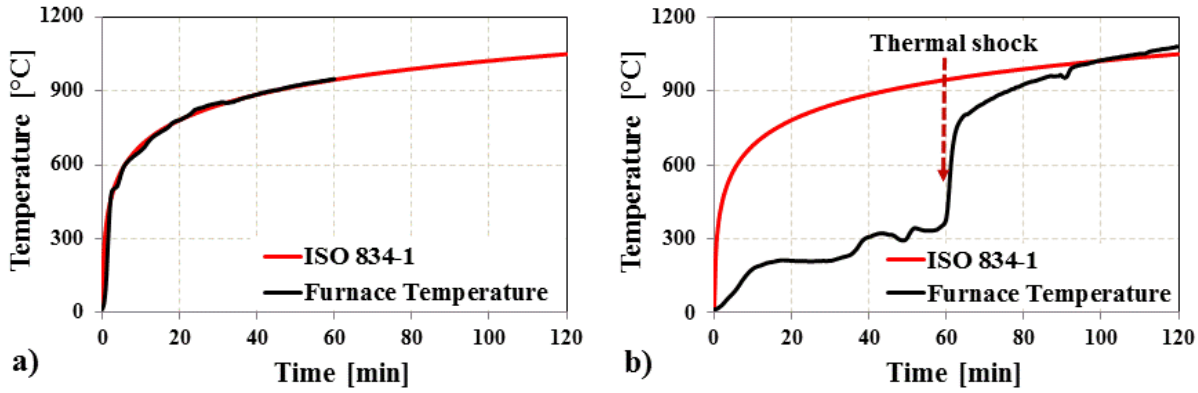

Figure 4.6: Evolution of furnace temperature during ISO 834-1 fire (a) and slow heating with thermal shock (b) test.

The concrete slabs were placed on the horizontal gas-burners furnace (feeding gas: propane) and exposed to fire on one single side only. The area of the specimen exposed to the fire was approximately 600 x 420 mm^2. The slabs were simply laid on two of their sides; the other two sides were not in contact with the furnace. The lateral sides of the slabs were insulated by rock wool (thickness ≈ 10 mm) in order to avoid the lateral heating. Temperature measurement inside the furnace was carried out with 2 thermoplates, which was placed inside the furnace, at 100 mm from the exposed surface of the slab. During the fire tests, both pore pressure and temperature were monitored at 4 different depths of 10, 20, 30 and 40 mm from the heated surface. The measurement of the pore pressure and the temperature was performed according to the system described by Kalifa et al. 2000 [2].

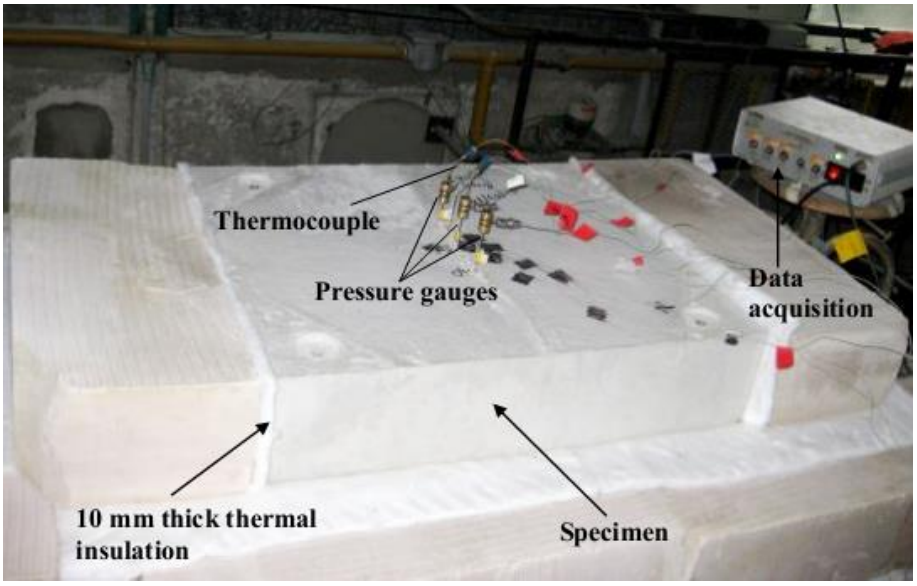

Figure 4.7: Concrete slab with the pressure-temperature measuring device before the fire test.

It is noted that the aim of this experimental campaign was to investigate pure heat-induced concrete spalling (i.e. no effect of external loading during heating), hence the specimens were not mechanically loaded or no restraint during the fire tests (free to expand during the fire test).

4.1.3 Fire spalling test under biaxial compressive loading

To investigate the interaction between pore pressure and thermo-mechanical stresses in triggering spalling, a joint research project was conducted by the Politecnico di Milano, Italy, the Centre Scientifique et Technique du Bâtiment (CSTB), France, and the University of Pau and Pays de l'Adour, SIAME, France. The fire spalling tests under biaxial compressive loading were carried out at the Politecnico di Milano, Italy. Fifteen mid-size unreinforced concrete slabs (800 x 800 x 100 mm^3) were subjected to ISO 834-1 fire curve at different levels of biaxial membrane compressive loading (see Figure 4.8). The concrete slabs were placed on top of the horizontal furnace (see Figure 4.8e), within a loading system consisting of a welded steel restraining frame fitted with hydraulic jacks. The thrust was exerted via spherical heads and thick steel plates working as load dividers. The spherical heads allow following the rotation of the slab edges induced by thermal curvature (see Figure 4.8g). In order to limit the temperature in the hydraulic jacks, only the central part of the slab (600 x 600 mm^2) was heated to keep the external concrete rim (100 mm from each side) colder. To reduce the confining effect exerted by this colder rim, 16 radial cuts (around 5 mm thick) were performed, aimed at breaking its mechanical continuity (see Figure 4.8a). The radial cuts were obtained by installing small insulating panels in the mould before casting.

The furnace was heated by a propane burner with a control system able to follow the ISO 834-1 fire curve. A constant biaxial compressive load was applied before heating (parallel to the heated face of the slab, 300 mm wide and 100 mm thickness on each side) with 8 hydraulic jacks (2 per side, see Figure 4.8c-d, g) and then the load was kept constant throughout the fire test. Seven different levels of biaxial compressive stress (0, 0.5, 0.75, 1.5, 3, 5 and 10 MPa) have been investigated on both concretes. Two series of tests have been carried out in 2015 and 2016. The summary of the experimental program is given in Table 4.4. In order to compare the amount of fire spalling at different levels of biaxial compressive loading, tests were stopped after 30 minutes of fire. However, the collapse of the slab occurred for 3 slabs loaded at 5 and 10 MPa before 30 minutes. Tests were then stopped.

Table 4.4: Summary of the experimental program for the biaxial fire spalling test

Applied stress [MPa]		0	0.5	0.75	1.5	3	5	10
2015	B40-II	1	1	/	/	/	1	1
	B40-III	/	1	/	/	/	1	1
2016	B40-II	1	/	1	1	1	/	/
	B40-III	1	/	1	1	1	/	/

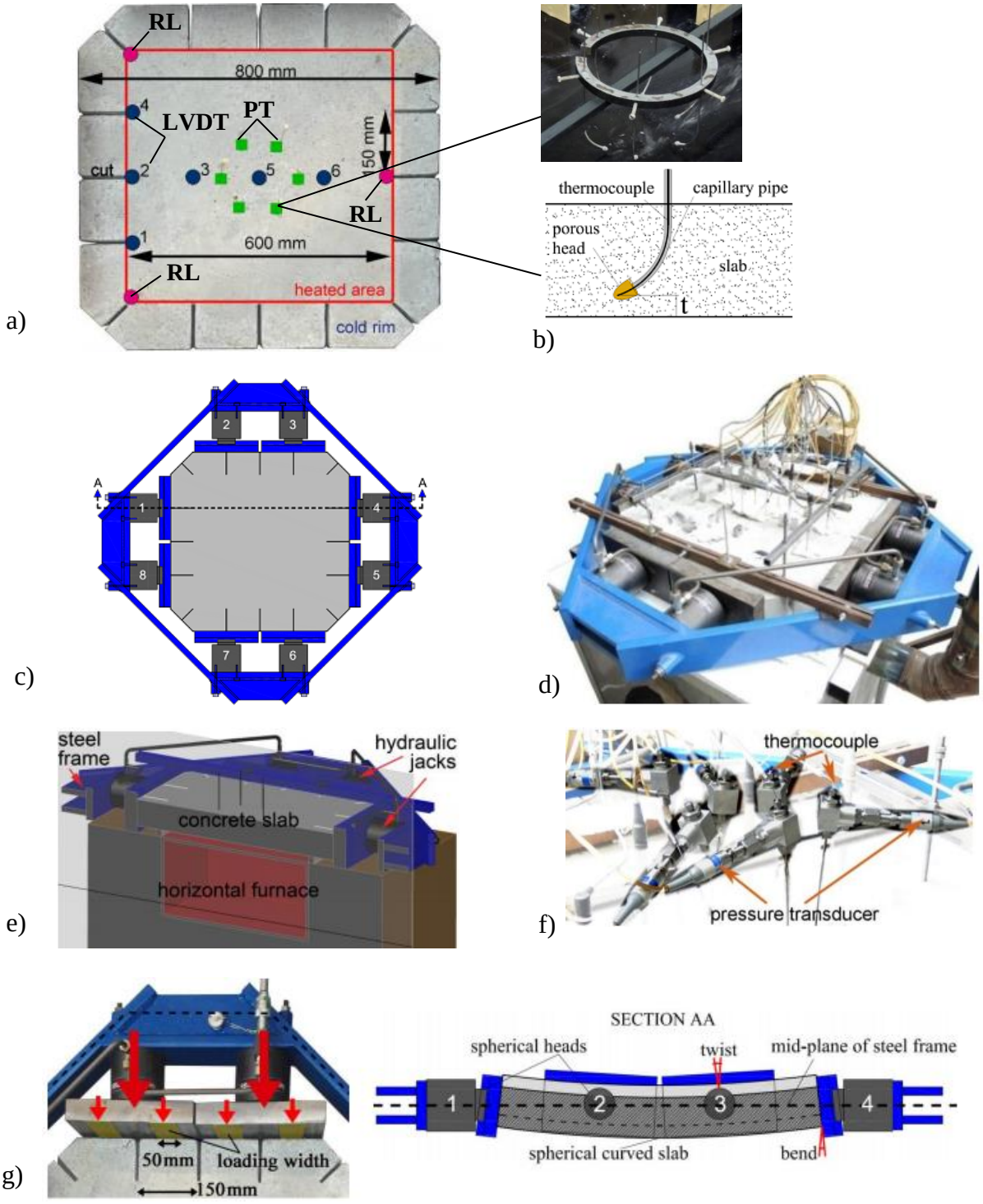

Figure 4.8: a-b) Concrete slab and measurement points of pressure-temperature and displacements, c-d) concrete slab within the loading system, e) section of the specimen positioned on the horizontal furnace, f) pressure-temperature sensors, and g) concrete slab within the loading system and section AA (see Fig. 4.8c) in deformed configuration. (PT=pressure–temperature sensors, LVDT= displacement transducers measuring the deflection, RL= 3 rigid legs of the LVDT-holding frame).

The specimens were instrumented with six pressure gauges placed at 6 different depths of 5, 10, 20, 30, 40 and 50 mm from the exposed surface of the slab for simultaneous pressure and temperature measurements (see Figure 4.8a-b). The measurement of the gas pore pressure and the temperature were monitored according to the system described by Felicetti et al. 2017 [3]. During the tests, the flexural behaviour was monitored through 6 Linear Voltage Displacement Transducers (LVDT) placed on one centre line and on one edge of the slab to measure the out of plane displacements at the top cold face. A more detailed description of the test set-up and the test method is given by Lo Monte et al. 2017 [1].

However, during the tests, special attention was paid to make visual observations of the exposed surface of the slab (i.e. spalling) through the opening of the furnace, as well as crack propagation of the top cold surface. The video was recorded continuously by an ordinary digital camera placed in front of the oven window, while the time and progress of spalling were documented by hearing the sound. Also, after the completion of fire tests, post-test observations were made to analyse the nature of spalling, cracking, and failure pattern of the specimen. After each test, the thickness profile of the spalled area was measured at room temperature by using a laser profilometer. Mean, maximum spalling depths and volume of the spalling were determined.

4.2 Experimental results and discussion

4.2.1 Fire spalling test under uniaxial compressive loading

4.2.1.1 Effect of uniaxial compressive loading and cement type on fire spalling

Figure 4.9 presents the mean spalling depth with some images of the heated faces of the cube specimens as a function of applied uniaxial compressive stress, while Table 4.5 presents the maximum spalling depth and spalling volume of all cubic specimens. A quite good repeatability of the tests has been observed for B40-III, while the repeatability was also observed for B40-II, except the results corresponding to 8 MPa that are rather scattered. The time of the first spall was in the range from 2.5 to 3.5 minutes of fire and the spalling was stopped at around 10 min of fire. The spalling events increased with the increased applied compressive stress. The oven temperature at the onset of spalling was in the range from 550 to 600 °C, whereas the measured temperature at the depth of 2 mm from the exposed surface was in the range from 90 to130 °C. Explosive spalling was observed in one of the B40-II concrete specimen loaded at 20 MPa at around 7 minutes of fire and the process involved almost the whole heated area of the specimen.

In Figure 4.9, on the one hand, no significant change in the measured spalling depths was observed from 0 to 4 MPa for B40-II and no spalling for B40-III. This result shows that a relatively low compressive stress does not significantly change the spalling depths of concrete, since the applied compressive stress was 12 times lower than the compressive strength of concrete (51 MPa at the day of the fire test). On the other hand, beyond 4 MPa, an increasing trend of spalling depths was observed with the increasing uniaxial compressive stress, except one

of the test result corresponding to B40-II subjected to 8 MPa exhibited a significantly higher spalling depth.

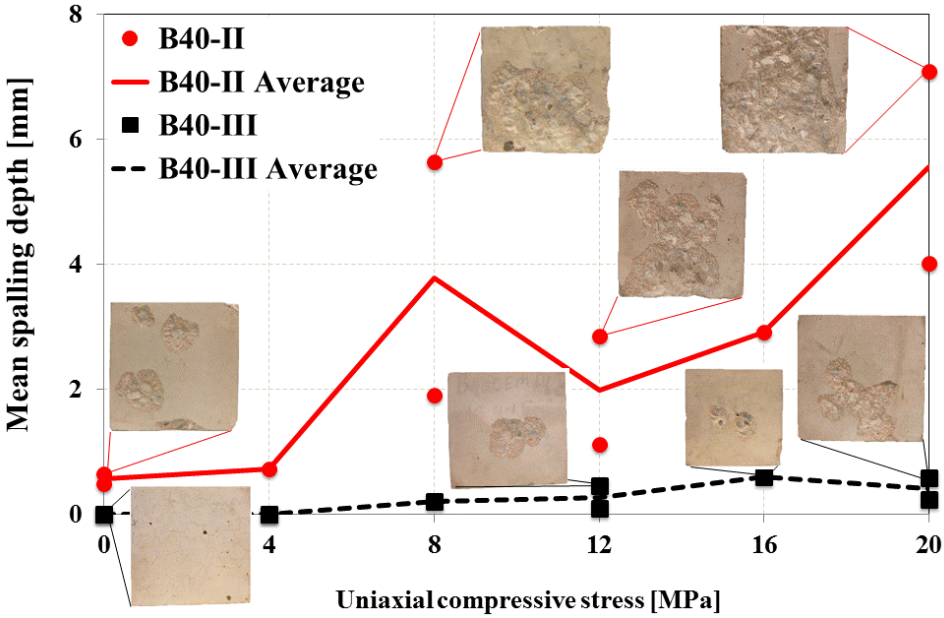

Figure 4.9: Mean spalling depth of B40-II and B40-III concrete cube specimens as a function of uniaxial compressive stress.

Table 4.5: Maximum spalling depth and spalling volume of B40-II and B40-III concrete cube specimens heated under different levels of uniaxial compressive stress (/ = no test)

	Load [MPa]	0	4	8	12	16	20
B40-II	Maximum depth [mm]	6	13	15	11	17	15
		7	/	13	14	/	18
	Volume [cm^3]	26	29	226	114	117	284
		20	/	76	45	/	161
B40-III	Maximum depth [mm]	0	0	3	2	4	5
		0	0	/	4	/	3
	Volume [cm^3]	0	0	8	4	24	23
		0	0	/	18	/	10

When the concrete specimens are heated under uniaxial compressive loading, the opening of cracks parallel to the loading direction increases (see Figure 5.13 in chapter 5), while it decreases for the cracks that are perpendicular to the loading direction (see Figure 5.12c-d, i.e. lower permeability in the direction perpendicular to the heated face). This tendency increases with the increasing applied uniaxial compressive loading during heating. In chapter 3, it has been shown that the radial gas permeability (perpendicular to the uniaxial load) decreases when uniaxial compressive stress increases due to the closing of cracks perpendicular to the load, see Figure

3.22. Similar results were found in the literature [4]. As a consequence, compression load affects the moisture transport inside the concrete by decreasing permeability which induces faster build-up and higher value of pore pressure (see Figures 4.14 and 4.15, i.e. higher tensile stress in the direction perpendicular to the heated surface). This higher pore pressure of the loaded specimen with the combination of stresses due to restrained strains and external load (see Figure 5.10 in chapter 5) increases the risk of fire spalling, which could be both violent (see images at 8 and 20 MPa in Figure 4.9) and non-violent. A more detailed description of the effect of loading on fire spalling is given in section 4.2.3 and chapter 6 as well.

When concrete specimens are heated in unloaded condition, multiple cracks could occur inside the concrete specimens such as orthogonal cracks in the concrete core and surface cracks parallel to the exposed face in the hot layers. Hence, the pore pressure and stresses should be lower [5-6] in the unloaded tests than the loaded tests. During the fire tests, it was found that the appearance of water from the side of the specimens was more evident in the unloaded tests than in the loaded tests, since the cracks are free to open in all directions, while the cracks are restricted to open in the perpendicular to the loading direction due to the presence of uniaxial compressive loading. As cracks were formed, a significant amounts of vapour and liquid water migrated out from the lateral side of the specimens, which reduces the build-up of pore pressure by favouring the moisture transport (comparatively low pore pressures were measured in the unloaded tests than loaded tests, see Figures 4.14 and 4.15), resulting in less risk of fire spalling in the unloaded specimens.

An important observation from Figure 4.9 and Table 4.5 is that the B40-II (3% of slag) exhibited significantly higher spalling than the B40-III (43% of slag) for all the applied values of compressive stress. At no load and low load tests (0 to 4 MPa), no spalling was observed for B40-III, while few spalling was measured for B40-II at both loading conditions. Maximum spalling depths at unloaded (0 MPa) and loaded (20 MPa) tests are, respectively, 7 mm and 18 mm for B40-II and 0 mm and 5 mm for B40-III, while spalling volume is 26 cm^3 and 284 cm^3 for B40-II and 0 cm^3 and 23 cm^3 for B40-III, respectively, see Table 4.5. This observation could be attributed to the lower permeability and porosity of B40-II at high temperatures than the B40-III (see Figures 3.15, 3.17, 3.20 and 3.22 in chapter 3), which prevents the passage of water vapour inside the concrete, as a result, steep build-up and higher value of pore pressure (see Figures 4.14 and 4.15), which enhance the risk of fire spalling.

It is noteworthy that most of the spalling occurred preferentially in front of large aggregates, see some examples in Figure 4.10. A similar observation was found in most of the specimens. This behaviour could be due to several phenomena, such as lower permeability of aggregates compared to the cement paste, the different expansion coefficient of cement paste and aggregates. The lower aggregates permeability could lead to higher pore pressures near the coarse aggregate in the vicinity of the heated surface. The thermal strain mismatch between cement paste and aggregates induces the development of cracks at the interface between cement paste and aggregates. This damage could involve a localisation of spalling in front of large aggregates.

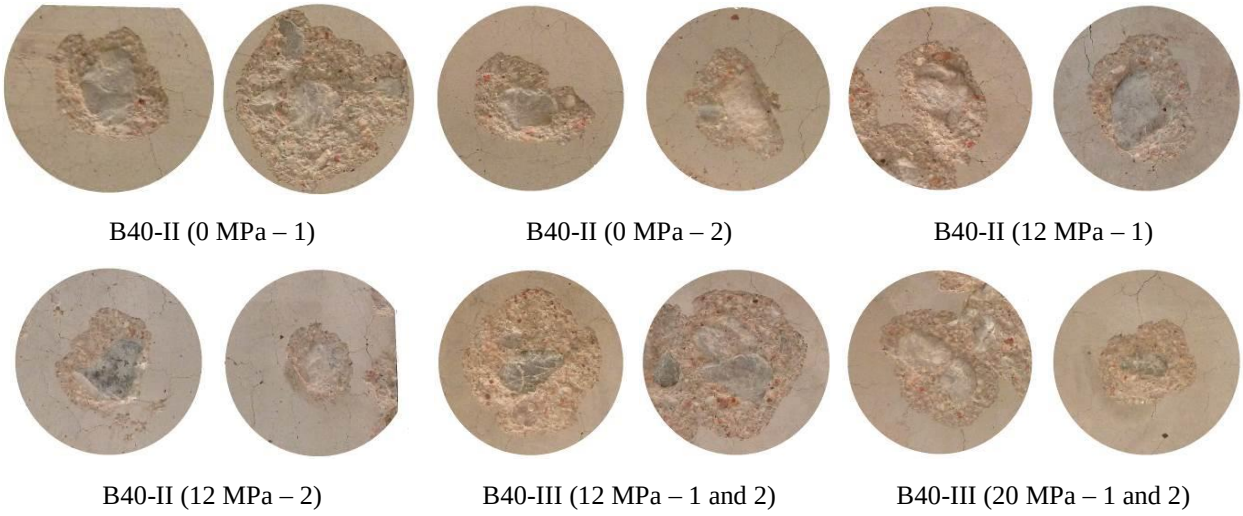

Figure 4.10: Images of several spalled areas (6.5 cm diameter) of the tested cube specimens.

In order to study the effect of variable loading during the fire, three different compressive loading-unloading cycles (see Figure 4.4) have been investigated on the prismatic specimens (200 x 200 x 100 mm^3). Figures 4.11 and 4.12 present the maximum spalling depth, spalling volume, and exposed faces of prismatic samples, respectively.

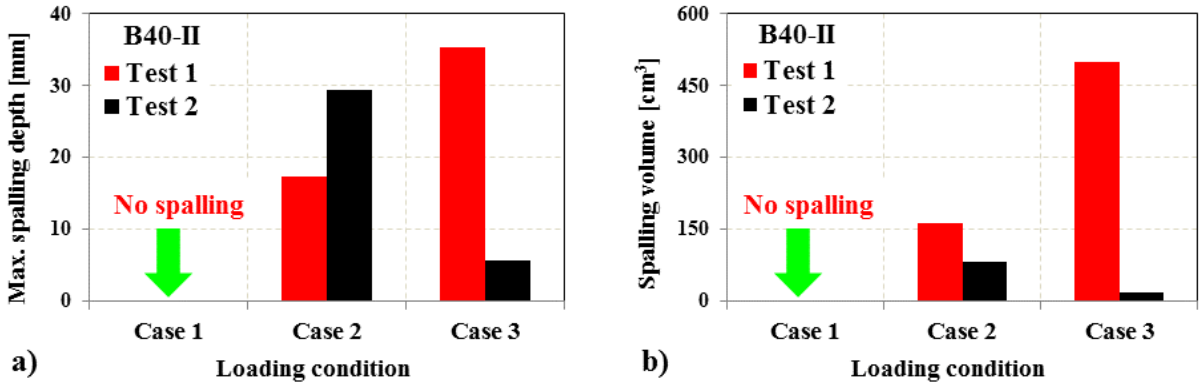

Figure 4.11: Maximum spalling depth (a) and spalling volume (b) of the prismatic specimens loaded under three different loading-unloading conditions.

It is important to note that no spalling was observed in B40-III specimens at three different loading-unloading cycles (Case 1, 2 and 3), except a minor spalling was observed in one of the B40-III specimen heated under load Case 2 (see Figure 4.12e). In B40-II, none of the specimens spalled in the Case 1, while a significant amount of spalling has been observed in the Case 2 (see Figure 4.11 and Figure 4.12b). The spalling occurred 1 min after the stabilisation of the load of 20 MPa (i.e. spalling occurred at around 6 min of fire). Probably, during 5 min of heating in the unloaded condition, the cracks (due to thermal incompatibility between the cement pastes and aggregates [7], and thermal stresses induced by the thermal gradients) are free to open, while

upon loading, a significant decrease of permeability can take place due to the closing of microcracks and cracks, which increase not only the pore pressure but also stresses (additional stress coming from the external uniaxial compressive stress), as a results higher risk of spalling.

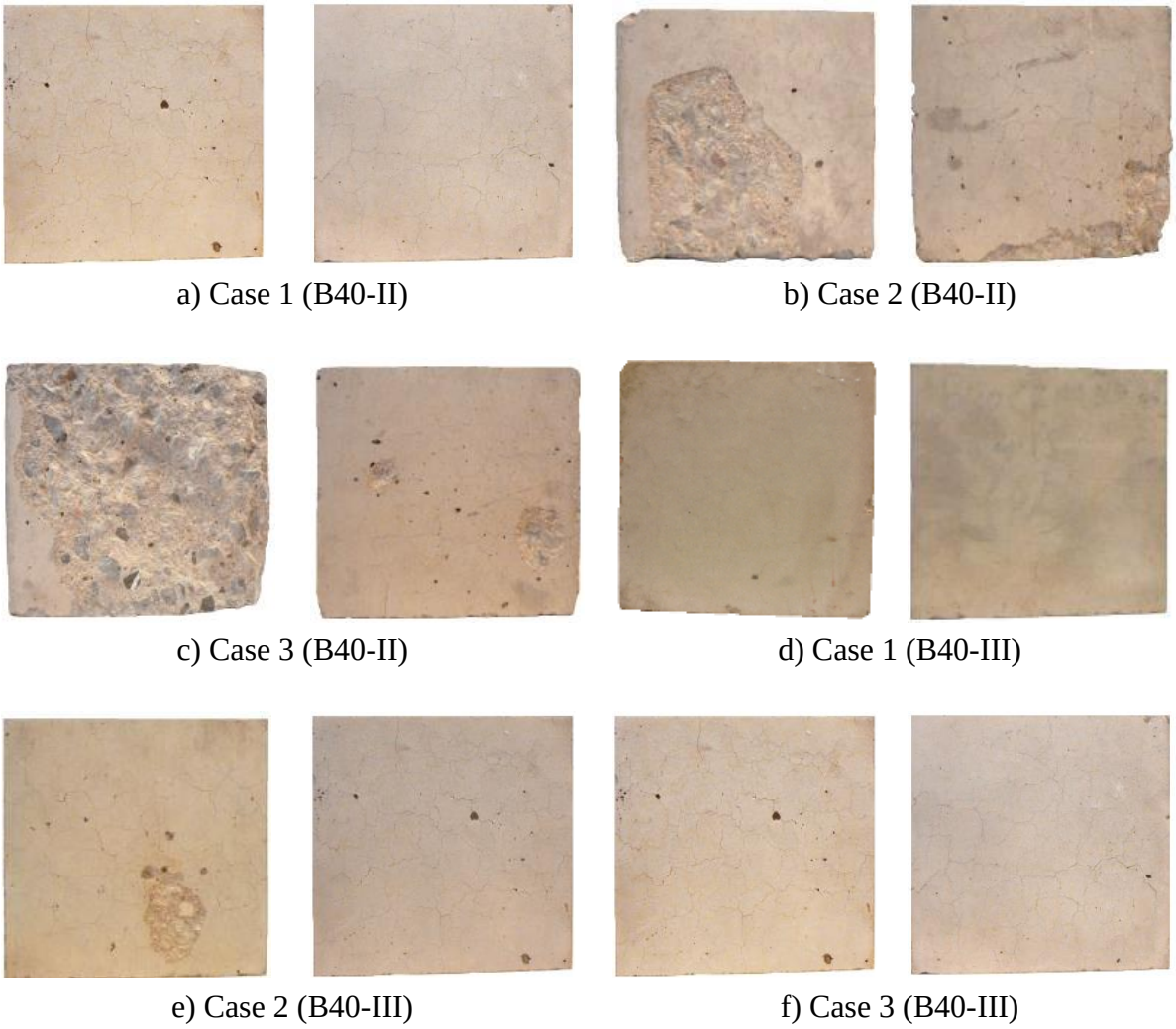

a) Case 1 (B40-II) b) Case 2 (B40-II)

c) Case 3 (B40-II) d) Case 1 (B40-III)

e) Case 2 (B40-III) f) Case 3 (B40-III)

Figure 4.12: Exposed face of the B40-II and B40-III specimens heated under loading-unloading.

In Case 3, explosive spalling was observed in the first specimen, while the second specimen did not spall (see Figure 4.12c). The exact reason for this behaviour is not known. The spalling occurred at around 3 min after reaching the target load (20 MPa). Among all the tests (cubic and prismatic specimens), highest spalling volume (≈ 500 cm^3) and highest maximum spalling depth (35.3 mm) has been observed in this loading condition (see Figures 4.11 and 4.12c). It is worth noting that the spalling process began with a severe single event which involved all the heated area of the specimen. Interestingly, in this loading condition, the spalling occurred after a relatively long exposure of heating (at around 8 min of fire from the start of the test) with a bigger mass, while a relatively early stage (within 2.5-3 min) with several events and relatively smaller size of the spalled fragments was observed in the cubic specimen tests. This behaviour

could be associated with the fact that longer heating period results in higher amounts of accumulated thermal energy, which predictably results in more energy being released upon spalling.

4.2.1.2 Thermal response and build-up of pore pressure of the cubes

A typical example of the temperature development at different depths of B40-II and B40-III concrete cube specimens exposed to ISO 834-1 fire curve in loaded (16 MPa) and unloaded (0 MPa) conditions are given in Figure 4.13. No significant change in the development of temperatures was observed in both concretes exposed to ISO 834-1 fire curve at loaded and unloaded conditions, except a bit scatter at 10 mm depth of the B40-II specimen. This scatter may be partly explained by the uncertainty of the thermocouple position due to technical offset during installation. For almost each measuring depths, a temperature plateau can be seen in range 100 to 180 °C in both concretes (onset of water vaporisation which consumes a significant amount of energy). Similar behaviour has been observed in the PT tests, see section 3.3.3 in chapter 3. A decreasing trend of temperature rise can be seen in this temperature plateau phase of both concretes. This highlights that the presence of moisture has a significant effect on the temperature development of concrete. The length of the temperature plateau increases with the increased amount of available moisture in that depth of concrete. As an example, the plateau can be seen clearly at the depth of 20 mm of both concretes, see Figure 4.13.

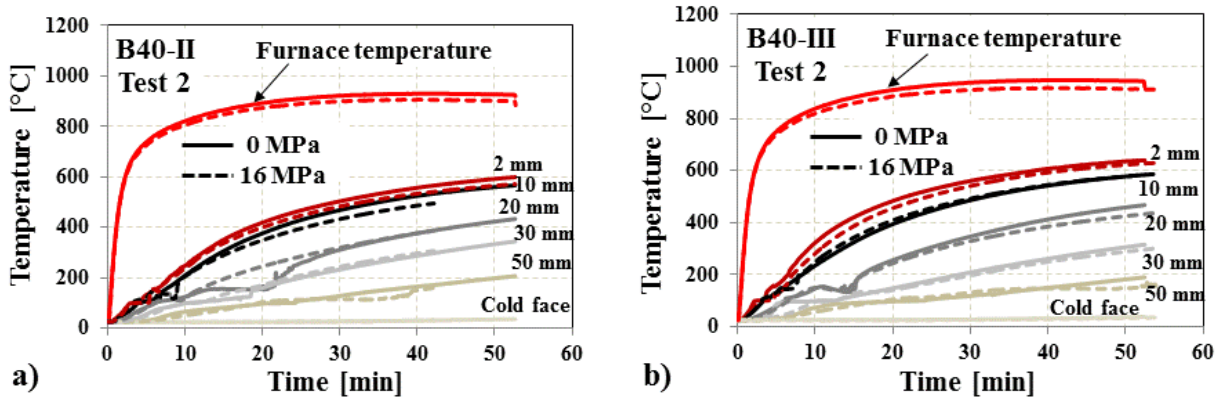

Figure 4.13: Development of temperature inside the B40-II and B40-III concrete cube specimens exposed to ISO 834-1 fire curve at loaded (16 MPa) and unloaded (0 MPa) conditions.

Figure 4.14 presents the development of pore pressure as a function of time of B40-II and B40-III concrete cube specimens exposed to ISO 834-1 fire curve. It can be seen that the development of pore pressure seems to be different for the specimens in loaded (16 MPa) and unloaded (0 MPa) conditions. In the loaded tests, steepest build-up of pore pressure was observed, while a slow rise of pore pressure was measured in the unloaded tests of both concretes. Maximum pore pressures determined during loaded and unloaded tests among all the depths are, respectively, 1.1 MPa and 0.45 MPa for B40-II and 0.76 MPa and 0.51 MPa for B40-III. From these values, it seems that there is an effect of compressive loading on the permeability

of concrete during heating. Since the permeability of concrete was identified as one of the key parameters controlling internal fluid transfer, which influences the build-up and the magnitude of the pore pressure within the concrete structure and then influence the risk of fire spalling.

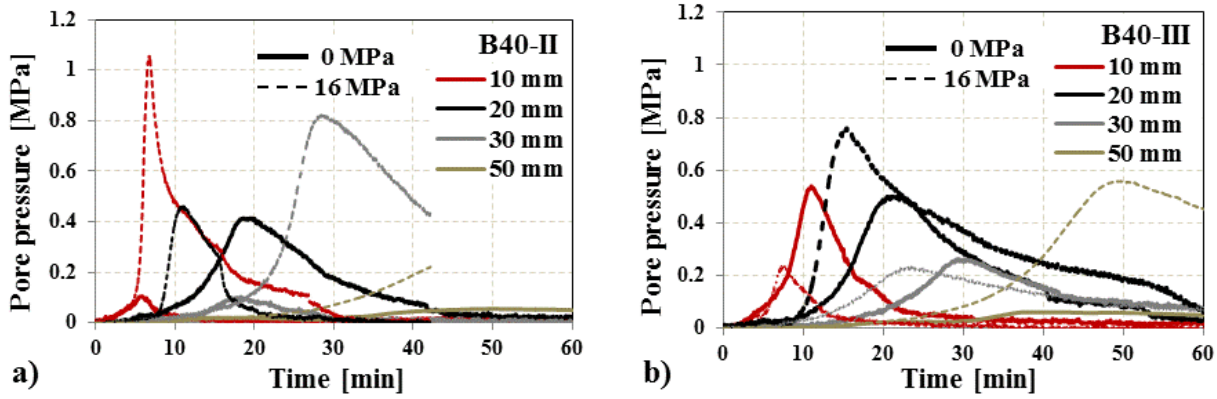

Figure 4.14: Development of pore pressure inside the B40-II and B40-III concrete cube specimens exposed to ISO 834-1 fire at loaded (16 MPa) and unloaded (0 MPa) conditions.

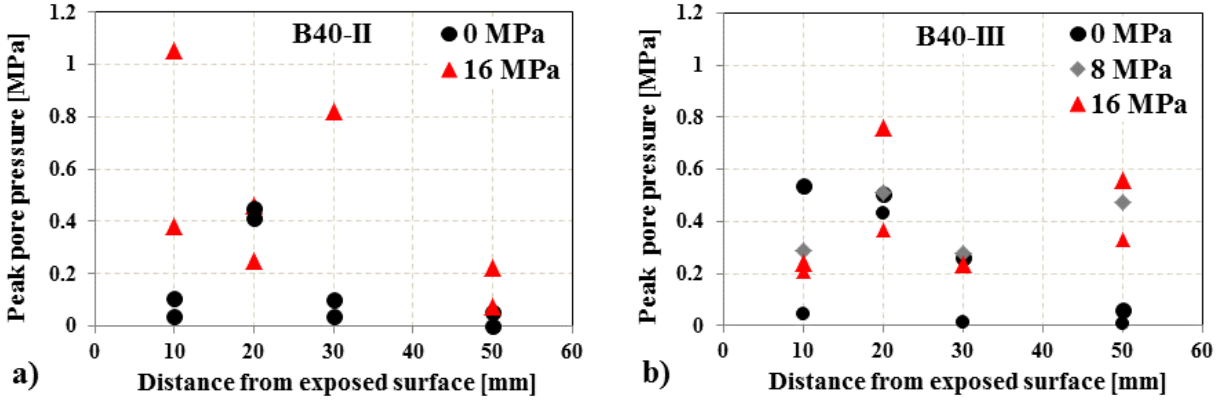

Figure 4.15: Maximum pore pressure measured in B40-II (a) and B40-III (b) concrete cube specimens exposed to ISO 834-1 fire at the loaded and unloaded condition.

The permeability of concrete increase is favoured by the thermal incompatibility between cement paste and aggregates [7] and thermal gradients. As a result, vapour and liquid water can escape from the specimen in the unloaded conditions, since the cracks are free to open in all directions in the unloaded tests due to the absence of compressive loading, thus significantly affecting the build-up of pore pressure. On the contrary, when the specimens are heated under a constant uniaxial compressive loading, the width of cracks parallel to the compressive loading direction increases, while it decreases for the cracks that are perpendicular to the compressive loading direction. Hence, it decreases the permeability in the direction perpendicular to the heated face of concrete, as a consequence, the presence of compressive loading could limit the moisture transport inside the concrete by decreasing permeability which induces faster build-up and higher value of pore pressure (see Figures 4.14 and 4.15). The evidence of decreasing

permeability with the increasing compressive loading was found in chapter 3, see Figures 3.17 and 3.22.

Similar results were found in the literature that the permeability of concrete during heating under uniaxial compressive loading (stress levels lower than 80% of the strength) is smaller than the permeability measured after unloading [4]. Since there is no additional connectivity of pores created, this slight decrease in permeability can be attributed to the effect of the applied compressive stress on the concrete specimen, i.e. the volumetric behaviour of the specimen is strictly contracting [4]. Likewise, Lun and Lackner 2013 [8] tested the gas permeability of concrete under thermal load (up to 350 °C) and uniaxial compressive stress (5, 10, 15 and 20 MPa). A reduction of the permeability was observed during heating and loading at 5 and 10 MPa. Lu and Fontana 2015 [9] thermo-hydro model have shown that the permeability decreased slightly with the compressive stress. Probably this is the reason why a steepest and higher pore pressure was measured close to the heated face (see Figure 4.14a), as well as a sudden decline in pore pressure, was observed, which could be due to spalling of the surrounding material close to the pore pressure measurement points. Once spalling occurred, the pore pressure could suddenly be released through the spalling cracks due to increased permeability which could affect the build-up of pore pressure in the next closest depth of the concrete specimen, probably this is the reason why the lower pore pressure was measured at the depth of 20 mm of B40-II, see Figure 4.14a.

4.2.2 Fire spalling tests on the unloaded slabs

It is important to note that no spalling was observed in all 3 slab specimens during 60 min of the ISO 834-1 test in the unloaded condition. These results are in good agreement with the fire spalling tests carried out by Carré et al. 2013 [10], none of the B40-II (named as B40 in the paper) slabs spalled in the unloaded condition. During heating, some long vertical cracks (at around 15 to 20 minutes of fire, see Figure 4.16 right) along the longer length (i.e. the sides which were laid on the furnace) of the specimens, as well as a more distributed network of fine cracks on the exposed side after cooling, were observed. As cracks were formed in the slabs, significant amounts of vapour and liquid water migrated out of the specimens on the lateral side during the fire test. After around 34 minutes of fire, water started to appear on the cold surface of the slab through the outer periphery of the pressure gauge tubes. Probably, these cracks somehow relieve the thermal stresses in the surrounding materials [5-6] as well as the release of vapour and liquid water, which reduces the build-up of pore pressure (comparatively low pore pressure was observed (see Figure 4.17c) than PT tests in chapter 3). As a result, low risk of fire spalling. This highlights the internal cracking is an important factor in the fire spalling behaviour of concrete, as we have seen in the rapid heating of PT (pressure and temperature) tests.

Figure 4.16: Exposed face (left); cracking and released of hot moisture (right) during the test.

The thermal response and build-up of pore pressure of B40-II and B40-III concrete specimens exposed to ISO 834-1 fire curve are presented in Figure 4.17. Almost same development of temperatures has been observed in both concretes. A temperature plateau can be seen in the range from 100 to 160 °C in both concretes, as we have seen in the PT and uniaxial fire spalling tests. Interestingly, in most of the depths, the steepest pore pressure rise occurred almost at the beginning of this temperature plateau, while the peak pore pressure was achieved at the end of this plateau, an example can be seen in Figure 4.17b. During this plateau phase, the increased production and release of vapour leads to drying out of the concrete specimens. The temperature increased again once all the moisture evaporates and the concrete becomes dry.

Figure 4.17c presents the development of pore pressure as a function of time of B40-II and B40-III concrete specimens exposed to ISO 834-1 fire curve. The comparison of the pore pressures of B40-II and B40-III in ISO 834-1 fire tests and PT tests (moderate heating: 600 °C in 5 minutes, see Figures 3.14 and 3.26c-d in chapter 3) shows that measured values are higher in the second type of tests. Maximum pore pressure determined during the ISO 834-1 fire tests and PT tests were, respectively, 0.26 MPa and 1.51 MPa for B40-II and 0.35 MPa and 0.73 MPa for B40-III. Similar value has been obtained when the cubic specimens were exposed to ISO 834-1 fire in the unloaded conditions. The maximum pore pressures of B40-II and B40-III cubic specimens were 0.45 MPa and 0.51 MPa respectively. These results are in good agreement with the observations made by Mindeguia et al. 2015 [11]. They are attributed to the higher thermal damage caused by ISO 834-1 fire, which reduces the build-up of pore pressure by favouring the moisture transport.

It can be observed that measured pore pressures in B40-II and B40-III followed the P_{sv} curve during the ascending branch, except one measured pore pressure (at 30 mm depth in B40-II) is slightly higher than the saturation vapour pressure curve (see Figure 4.17d). This overpressure was also observed in the PT tests. As explained before that this behaviour could be attributed to the partial pressure of the dry air enclosed within the porous network [2, 12].

After being heated 60 minutes at a slow heating rate, one B40-III slab was exposed to a thermal shock before pore pressure reached their maximum value (see Figure 4.18). This thermal

shock did not induce spalling of the B40-III. As soon as the thermal shock was applied, a sudden increase followed by a sharp decrease in pore pressure was found in all depths of B40-III concrete specimen (see Figure 4.18b). When the thermal shock was applied, more surface cracks on the exposed surface of the specimen as well as large vertical cracks on the side faces were observed. The cracks allow significant amounts of vapour and liquid water to be drained out from the specimen, which avoids the risk of fire spalling.

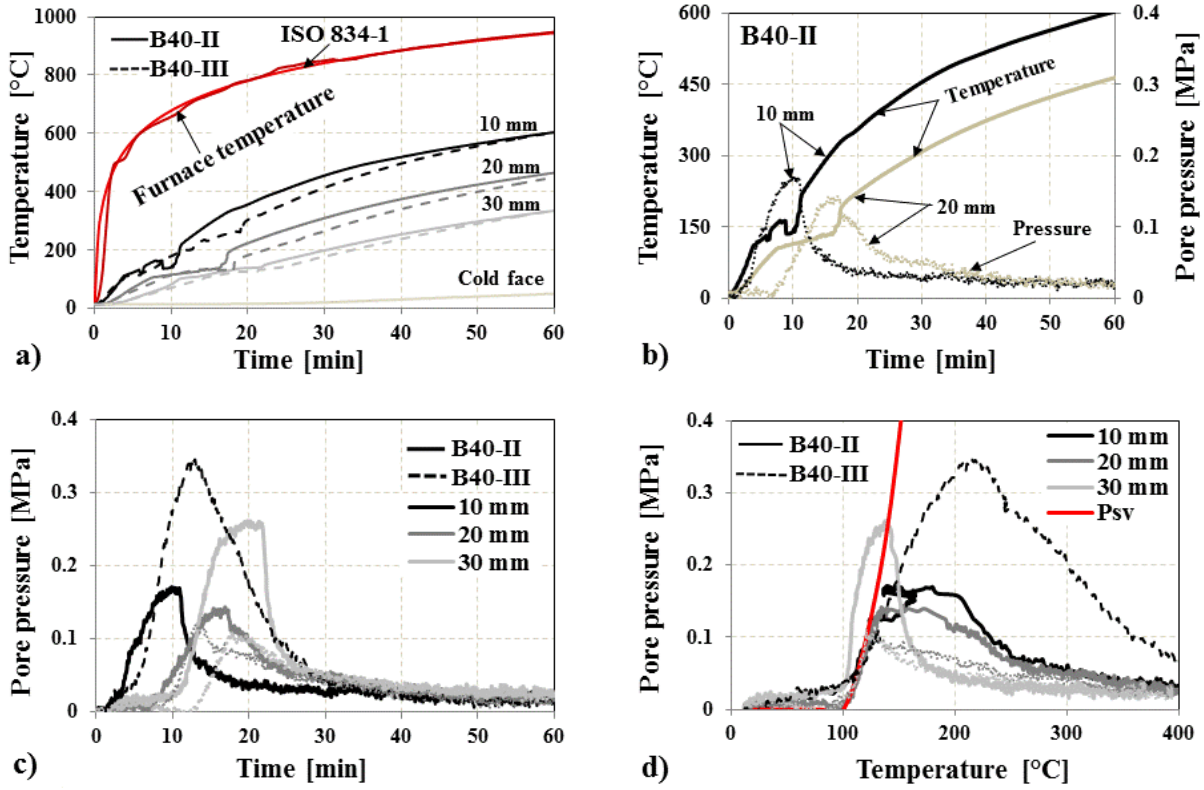

Figure 4.17: Evolution of temperature and pore pressure of B40-II and B40-III concrete specimens exposed to ISO 834-1 fire curve.

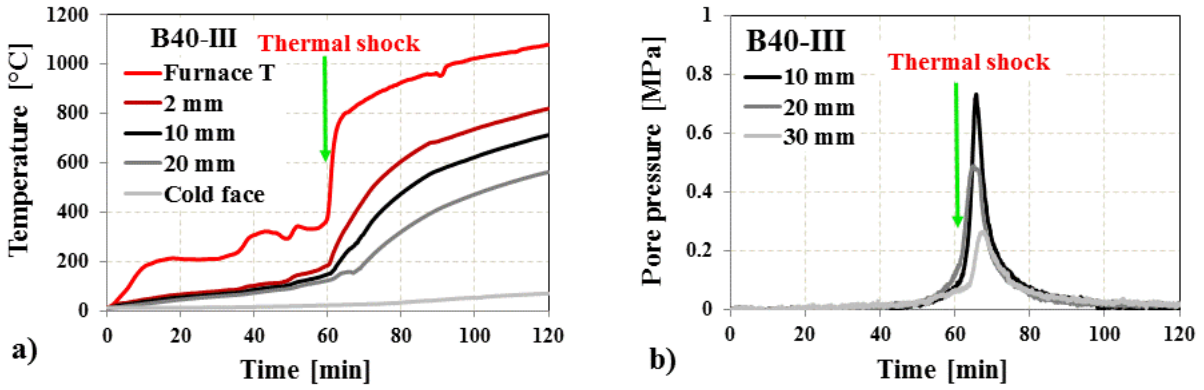

Figure 4.18: Development of temperature (a) and pore pressure (b) inside B40- III concrete during slow heating and thermal shock test.

4.2.3 Fire spalling tests under biaxial compressive loading

4.2.3.1 Effect of biaxial compressive loading on fire spalling

Figures 4.19 and 4.20 present the images of the exposed face of B40-II and B40-III concrete slabs exposed to ISO 834-1 fire at the 7 different levels of biaxial compressive loading. The experimental results have shown that the loaded specimens are more prone to spalling than unloaded specimens. Similar behaviour has been observed in the uniaxially loaded concrete cubes during ISO 834-1 fire tests (see section 4.2.1.1). Even though the size and the shape of the slabs were little different in two different tests set-up (described in sections 4.1.2 and 4.1.3), a similar fire behaviour has been observed in both tests. None of the specimens spalled when exposed to ISO 834-1 fire curve in the unloaded condition, which is a good agreement from one test set-up to another one. Similarly, none of the specimens spalled in the PT and uniaxial fire spalling tests in the unloaded conditions.

In this biaxial fire test, spalling was accompanied by a loud "popping" sound as concrete fragments were released layer-by-layer from the concrete surface. The time of the first spall was in the range from 6 to10 minutes of fire and the spalling events increased with the increased applied compressive stress. A similar behaviour was observed in the uniaxial fire spalling test. The oven temperature at the onset of spalling was in the range from 600 to 670 °C, whereas the measured temperature at the depth of 5 mm from the exposed surface was in the range from 150 to 200 °C. After cool down the furnace, the mass of the concrete spalled fragments were collected and weighed. The mass of the B40-II concrete spalled fragments loaded at 1.5, 3, 5 and 10 MPa are, respectively, 22.6 kg, 30.6 kg, 35.3 kg and 33.1 kg. In order to minimise the cold rim effect on the spalling depths, the mean spalling depths were calculated in the area of 500 x 500 mm^2, while the area of the exposed face was 600 x 600 mm^2. Mean spalling depths as a function of applied biaxial compressive stresses are reported in Figure 4.21 (see more detail in Table 4.6).

In Figure 4.21, the effect of compressive loading on the spalling behaviour of concrete can be defined in two stages: effect of the intermediate load (0 to 5 MPa) and higher load (5 to 10 MPa). No spalling was observed in unloaded tests of both concretes and on B40-II loaded at 0.75 MPa. Very limited spalling was observed on B40-III at 0.5 MPa. On the other hand, a uniform erosion extended to the whole heated area has been observed at 0.5 MPa for B40-II and 0.75 MPa for B40-III. The determined average spalling depths for these 2 last tests were respectively 12 mm and 14 mm. The observed spalling depth decrease on B40-II from 0.5 to 0.75 MPa may appear inconsistent with the other test results. The exact reason for this behaviour is not known.

Interestingly, a higher increase of spalling depth was observed in both concretes when the applied compressive stress was increased from 0.75 MPa to 1.5, 3 MPa (higher than 40 mm), and 5 MPa (close to 60 mm over the 100 mm slab thickness).

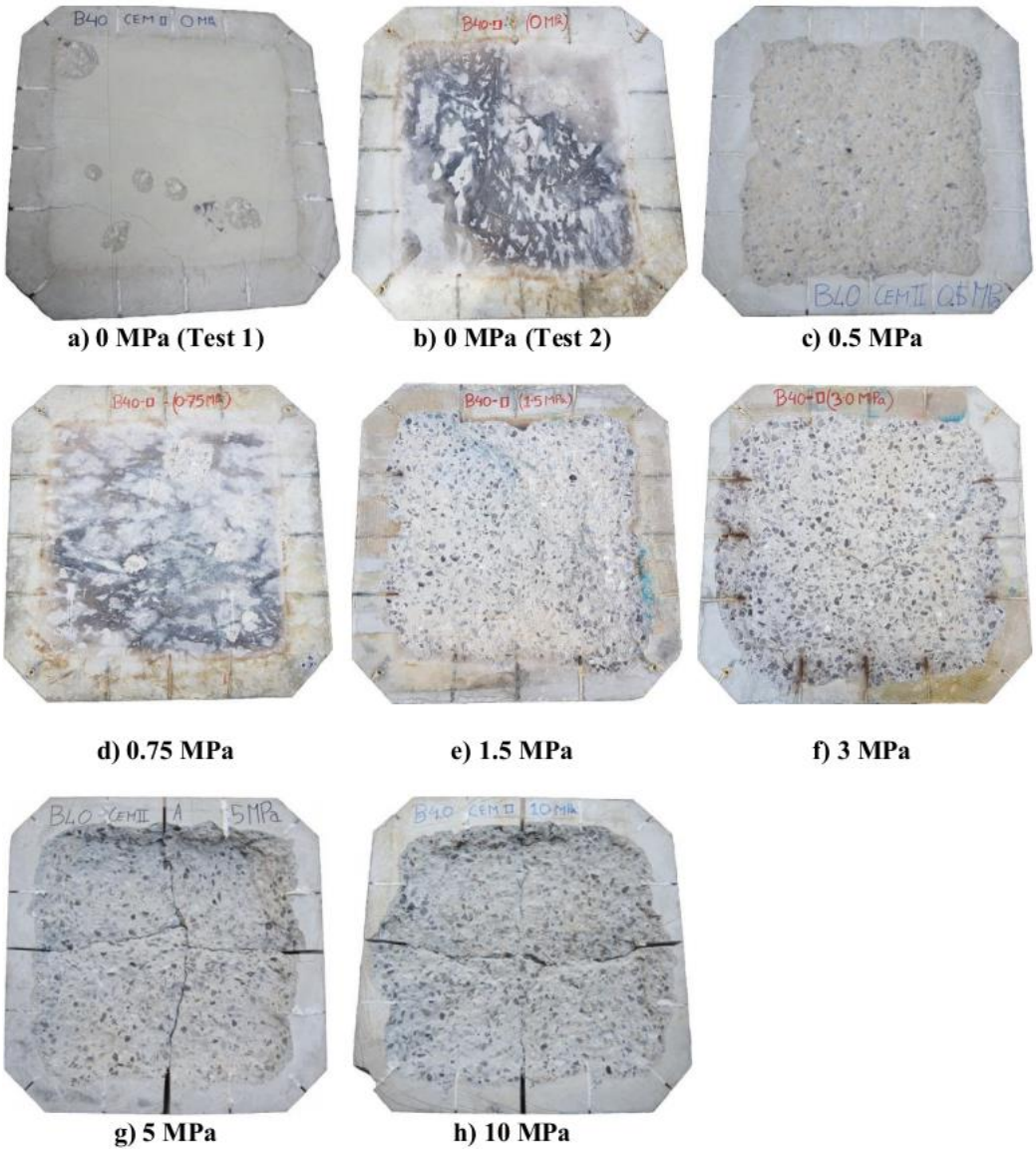

Figure 4.19: Exposed faces of the B40-II slabs after ISO 834-1 fire test.

As already stated in section 4.2.1.1, the possible following explanation is proposed to explain the mechanism:

When the concrete specimens are heated under biaxial compressive loading, the opening of cracks parallel to the loading direction increases [13], while it decreases for the cracks that are perpendicular to the loading direction (see Figure 5.11 in chapter 5, i.e. lower permeability). As a result, the moisture could not drain from the critical spalling zone of the heated concrete, which induces a very steep and higher pore pressure (see Figure 4.25). This higher pore pressure of the loaded specimens with a combination of stresses (due to restrained strains and external load) increases the risk of fire spalling. This mechanism is discussed more in details in chapter 6.

When the concrete is heated at the bottom surface of the slab in unloaded conditions, multiple cracks could occur inside the concrete specimens such as orthogonal cracks in the concrete core

perpendicular to the heated surface and surface cracks parallel to the exposed face in the hot layers. These cracks are often beneficial to limit the development of thermal stresses [5-6] as well as pore pressure.

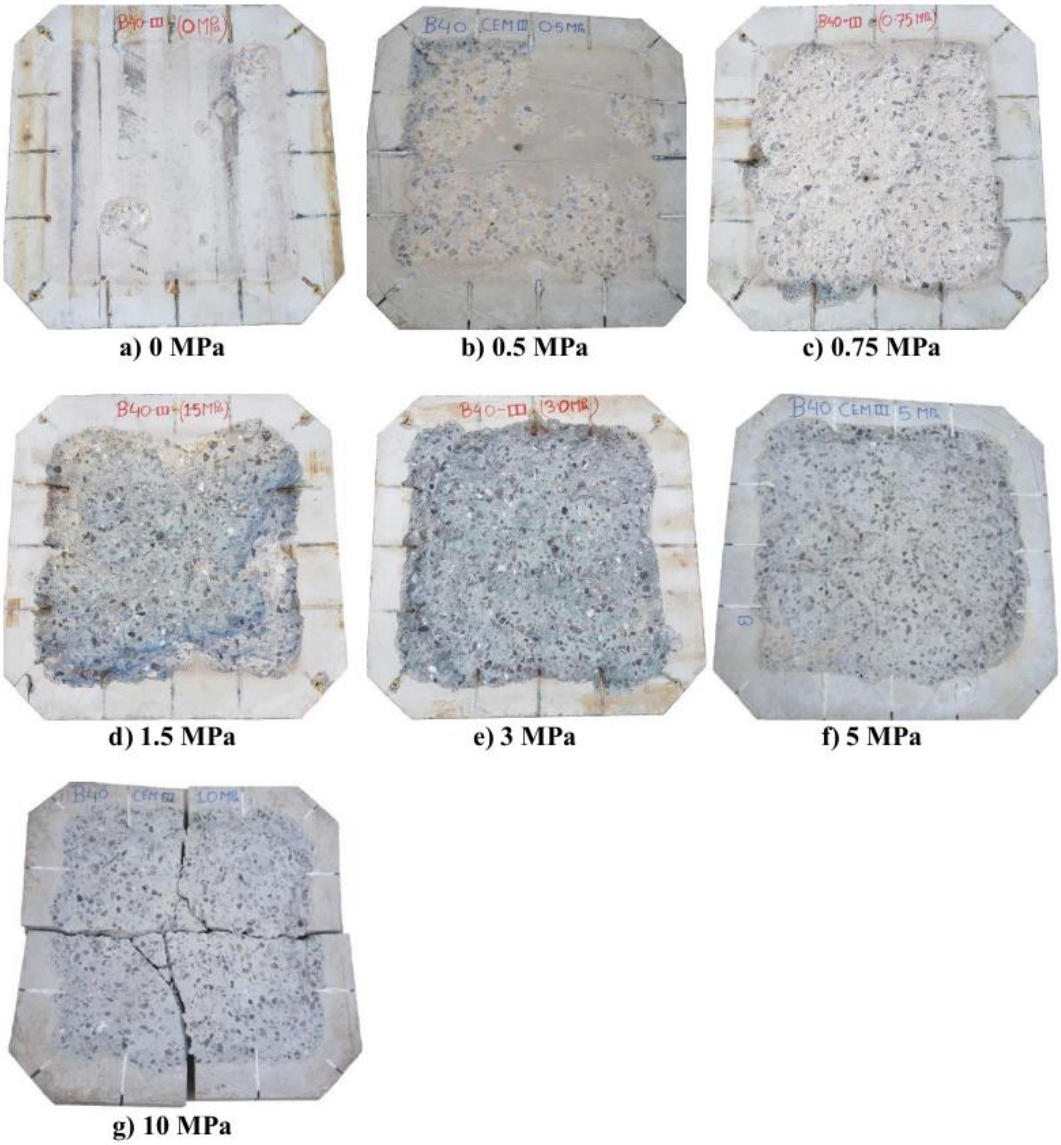

Figure 4.20: Exposed faces of the B40-III slabs after ISO 834-1 fire test.

During the fire tests, it was found that the appearance of water is more evident in the unloaded tests than the loaded tests, since the cracks are free to open in all directions. A similar behaviour was found during the ISO 834-I fire tests on the cube and mid-size slabs in the unloaded condition. After approximately 13-16 minutes of fire test, water started to appear on the cold surface of the slab through multiple routes on the specimens (e.g. through the cut notches and the outer periphery of the pressure gauge tubes, see an example in Figure 4.22). Since the thickness

of the slab was not so high, 100 mm, hence slabs were able to deform (towards the fire) easily during heating (i.e. higher cracking), thus diminished the thermally induced stresses near the heated surface as well as reduced the build-up of pore pressure (comparatively low pore pressures and higher displacement were measured in the unloaded tests than loaded tests, see Figures 4.26 and 4.28). The reduction in these thermal stresses with the combination of low pore pressure may have helped to avoid the risk of spalling. These observations highlight the importance of the moisture migration inside the concrete on the fire spalling of concrete.

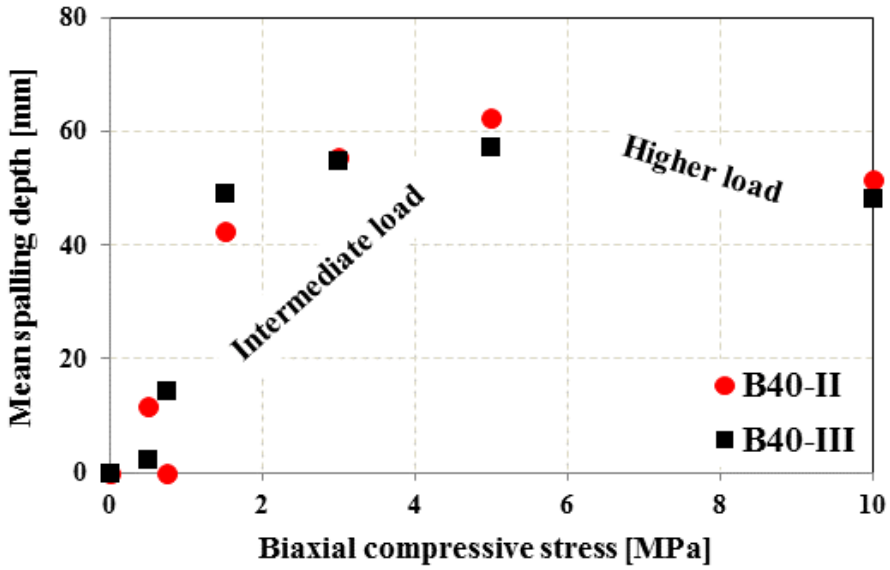

Figure 4.21: Mean spalling depth as a function of applied compressive stress

Table 4.6: Maximum, mean spalling depth, and spalling volume of B40-II and B40-III concrete.

	Load [MPa]	0	0.5	0.75	1.5	3	5	10
Maximum depth [mm]	B40-II	0	55	5	59	72	73	87
	B40-III	0	39	40	65	71	75	76
Mean depth [mm]	B40-II	0	12	0	43	55	62	51
	B40-III	0	2	14	49	55	57	48
Volume [cm^3]	B40-II	0	2886	0	10101	14160	15570	12867
	B40-III	0	563	3682	11922	14049	14323	12074

As it can be seen in Figure 4.21, the mean spalling depth of both concretes decreased from 5 to 10 MPa. However, the collapse of the 3 slabs occurred when the bending bearing capacity of the slabs was reached: 29 min for B40-II at 5 MPa, 25 min for B40-II at 10 MPa and 24 min for B40-III at 10 MPa, see Figure 4.19g-h and 4.20g. This behaviour could be due to a hogging bending moment caused by the eccentricity of the external loads (due to the decay of concrete

stiffness at the bottom face of the slab and higher reduction of thickness, maximum spalling depth exceeded half of its thickness) and lack of reinforcement, for more details see section 4.2.3.4. The spalling depth at 10 MPa could then be equal or higher than at 5 MPa if the collapse had not occurred and the tests could have continued for the same fire duration (30 min).

Figure 4.22: Released of hot moisture during the fire tests of B40-II in the unloaded (left) and loaded at 3 MPa (right).

At the low compressive loading (0.5 MPa), lower spalling has been observed in B40-III than the B40-II, while the spalling differences of both concretes are much lower from the compressive loading of 1.5 MPa to 10 MPa. This result is opposite than the one we observed by carrying out spalling test on the same concrete under uniaxial load (see section 4.2.1.1). Since the initial permeability of B40-III was higher than B40-II (see Figure 3.15), when concretes are heated under low compressive loading (e.g. 0.5 MPa), a small change of permeability due to the thermal mismatch between cement paste and aggregates and thermal gradients can be sufficient to prevent the development of pore pressure (at 0.5 MPa, the pore pressure of B40-III is lower than B40-II, Figure 4.26a-b) to exceed a value that favours spalling. While at higher biaxial compressive load, it can be considered that, most of the internal microcracks and cracks (perpendicular to the heated surface) are closed (see Figure 5.11). Hence, permeability (i.e. pore pressure) and stresses should not be different for two different concretes. Therefore, the spalling difference due to cement type is almost nil at the intermediate and higher biaxial compressive loading (e.g. 1.5 to 10 MPa) compared to the low compressive loading (0.5 MPa).

4.2.3.2 Thermal response of the slabs

Figure 4.23a-g presents the evolution of temperatures inside the concrete specimens exposed to ISO 834-1 fire curve under different levels of compressive load. The sudden rise of temperatures indicates the exposure of thermocouples to hot air due to spalling. The almost similar thermal response has been observed in both concretes in the unloaded tests (see Figure 4.23a). The furnace temperatures were obtained as average values of 2 measurements by a plate thermometer. It is worth noting that the measured air temperature inside the furnace followed the target ISO 834-1 fire curve very closely, except after the first spalling event.

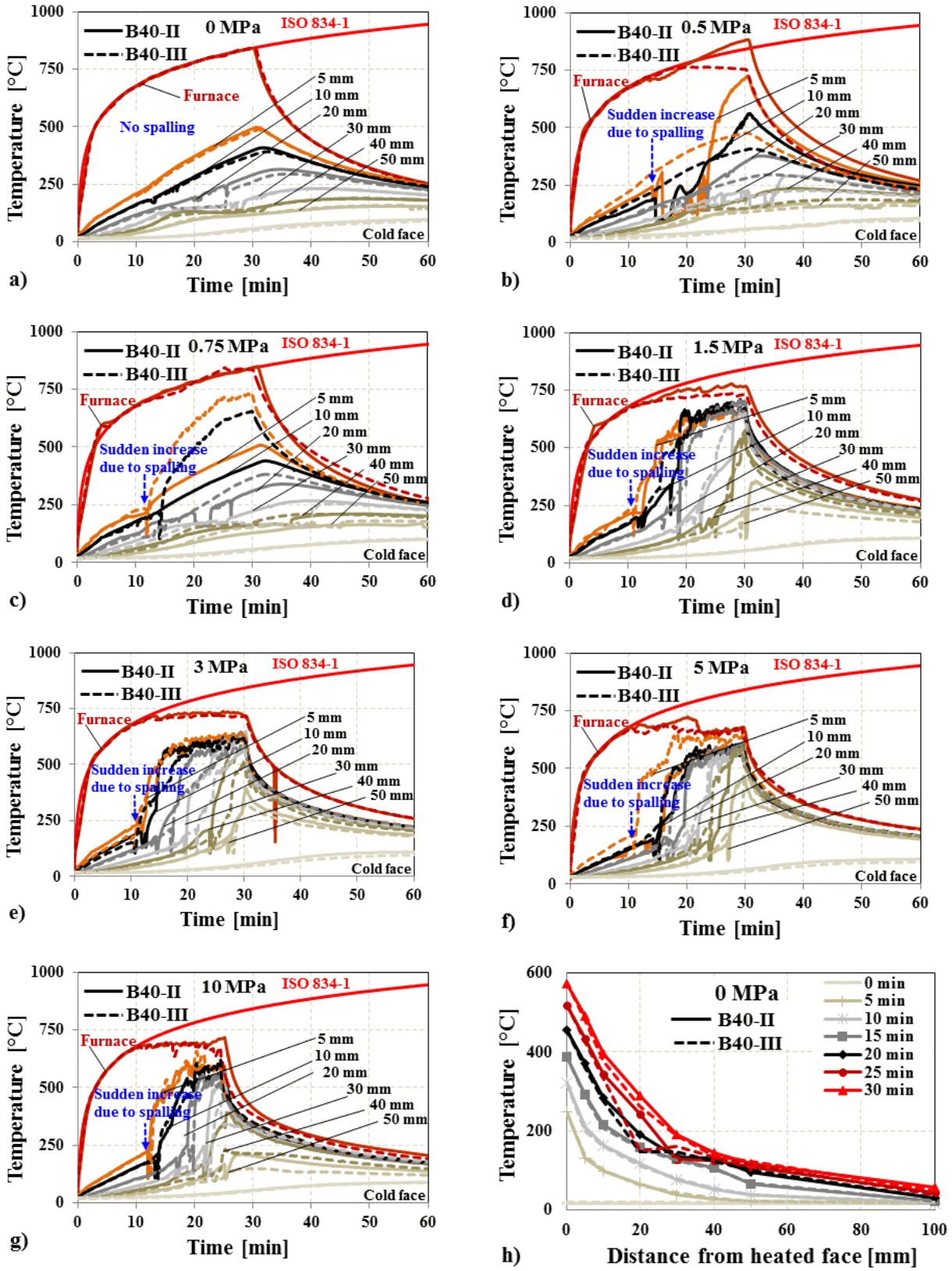

Figure 4.23: Development of temperature as a function of time (a-g); temperature profile through the thickness of concretes (h).

A few minutes after spalling, the temperature of the furnace did not reach the target temperature, even if the opening of the valve of the gas burner was set to its maximum value. Since the spalling debris was collected at the bottom of the furnace, which may increase the thermal inertia in the bottom of the furnace. As a result, the bottom of the furnace absorbs more heat during heating, therefore it needs more time to raise the furnace temperature. Hence, for homogeneity of all tests, a constant opening of the burner was set after around 15 minutes of fire that is the reason why the temperature of the furnace is colder than the ISO 834-1 fire cure for the all loaded tests.

Figure 4.23h presents interior temperature profiles measured at eight different depths through the thickness of the unloaded slab (triangular symbols on each line depict the measurement points). After being heated 10 minutes of ISO 834-1 fire, the measured temperatures at the hot face and at 5 mm are, respectively, 322 °C and 210 °C for B40-II and 319 °C and 200 °C for B40-III. The temperature difference between B40-II and B40-III concretes are almost negligible.

In all the tests, it was observed that spalling behaviour was homogeneous all over the central part of the exposed section (500 mm x 500 mm) and for all the samples. Then, interestingly, spalling kinetics could be reasonably determined from the sudden rise of temperature determined on the different thermocouples (see Figure 4.24). It can be observed that for most of the tests, spalling rates were almost constant and very close to each other (parallel curves). The spalling rate is approximately 100 mm/h. A particular trend was observed on tests loaded at 10 MPa. Spalling rate increased after 22 min in both samples. This has led to the collapse of the 2 slabs at 24 and 25 min.

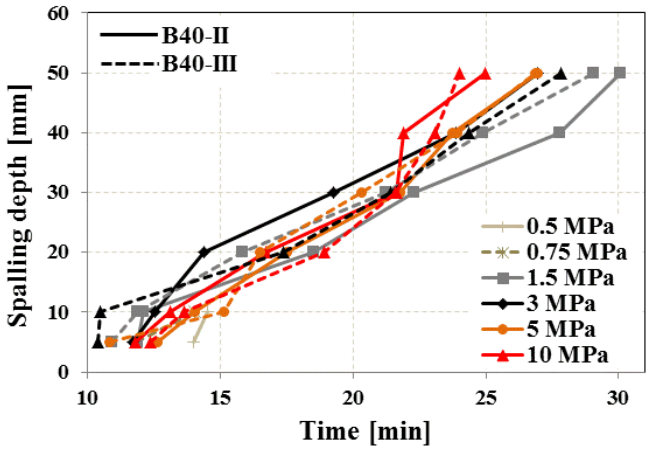

Figure 4.24: Determined spalling kinetics based on the observed sudden temperature increase caused by thermocouples exposition to fire.

4.2.3.3 Build-up of pore pressure of the slabs

Figure 4.25 presents the development of pore pressure as a function of time of B40-II and B40-III concrete specimens exposed to ISO 834-1 fire curve under different levels of biaxial compressive loading. Two curve shapes have been observed.

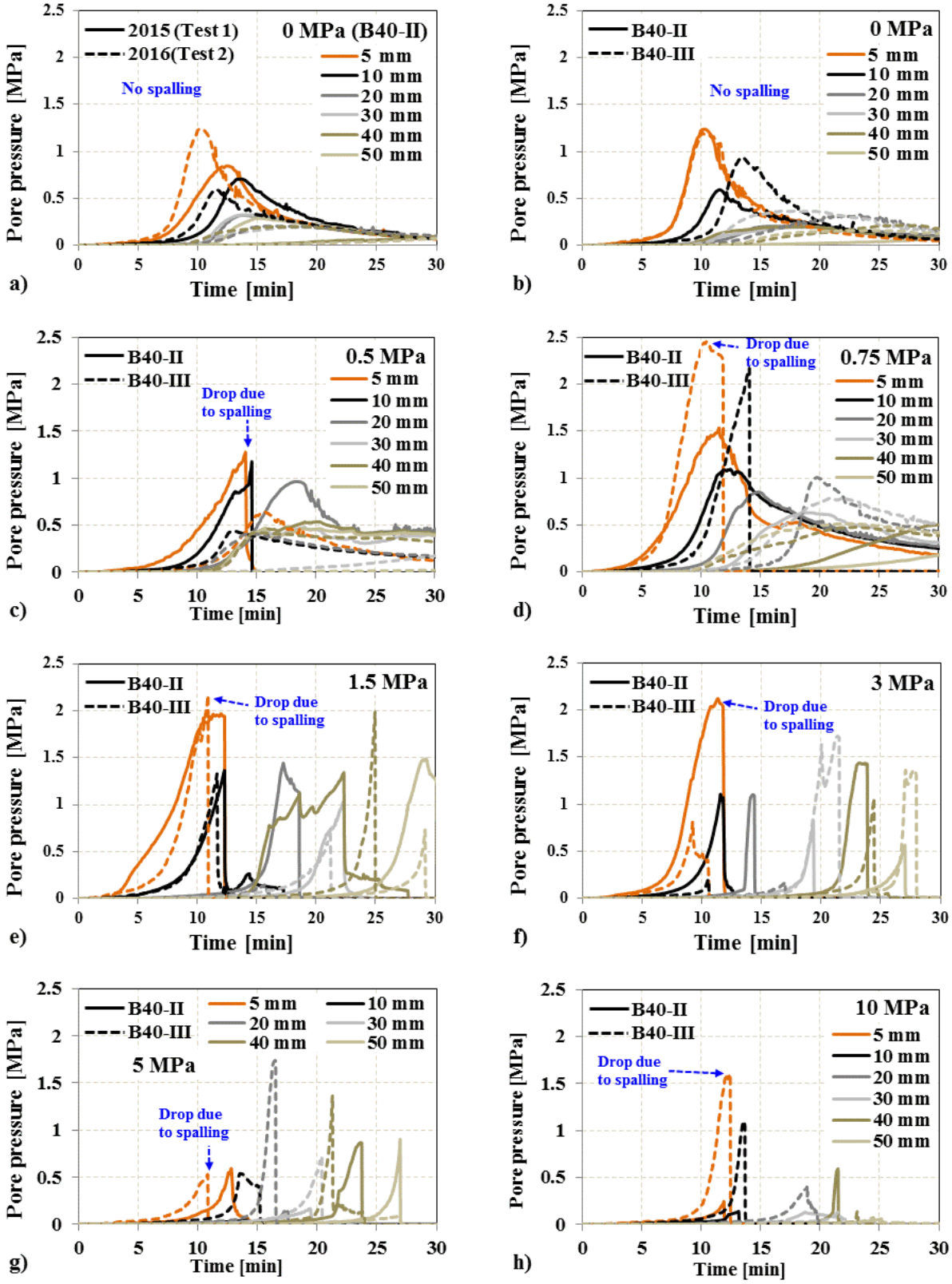

Figure 4.25: Development of pore pressure in B40-II and B40-III concretes as a function of time.

Some curves have a bell-shape when no spalling occurred. This can be observed on unloaded tests, at 0.5 MPa on B40-III and at 0.75 MPa on B40-II. A sudden decrease of pore pressure was observed when concrete spalls. This sudden decrease in pore pressure due to spalling was more evident for the tests at 1.5 MPa to 10 MPa.

In the limited load zone (0.75 to 3 MPa), maximum pore pressure increased when biaxial applied stress increased. In unloaded samples, maximum pore pressures are respectively 0.8 MPa / 1.2 MPa (Test 1 / Test 2) and 0.9 MPa for B40-II and B40-III (see Figures 4.25a and 4.26a-b) and no spalling was observed. At 1.5 MPa, the maximum pore pressure are 2.0 and 2.2 MPa, respectively (see Figures 4.25e and 4.26a-b). Spalling was then observed. It can be confirmed from these observations that membrane compressive loading can affect the build-up of pore pressure during heating.

The following explanation is proposed.

In the unloaded situation, the permeability close to the exposed surface increases with temperature because of the development of cracks and microcracks (due to thermal incompatibility between the cement pastes and aggregates [7], and thermal stresses induced by the thermal gradients). Since at high temperature the cement paste shrinks due to drying and dehydration, while the aggregates dilate due to their positive thermal expansion. This mismatch brings in tensile stresses in the matrix and compressive stress in the aggregates leading cracking. As a result, vapour and liquid water can escape more easily from the specimen since the cracks are free to open in all directions. This higher permeability significantly affects the build-up of pore pressure.

On the contrary, when the specimens are heated under a constant biaxial compressive loading, the applied load tends to close the cracks perpendicular to the loading directions. Felicetti and Lo Monte 2016 [14], by implementing on the same biaxial fire tests an innovative technique based on ultrasonic pulse-echo have shown that damage is significantly reduced when samples are loaded, even at a very low stress (0.5 MPa). As a result, the presence of load limits the moisture transport inside the concrete by decreasing permeability which induces the steep build-up and higher value of measured pore pressure (see Figure 4.25d-f).

The maximum measured pore pressures as a function of applied compressive stress are plotted in Figure 4.26c. From this graph, the following trend can be observed:

Under low stress, maximum pore pressure tends to increase with the applied stress. This can be due to, as explained earlier to the permeability decrease when applied stress increase. In the higher stresses range where spalling occurs, maximum pore pressure tends to decrease when applied stress increases. This can be explained by the fact that spalling can occur when the state of stresses combining thermal stresses, applied stresses and pore pressure reaches a given threshold. Then to reach this threshold, the higher is the applied stresses lower will be the pore pressure, see Figure 4.26c. From this graph, it can be observed that, except at 5 and 10 MPa, maximum pore pressures are globally in the same range for B40-II and B40-III.

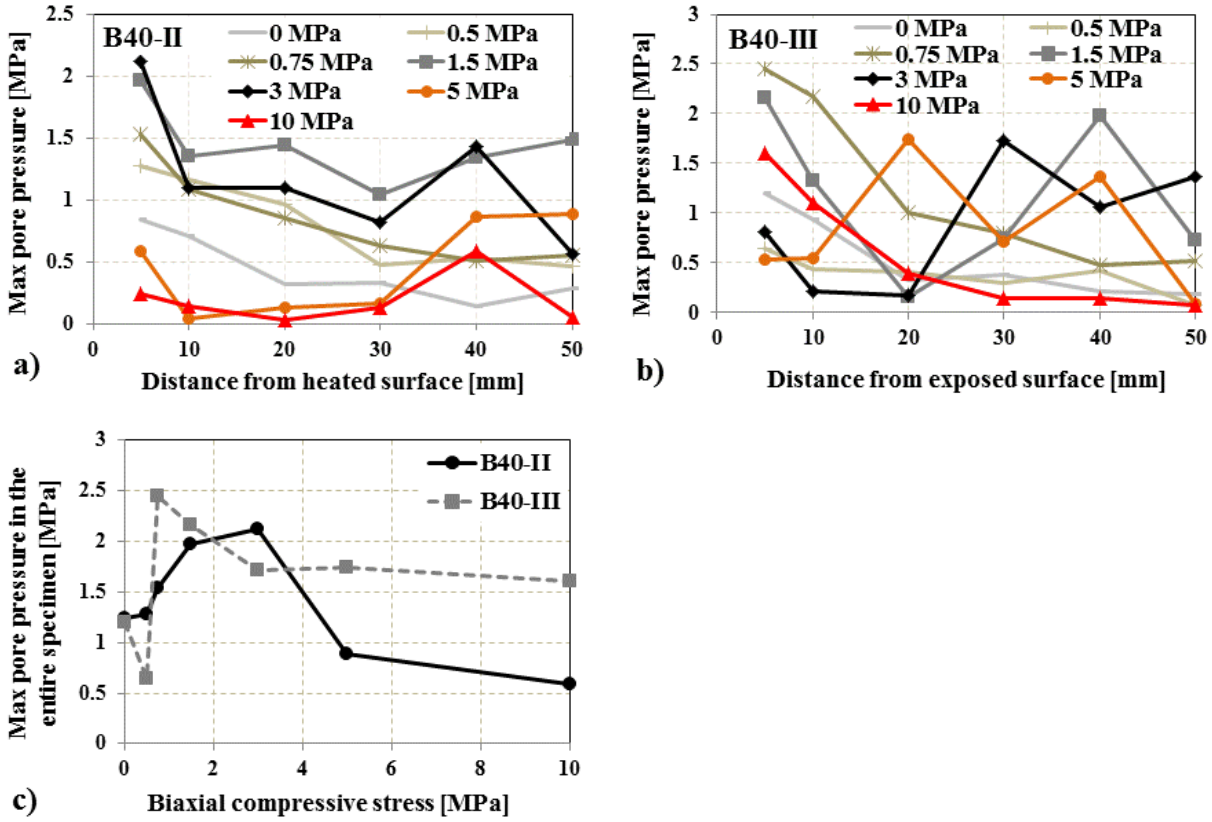

Figure 4.26: Maximum pore pressure along the slab thickness measured in B40-II and B40-III concretes under different compressive stress (a-b) and maximum measured pore pressure of the entire specimen as a function of applied compressive stress (c).

4.2.3.4 Out of plane displacement of the slabs

The effect of compressive loading on the fire spalling behaviour of concrete can also be described by comparing the deflections at different loading levels, since the presence of load during heating plays an important key role in the development of thermal curvature of the slab. The displacement of the slabs was measured in two directions (X and Y) as discussed in the test method. The three legs of the LVDT-holding frame was laid on the slab points A, B and C. Figure 4.27_left presents the positions of the LVDTs on the concrete slab specimens in the direction of X and Y, while Figure 4.27_right presents the calculation method of the displacement for LVDT3, LVDT5 and LVDT6, since the support conditions along the X and Y directions were not same.

The modified displacements are as follows:

LVDT3* = LVDT3 – 0.75 * LVDT2

LVDT5* = LVDT5 – 0.50 * LVDT2

LVDT6* = LVDT6 – 0.25 * LVDT2

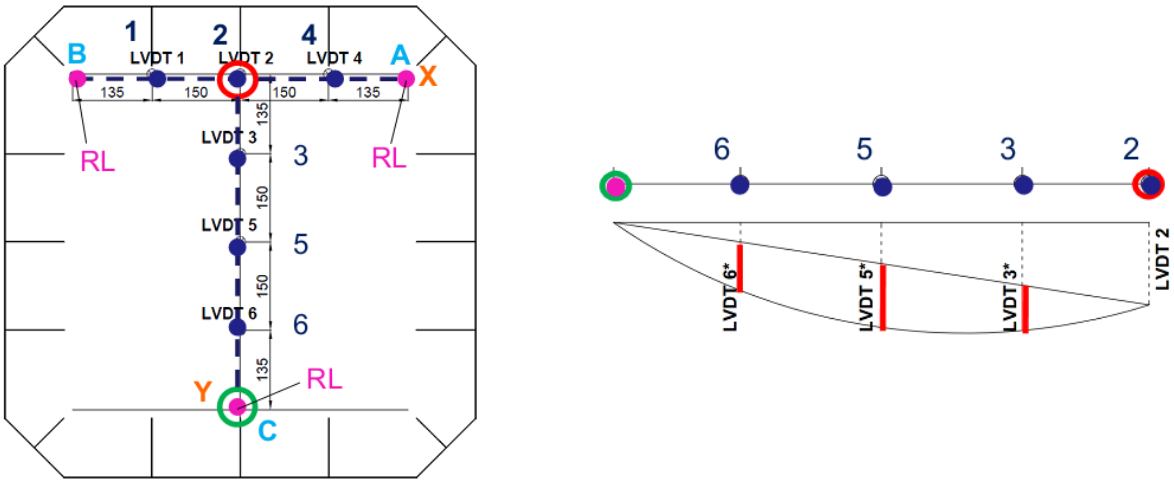

Figure 4.27: Schematic diagram of the measurement points of displacements (left) and an explanation of the displacement calculations for LVDT3, LVDT5 and LVDT6 (right) (RL= 3 rigid legs of the LVDT-holding frame).

The deformed shape of the B40-III specimens as a function of time subjected to different levels of compressive loading along the X and Y directions are given in the Figure 4.28a-g (symbols on each line depict the measurement points). The values along the X axis and Y axis are given in dashed and solid lines respectively. The deformed shape of the B40-II specimens is presented in Figure A1 in the Appendix A. Deflections at the centre of the sample (LVDT n° 5) versus time and for all the tests are plotted in Figure 4.28h. From this graph, it can be seen that the applied external membrane compressive loading reduces the displacement of the slabs.

During heating of concrete, initial sagging curvature towards the fire is due to the higher thermal dilation of the bottom heated face than the top colder face. At the same time, because of the decay of concrete stiffness in the hot layers (corresponding to the decrease of the modulus of elasticity (E) with temperature, i.e. $E_{hot} < E_{cold}$) and because of the spalling phenomena, the stiffness centre rises. As the external load is continuously applied at the mid-plane, this turns into the upward eccentricity (hogging bending moment) and the displacement trend is reversed. As a consequence, the combined effects (sagging curvature due to thermal loading and hogging curvature due to the presence of compressive loading caused by eccentric force) lead to lower curvature in the loaded specimen than in unloaded specimens. As a result, upward deflections increases when applied load increases (see Figure 4.28e-h). This trend is enhanced with spalling kinetics increase. The increasing rate of the upward displacement of both concretes was much higher than the downward displacement, especially after 20 minutes of fire test loaded at 10 MPa (see Figure 4.28h).

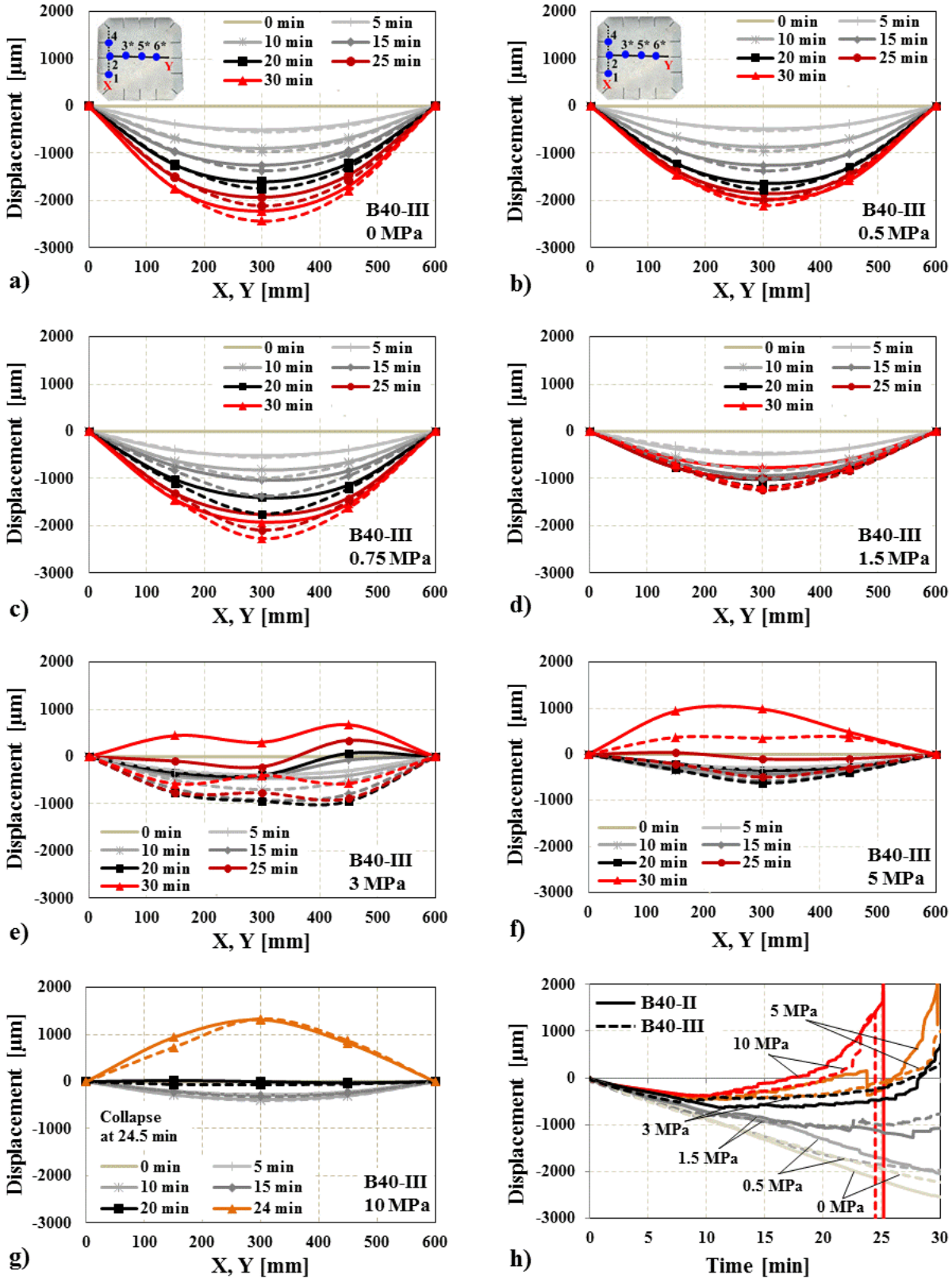

Figure 4.28: (a-g) Deformed shape of B40-III slabs in the X and Y-axes and (h) vertical displacement of concretes versus time (comparison of the top-mid displacements, i.e. LVDT 5).

4.3 Summary and conclusions

Fire spalling of concrete is a complex phenomenon, which might occur due to pressure build-up in the pores, thermal and load-induced stresses. This chapter aimed to contribute determining the effect of compressive loading (uniaxial and biaxial) and cement type on the fire spalling behaviour of concrete. The following conclusions can be drawn based on the results presented in this chapter:

The experimental test results have clearly shown that the compressive loading (uniaxial and biaxial) and their levels have a significant influence on the fire spalling behaviour of concrete. Compressive loaded specimens are more prone to spalling than unloaded specimens. It is worth to note, that unloaded samples made with the 2 concretes in three different tests (uniaxial and biaxial fire tests; and unloaded mid size slab tests) did not spall.

In the uniaxial fire spalling test, the amount of spalling was increased with the increased applied compressive stress, while in the biaxial test, an increased trend of spalling depths was found up to 5 MPa, then it decreased at 10 MPa due to the early collapse behaviour of the slabs.

From the sudden temperature increase related to spalling of the slabs, it has been able to determine the spalling kinetics for all the tests. It appears that the spalling rate is almost constant during all the tests and very close from one test to the other. In the biaxial fire tests, the spalling rate was approximately 100 mm/h.

It was found that under low stress, maximum pore pressure tends to increase with the applied stress. In the higher stresses range where spalling occurs, maximum pore pressure tends to decrease when applied stress increases. The fire spalling can occur when the state of stresses combining thermal stresses, applied stresses and pore pressure reaches a given threshold. Then to reach this threshold, the higher is the applied stresses lower will be the pore pressure. The amount of pore pressure is well known as a key parameter that influences spalling risk.

It has been found that the amount of spalling was much higher when samples have been subjected to biaxial loading than uniaxial loading (see Figure 4.29). Under biaxial loading during heating, the cracks generated by the state of stresses are mainly orientated parallel to the heated surface. These cracks are certainly the ones which induce the more important risk of spalling. Under uniaxial loading, the cracks and microcracks tend to open vertically in all the directions along the compressive loading axis and tends to close the cracks perpendicular to the loading direction (i.e. lower permeability in the direction perpendicular to the heated face). Hence, the permeability should be higher (i.e. lower pore pressure) in the specimens under uniaxial load test than the specimens under biaxial load tests due to the absence of loading in the second axis of the uniaxial load test specimens. As a result, lower spalling in the uniaxial test than the biaxial test, since the cracks not only release the pore pressure as well as stresses. Moreover, the size of the specimen itself has an effect on the rate of moisture escaping during the test. In cube specimens, the spalling started close to the central area of the exposed surface and decreases when reaching the edges, since the water can be transported out from the specimen due to the shorter path of the smaller specimen. Hence, the vapour pressure decreases towards the edges, thereby the risk of spalling is reduced. As can be seen the image in Figure 4.9 and 4.12, almost no spalling took

place around the boundary of the specimens. Finally, it should be noted that the initial water content of the biaxial load test specimens was about 1.0% higher than the uniaxial load test specimens (see Table 3.5 in chapter 3), which can induce higher pore pressure (the maximum pore pressure of uniaxial and biaxial tests are, respectively, 1.1 MPa and 2.1 MPa for B40-II and 0.7 MPa and 2.45 MPa for B40-III) and then enhance the risk of fire spalling.

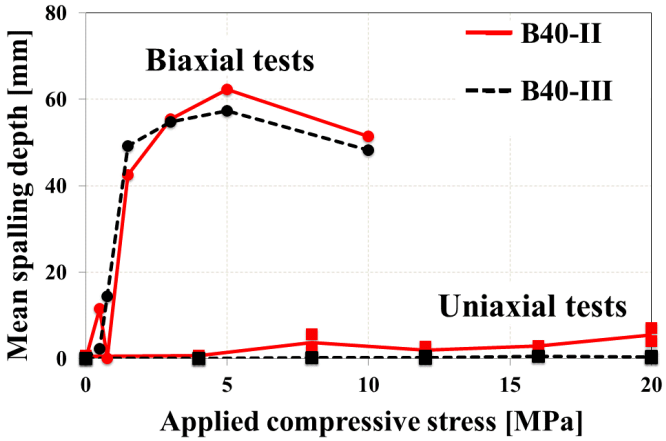

Figure 4.29: Mean spalling depth for uniaxial and biaxial loading as a function of applied stress.

Another difference appears when comparing the two series of tests. In uniaxial tests, spalling was much higher for B40-II (3% of slag) than B40-III (43% of slag) for all the applied values of compressive stress. This behaviour is mainly explained by the lower permeability and porosity of B40-II than B40-III concrete at high temperature. A similar difference was observed between the results obtained in biaxial tests at lower load (0.5 MPa). On the contrary, the difference appears not so significant from 1.5 to 10 MPa of biaxial fire tests. This could lead to the conclusion that the relative effect on spalling of permeability decreases when the biaxial load becomes relatively high.

4.4 References

[1] Lo Monte F. and Felicetti R. “Heated slabs under biaxial compressive loading: a test set-up for the assessment of concrete sensitivity to spalling”, Materials and Structures (2017) 50:192.
[2] Kalifa, P., Menneteau, FD and Quenard, D. (2000). “Spalling and pore pressure in HPC at high temperatures”, Cement and Concrete Research (2000), Vol. 30, pp. 1915-1927.
[3] Felicetti, R., Lo Monte, F and Pimienta, P. (2017). “A new test method to study the influence of pore pressure on fracture behaviour of concrete during heating”, CCR 94 (2017) 13–23.
[4] Choinska, M., Khelidj, A., Chatzigeorgiou, G., Pijaudier-Cabot, G. (2007). “Effects and Interactions of Temperature and Stress-level Related Damage on Permeability of Concrete”, Cement and Concrete Research 37 (2007) 79–88.
[5] Dougill, J.W., “Some observations on failure of quasi brittle materials under thermal stress”, Cement and Concrete Research, Vol. 3, pp. 469-474, 1973.

[6] Lottman, B.B.G., Koenders, E.A.B., Blom, C.B.M., and Walraven, J.C. (2015). "Spalling of fire exposed concrete based on a coupled material description: an overview", Proceedings of the 4th IWCS, October 08-09, 2015, Leipzig, Germany.
[7] Kalifa, P., Chéné, Grégoire., and Gallé. (2001). "High-temperature behaviour of HPC with polypropylene fibres From spalling to microstructure", CCR 31 (2001) 1487–1499.
[8] Lun, H and Lackner, R. (2013). "Permeability of concrete under thermal and compressive stress influence; an experimental study", 3rd IWCS, September 25-27, 2013, Paris, France.
[9] Lu, F., and Fontana, M. "A thermo-hydro model for predicting spalling and evaluating the protective methods", 4th IWCS due to Fire exposure, Oct. 08-09, 2015, Leipzig, Germany.
[10] Carré, H., Pimienta, P., La Borderie, C., Pereira, F., and Mindeguia, J. C. (2013). "Effect of Compressive Loading on the Risk of Spalling," Proceedings of the 3rd International Workshop on Concrete Spalling due to Fire Exposure, pp. 01007, Paris, France.
[11] Mindeguia, J-C., Carré, H., Pimienta, P and La Borderie, C. (2015). "Experimental discussion on the mechanisms behind the fire spalling of concrete", Fire Mater.2015;39:619-635.
[12] Mindeguia, J-C., Pimienta, P., Noumowé, A and Kanema, M. (2010). "Temperature, pore pressure and mass variation of concrete subjected to high temperature—Experimental and numerical discussion on spalling risk", Cement and Concrete Research 40 (2010) 477–487.
[13] Sertmehmetoglu, Y. (1977). "On a mechanism of spalling of concrete under fire conditions", PhD Thesis, King's College, London, 1977.
[14] Felicetti, R and Lo Monte, F. (2016). "Pulse-Echo Monitoring of Concrete Damage and Spalling during Fire", 9th International Conference on SIF, June 8-10, 2016, Princeton, USA

5 The Thermo-Mechanical Model

The experimental test results described in chapter 4 clearly shown that the compressive loading (uniaxial and biaxial) and their levels have a significant influence on the fire spalling behaviour of concrete. In chapter 3, it was found that the load decreases the permeability, which increases the pore pressure and then increases the risk of fire spalling. The results described in chapter 3 and 4 allowed that an additional research is needed for deeper understanding the effect of loading on the fire spalling mechanisms of concrete. For this, the calculation of stress profiles and crack opening along the thickness of the concrete specimens during heating could be a useful tool to better explain the fire spalling mechanism of concrete.

Since there is no convenient experimental method available for obtaining the internal stress field (except indirect measurement via strains) and the crack opening during heating until now, mainly because of the limitation of equipment and the complex structure of a composite material. Hence, the finite element model could be used for determining and monitoring the concrete mechanical response (e.g. stress profile and crack opening) during heating under loading which is difficult to be examined experimentally.

Although numerous finite element models have been developed to study the spalling mechanisms of concrete in fire conditions, such as those presented by de Morais et al 2010 [1], Fu and Li 2011 [2] and Lottman et al. 2015 [3] even if the mechanisms of fire spalling is still not fully understood. Within this context, in the present chapter, the thermo-mechanical (TM) computations are conducted only for B40-II ($f_{c28days} \approx 40$ MPa) with the finite element code CAST3M (version 2015) [4] and verified against the experimental data by comparing the predicted temperature profiles and out of plane displacements with the measured values from the fire tests of B40-II concrete (described in chapter 4). This model was already implemented in SIAME by Hatem Kallel during his post-doc research activities in SIAME. In this thesis, this existing model was used to deeper analyse the experimental results obtained in chapters 3 and 4 and to better understand the influence of compressive loading on the spalling mechanism of concrete. The main objective of this chapter is to investigate the evolution of internal stresses (due to thermal gradients and external compressive loading) as well as the crack opening (i.e. damage due to fire and external compressive loading) through the thickness of the slab and the cube during heating under loading.

The following parts of this chapter are structured as follows: in section 5.1, the description of the thermal and mechanical model for uniaxial and biaxial fire tests where the geometry, boundary conditions, thermal and mechanical properties of the tested concrete are introduced. In section 5.2, the computational results of the thermal and mechanical response of the specimens (cube and slab) are presented, including temperature distribution, out of plane displacements,

stresses distribution through the thickness, damage and the crack opening. The computational prediction results are verified by comparison with the experimental observation of both tests. The chapter closes with concluding remarks given in section 5.3.

5.1 Finite element model

The thermo-mechanical (TM) computations were conducted using the finite element code CAST3M (version 2015) developed at the French Alternative Energies and Atomic Energy Commission (CEA) [4]. In the mechanical analysis, the concrete damage model was used which was developed by Fichant et al. 1999 [5] and Matallah et al. 2009 [6], while the elastic model was considered for the load supporting steel plates.

5.1.1 Thermal model

3D finite element heat transfer analysis was undertaken to determine the distribution of temperatures through the thickness of the cube and slab specimens. The heat transfers are assumed to be unidirectional in the direction perpendicular to the exposed face of the cube and slab specimens. For a more direct (as closely as possible) thermal comparison against the experimental tests, the temperature history recorded during the test (at the exposed surface) was taken as an input thermal boundary condition. The temperature inside the concrete was computed based on thermal conduction laws by Fourier's differential [7] as shown in Equation 5.1.

$$div\left(\lambda \nabla T\,(r,t)\right) + s\,(r,t) = \rho\, C_p\, \frac{\partial T\,(r,t)}{\partial t} \tag{5.1}$$

where q = heat flux vector ($q\,(r,t) = -\lambda \nabla T(r,t)$),
s = heat per unit of volume dissipated by the internal sources,
$\rho\, C_p$ = volumic heat with constant pressure, T = temperature, r = variable of space,
t = variable time and λ = thermal coefficient of conductivity.

5.1.2 Mechanical model

For the mechanical analysis, damage model has been used for concrete and the elastic model has considered for the load supporting steel plates (Young modulus of elasticity, E = 210 GPa, Poisson's ratio, υ = 0.3 and coefficient of thermal expansion, α = 10 x 10^{-6} per K^{-1}). The damage model used is the isotropic damage model developed by Fichant et al. 1999 [5], which is an extension of Mazars' model [8] taking into account the unilateral effect of concrete and inelastic strains (plasticity). The microcracking effect is directly linked to the internal state damage variable D. This damage variable ranges from 0, for an undamaged material, to 1, for a fully damaged material. The notions of damaged and undamaged lead to the concept of effective stress $\tilde{\sigma}$ (5.2), which represents the necessary stress to apply to an undamaged material element so that it deforms the same way as a damaged element under total stress σ (5.3).

$$\tilde{\sigma}_{ij} = C^{O}_{ijkl} : \varepsilon^{e}_{kl} \tag{5.2}$$

where ε^{e}_{kl} is the local elastic strain fields and C^{O}_{ijkl} is the initial isotropic elastic stiffness tensor. The total stress is described by:

$$\sigma_{ij} = C^{damaged}_{ijkl} : \varepsilon^{e}_{kl} \tag{5.3}$$

where $C^{damaged}_{ijkl}$ is the damaged material stiffness tensor. Based on Equation (5.2) and (5.3), the relation between total and effective stress can be written as follows:

$$\sigma_{ij} = C^{damaged}_{ijkl} : (C^{O}_{klmn})^{-1} : \tilde{\sigma}_{mn} = (1 - D)\tilde{\sigma}_{mn} \tag{5.4}$$

where $(C^{O}_{klmn})^{-1}$ is the initial compliance tensor and D is the scalar variable of the isotropic model. The evolution of the isotropic damage variable D is expressed as an exponential law:

$$\mathrm{D} = 1 - \frac{\varepsilon_{do}}{\varepsilon_{eq}} \, exp\left(B_t(\varepsilon_{do} - \varepsilon_{eq})\right) \tag{5.5}$$

where $B_t = \frac{h f_t}{G_f - 0.5 \, f_t \, \varepsilon_{do} h}$ is a damage parameter driving the shape of the strain softening and in which f_t is the tensile strength and E is the young modulus of elasticity, G_f is the fracture energy and h corresponds to the size of the finite element.

Moreover, in Eq. (5.5) ε_{do} is the damage threshold expressed in strain, i.e., ($\varepsilon_{do} = \frac{f_t}{E}$) where E is the young modulus of elasticity, and ε_{eq} is the equivalent strain defined by Mazars which drives damage evolution and describes the state of local extension induced by stress:

$$\varepsilon_{eq} = \sqrt{\sum \langle \varepsilon_i \rangle^2} \tag{5.6}$$

Unitary Crack Opening strain variable is computed using the following procedure:
The total strain in the fracture element is written as

$$\varepsilon_{ij} = \varepsilon^{e}_{ij} + \varepsilon^{uco}_{ij} \tag{5.7}$$

The total strain is decomposed into two parts: an elastic part ε^{e} and a cracking part represented by the Unitary Crack Opening strain variable ε^{uco}. Multiplying (5.7) by the elastic stiffness tensor C_{ijkl}, the equation can be written as

$$\tilde{\sigma}_{ij} = C_{ijkl}\varepsilon_{kl} = C_{ijkl} \, \varepsilon^{e}_{kl} + C_{ijkl} \, \varepsilon^{uco}_{kl} = \sigma_{ij} + \sigma^{in}_{ij} \tag{5.8}$$

Hence, the tensor of the crack opening strain is given by

$$\varepsilon_{ij}^{uco} = C_{ijkl}^{-1}\,\sigma_{ij}^{in} \tag{5.9}$$

From the finite element computation, we get a nominal (total) stress σ. The effective stress is computed using the total strain equation (5.2). The inelastic stress tensor is therefore given by

$$\sigma_{ij}^{in} = \sigma_{ij} - \tilde{\sigma}_{ij} \tag{5.10}$$

Equation (5.9) gives the Unitary Crack Opening strain tensor. The normal crack opening displacement value is given by

$$\delta_n = n_i \delta_{ij} n_j = n_i h \varepsilon_{ij}^{uco} n_j \tag{5.11}$$

where n is the unit vector normal to the crack.

5.1.3 Material properties

A good representation of the material properties plays an important role in the success of model to analyse the thermal and mechanical response. Hence, to fit with the real thermal and mechanical response of concrete specimens during the fire, the material properties of concrete need to be temperature dependent. The evolution of thermal and mechanical properties of the tested concrete (B40-II, concrete means skeleton) with temperatures was taken from the previous research work, which was studied by J-C Mindeguia in his PhD thesis 2009 [9], EC2 [10] and the experiments carried out by Hélène Carré on the B40-II [11]. In the model, the water and the flow of water were not taken into account. This was adopted with the consideration of the evolution of specific heat (discussed in the following section). The material's properties were calibrated for B40-II concrete, as discussed below.

5.1.3.1 Thermal properties

The density of concrete (ρ) under virgin condition (at 20 °C) was assumed to be 2300 kg/m^3 and the density variation with temperature due to water loss was considered as suggested in EC2 [10]. The evolution of conductivity with temperature was adopted based on the normalised value reported in Mindeguia PhD thesis 2009 [9], while the specific heat with temperature was determined from the normalised standard trends provided by EC2 [10]. To do that, the conductivity (λ) and specific heat (Cp) tests were carried out on B40-II concrete at room temperature (20 °C) in SIAME and then the evolutions with the temperature were calculated based on the normalised value as described above. Since the thermal conductivity of the concrete was reported up to 400 °C in reference [9], therefore, at 600 °C, the thermal conductivity was calculated based on the normalised value provided by EC2 [10], since the values are very similar to EC2 from 200 °C, see Figure 5.1b. It is important to note that the role of water vaporisation taken into account with the evolution of Cp. In order to capture that with the numerical model, the time step must be small enough (time step of 1 second was used) to ensure that the

temperature evolution of each node follows correctly the Cp curve. As an example, if the temperature at a point for time step i is 80 °C and at time step i+1 is 220 °C, the effect of water vaporisation is missed. For other cases, it can be only partly taken into account. The variations of mass density, thermal conductivity and specific heat are represented in Figure 5.1.

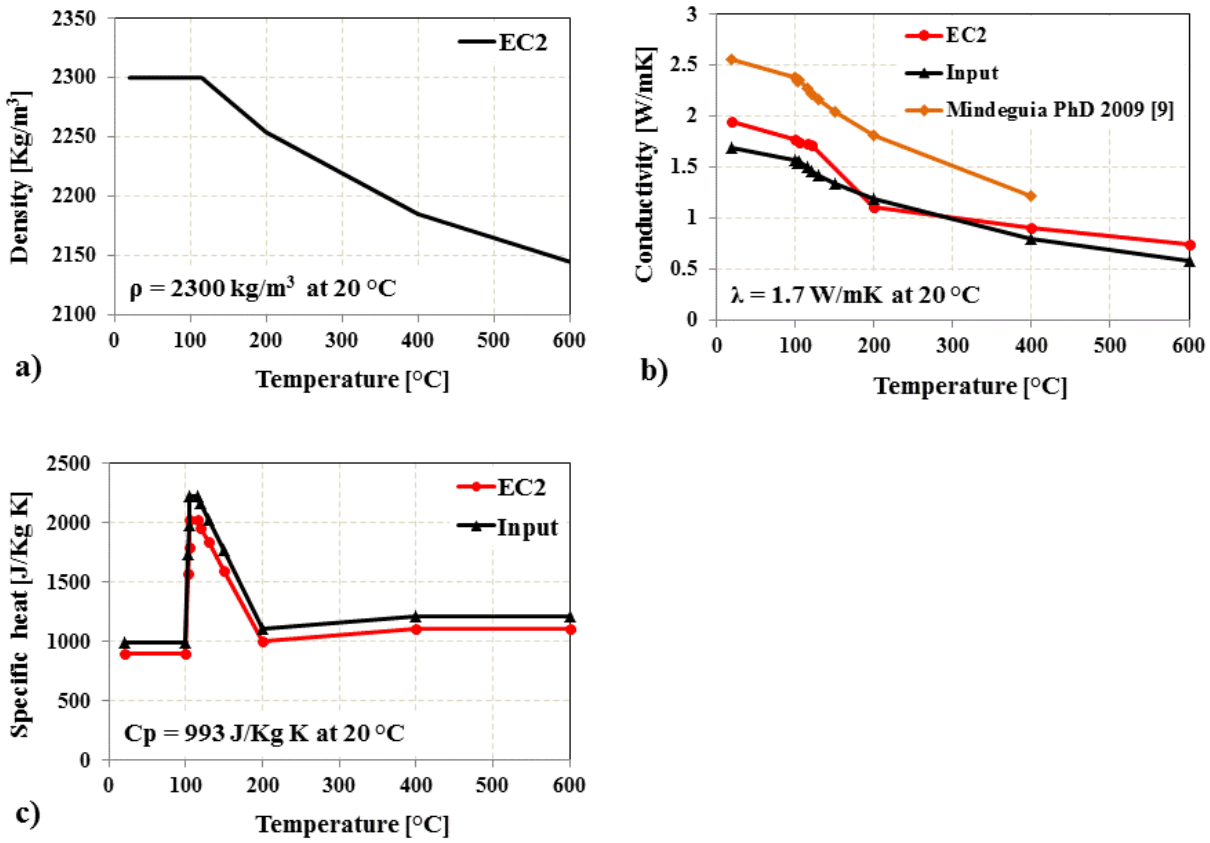

Figure 5.1: Variations of concrete density (a), thermal conductivity (b) and specific heat (c) as a function of temperature.

5.1.3.2 Mechanical properties

The variation of modulus of elasticity (E) and coefficient of thermal expansion (α) of the tested concrete with respect to temperature was taken from the experimental results of the reference [9], while the tensile strength (f_t) and fracture energy (G_f) was taken from the experiment carried out by Hélène Carré on the B40-II [11]. In order to obtain the possible shape of the displacement curve measured in the experimental test, the coefficient of thermal expansion (α) was adjusted with the unloaded experimental test. It can be noticed that the α curve has three segments, almost constant from 20 °C to 364 °C ($\alpha = 1 \times 10^{-5}$ µm/m/°C), then increased until 508 °C ($\alpha = 1 \times 10^{-5}$ to 1.5×10^{-5} µm/m/°C) and again constant from 508 °C to 619 °C ($\alpha = 1.5 \times 10^{-5}$ µm/m/°C), see Figure 5.2d. The detailed information about the testing apparatus, the geometry of the specimens, standards and loading rates for measuring the mechanical properties of the tested concrete under high temperatures are given in references [9, 11]. While the evolution of Poison's

ratio of concrete with temperature was evaluated according to the Equation (5.12) proposed by Bahr et al. 2013 [12].

$$\vartheta_T = a.e^{-b.T} = 0.204.e^{-0.002.T} \text{ with } 20\ °C \leq T \leq 500\ °C \quad (5.12)$$

where T is temperature, ϑ is Poison's ratio; a and b are regression coefficients.
The mechanical properties of concrete with the increased temperature are presented in Figure 5.2.

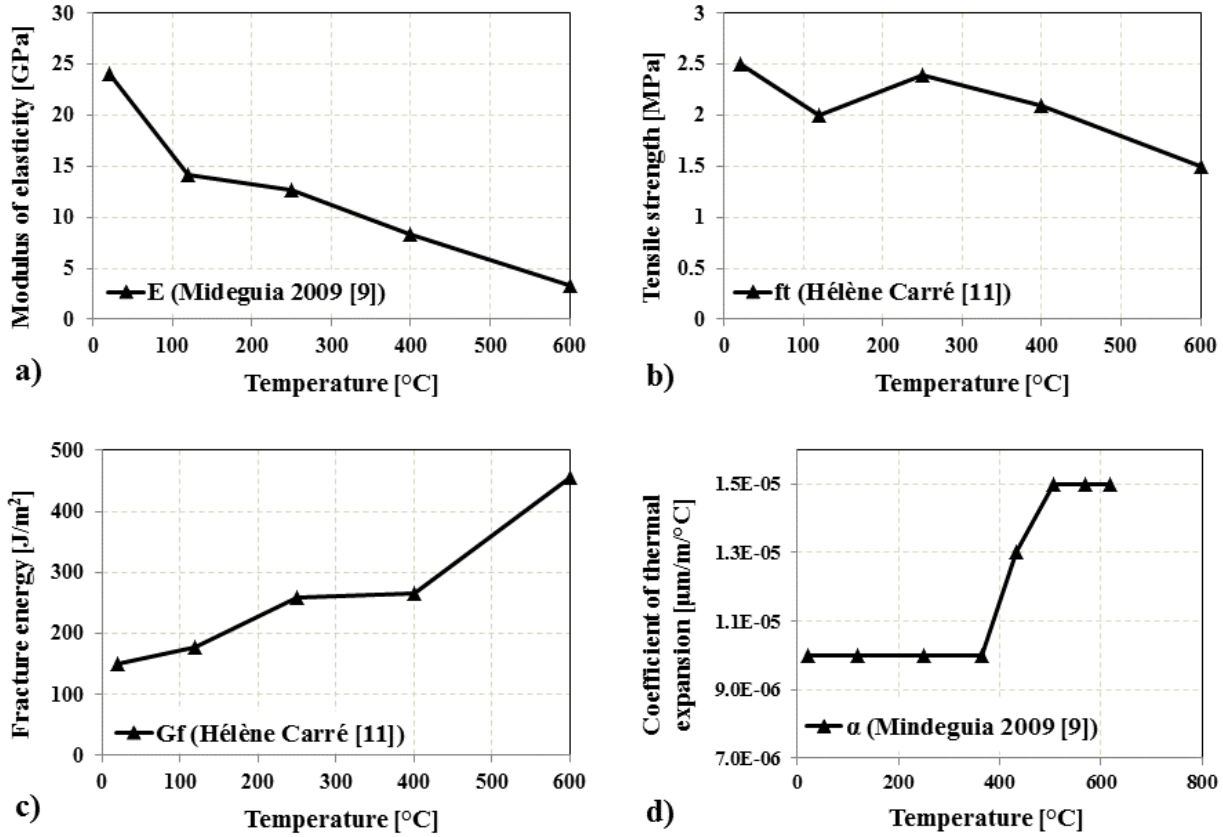

Figure 5.2: Evolution of mechanical properties as a function of temperature.

5.1.4 Geometry and mesh

One-quarter of the specimens (slab and cube) were modelled, given its symmetrical configuration in the longitudinal and transverse directions for the geometry and load, to reduce the computational effort required to perform the analysis. 3D geometry cubic with 8 nodes and prismatic with 6 nodes elements mesh for biaxial slab and cubic with 8 nodes elements mesh for uniaxial cube models were used. The total number of nodes and elements were, respectively, 11968 and 10430 for biaxial slab and 12177 and 10400 for the uniaxial cube model. The size of the modelled slab was 400 x 400 x 100 mm^3, while the size of the load supporting steel plate was 100 x 300 x 50 mm^3. The size of the modelled cube was 100 x 200 x 100 mm^3. Linear

propagation of the mesh (2 mm starting from the hot face to 10 mm in maximum towards the cold face) has been used in both models (uniaxial and biaxial model).

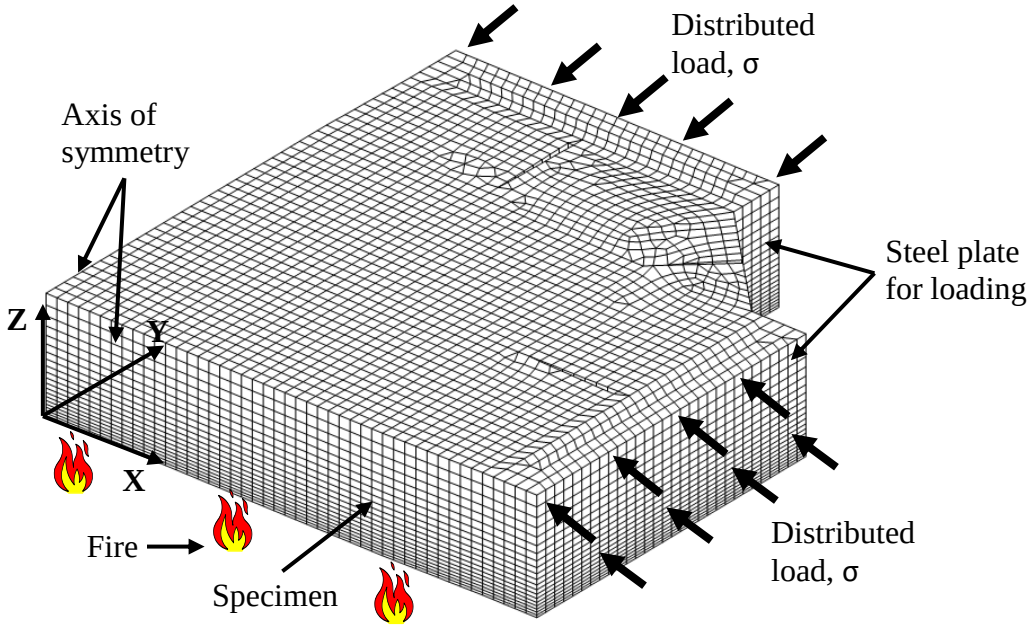

Figure 5.3: Finite element mesh for one-quarter of the slab.

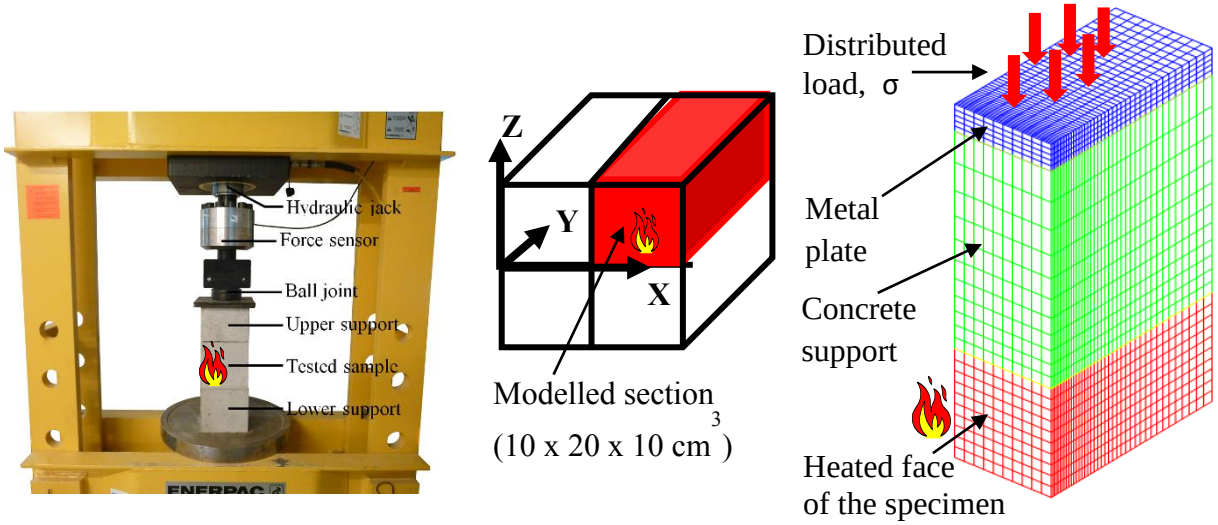

a) Experimental set-up, sample in the hydraulic press

b) Modelled 1/4th of the cubic specimen

c) Finite element mesh of the cube specimen with supports.

Figure 5.4: Uniaxial modelled cube specimen with the concrete support and metal plate.

In order to achieve the real situation as in the experimental set-up during the fire tests, the concrete cube support (100 x 200 x 200 mm^3) with a load supporting steel plates (100 x 200 x 50

mm^3) on the specimen was modelled as well. A typical geometry with the mesh of the specimens (biaxial slab and uniaxial cube) is shown in Figures 5.3 and 5.4. In the uniaxial cube model, the maximum mesh size of 10 mm (width) by 10 mm (height) was used for the specimen and a bit bigger size of mesh was used for the concrete support to limit the duration of the computation.

5.1.5 Boundary conditions

The boundary conditions and load application were identical to that used in the experimental tests (uniaxial and biaxial test). In both models (biaxial and uniaxial model), the temperature history recorded during the fire test (at the exposed surface) was taken as an input thermal boundary condition. Intermediate temperatures in the specimens (slab and cube) were calculated based on 3D finite element heat transfer analysis based on thermal conduction laws by Fourier's differential as shown in Equation 5.1.

In the biaxial slab model, only the central part of the bottom slab (300 x 300 mm^2) was heated to keep the external concrete rim colder, while in the uniaxial cube model, the whole face of the specimen (100 x 100 mm^2) was heated as in the experiment. The initial temperature on the exposed surface of the specimens was equal to the ambient temperature (T_0 = 20 °C). No heat exchange between the cold face and air were considered, hence the temperature at the cold face remains constant (i.e. T = 20 °C) throughout the whole test (30/60 min). In order to achieve the real situation as in the both experimental set-up during the fire tests, the heat transfer was allowed from the heated specimens (slab and cube) to the load supporting concrete cube and steel metal plates.

In the biaxial model, zero displacement was imposed at the centre of the bottom surface (in the Z direction at the point O, Uz = 0, see Figure 5.5) to ensure isostaticity (the reference 0 Uz displacement is not the same for experiments, but since all measurements are relative, we will be able to compare them). In the uniaxial cube model, the displacements were restrained in the Y direction at the point O (Uy = 0) and the symmetry axis in X and Z directions (Uz = Ux = 0), since this is the cut section of the whole cube specimen, see Figure 5.6.

In both models, a constant distributed compressive load (uniaxial or biaxial load) was applied before heating and then the load was kept constant throughout the fire test, while the temperature of the specimen increased. In the biaxial model, the load was applied parallel to the heated face of the slab on the steel metal plates (300 mm long and 100 mm wide on each side), which transfers the load to the specimen. While in the uniaxial model, the load was applied at the rectangular metal plate which transfers the load to the concrete support and then transfers to the top of the specimen. During application of the load, the temperature on the exposed surface of the specimens was equal to the ambient temperature (T_0 = 20 °C) for at about 100 seconds, once the target load was reached, the thermal load was applied to the specimen. Four different levels of biaxial compressive stress (0, 1.5, 5 and 10 MPa) and six different levels of uniaxial compressive stress (0, 4, 8, 12, 16 and 20 MPa) have been investigated as in the experiment. In the both models, the stresses resulting from the self-weight of the specimens (slab and cube), load induced thermal strain (LITS) and creep strain were not taken into account. As already

mentioned before, in order to achieve reliable results and to consider the role of water vaporization, a small time step of 1 second was used.

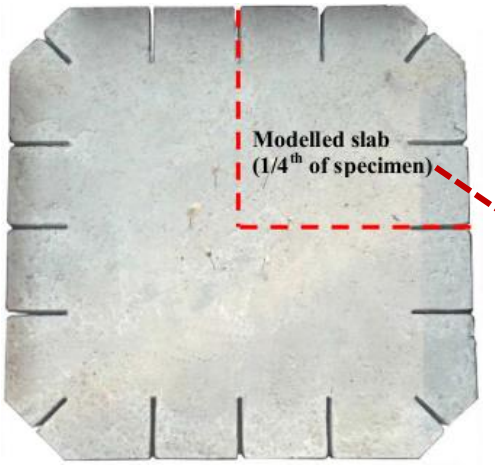

a) Concrete slab specimen

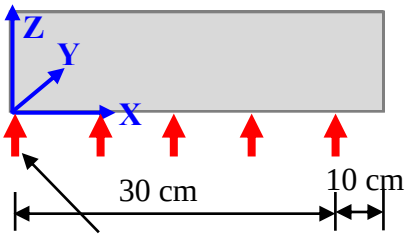

● Thermal load (i.e. hot face temperature) at the bottom face of the slab, T_0 = 20 °C

● No heat exchange between the cold face and air. T constant at cold face (T_{cold} = 20 °C)

b) Thermal boundary condition

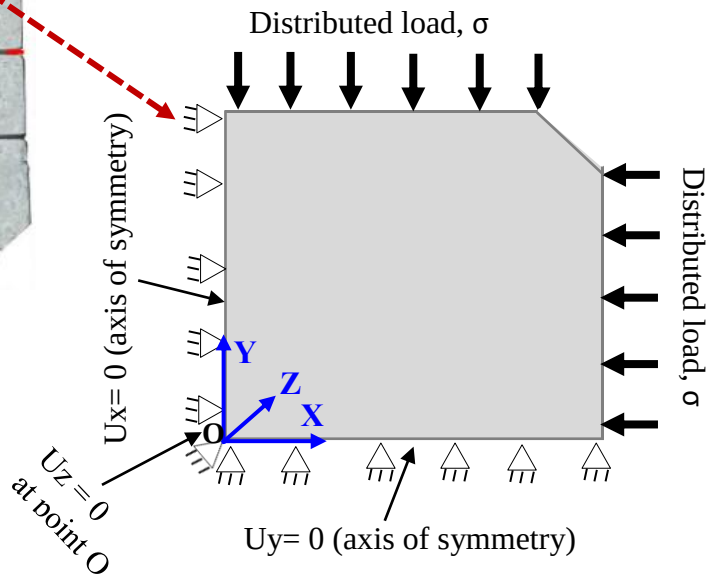

c) Mechanical boundary condition

Figure 5.5: Boundary conditions of the modelled slab.

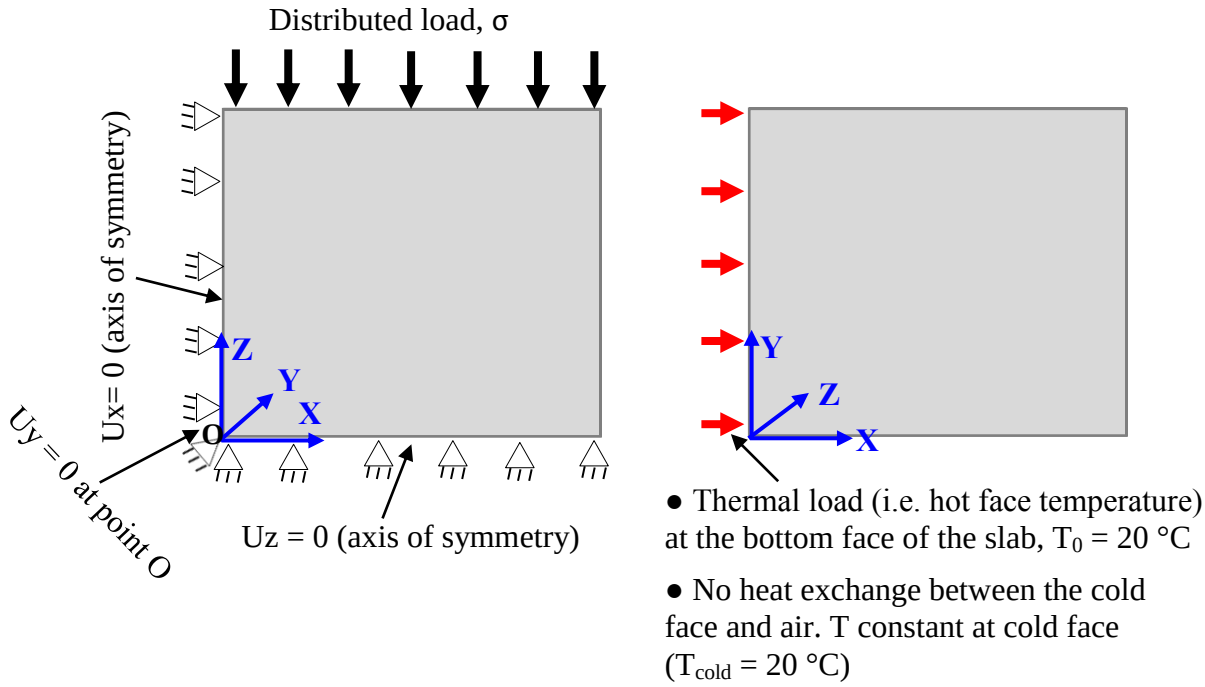

a) Mechanical boundary condition b) Thermal boundary condition

Figure 5.6: Boundary conditions of the modelled cube.

5.2 Numerical results and discussion

In order to validate the thermo-mechanical model, the predicted results from the numerical model were compared with the experimentally measured temperature distribution at different depths from the exposed surface of the specimens and out of plane displacements at the cold face. To expand these comparisons, a broad discussion is made in the sections below.

5.2.1 Predicted thermal response and comparisons with experimental results

Predicted and experimentally measured temperatures at different depths from the exposed surface of biaxial and uniaxial fire test specimens are compared in Figure 5.7. The 3D image of the temperature distribution of the slab and cube specimens can be seen in Figure B1 in the Appendix B. It can be seen that the predicted temperatures are generally in good agreement with the experimentally measured temperatures throughout the fire exposure time. In biaxial computation, in all depths (except at 10 mm) from the exposed surface of the specimens, the predicted results were very close to the experimental results during the first 10 min of fire, thereafter dropped slightly and lagged the model predictions up to 30 min of computation (see Figure 5.7b). At a later stage (after 30 min of computation), an excellent match was found between the predicted and experimental results, which is the important stage from the point of view of predicting the fire resistance of the concrete, since the influence of migration of moisture was less evident due to the completed evaporation process of the moisture (i.e. concrete became

dry). Interestingly, the predicted temperature was fitted well with the experimental temperature measured at 20 mm from the exposed surface of concrete throughout the whole test (60 min), probably this was due to the less evidence of the temperature plateau at that depth. While in the uniaxial computation, the numerical model predictions show a quite good agreement with the experimental temperatures throughout the whole test (30 min). The minor discrepancies could be attributed to the differences in the thermal properties, such as thermal conductivity and specific heat, since these properties were not experimentally measured for this concrete at the elevated temperatures. Since the positions of the thermocouples are not known precisely, hence this discrepancy may also be partly explained by the uncertainty of the thermocouple position due to technical offsets during installation.

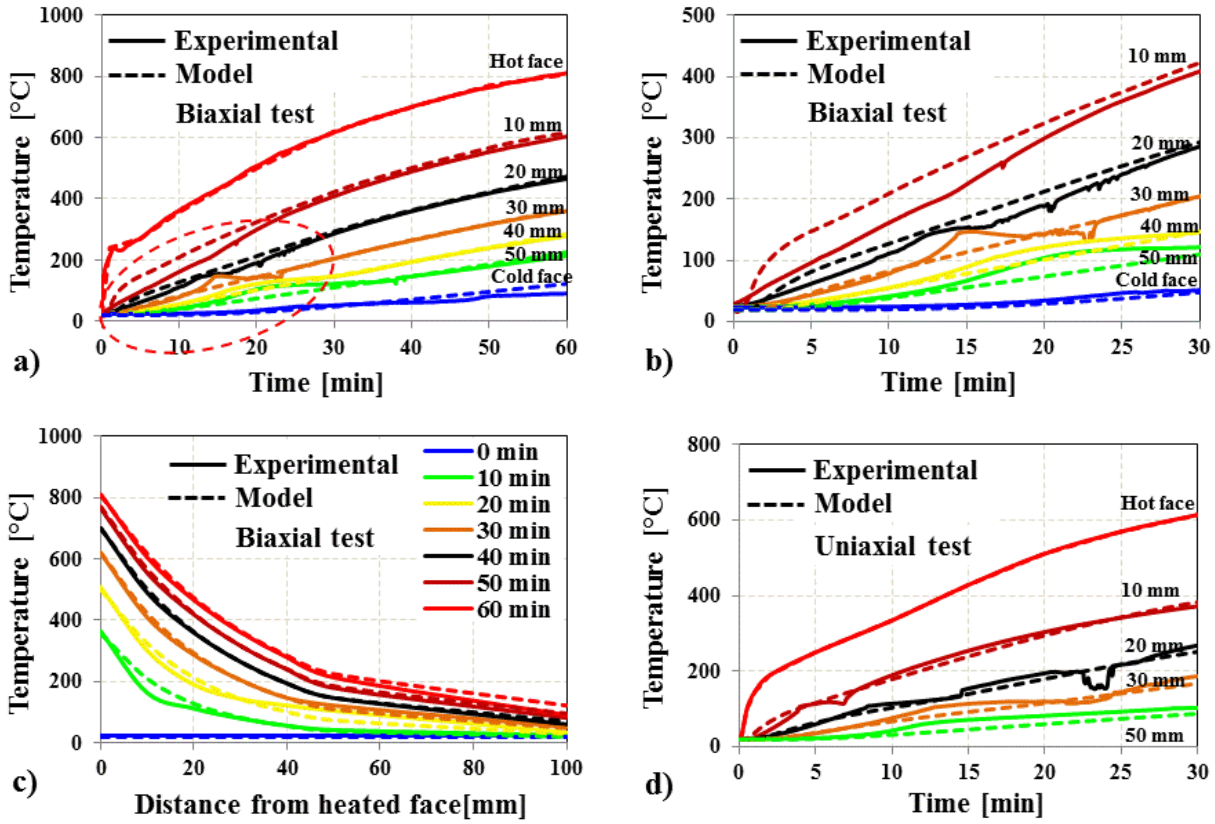

Figure 5.7: Predicted and experimentally measured temperatures of the unloaded test specimen as a function of time: (a) biaxial fire test and (d) uniaxial fire test; (b) zoom of the circle point of Figure 5.7a to show detail in data and (c) predicted and experimentally measured temperature profile through the thickness of concrete slab specimen.

As discussed above in section 5.1.3.1, the evolution of thermal properties with temperature was adopted based on the normalised value reported in Mindeguia PhD thesis 2009 [9] and standard trends provided by EC2 [10] due to the lack of data on the thermal properties of this concrete, which does not represent the exact thermal properties of the modelled concrete. However, in biaxial computation, at 10 mm from the exposed face, the model predicts slightly higher

temperatures during the first 20 min of fire than the measured ones (see Figure 5.7b). This discrepancy may be partly explained by the uncertainty of the thermocouple position due to technical offsets during installation, since the other temperatures were followed more closely the trends of the experimental curve.

In both fire tests, it can be noticed that an initiation of the temperature plateau has been observed close to the heated surface at approximately the boiling temperature of water at around 100 °C. Once the thermocouples reached a plateau, the temperatures almost remained constant for a few minutes until the water phase change was completed, which is quite challenging and difficult to capture in the numerical model. It was also found that some of the thermocouples (far away from the hot face) did not experience a clear temperature plateau. This is probably due to thermal damage (i.e. cracking) inside the concrete (caused by thermal mismatch between cement pastes and aggregates), which allow a greater amount of moisture loss during the fire test (a significant amount of moisture was observed on the cold face of the biaxial slab and cold sides of the uniaxial cube tests). As a result, the drying process is different at different locations due to the least amount of water in that location, which is also quite challenging and difficult to capture in the numerical model.

In order to compare the thermal response inside the concrete slab, the predicted and measured thermal gradients through the slab thickness was drawn (see Figure 5.7c) at 0 to 60 min with the interval of 10 minutes of fire exposure. Numerical and experimental results showed that the heating of concrete involves significant high temperature gradients particularly in the first centimetre of the heated surface of the slab and these temperature gradients raised gradually with the increasing temperature. Except for the early stages of the test (at 10 min of fire exposure), comparatively low discrepancies between the predicted and measured temperatures was found throughout the thickness of the slab.

5.2.2 Predicted out of plane displacement and comparisons with experimental results

The out of plane displacement measured at the centre of the slab as a function of time obtained from the test and finite element analysis are compared, as shown in Figure 5.8. The Figure 5.8a shows that there is a good agreement between the measured and the predicted displacement of the unloaded slab throughout the fire exposure time, since the coefficient of thermal expansion was adjusted with this unloaded test. In the model, the shape of the displacement curve is a bit different than the experimental one. A bit higher rate of vertical displacement was observed during the early stage of heating (up to 7 min of fire), afterwards, there is a good agreement with the experimental curve from 8 min to 12 min of fire and then decreased and followed by an increasing rate of displacement. This behaviour could be due to the input value of the coefficient of thermal expansion (CTE, i.e. α) of the modelled concrete (see Figure 5.2d). Since the CTE triggers the deformation of the concrete slab, hence this shape of the CTE can explain the displacement shape of the modelled slab. The maximum vertical displacements of the measured and predicted are, respectively, -4.0 mm and -4.40 mm, while the

maximum difference between predicted and measured vertical displacement are about 0.44 mm, see Figure 5.8a.

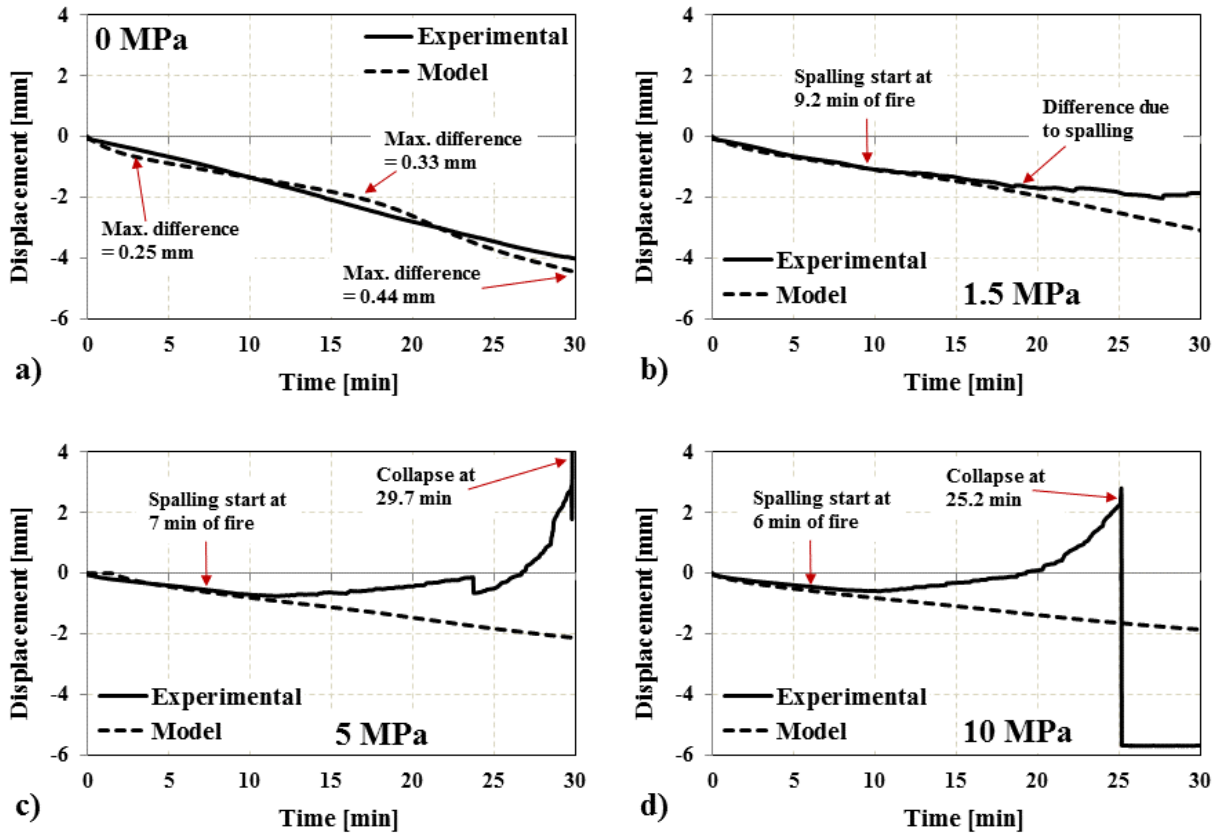

Figure 5.8: Comparison between predicted (model) and experimentally measured out of plane displacement at the top-mid of the slab (i.e. LVDT 5) subjected to ISO 834-1 fire under different levels of biaxial compressive stress.

As concern the loaded tests, the predicted displacements are in good agreement until the specimen did not spall in the experimental tests. As described in the section 4.2.3.4 (chapter 4), the presence of load during heating plays an important key role in the development of thermal curvature of the slab due to the eccentricity of the external load (caused by the decay of concrete stiffness in the hot bottom layers and reduction of thickness, e.g. spalling). Since the spalling occurred in the loaded tests, a lower downward curvature was observed in the experimental test (due to the eccentricity of the external load). And then, upward deflections was observed in the most loaded specimens (see Figure 5.8c-d) due to the larger eccentricity caused by the higher reduction of thickness (maximum spalling depth exceeded half of its thickness, see Figure 4.21 in chapter 4). Since the reduction of thickness due to spalling with time has not been considered in the model, this could explain the difference in this behaviour between predicted and measured displacement as shown in Figure 5.8b-d.

5.2.3 Distribution of stresses in the concrete

The experimental test results described in chapter 4 clearly shown that the amount of spalling was increased with the increased applied compressive stress (biaxial and uniaxial). In order to deeper understanding the role of external loading on the mechanism of fire spalling of concrete, the stress profiles along the cross-section of the concrete slab (stress parallel to the loading direction, σ_{xx} for the biaxial test) and cube (stress parallel to the loading direction, σ_{zz} for the uniaxial test) are plotted in Figure 5.9 and 5.10, respectively for different fire durations under different external compressive loading. The extraction points of the stress profile for the biaxial slab and uniaxial cube models were X = 10 mm, Y = 10 mm, Z = 0, 2, 4, 6….100 mm and X = 10 mm, Y = 0, 2, 4, 6…..200 mm and Z = 30 mm, respectively. On the origin of the Y-axis in the plots 5.9 and 5.10, 0 mm denotes the exposed surface of the specimens (slab or cube) while 100 mm (for slab) or 200 mm (for the cube) corresponds to the unexposed face of the specimens. The sign convention for stresses in the x-axis, the positive values represent tension and negative values represent compression.

In general, as the concrete specimen (slab or cube) was heated, the hot surface of the specimen becomes compressed and tensile stress initiated at a certain distance between hot and cold faces (mostly at the centre part of the specimen), while the cold surface becomes compressed to maintain the equilibrium and tends to restrain expansion. This behaviour is due to the temperature gradient generated across the concrete cross section of the specimens (see Figure 5.7c). The extremum tensile and compressive stress in unloaded tests heated after 30 min of fire could reach up to approximately 3.3 MPa and -36.8 MPa, respectively in the biaxial slab and 3.6 MPa and -25.6 MPa, respectively in the uniaxial cube. At the 30 min of heating, the hot face temperature of biaxial slab and uniaxial cube models are 621 °C and 614 °C. The maximum hot tensile strength (f_t) of the B40-II tested concrete at 600 °C is 1.5 MPa (see Figure 5.2b), which is about 2.4 times lower than the tensile stress inside the concrete specimens (slab and cube). Even though the model we used, the damage and then the cracks are due to positive strain (see section 5.1.2), the above values demonstrated that the multiple cracks could occur inside the concrete specimens such as orthogonal cracks perpendicular to the heated surface in the concrete core and surface cracks parallel to the exposed face in the hot layers. As a consequence, these cracks increase the permeability and decrease the stresses in the surrounding material [3], which help to mitigate the build-up of pore pressure by favouring vapour migration and may prevent moisture clog. Thereby, the risk of fire spalling is avoided.

When an external compressive load was introduced, the tensile stress was remarkably reduced and even it was completely avoided in the higher compressive loading (10 MPa for biaxial slab and 12-20 MPa for the uniaxial cube, see Figures 5.9-5.10). At the same time, the compressive stress increases in the hot and cold surfaces with the increasing applied compressive loading. These numerical results are in good agreement with non-linear finite element analysis carried out by Lo Monte and Felicetti 2017 [13].

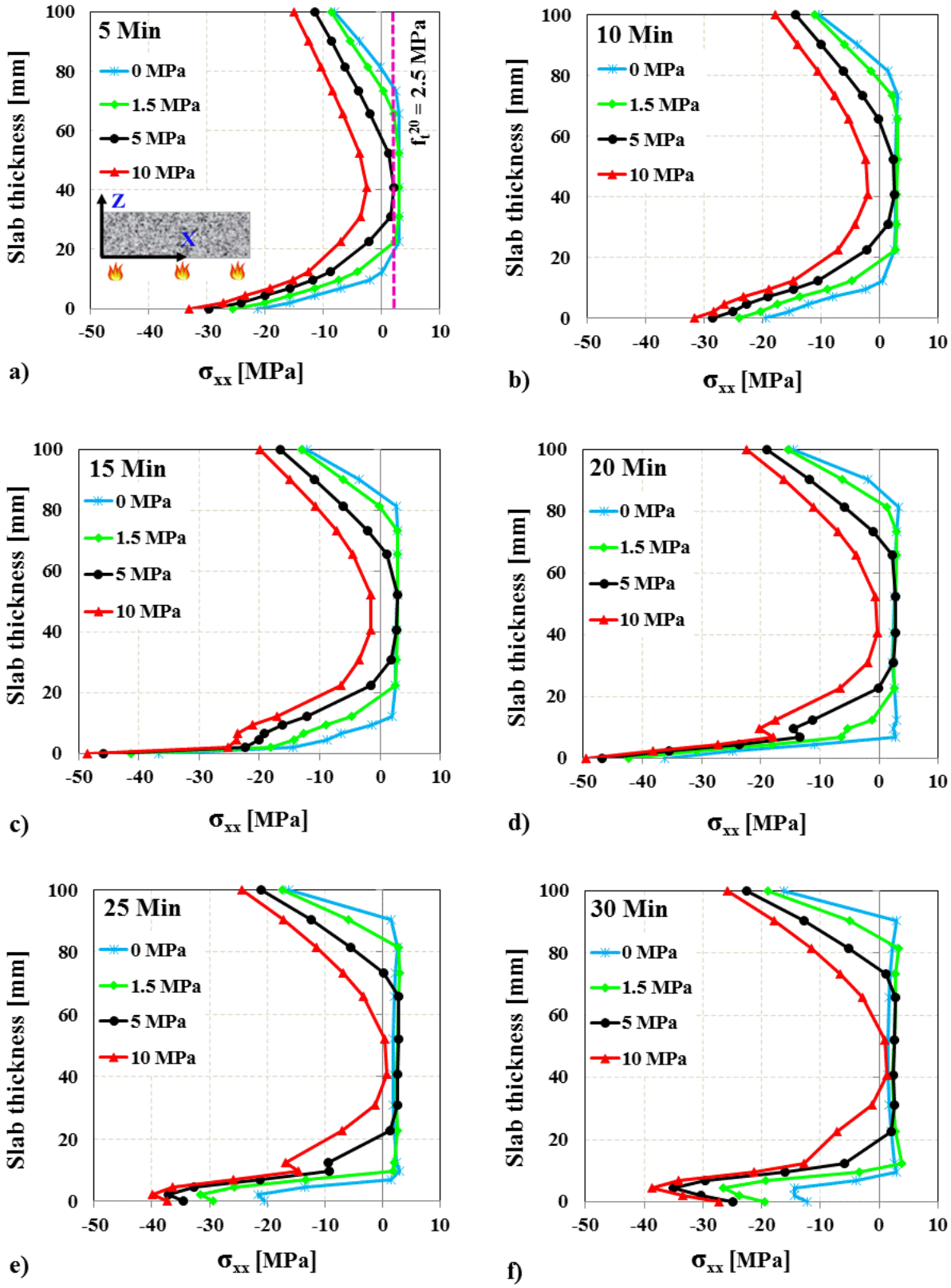

Figure 5.9: Evolution of concrete stress profiles in the x-direction (σ_{xx}) through the thickness (towards fire) of the slab for different fire durations under different biaxial compressive stress.

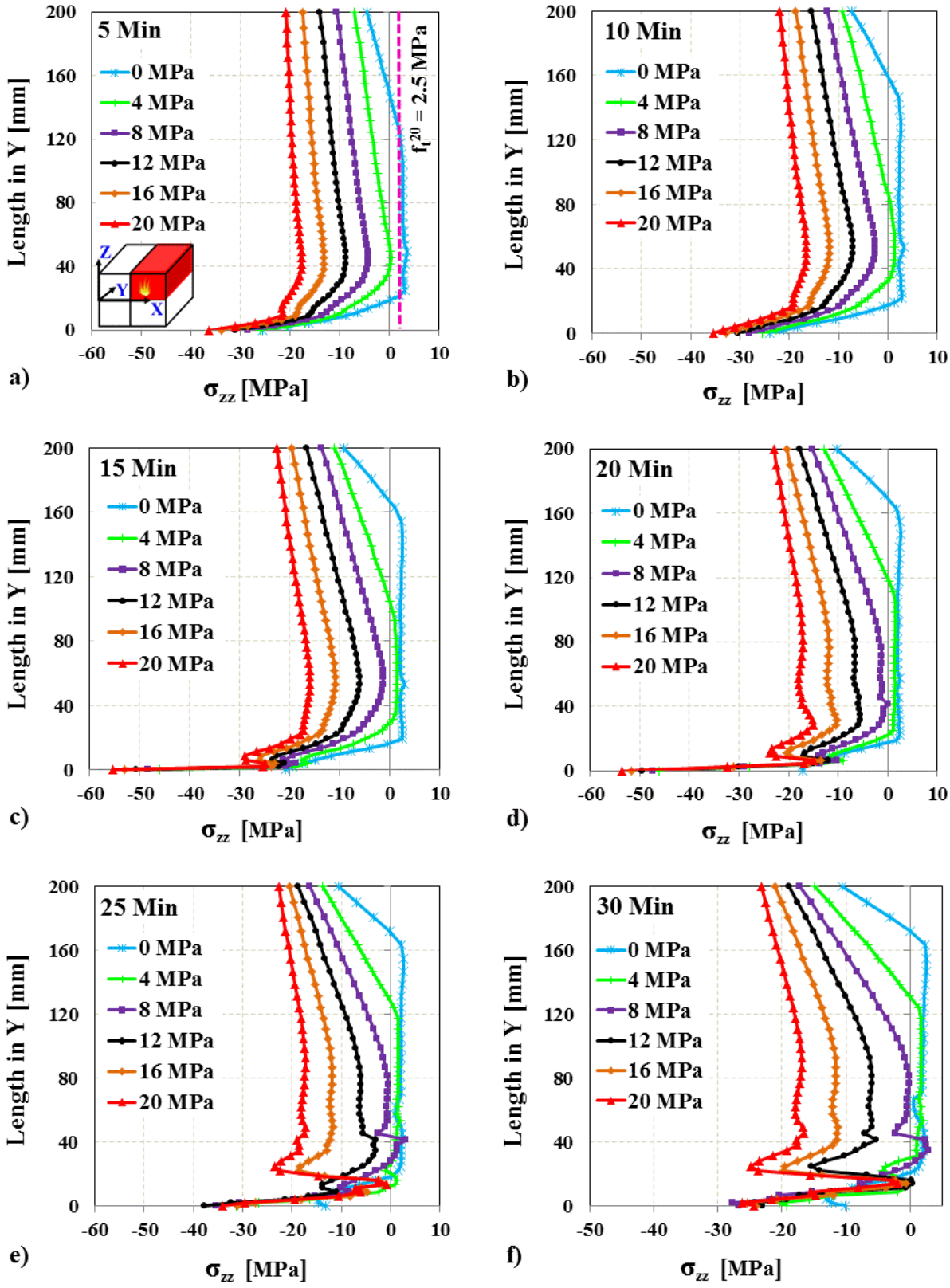

Figure 5.10: Evolution of concrete stress profiles in the z-direction (σ_{zz}) through the thickness of the cube (towards fire) for different fire durations under different uniaxial compressive stress.

Hence, the cracks parallel to the heated surface of the slabs should be increased with the increased applied compressive loading [14] (due to stresses induced by thermal gradients and external compressive loading), see an example in Figure 5.13, while it decreases for the cracks that are perpendicular to the heated surface, see Figures 5.11-5.12. A more detailed presentation of the effect of loading on cracking is given in the section 5.2.4. As a result, fire spalling should be higher in the loaded tests than the unloaded tests due to higher stresses with the combination of higher pore pressure (see Figures 4.15 and 4.26 in chapter 4). These effects will be more pronounced with the increasing applied compressive loading. The spalling mechanism is discussed more in details in chapters 6.

As Majorana et al. 2010 [15] described that the internal cracking has a dual and opposite effect upon explosive spalling. On the one hand, the cracks can be regarded as 'channels' for the vapour pressure to escape during heating, on the other hand, they facilitate the process of spalling by providing a source for crack propagation.

It can be noticed that after being 30 minutes of heating, the compressive stress in the hot layer decreases and this is more evident for the higher compressive loading. This behaviour could be due to the higher reduction of the young modulus of elasticity of concrete at high temperatures. At the 30 min of heating, the hot face temperature of biaxial slab and uniaxial cube models are 621 °C and 614 °C. The maximum hot young modulus of elasticity (E) of the B40-II tested concrete at 600 °C is 2.9 GPa, see Figure 5.2a, which could be very close to zero above 600 °C.

5.2.4 Damage fields and crack patterns

The study of damage field and crack opening of the slab and cube specimens heated under different levels of compressive load are illustrated in Figures 5.11-5.13 and Figures B2 and B3 in the Appendix B. In Figure 5.12, the scale "Dom" represent the global damage of the specimen (1 = fully damaged and 0 = undamaged), while the scale "EPzz" represent the crack opening (in m) perpendicular to the heated surface of the specimen. In Figure 5.11, it can be seen that the external compressive load is a key factor affecting the crack opening of the concrete during heating. In the unloaded biaxial fire test, with the increasing temperature, the vertical thermal cracks (perpendicular to the heated face) were increased due to the gradual increase of thermal stresses. These cracks are mainly initiated nearly at the centre part of the specimen and then propagated through the thickness of the specimen with time.

While an external compressive load was introduced, these cracks remarkably reduced and going to be zero for the higher compressive load (10 MPa) (see Figure 5.11). This reduction of vertical cracks caused by loading decreased the permeability of concrete, which explains the higher risk of spalling due to higher pore pressure and higher stresses, since these cracks not only release the pore pressure as well as stresses (an example can be seen where the cracks initiated at 13.7 mm from the exposed face of the cube, see Figures 5.10f and 5.13a). Similar behaviour has been observed in the uniaxial model. As an example can be seen in Figure 5.12, clear horizontal cracks can be seen in the unloaded cube (0 MPa, see Figure 5.12c), while these cracks were completely disappeared for the loaded cube (20 MPa, see Figure 5.12d) test.

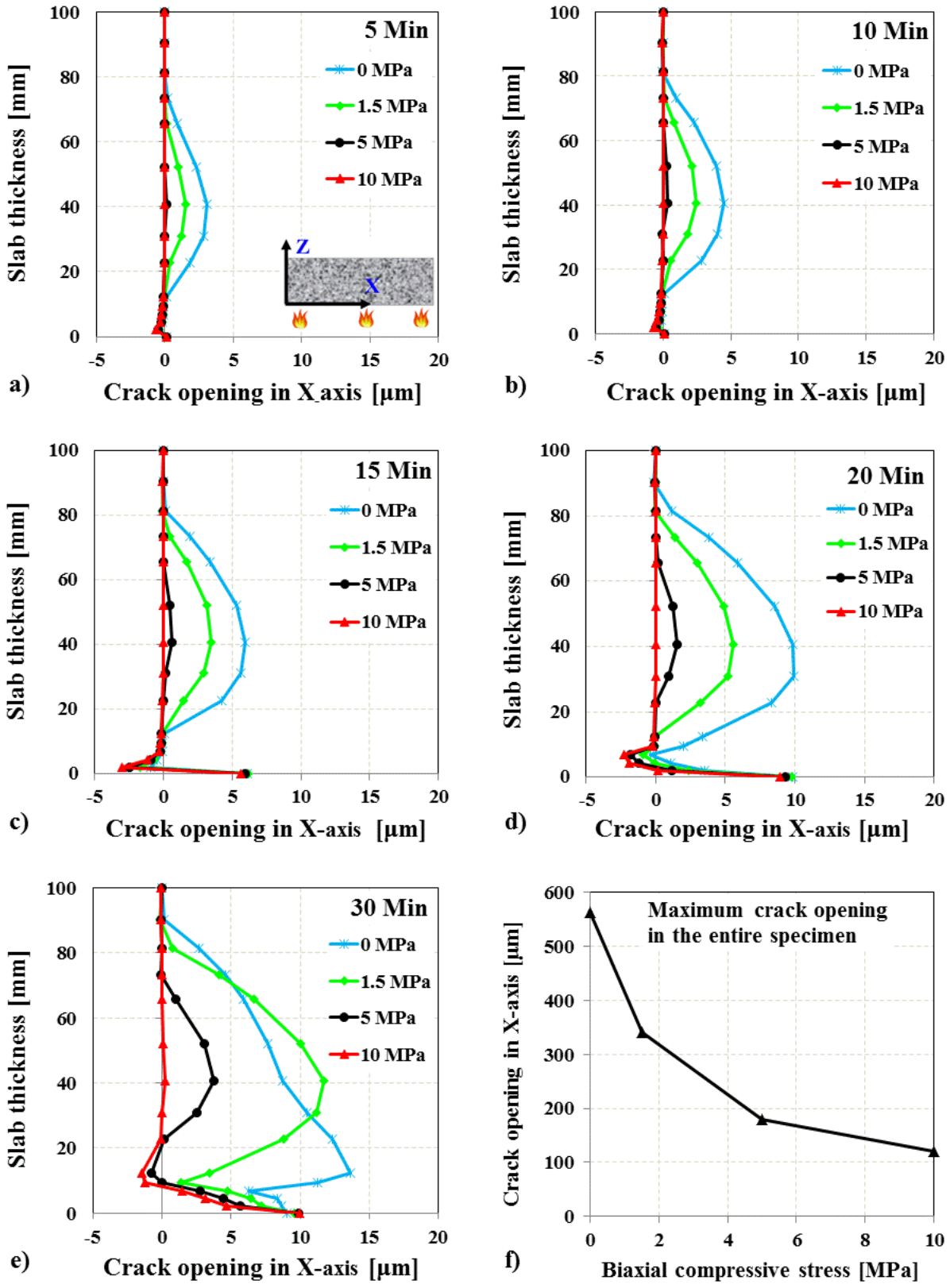

Figure 5.11: Crack opening perpendicular to the heated surface of the slabs for different fire durations under different biaxial compressive stress.

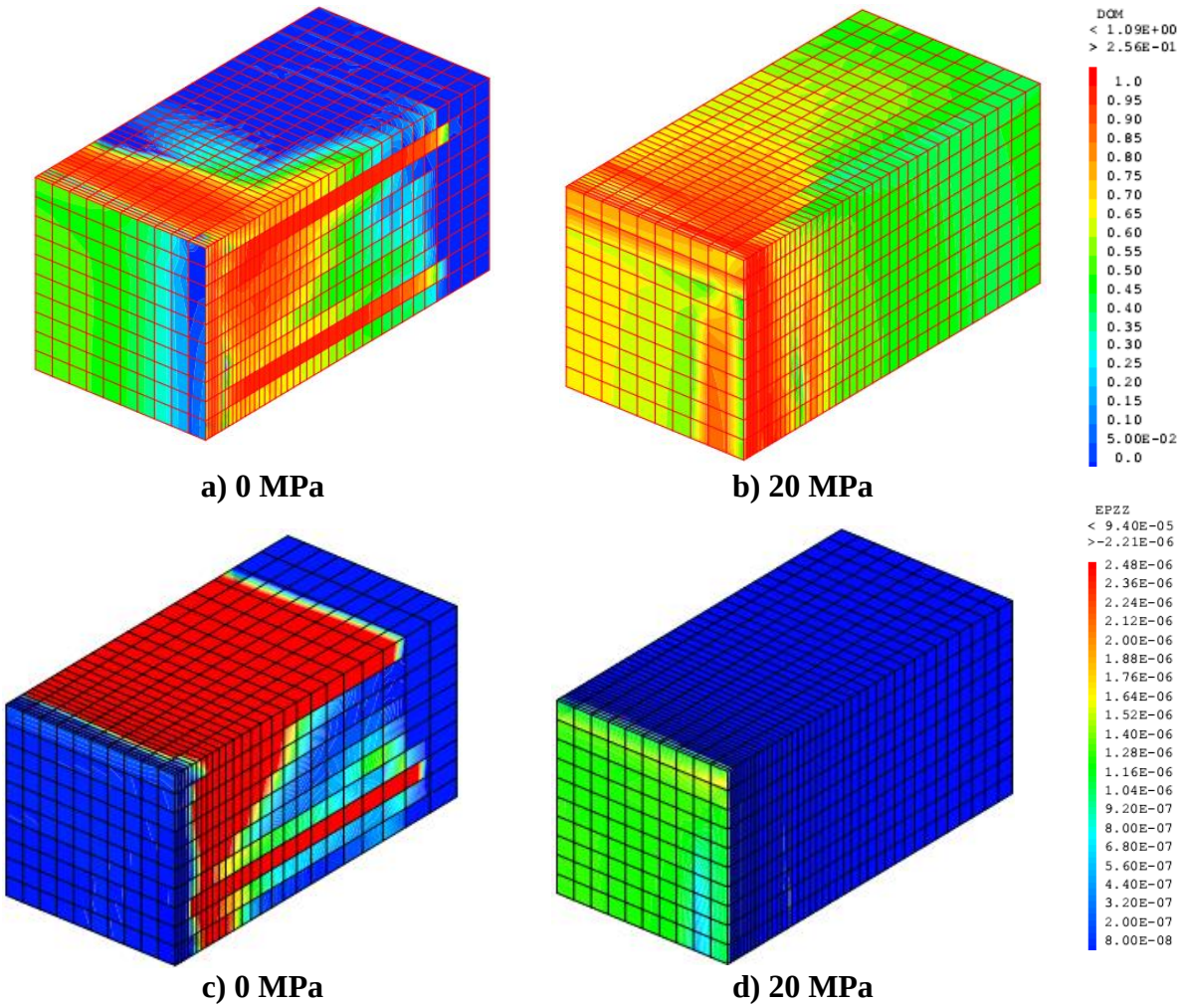

a) 0 MPa **b) 20 MPa**

c) 0 MPa **d) 20 MPa**

Figure 5.12: Typical damage fields of the unloaded (a) and loaded (b) test; Crack opening perpendicular to the heated surface of the cubes in unloaded (c) and loaded (d) test.

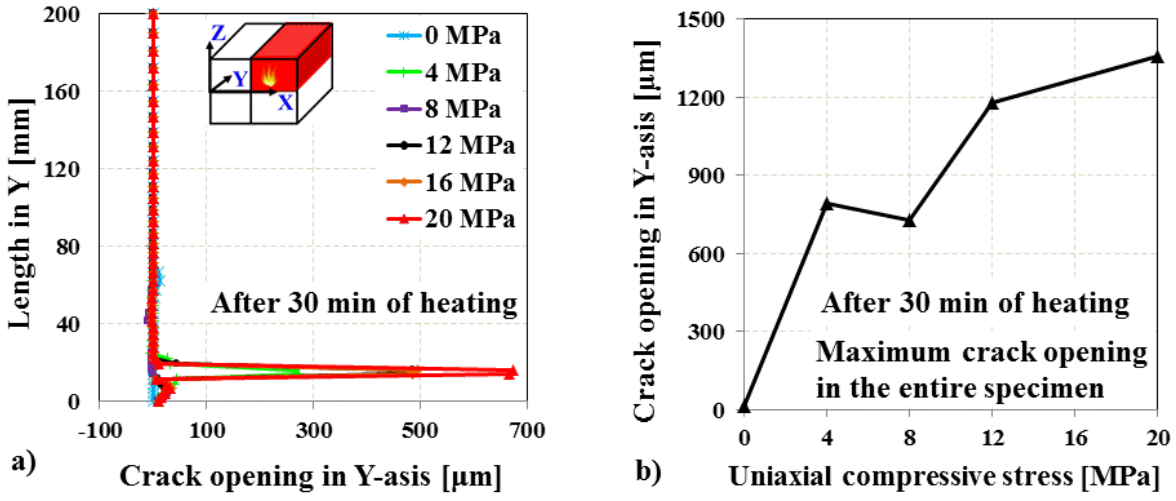

Figure 5.13: Crack opening parallel to the uniaxial load: a) extracted at X = 10 mm, Y = 0, 2, 4, 6…..200 mm and Z = 30 mm, and b) from entire section.

Interestingly, an increasing trend of the crack opening (parallel to the loading direction) was observed with the increased uniaxial compressive loading during heating, see Figure 5.13. These results are in good agreement with the measurement of the residual axial permeability tests after preheating under uniaxial loading. The axial permeability was increased with the increased uniaxial compressive loading during heating-cooling, a clear vertical crack was observed in the loaded specimen, see Figures 3.20 and 3.21 in chapter 3. This increasing trend of crack (parallel to the direction of loading or heated surface) of the loaded cube can increase the risk of fire spalling. The maximum crack opening occurred at the depth of 13.7 mm from the exposed face of the cube, which could demonstrate the initial spalling depth of the loaded test (Figure 5.13a).

5.3 Summary and conclusions

Based on the predicted results and discussion presented herein, the following conclusions can be made on the role of compressive loading on the fire spalling behaviour of concrete:

In the biaxial slab model, in all depths (except at 10 mm), the predicted temperatures were very close to the experimental temperatures during the first 10 min of fire, thereafter dropped slightly and lagged the model predictions up to 30 min of computation. Beyond 30 min of computation, an excellent match was found between the predicted and experimental results. While in the uniaxial computation, the numerical model predictions show a quite good agreement with the experimental temperatures throughout the whole test (30 min).

In the biaxial unloaded model, a good agreement between the measured and the predicted displacement throughout the fire exposure time was observed. While in the loaded models, the predicted displacements are perfectly matched with experiment until the specimen did not spall.

In both unloaded computations, a significantly higher tensile stress occurred in the central part of the specimens and compression stress at the hot and cold surface. When an external compressive load was introduced, the tensile stress was remarkably reduced and even it was completely avoided in the higher compressive loading. At the same time, the compressive stress increases in the hot and cold surfaces with the increasing applied compressive loading (i.e. higher spalling due to higher cracks parallel to the heated face of the specimens).

It has been found that the opening of cracks perpendicular to the loading direction decreased with the increased load, while it increased for the cracks that are parallel to the loading direction. As a consequent, permeability decreased in the direction perpendicular to the heated surface, which affect the migration of moisture from the critical spalling zone of the heated concrete, therefore a higher pore pressure with the combination of higher stresses (due to restrained strains and external load) increase the risk of fire spalling of the loaded tests than the unloaded tests.

5.4 References

[1] de Morais, M.V.G., Pliya, P., Noumowé, A., Beaucour, A-L., and Ortola, S. (2010). "Contribution to the explanation of the spalling of small specimen without any mechanical restraint exposed to high temperature", Nuclear Engineering and Design 240 (2010) 2655–2663.
[2] Fu, Y and Li, L. (2011). "Study on mechanism of thermal spalling in concrete exposed to elevated temperatures", Materials and Structures (2011) 44:361–376.
[3] Lottman, B.B.G., Koenders, E.A.B., Blom, C.B.M., and Walraven, J.C. (2015). "Spalling of fire exposed concrete based on a coupled material description: an overview", 4th IWCS due to Fire Exposure, October 08-09, 2015, Leipzig, Germany.
[4] CEA, CAST3M finite element code, Tech. rep., French Alternative Energies and Atomic Energy Commission. http://www-cast3m.cea.fr/
[5] Fichant, S., La Borderie, C. and Pijaudier-Cabot, G. "Isotropic and anisotropic descriptions of damage in concrete structures", Mec. of Cohesive-Frictional Mat. 4, 339-359 (1999).
[6] Matallah, M., La Borderie, C. and Maurel, O. (2009). "A practical method to estimate crack openings in concrete structures", Int. J. Numer. Anal. Meth. Geomech. (2009).
[7] Code_Aster (2010). "Algorithm of linear thermal transient", Responsable: HAELEWYN Jessica, R5.02.01, Révision: 2d954e843624.
[8] J. Mazars. (1986). "A description of micro- and macroscale damage of concrete structures", Eng. Fract. Mech. 25 (5–6) (1986) 729–737.
[9] Mindeguia JC. (2009). "Contribution Expérimental a la Compréhension des risqué d'Instabilité Thermiques des Béton", PhD Thesis (French), UPPA, Pau (France).
[10] Eurocode 2, 1992-1-2. (2005). "Design of concrete structures. Part 1–2: General rules – structural fire design", Brussels, Belgium.
[11] Carré, H., Pimienta, P and La Borderie, C. "Bending test on concrete at high temperature: evaluation of tensile strength and fracture energy", (not yet published).
[12] Bahr, O., Schaumann,P., Bollen, B and Bracke, J. "Young's modulus and Poisson's ratio of concrete at high temperatures: Experimental investigations", Mat. and Des. 45 (2013) 421–429.
[13] Lo Monte F. and Felicetti R. "Heated slabs under biaxial compressive loading: a test set–up for the assessment of concrete sensitivity to spalling", Materials and Structures (2017) 50:192.
[14] Sertmehmetoglu, Y. (1977). "On a mechanism of spalling of concrete under fire conditions", PhD Thesis, King's College, London, 1977.
[15] Majorana, C.E., Salomoni, V.A., Mazzucco, G and Khoury, G.A. (2010) "An approach for modelling concrete spalling in finite strains", Mathematics and Computers in Simulation 80 (2010) 1694–1712.

6 Fire Spalling Mechanism of the Ordinary Concrete

As described in chapter 2, in the literature, two main hypothesis have been proposed to explain the fire spalling mechanism of concrete, namely: the build-up of pore pressure [1] and the development of thermal stresses [2] in concrete when exposed to rapidly increasing temperature. However, some other authors recommended that the spalling is the combined action of both pore pressures and thermal stresses [3-5]. According to pioneer investigations in the literature (see chapter 2), it is shown that the occurrence of fire spalling is influenced by various parameters, the external compressive load being one of them, which role is not well known in detail.

In order to deeper understand the fire spalling mechanism of the ordinary concrete, a possible mechanism is discussed based on the results presented in this thesis.

6.1 Fire spalling mechanism

6.1.1 Effect of biaxial compressive loading

In order to give a broad idea of the role of external biaxial compressive loading on the fire spalling mechanism of the ordinary concrete, a 2D schematic diagram of the heated slab has been drawn, see Figure 6.1. In Figure 4.21 (see chapter 4), the effect of biaxial compressive loading on the fire spalling behaviour of the ordinary concrete has been categorised into 2 stages: intermediate load (0 to 5 MPa) and higher load (5 to 10 MPa). Therefore, the schematic diagrams of the heated slab have been drawn for these two loading ranges to better explain the fire spalling mechanism of concrete, see Figure 6.1b-c.

When concrete is heated at the bottom surface of the slab in unloaded condition, the hot surface of the specimen becomes compressed and tensile stress initiated at a certain distance between hot and cold faces (mostly at the centre part of the specimen), while the cold surface becomes compressed to maintain the equilibrium and tends to restrain expansion. As a result, multiple cracks could occur inside the concrete specimens such as orthogonal cracks perpendicular to the heated surface in the concrete core and surface cracks parallel to the exposed face in the hot layers, see Figure 6.1a. These cracks are often beneficial to limit the development of thermal stresses [6-7] as well as pore pressure. A quite slow rise with the low magnitude of pore pressure (see Figures 4.25 and 4.26) and lower thermal stress (see Figure 5.9) were observed in the unloaded fire tests than the loaded tests. Thereby, the risk of fire spalling is avoided.

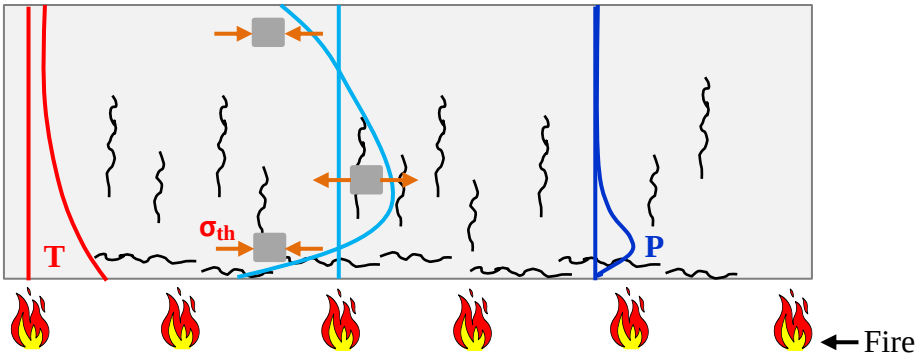

a) Cracking in the slab due to thermal stress (σ_{th}), thermal mismatch and pore pressure (P)

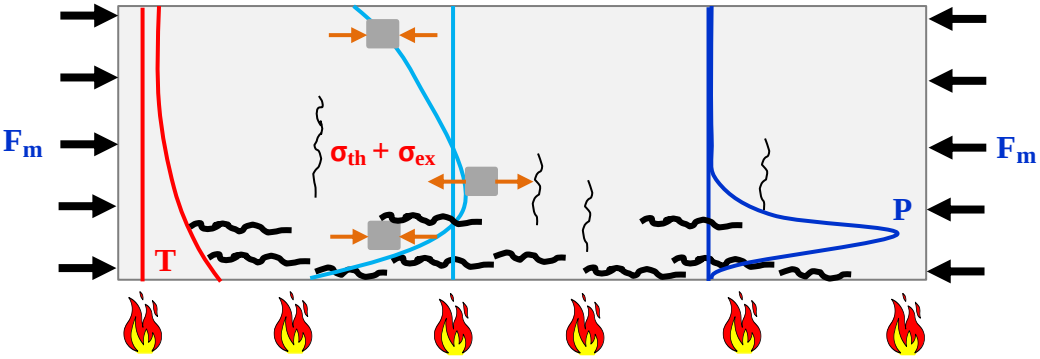

b) Cracking in the slab due to thermal and intermediate external load induced stress, thermal mismatch and pore pressure (P)

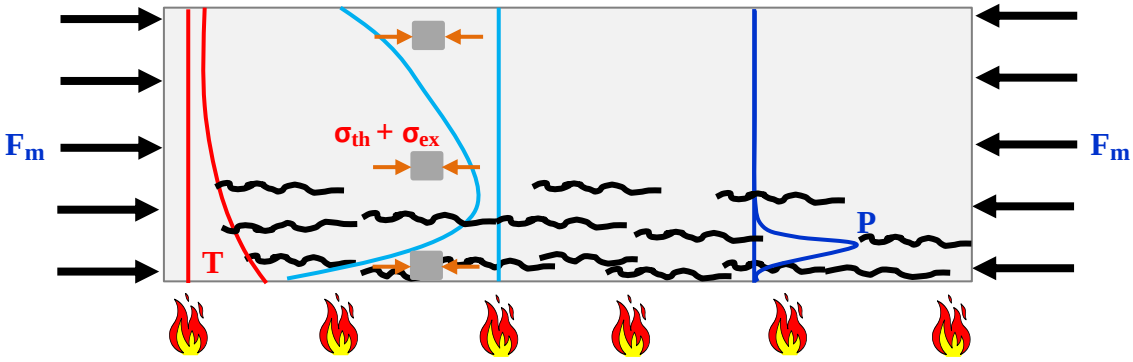

c) Cracking in the slab due to thermal and higher external load induced stress, thermal mismatch and pore pressure (P)

Figure 6.1: Schematic diagram of the cracking in the slab heated in unloaded (a) and loaded (b-c) conditions (F_m = mechanical load, T = temperature, P = pore pressure, σ_{th} = thermal stress, and σ_{ex} = load-induced stress). **Note**: stresses and cracks due to thermal mismatch are not drawn.

When an external biaxial compressive load was introduced, the tensile stress was remarkably reduced and even it was completely avoided in the higher compressive loading (see Figure 5.9 in chapter 5 and Figure 6.1b-c). At the same time, the compressive stress increases in the hot and

cold surfaces with the increasing applied compressive loading. Hence, the cracks parallel to the heated surface of the slabs should be increased with the increased applied biaxial compressive loading during heating [5], while the opening of the cracks that are perpendicular to the heated surface decreases, see Figure 5.11. In the permeability tests (see chapter 3), it has been shown that the axial permeability decreases when the confining pressure (i.e. biaxial loading) increases by reducing the opening of the axial cracks (perpendicular to the confining pressure), see Figure 3.17, while the axial permeability increases with uniaxial compressive stress applied during preheating due to the formation of cracks parallel to the direction of compressive stress, see Figure 3.20 and 3.21. As results, lower permeability in the direction perpendicular to the heated surface, which induce a steep build-up and higher magnitude of pore pressure, see Figures 4.25 and 4.26.

As the temperature increased under biaxial compressive loading, a reduction of tensile strength of concrete could occur in the direction perpendicular to the heated surface caused by the cracks parallel to the heated surface of the slab [5]. This effect is directly taken into account by the equivalent strain (see equations 5.5 and 5.6 in chapter 5). A biaxial compression creates an extension in the perpendicular direction due to Poison's ratio. This extension is added to the one created by a potential tension stress to reach the damage limit. Zeiml et al. 2013 [8] carried out the thermo-hygro-chemo-mechanical computations to investigate the spalling mechanisms of concrete. The authors found that thermo-mechanical processes cause a build-up of compressive stresses parallel to the heated surface, leading to a decrease of the tensile strength perpendicular to the heated surface of concrete. Sertmehmetoglu 1977 [5] proposed that these cracks fill with vapour produced by the desorption of pore water [4], resulting in tensile stresses at right angles to the compressive stress (i.e. higher pore pressure due to lower permeability in the direction perpendicular to the heated surface, which induces higher tensile stress in the direction perpendicular to the heated surface, see an example in Figure 6.3c). As the heating continues under biaxial compressive loading, the number and size of the cracks would increase (see Figure 6.1b-c) and when the tensile stresses in the cross section decrease the capability of the concrete to withstand tensile stresses due to the build-up of pore pressure, the material between the cracks and the heated surface would be expelled. This probability increases with the increasing applied load. As Zhukov 1976 [3] proposed that the occurrence of the explosive spalling is the development of unstable cracks under the action of the internal compressive stresses, compressive stresses caused by external loading and tensile stresses due to the pore pressure.

Concerning the effect of biaxial compressive loading levels on the fire spalling, in the intermediate load (e.g. 0.5 to 5 MPa), as mentioned earlier that the size, number, and the opening of cracks increased and the cracks are decreased perpendicular to the heated surface (see Figure 6.1b). Since a very high pore pressure occurred in the intermediate load tests (e.g. more than 2 MPa for the both biaxial loads at 1.5 and 3 MPa was observed, see Figure 4.25e-f), a small crack parallel to the heated face might be enough to induce spalling. While in the higher load (5 to 10 MPa), the cracks linked together and developed into larger cracks in the length and the width (see Figure 6.1c), as soon as the pressure increase, the cracks reach the critical value and initiate

the spalling. This behaviour could occur at the earlier stage of heating than the intermediate loading test. The time of the first spall of the slabs loaded at 3, 5 and 10 MPa are, respectively, 11.1 min, 7 min and 6 min. Since the cracks number, length and opening are higher for the higher load, a small pore pressure could be high enough to induce spalling (lower pore pressures were observed in the higher loaded tests than intermediate load tests, see Figures 4.25, 4.26 and 6.2).

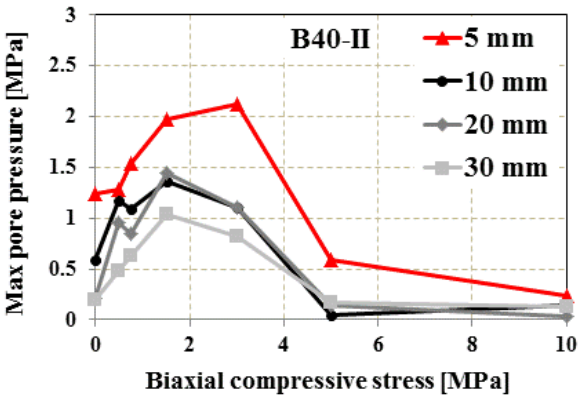

Figure 6.2: Maximum measured pore pressure in different depths of the specimen as a function of applied biaxial compressive stress.

6.1.2 Effect of uniaxial compressive loading

3D schematic diagram of the heated cube in unloaded and uniaxially loaded conditions have been drawn (see Figure 6.3) to explain the spalling mechanism of the ordinary concrete.

When the concrete cube specimens are heated under uniaxial compressive loading, the cracks and microcracks tend to open vertically in all the directions along the compressive loading axis (see Figures 6.3b and 5.13), while it decreases for the cracks that are perpendicular to the loading direction (see Figures 6.3b and 5.12d).

In the permeability tests (see chapter 3), it has been shown that the radial permeability decreases when the uniaxial compressive stress increases due to the closing of cracks perpendicular to the uniaxial compressive load, see Figure 3.22. As a consequence, uniaxial compressive load affects the moisture transport inside the concrete by decreasing permeability in the direction perpendicular to the heated face, as a result, induces faster build-up and higher value of pore pressure (see Figures 4.14 and 4.15, i.e. higher tensile stress perpendicular to the heated surface, see Figure 6.3c) in the specimen, which could exceed a value that favours spalling.

It is important to note that the amount of fire spalling should be higher when samples are subjected to biaxial loading than uniaxial loading (see Figure 4.29). Under biaxial loading during heating, the cracks generated by the state of stresses are mainly orientated parallel to the heated surface. These cracks are certainly the ones which induce the more important risk of spalling. At the same time, the opening of cracks perpendicular to the loading direction decreases in both

directions of biaxial loading (i.e. lower permeability and very high pore pressure). As stated above, under uniaxial loading, the cracks and microcracks tend to open vertically in all the directions along the compressive loading axis and tend to close the cracks that are only perpendicular to the loading direction (i.e. cracks close in the loading direction and cracks open a little bit in the other direction due to the absence of loading in that direction). Hence, crack closure is higher in the biaxial load than uniaxial load tests in the direction perpendicular to the heated surface of the concrete specimens. As a consequence, the permeability should be higher (i.e. lower pore pressure) in the specimens under uniaxial load test than the specimens under biaxial load tests.

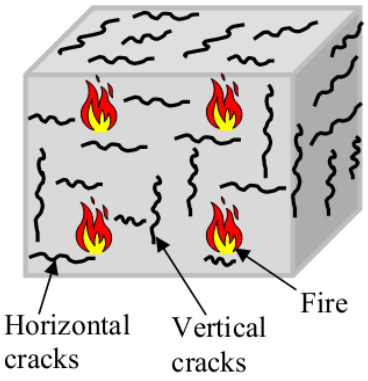

a) Crack patterns of unloaded test

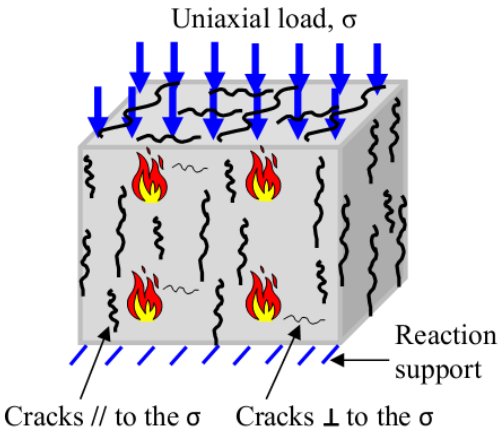

b) Crack patterns of loaded test

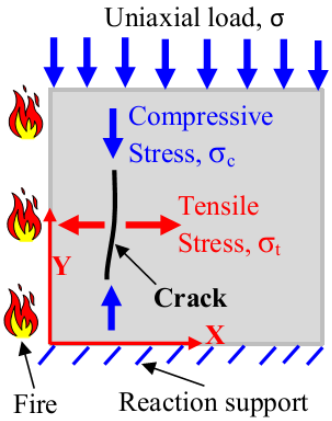

c) Stresses distribution and the crack in the loaded concrete

Figure 6.3: Schematic diagrams of the cracking in the cube heated in unloaded and loaded conditions (Note: // = parallel and ⊥ = perpendicular).

An example can be given by comparing the axial and radial permeability presented in chapter 3. At 600 °C, a sharp decrease of axial permeability was observed when the confining pressure (i.e. biaxial loading) was doubled (Pc = 0.6 MPa) than the reference pressure (Pc = 0.3 MPa) (see

Figure 3.17b), while no significant change of radial permeability was observed up to 1.2 MPa of uniaxial compressive loading (see Figure 3.22b). This behaviour demonstrated that the confining pressure (i.e. biaxial loading) leads to a higher decrease (i.e. higher crack closure) of gas permeability than uniaxial loading. These results are in good agreement with the measurement of pore pressure in both loading conditions. The maximum pore pressure of uniaxial load test at 16 MPa and biaxial load test at 1.5 MPa were, respectively, 1.1 MPa and 2.0 MPa for B40-II and 0.7 MPa and 2.2 MPa for B40-III. As stated before, the pore pressures were lower in the higher compressive load (10 MPa) than the moderate load (e.g. 0.75–3 MPa) due to higher mechanical damage (i.e. spalling), see Figure 6.2. These results demonstrated that biaxial compressive load (e.g. 1.5 MPa) increases very high pore pressure than uniaxial load (e.g. 16 MPa), which induces higher tensile stress in the direction perpendicular to the heated surface in the specimens under biaxial load test than the specimens under uniaxial load tests. Also, as stated in section 6.1.1, a higher reduction of tensile strength of concrete could occur in the direction perpendicular to the heated surface in the specimens under biaxial load test than the specimens under uniaxial load tests due to the absence of loading in the second axis of the uniaxial load test specimens. As a result, lower spalling in the uniaxial test than the biaxial test. Moreover, the size of the specimen itself has an effect on the rate of moisture escaping during the test. In cube specimens, the spalling started close to the central area of the exposed surface and decreases when reaching the edges, since the water can be transported out from the specimen due to the shorter path of the smaller specimen. Hence, the vapour pressure decreases towards the edges, thereby the risk of spalling is reduced.

6.2 Effect of cement type on fire spalling

In uniaxial fire tests, the amount of spalling was much higher for B40-II (3% of slag) than B40-III (43% of slag) for all the applied values of compressive stress. This behaviour is mainly explained by the lower permeability and porosity of B40-II than B40-III concrete at high temperatures (see Figure 3.15). While in the biaxial fire tests, at the low compressive loading (0.5 MPa), lower spalling has been observed in B40-III than the B40-II, while the spalling differences of both concretes are much lower from the compressive loading of 1.5 MPa to 10 MPa. The difference in the behaviour of both concretes cannot be explained by the difference of the mechanical properties (since the compressive and tensile strengths at the day of the fire tests are almost same, see table 3.3 in chapter 3) but by the difference of gas permeability. B40-III exhibited higher permeability than B40-II at any temperature (see Figures 3.15, 3.17, 3.20 and 3.22). Since the initial permeability of B40-III is higher than the B40-II, when concrete specimens (B40-II and B40-III) are heated under low load (e.g. 0.5 MPa), a small change of permeability (i.e. permeability of crack) due to the thermal mismatch between cement paste and aggregates and thermal gradients can be sufficient to prevent the development of pore pressure to exceed a value that favours spalling. For example, in the same fire and external loading condition, if the permeability of crack is equal to one order of magnitude in both concretes, then the final permeability of concrete (i.e. initial permeability + permeability of crack) will be higher

in B40-III than B40-II (as stated before, higher permeability in B40-III than B40-II in all temperatures), which is very important to prevent the development of pore pressure, resulting lower spalling in B40-III than B40-II. This behaviour consistent with the measurements of pore pressure at low load (0.5 MPa). Maximum pore pressures determined during biaxial loading at 0.5 MPa of B40-II and B40-III were 1.3 MPa and 0.6 MPa (see Figure 4.26), respectively. Therefore, this higher pore pressure of B40-II could explain the higher spalling of B40-II than B40-III.

While at the intermediate and higher biaxial compressive loading, it can be considered that, most of the internal microcracks and cracks (perpendicular to the heated surface) are closed (see Figure 5.11). Hence, permeability (i.e. pore pressure) and internal stresses should not be different for both concretes. This behaviour consistent with the measurements of pore pressure of both concretes. Maximum pore pressures determined during fire under biaxial load at 1.5 MPa and 3 MPa were, respectively, 2.0 MPa and 2.1 MPa for B40-II and 2.2 MPa and 1.7 MPa for B40-III, which is very close from one concrete to other, see Figure 4.26. Therefore, the spalling difference due to cement type is almost nil at the intermediate and higher biaxial compressive loading (1.5 to 10 MPa) compared to the low compressive loading (0.5 MPa).

6.3 References

[1] Harmathy, T. Z. (1965). "Effect of moisture on the fire endurance of building elements", ASTM Special Technical Publication, No. 385, pp. 74-95, 1965.

[2] Bazant, Z.P. (1997). "Analysis of pore pressure, thermal stress and fracture in rapidly heated concrete", in: Proceedings, International Workshop on Fire Performance of High-Strength Concrete, NIST, February 13-14, 1997, pp. 155–164.

[3] Zhukov, V. V. (1976). "Reasons of explosive spalling of concrete by fire", Beton i zhlezobeton (Concrete and Reinforcement Concrete), Issue 3.

[4] Khoury G. A and Anderberg Y. (2000). "Concrete spalling review", Fire safety design, report submitted to the Swedish National Road Administration, Sweden.

[5] Sertmehmetoglu, Y. (1977). "On a mechanism of spalling of concrete under fire conditions", PhD Thesis, King's College, London, 1977.

[6] Dougill, J.W., "Some observations on failure of quasi brittle materials under thermal stress", Cement and Concrete Research, Vol. 3, pp. 469-474, 1973.

[7] Lottman, B.B.G., Koenders, E.A.B., Blom, C.B.M., and Walraven, J.C., "Spalling of fire exposed concrete based on a coupled material description: an overview", Proceedings of the 4th International Workshop on the Concrete Spalling of Fire Exposure, October 08-09, 2015, Leipzig, Germany.

[8] Zeiml, M., Zhang, Z., Pichler, C., Lackner, R. and Mang, H. A. (2013). "A coupled thermo-hygro-chemo-mechanical model for the simulation of spalling of concrete subjected to fire loading", Proceedings of the 3rd International Workshop on Concrete Spalling due to Fire Exposure, 25-27 September, 2013, Paris, France.

7 Conclusions and Recommendations for Future Research

The aim of this thesis was to investigate the effect of compressive loading and cement type on the fire spalling behaviour of two ordinary concretes. For this purpose, comprehensive experimental studies have been performed within the scope of the work presented in this thesis. Two ordinary concrete (B40-II and B40-III: $f_{c28days} \approx 40$ MPa) specimens (slab, cube and prismatic shape) were exposed to ISO 834-1 fire curve, while a constant uniaxial or biaxial compressive load was applied. In order to better understand the mechanism of the fire spalling role played by the external compressive loading and incorporation of slag in cement, comprehensive experimental studies have been conducted, such as water absorption porosity and axial gas permeability tests on the unloaded preheating specimens, axial and radial gas permeability tests under different loading conditions (i.e. confining pressure and uniaxial compressive load) after preheating under loading and unloading conditions. In order to better analyse the experimental results and to provide more insight into the mechanism behind the fire spalling behaviour of concrete role played by the external compressive loading, numerical computations were carried out by using the existing thermo-mechanical (TM) model implemented in a finite element code CAST3M.

A number of conclusions can be drawn on the basis of the research studies presented and discussed in this thesis. The main conclusions are:

7.1 Effect of compressive loading and cement type on the fire spalling of concrete

On the basis of the experimental results presented in chapter 4, the following conclusions can be drawn:

- The experimental test results have clearly shown that the external compressive loading (uniaxial and biaxial load) and their levels have a significant influence on the fire spalling of concrete. Loaded specimens are more prone to spalling than unloaded specimens. It is worth to note, that unloaded samples made with the 2 concretes in three different tests (uniaxial and biaxial fire tests; and unloaded mid size slab tests) did not spall. In the biaxial fire test, a significant difference of spalling depths was observed in the tests between without load and under the lower load (0.5 MPa for B40-II and 0.75 for B40-III). On the contrary, in the uniaxial test results have shown no significant changes from 0 to 4 MPa.
- In the uniaxial fire spalling test, the amount of spalling was increased with the increased applied compressive stress, while in the biaxial test, an increased trend of spalling depths

was found up to 5 MPa, then it decreased at 10 MPa due to the early collapse behaviour of the slab specimens. The collapse of the 3 slabs occurred when the bending bearing capacity of the slabs was reached: 29 min for B40-II at 5 MPa, 25 min for B40-II at 10 MPa and 24 min for B40-III at 10 MPa, while in the uniaxial tests, the maximum load of 20 MPa was not sufficient to induce collapse, hence the spalling depths were not reduced at higher uniaxial compressive loading.

- From the sudden temperature increase related to spalling of the slabs, it has been able to determine the spalling kinetics for all the tests. It appears that the spalling rate is almost constant during all the tests and very close from one test to the other. In the biaxial fire tests, the spalling rate was approximately 100 mm/h.
- The fire spalling can occur when the state of stresses combining thermal stresses, applied stresses and pore pressure reaches a given threshold. Then to reach this threshold, the higher is the applied stresses lower will be the pore pressure.
- It has been found that the amount of spalling was much higher when samples have been subjected to biaxial loading than uniaxial loading. Under biaxial loading during heating, the cracks generated by the state of stresses are mainly orientated parallel to the heated surface. While in the uniaxial loading, the cracks and microcracks tend to open vertically in all the directions along the compressive loading axis. Hence, lower pore pressure (due to higher permeability) and lower stresses in uniaxial than biaxial fire tests, resulting lower spalling in the uniaxial fire test than the biaxial fire test.
- In uniaxial tests, spalling was much higher for B40-II (3% of slag) than B40-III (43% of slag) for all the applied values of compressive stress. This behaviour is mainly explained by the lower permeability and porosity of B40-II than B40-III concrete at high temperature. A similar difference was observed between the results obtained in biaxial tests at lower load (0.5 MPa). On the contrary, the difference appears not so significant from 1.5 to 10 MPa of biaxial fire tests due to the lower influence of the permeability of two different concretes when the biaxial load becomes relatively high (due to complete closure of the cracks perpendicular to the heated surface of both concretes).
- In both uniaxial and biaxial tests, the steepest build-up and higher value of pore pressure were measured in loaded tests, while a quite slow rise and lower magnitude of pore pressures were measured in the unloaded tests of both concretes (B40-II and B40-III). It has been shown that pore pressures are higher in the biaxial fire tests than the uniaxial fire tests. The maximum pore pressure of uniaxial and biaxial tests were, respectively, 1.1 MPa and 2.1 MPa for B40-II and 0.7 MPa and 2.45 MPa for B40-III. In the biaxial tests, the pore pressures were lower in the higher compressive load (10 MPa) than the moderate load (e.g. 0.75-3 MPa) due to higher mechanical damage (i.e. spalling).
- The presence of compressive loading during heating play a key important role on the thermal curvature of the slab. The experimental test results have shown that the displacement of the slabs decreased with the increased applied external compressive loading during heating.

7.2 The Thermo mechanical modelling of fire spalling of concrete

Based on the predicted results and discussion presented in chapter 5, the following conclusions can be made on the role of compressive loading on the fire spalling behaviour of concrete:

- In the biaxial slab model, in all depths (except at 10 mm), the predicted temperatures were very close to the experimental temperatures during the first 10 min of fire, thereafter dropped slightly and lagged the model predictions up to 30 min of computation. Beyond 30 min of computation, an excellent match was found between the predicted and experimental results. While in the uniaxial computation, the numerical model predictions show a quite good agreement with the experimental temperatures throughout the whole test (30 min).
- In the biaxial unloaded model, a good agreement between the measured and the predicted displacement throughout the fire exposure time was observed. While in the loaded models, the predicted displacements are perfectly matched with experiment until the specimen did not spall.
- In both unloaded computations (biaxial and uniaxial model), tensile stress occurred in the central part of the specimens and compression stress at the hot and cold surfaces. When an external compressive load was introduced, the tensile stress was remarkably reduced and even it was completely avoided in the higher compressive loading. At the same time, the compressive stress increases in the hot and cold surfaces with the increasing applied compressive loading.
- It has been found that the opening of cracks perpendicular to the loading direction decreased with the increased load, while it increased for the cracks that are parallel to the loading direction.

7.3 Effect of loading on the residual gas permeability of concrete

This research aimed to contribute determining the effect of loading on the residual gas permeability of concrete (discussed in chapter 3), which is a key parameter of concrete fire spalling. Axial and radial gas permeability tests were carried out on two concretes (B40-II and B40-III) under different preheating and loading conditions. The main conclusions are:

- It has been clearly shown that the presence of loading and their levels have a significant influence on the gas permeability of concrete.
- The specimens preheated in an unloaded condition, the axial permeability decreases when confining pressure (perpendicular to the gas flow) increases by reducing the opening of the axial cracks.
- The specimens preheated under uniaxial compressive stress tests showed that the axial permeability increases with uniaxial compressive stress applied during preheating due to induced cracks parallel to the direction of compressive stress.

- The specimens preheated in unloaded condition, at lower temperatures (120 and 250 °C), the radial permeability decreases when applied compressive stress increases, while at the higher temperatures (400 °C and 600 °C), the permeability decreases up to a certain level of load, after that stabilises and then increases when the compressive stress increases.
- The permeability increases or decreases depends on the orientation and opening of cracking and these two parameters are influenced by compressive loading. Hence, the stress state, by governing the orientation and opening of the cracks is very important key factors which control the internal fluid transfer (i.e. permeability) and then directly triggers the build-up and magnitude of the pore pressure within the concrete structure. Stress state has then 2 major roles on concrete fire spalling: (i) a direct influence in the thermo mechanical mechanism and (ii) an indirect influence in themo-hydral mechanism by influencing the cracks opening and orientation and then, the permeability.
- The effect of compressive loading on the gas permeability of concrete is visible even if the load is very small compared to the compressive strength of concrete. A sharp decrease of axial permeability was observed when the confining pressure was doubled (Pc = 0.6 MPa) than the reference pressure (Pc = 0.3 MPa).
- The confining pressure (i.e. biaxial loading) leads to a higher decrease (i.e. higher crack closure) of gas permeability than uniaxial loading.
- The effects of loading on the residual gas permeability of specimen slowly heated in free mechanics conditions have been discussed here in this thesis. The heating of the specimens creates some cracking principally due to thermal mismatch. In the case of a structure submitted to a fire, the thermal gradients are much more important and the cracking of the structure is not only governed by the thermal mismatch. Nevertheless, the presence of a compressive stress and moreover a confining compressive stress reduces the risk of cracking and by the way, increases the risk of fire spalling.
- It was found that the permeability of concrete made with CEM III cement (B40-III: 43% of slag) is higher than the one of concrete made with CEM II cement (B40-II: 3% slag) in all heating and loading conditions.

7.4 Effect of heating on the residual porosity, permeability, and pore pressure of concrete

In order to gain a better understanding of the fundamental physics behind the fire spalling behaviour of concrete, residual gas permeability and water absorption porosity measurements were carried out on the preheated specimens in the unloaded conditions. Additionally, the build-up of pore pressure and temperature (PT) were measured to a deeper understanding the thermo-hydral process of spalling. The following conclusions can be drawn based on the results presented in chapter 3.

- As the temperature increased, the porosity and permeability increased, especially higher increment at the higher thermal load. At temperatures ranging from 80 °C to 120 °C, a sharp increase of porosity and permeability was observed for both concretes. At a temperature higher than 400 °C, the increased permeability is attributed to the

development of cracks mainly caused by the thermal incompatibility between the cement paste and the aggregates.

- Concrete made with CEM III cement (B40-III: 43% of slag) exhibited higher values of residual porosity and permeability at high temperature than CEM II cement concrete (B40-II: 3% of slag).
- B40-II (3% of slag) presented higher pore pressure for moderate and slow thermal loadings than B40-III (43% of slag). This result is in good agreement with the lower B40-II permeability and porosity at high temperature.
- During rapid heating, low values of pore pressure were observed in B40-II due to a larger number of surface cracks and few long cracks induced by the higher thermal gradient of rapid heating. The cracks allow significant amounts of vapour and liquid water to be drained out from the specimen. Hence, a thermal gradient is found to be an influencing factor in the process of pore pressure build-up. This suggests that the internal cracking is an important factor for pore pressure development when concrete is exposed to fast heating rate.

7.5 Fire spalling mechanism of the ordinary concrete

Based on the results presented in this thesis, a possible mechanism is discussed to explain the role of external compressive loading on the fire spalling mechanism of the ordinary concrete.

- **Unloaded fire tests:** When concrete is heated in unloaded condition, a multiple cracks could occur inside the concrete specimens such as orthogonal cracks perpendicular to the heated surface in the concrete core and surface cracks parallel to the exposed face in the hot layers. These cracks are often beneficial to limit the development of pore pressure as well as stresses. Thereby, the risk of fire spalling is avoided.
- **Fire test under biaxial compressive loading:** When the concrete specimens are heated under compressive loading, the opening of cracks parallel to the loading direction increases, while it decreases for the cracks that are perpendicular to the loading direction (i.e. lower permeability in the direction perpendicular to the heated surface). This tendency increases with the increasing applied load. As a result, the moisture could not drain from the critical spalling zone of the heated concrete, which induces a very steep and higher pore pressure. As the temperature increased, a reduction of tensile strength of concrete could occur in the direction perpendicular to the heated surface caused by the cracks parallel to the heated surface of the slab. As the heating continues, the number and size of the cracks would increase and when the tensile stresses in the cross section decrease the capability of the concrete to withstand tensile stresses due to the build-up of pore pressure, the material between the cracks and the heated surface would be expelled. The pore pressure required to cause spalling depends on the stress state, hot mechanical properties, and number, length and width of the cracks. For the intermediate loading, the cracks parallel to the heated surface would be less, hence higher pore pressure is needed

to induce spalling, while in the higher load, the cracks parallel to the heated surface would be higher, therefore a small magnitude of pore pressure could be high enough to induce spalling.

- **Fire test under uniaxial compressive loading:** When the concrete specimens are heated under uniaxial compressive loading, the cracks and microcracks tend to open vertically in all the directions along the compressive loading axis, while it decreases for the cracks that are only perpendicular to the loading direction (i.e. lower crack closure than biaxial loading). As a consequence, compressive load affects the moisture transport inside the concrete by decreasing permeability in the direction perpendicular to the heated face, as a result, induce very high pore pressure (i.e. higher tensile stress perpendicular to the heated surface) in the specimen, which could exceed a value that favours spalling.

During a real fire, concrete structural members are always loaded or restrained. The presence of compressive loading during heating significantly increases the compressive stress (decreases the tensile stress) and the magnitude of pore pressure, which increase the risk of fire spalling. ***Then, the applied compressive stress is a very important key factor that the fire resistance design of concrete structures should take into account when considering spalling. Hence, it is recommended that the fire spalling test should not be carried out only on unloaded specimens, especially for the ordinary concrete.***

7.6 Recommendations for future research

Data generated from this thesis can be used for future modelling and the development of appropriate design guidelines on the fire spalling behaviour of concrete when exposed to fire and external compressive loading. Although a number of significant conclusions have been drawn from the research work presented in this thesis, more experimental investigations, as well as model developments and numerical computations are needed in order to progress in the understanding of the phenomena of fire spalling behaviour of concrete.

Experimental studies:

- Since a clear link between compressive load and the fire spalling depth has been found in the ordinary concrete, hence it is encouraging to investigate the spalling behaviour of high performance concrete with and without fibres heated under different levels of compressive loading (uniaxial and biaxial).
- Since the permeability was identified as one of the main key parameters of concrete fire spalling by directly influencing the build-up of pore pressure during heating (a good agreement has been found in this thesis). The concrete permeability at high temperatures under different level of compressive loading can be measured to deeper analyse the spalling mechanism of concrete, also the outcome of this research can be used as a good input parameter for the future spalling modelling.

- To date, in the literature, there is no measurement of liquid pressure of concrete during heating, hence this research can give us a new information to better understand the mechanism of spalling.
- Moisture migration and the presence of moisture clog inside the concrete during heating are well explained in the literature, except few tests on the visualisation of moisture profile during heating, no detail investigation exists in the literature. Therefore, it is encouraging to study the moisture migration and the presence of a moisture clog inside the concrete at high temperatures.
- In this thesis, it has been shown that the incorporation of slag (CEM III cement: 43% of slag) in cement is less sensitive to fire spalling. Hence, it is also encouraging to investigate the fire spalling behaviour of concrete made with the different percentage of slag (e.g. 0, 20, 50, 70 and 90%) in cement to answer the question whether concrete members and structures made with slag based cements can give the same fire safety level as those made with 100% Ordinary Portland Cement. This research will allow to find an optimum percentage of slag which could be used in the concrete structures when exposed to high temperatures, which will also decrease negative environmental effects as well as economic benefits.
- Non-destructive evaluation methods can be developed to monitor the concrete damage (e.g. crack pattern), migration of water (e.g. moisture clog), and spalling progression in structural members during fire tests.

Numerical studies:

- Numerical results presented in this thesis allow us to deeper understanding the mechanism of fire spalling of concrete role played by external compressive loading. In this thesis, thermo-mechanical (TM) model has been studied without considering creep, load induced strain, and the reduction of the thickness (due to spalling) with time, these parameters can be considered to improve the future TM model.
- In this thesis, it has been shown that the cracking plays an important key role during heating under loading, which probably cooperates to induce spalling, hence the development of crack pattern and the crack opening can be analysed deeply in particular at the meso-scale.
- In order to deeper understanding, the actual mechanism of spalling, hygro-thermo-mechanical analysis should be developed.

Appendix A: Fire spalling test under biaxial compressive loading

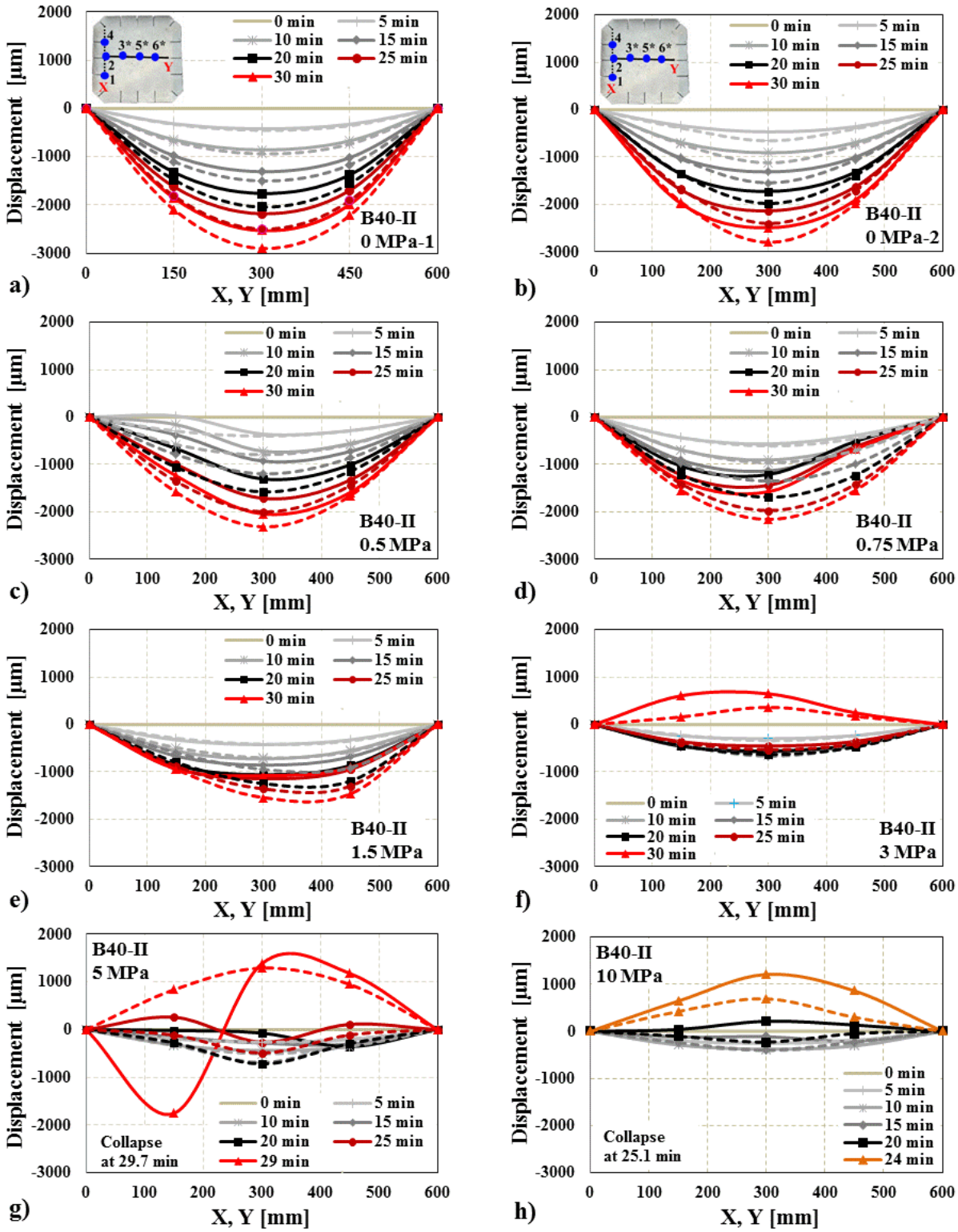

Figure A1: Deformed shape of B40-II slabs in the X and Y-axes (see top-left plot).

Appendix B: The thermo-mechanical model

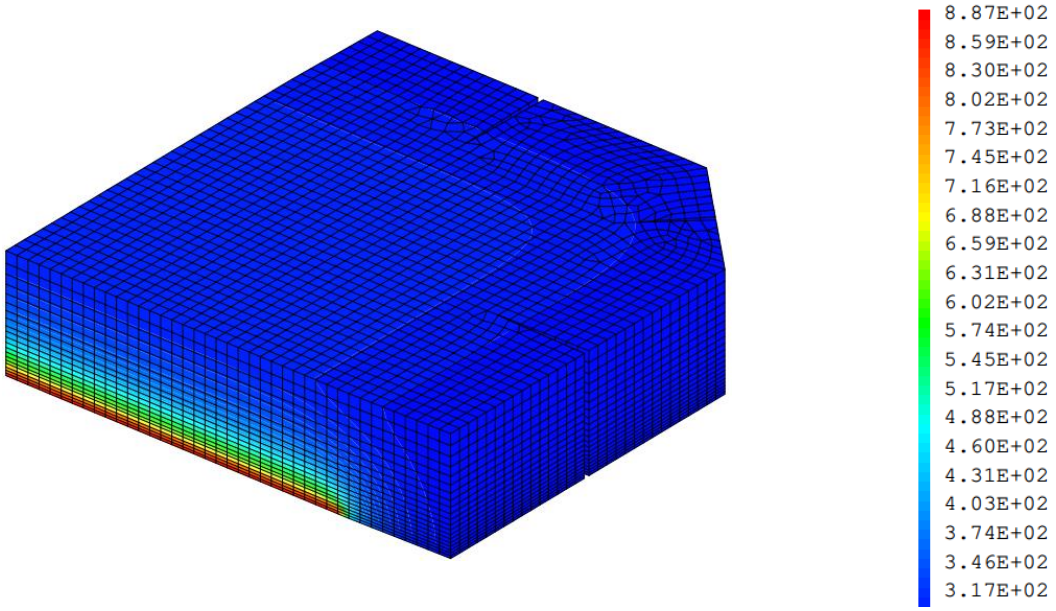

a) Slab specimen

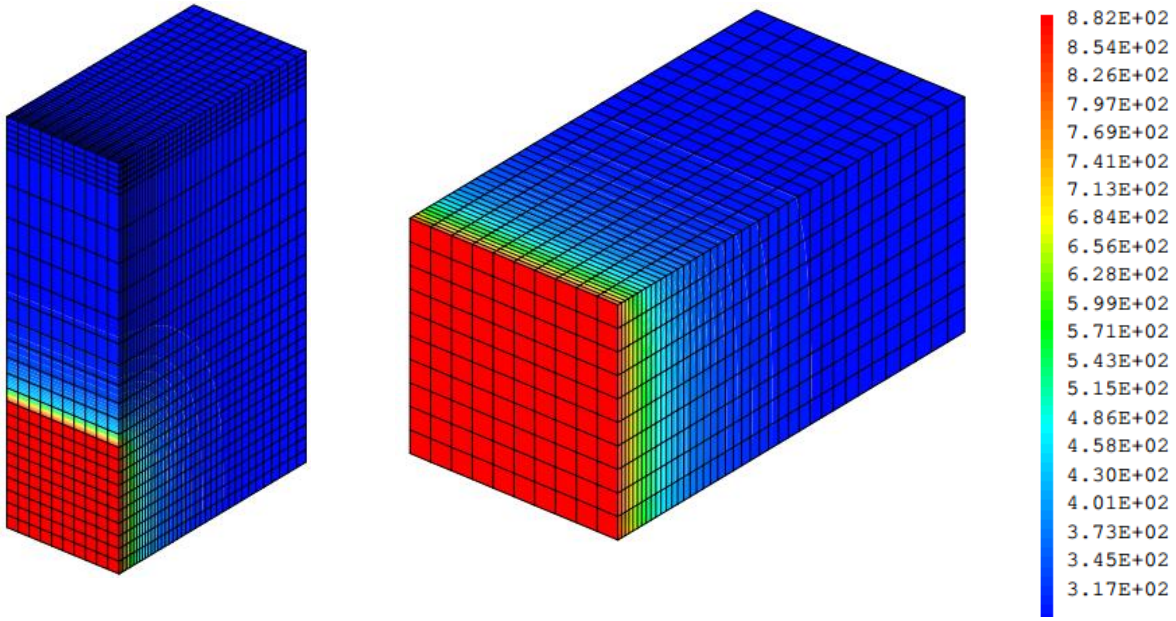

b) Cube with supports

c) Cube specimen

Figure B1: 3D thermal image of one-quarter section of the biaxial slab (a) and uniaxial cube (b-c) specimens.

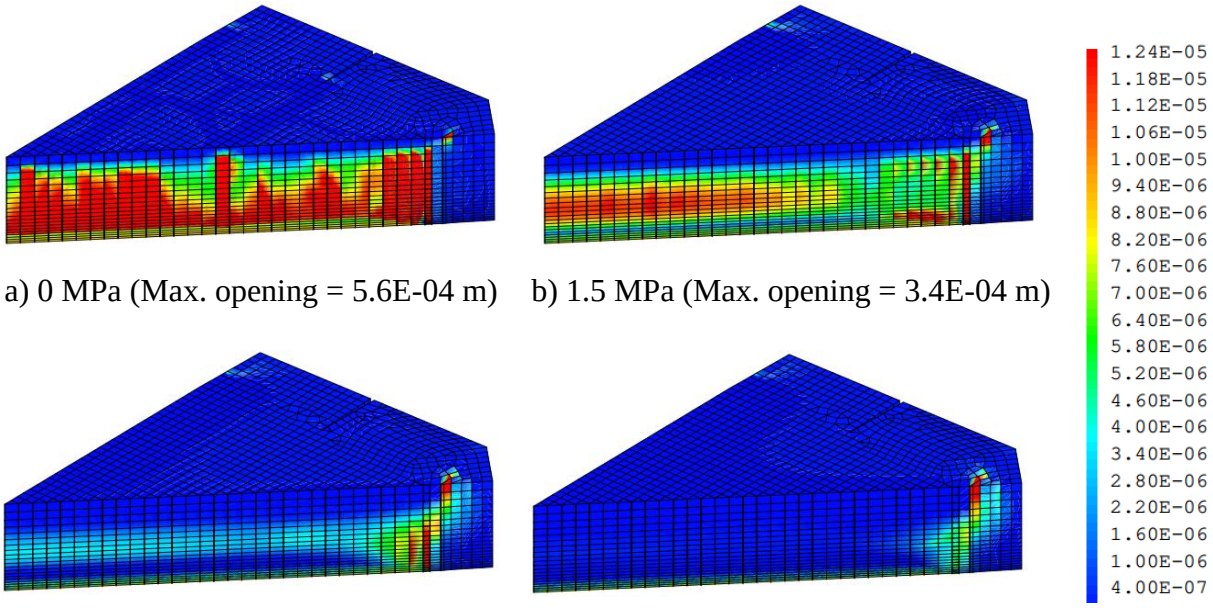

a) 0 MPa (Max. opening = 5.6E-04 m) b) 1.5 MPa (Max. opening = 3.4E-04 m)

c) 5 MPa (Max. opening = 1.8E-04 m) d) 10 MPa (Max. opening = 1.2E-04 m)

Figure B2: Crack opening perpendicular to the heated surface of the slabs after 30 minutes of heating under different levels of biaxial compressive stress.

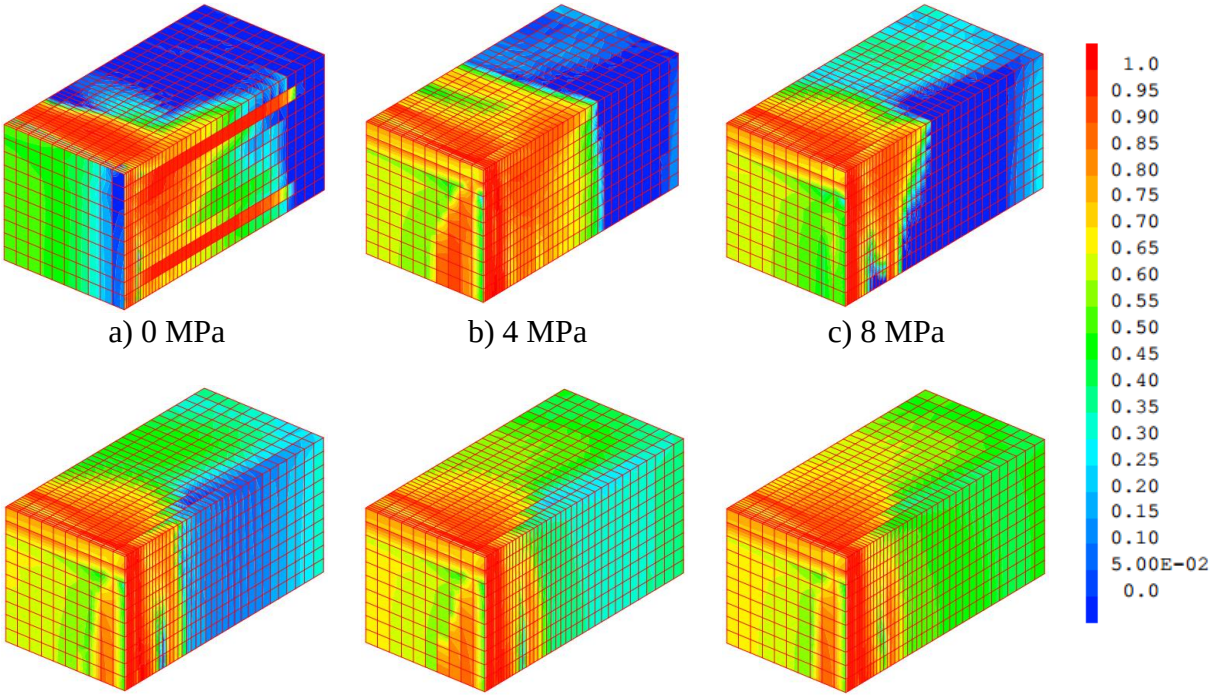

a) 0 MPa b) 4 MPa c) 8 MPa

d) 12 MPa e) 16 MPa f) 20 MPa

Figure B3: Typical damage fields of the cubes after 30 min of fire at different levels of uniaxial compressive stress (1 = fully damaged and 0 = undamaged).

About the author

Name:	**Md Jihad MIAH**
October 30th, 1984:	Born in Jimmapara, Rangpur, Bangladesh.
Parents:	Most Rahema Begum (mother) and Noor Mohammad Bapary (father)
Married:	Shamima Aktar MIAH
2000 – 2004:	Diploma in Civil Engineering
	Rangpur Polytechnic Institute, Bangladesh
2006 – 2010:	B.Sc. in Civil Engineering
	University of Asia Pacific, Bangladesh
2011 – 2013:	M.Sc. in Civil Engineering for Risk Mitigation
	Politecnico di Milano, Italy
2014 – 2017:	PhD candidate, Centre Scientifique et Technique du Bâtiment (CSTB)
	and University of Pau and Pays de l'Adour, France

Publications during PhD thesis

Journal Papers

[1] Miah, M.J., Carré, H., Pimienta, P and La Borderie, C. "Factors Influencing Fire Spalling Behaviour of Concrete: Effect of Uniaxial Compressive Loading and Cement Type", 2017 (in preparation).

[2] Miah, M.J., Lo Monte, F., Felicetti, R., Pimienta, P., Carré, H and La Borderie, C. "The Effect of Biaxial Compressive Loading on the Fire Spalling Behaviour of Concrete – Part 1: Experimental", 2017 (in preparation).

[3] Miah, M.J., Kallel, H., Carré, H., Pimienta, P., La Borderie, C., Lo Monte, F and Felicetti, R. "The Effect of Loading on the Residual Gas Permeability of Concrete", 2017 (in preparation).

Conference Papers

[4] Miah, M.J., Lo Monte, F., Felicetti, R., Pimienta, P., Carré, H and La Borderie, C. "Experimental Investigation on Fire Spalling Behaviour of Concrete: Effect of Biaxial Compressive Loading and Cement Type", 5th International Workshop on Concrete Spalling due to Fire Exposure, 12-13 October 2017, Borås, Sweden, 10 pp. (in press).

[5] Miah, M.J., Kallel, H., Carré, H., Pimienta, P., La Borderie, C., Lo Monte, F and Felicetti, R. "The Effect of Loading on the Residual Gas Permeability of Concrete", 5th International Workshop on Concrete Spalling due to Fire Exposure, 12-13 October 2017, Borås, Sweden, 10 pp. (in press).

[6] Miah, M. J., Lo Monte, F., Felicetti, R., Carré, H., Pimienta, P and La Borderie, C. (2016). "Fire Spalling Behaviour of Concrete: Role of Mechanical Loading (Uniaxial and Biaxial) and Cement Type", Key Engineering Materials, ISSN: 1662-9795, Vol. 711, pp. 549-555, CONSEC 2016, Politecnico di Milano, Lecco, Italy.

[7] Carré, H., Céline, P., Atef, D., **Miah, M. J** and Bassem, A. (2016). "Durability of Ordinary Concrete after Heating at High Temperature", Key Engineering Materials, ISSN: 1662-9795, Vol. 711, pp. 428-435, CONSEC 2016, Politecnico di Milano, Lecco, Italy.

[8] Bamonte, P., Felicetti, R., Kalaba, N., Lo Monte, F., Pinoteau, N., **Miah, M. J** and Pimienta, P. (2016). "On the Structural behavior of Reinforced Concrete Walls Exposed to Fire", Key Engineering Materials, Vol. 711, pp. 580-587, CONSEC 2016, Politecnico di Milano, Lecco, Italy.

[9] Miah, M. J., Lo Monte, F., Pimienta, P and Felicetti, R. (2016). "Effect of Biaxial Mechanical Loading and Cement Type on the Fire Spalling Behaviour of Concrete", 9th International Conference on Structures in Fire, June 8-10, 2016, Princeton, USA.

[10] Miah, M. J., Pinoteau, N and Pimienta, P. (2016). "A Thermo Mechanical Experimental Investigation on 3 Loaded Concrete Walls Exposed to ISO 834-1 Fire", 9th International Conference on Structures in Fire, June 8-10, 2016, Princeton, USA.

[11] Miah, M.J., Pimienta, P., Carré, H., Pinoteau, N**.**, and La Borderie, C. (2015). "Fire Spalling of Concrete: Effect of Cement Type", 4th International Workshop on Concrete Spalling (IWCS) due to Fire Exposure, October 8-9, 2015, Leipzig, Germany.

[12] Miah, M. J., Carré, H., Pimienta, P., Pinoteau, N., and La Borderie, C. (2015). "Effect of Uniaxial Mechanical Loading on Fire Spalling of Concrete," 4th International Workshop on Concrete Spalling (IWCS) due to Fire Exposure, October 8-9, 2015, Leipzig, Germany.

[13] Miah M.J., Pimienta, P., Carré, H., Pinoteau, N**.**, and La Borderie, C. (2015). "Effect of Cement Type on Pore pressure, Temperature and Mass Loss of Concrete Heated up to 800°C", AUGC 2015, 33e Rencontres Universitaires de Génie Civil, Université de Pau et des pays de l'Adour, p. 432-439, May 27 – 29, 2015, Anglet, France.